

การเตรียม การวิเคราะห์ลักษณะและสมรรถนะการเร่งปฏิกิริยาของ  
ตัวเร่งปฏิกิริยา Pt-Ru บนตัวรองรับที่เตรียมจากคลัสเตอร์ของโลหะ

นางสาวเสาวภา โชติสุวรรณ

วิทยานิพนธ์นี้เป็นส่วนหนึ่งของการศึกษาตามหลักสูตรปริญญาวิทยาศาสตรดุษฎีบัณฑิต

สาขาวิชาเคมี

มหาวิทยาลัยเทคโนโลยีสุรนารี

ปีการศึกษา 2547

ISBN 974-533-381-6

**PREPARATION, CHARACTERIZATION AND  
CATALYTIC PERFORMANCE OF SUPPORTED Pt-Ru  
CATALYSTS PREPARED FROM A METAL CLUSTER**

**Miss Saowapa Chotisuwan**

**A Thesis Submitted in Partial Fulfillment of the Requirements**

**for the Degree of Doctor of Philosophy in Chemistry**

**Suranaree University of Technology**

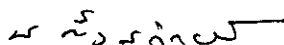
**Academic Year 2004**

**ISBN 974-533-381-6**

**PREPARATION, CHARACTERIZATION AND CATALYTIC  
PERFORMANCE OF SUPPORTED Pt-Ru CATALYSTS  
PREPARED FROM A METAL CLUSTER**

Suranaree University of Technology has approved this thesis submitted in partial fulfillment of the requirements for the Degree of Doctor of Philosophy.

Thesis Examining Committee



(Asst. Prof. Dr. Malee Tangsathitkulchai)

Chairperson



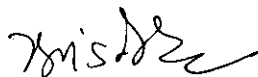
(Asst. Prof. Dr. Jatuporn Wittayakun)

Member (Thesis Advisor)



(Prof. Dr. Bruce C. Gates)

Member



(Assoc. Prof. Dr. Nurak Grisdanurak)

Member

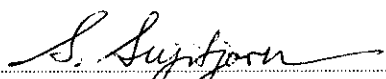


(Assoc. Prof. Dr. Vichitr Rattanaphani)

Member



(Assoc. Prof. Dr. Prasart Suebka)



(Assoc. Prof. Dr. Sarawut Sujitjorn)

Vice Rector for Academic Affairs

Dean of Institute of Science

เสาวภา โชติสุวรรณ : การเตรียม การวิเคราะห์ลักษณะและสมรรถนะการเร่งปฏิกิริยาของ  
ตัวเร่งปฏิกิริยา Pt-Ru บนตัวรองรับที่เตรียมจากคลัสเตอร์ของโลหะ (PREPARATION,  
CHARACTERIZATION AND CATALYTIC PERFORMANCE OF  
SUPPORTED Pt-Ru CATALYSTS PREPARED FROM A METAL  
CLUSTER) อาจารย์ที่ปรึกษา : ผู้ช่วยศาสตราจารย์ ดร.จตุพร วิทยาคูณ, 247 หน้า.  
ISBN 974-533-381-6

วิทยานิพนธ์นี้กล่าวถึงการเตรียม การวิเคราะห์ลักษณะ และการทดสอบสมรรถนะการเร่ง  
ปฏิกิริยาของตัวเร่งปฏิกิริยาโลหะคู่แพลตินัมนรูทีเนียมที่มีการกระจายตัวสูงบนตัวรองรับซึ่งเตรียม  
โดยการดูดซับคลัสเตอร์  $Pt_3Ru_6(CO)_{21}(\mu_3-H)(\mu-H)_3$  จากไดคลอโรโรมีเรนบนตัวรองรับอะลูมินา  
แมกนีเซียและไทเทเนีย จะสังเกตการเปลี่ยนแปลงของคลัสเตอร์ตั้งต้นและอันตรกิริยากับผิวหน้า  
ของตัวรองรับหลังจากการดูดซับได้จากการวิเคราะห์ลักษณะของตัวอย่างที่ผ่านการทำให้แห้งภายใต้  
สูญญากาศด้วยอินฟราเรด (IR) และเอกซ์เทนเดดเอกซ์เรย์แอบซอร์ปชันไฟน์สตรักเจอร์ (EXAFS)  
สเปกโทรสโกปี การดูดซับของคลัสเตอร์ตั้งต้นบนตัวรองรับทุกตัวเป็นเชิงเคมีและไม่สามารถสกัด  
กลับออกมาได้อีกด้วยตัวทำละลายไดคลอโรมีเรน หลังการดูดซับบนอะลูมินา แกนโลหะของคลัส  
เตอร์ยังคงสภาพเดิม แต่เมื่ออยู่บนแมกนีเซียและไทเทเนียจำนวนพันธะระหว่างแพลตินัมกับ  
รูทีเนียมจะลดลง นอกจากนี้ลิแกนด์ไฮโดรเจนอาจหลุดออกไปได้ระหว่างการดูดซับ การดูดซับ  
ของคลัสเตอร์บนอะลูมินาเกิดจากอันตรกิริยาระหว่างโลหะของสารตั้งต้นและออกซิเจนที่ผิว  
ตัวรองรับ และเกิดจากอันตรกิริยาระหว่างออกซิเจนของลิแกนด์คาร์บอนิลและหมู่ไฮดรอกซิลที่ผิว  
ตัวรองรับและ/หรือที่ตำแหน่งกรด  $Al^{3+}$  ได้เช่นเดียวกัน ส่วนอันตรกิริยาบนแมกนีเซียและไทเทเนีย  
เกิดระหว่างออกซิเจนของลิแกนด์คาร์บอนิลของสารตั้งต้นกับหมู่ไฮดรอกซิลที่ผิวตัวรองรับโดย  
เกิดเป็นหมู่คาร์บอเนตและคาร์บอกซิเลต จะสังเกตเห็นพันธะไฮโดรเจนในการดูดซับบนแมกนีเซีย  
ส่วนบนไทเทเนียจะสังเกตเห็นว่าอะตอมรูทีเนียมมีการสูญเสียลิแกนด์คาร์บอนิลบางส่วน อย่างไรก็ตาม  
ก็ตามลิแกนด์คาร์บอนิลบนสารตั้งต้นที่ถูกดูดซับบนตัวรองรับจะหลุดออกอย่างสมบูรณ์เมื่อให้  
ความร้อน ณ อุณหภูมิ 300 องศาเซลเซียส เป็นเวลา 2 ชั่วโมงในบรรยากาศของฮีเลียม เป็นผลทำให้  
อนุภาคโลหะคู่แพลตินัมนรูทีเนียมบนตัวรองรับมีการกระจายตัวสูง ความยาวเฉลี่ยของพันธะ  
โลหะ-โลหะในตัวเร่งปฏิกิริยาแพลตินัมนรูทีเนียมบนตัวรองรับอะลูมินา แมกนีเซียและ  
ไทเทเนียมีค่าตามลำดับดังนี้ พันธะแพลตินัม-แพลตินัม เท่ากับ 2.64, 2.69 และ 2.65 อังสตรอม  
พันธะแพลตินัม-รูทีเนียม เท่ากับ 2.68, 2.69 และ 2.69 อังสตรอม และพันธะรูทีเนียม-รูทีเนียม  
เท่ากับ 2.62, 2.63 และ 2.65 อังสตรอม ส่วนเลขโคออร์ดิเนชันเฉลี่ยของโลหะ-โลหะในตัวเร่ง

ปฏิกิริยาแพลตินั่มรูทีเนียมบนตัวรองรับอะลูมินา แมกนีเซียและไทเทเนียมมีค่าตามลำดับดังนี้ แพลตินั่ม-แพลตินั่ม เท่ากับ 1.7, 1.3 และ 1.8 แพลตินั่ม-รูทีเนียม เท่ากับ 2.2, 0.9 และ 1.9 รูทีเนียม-รูทีเนียม เท่ากับ 2.1, 2.6 และ 2.4 และรูทีเนียม-แพลตินั่ม เท่ากับ 1.0, 1.1 และ 0.9

ตัวเร่งปฏิกิริยาแพลตินั่มรูทีเนียมบนตัวรองรับที่เตรียมจาก  $\text{Pt}_3\text{Ru}_6(\text{CO})_{21}(\mu_3\text{-H})(\mu\text{-H})_3$  สามารถเร่งปฏิกิริยาการเติมไฮโดรเจนในเอธิลีนและปฏิกิริยาการแตกตัวของนอร์มอลบิวเทนเมื่อเติมไฮโดรเจนได้ พลังงานก่อกัมมันต์ปรากฏสำหรับปฏิกิริยาการเติมไฮโดรเจนในเอธิลีนของตัวเร่งปฏิกิริยาบนตัวรองรับอะลูมินา แมกนีเซียและไทเทเนียมเท่ากับ 8.4, 7.6 และ 8.1 กิโลแคลอรีต่อโมล ตามลำดับ ในขณะที่พลังงานก่อกัมมันต์ปรากฏสำหรับปฏิกิริยาการแตกตัวของนอร์มอลบิวเทนเท่ากับ 30.9, 15.5 และ 28.2 กิโลแคลอรีต่อโมล

ได้เปรียบเทียบตัวเร่งปฏิกิริยาแพลตินั่มรูทีเนียมที่เตรียมจาก  $\text{Pt}_3\text{Ru}_6(\text{CO})_{21}(\mu_3\text{-H})(\mu\text{-H})_3$  บนตัวรองรับอะลูมินาและแมกนีเซียกับตัวเร่งปฏิกิริยาแพลตินั่มรูทีเนียมที่เตรียมจากสารผสมของ  $\text{Pt}(\text{acac})_2$  และ  $\text{Ru}(\text{acac})_3$  แม้ว่างานนี้จะเป็นงานแรกที่เตรียมตัวเร่งปฏิกิริยาแพลตินั่มรูทีเนียมบนตัวรองรับจากสารผสมของ  $\text{Pt}(\text{acac})_2$  และ  $\text{Ru}(\text{acac})_3$  แต่กลับไม่พบพันธะแพลตินั่ม-รูทีเนียมบนวัสดุที่ได้หลังจากนำตัวอย่างไปกำจัดลิแกนด์ด้วยความร้อนในบรรยากาศของไฮโดรเจน ณ อุณหภูมิ 300 องศาเซลเซียส เป็นเวลา 2 ชั่วโมง ตัวเร่งปฏิกิริยาแพลตินั่มรูทีเนียมที่เตรียมจากสารผสมของสารตั้งต้นโลหะอินทรีย์นี้สามารถเร่งปฏิกิริยาการเติมไฮโดรเจนในเอธิลีนได้และมีพลังงานก่อกัมมันต์ปรากฏอยู่ในช่วงเดียวกัน

สาขาวิชาเคมี

ปีการศึกษา 2547

ลายมือชื่อนักศึกษา.....

ลายมือชื่ออาจารย์ที่ปรึกษา.....

ลายมือชื่ออาจารย์ที่ปรึกษาร่วม.....

SAOWAPA CHOTISUWAN : PREPARATION, CHARACTERIZATION  
AND CATALYTIC PERFORMANCE OF SUPPORTED Pt-Ru  
CATALYSTS PREPARED FROM A METAL CLUSTER.  
THESIS ADVISOR : ASST. PROF. JATUPORN WITTAYAKUN, Ph.D.  
247 PP. ISBN 974-533-381-6

This thesis reported the preparation, characterization and catalytic performance of supported bimetallic PtRu catalysts with extremely high dispersion prepared by adsorption of  $\text{Pt}_3\text{Ru}_6(\text{CO})_{21}(\mu_3\text{-H})(\mu\text{-H})_3$  cluster from  $\text{CH}_2\text{Cl}_2$  onto  $\gamma\text{-Al}_2\text{O}_3$ , MgO and  $\text{TiO}_2$ . Changes in cluster precursor and interaction with the support surface after adsorption of the vacuum-dry samples were observed by infrared (IR) and extended X-ray absorption fine structure (EXAFS) spectroscopy. The cluster precursor adsorbed chemically in the form of bimetallic carbonyl species on all supports and was unable to be re-extracted by  $\text{CH}_2\text{Cl}_2$  solvent. However, the metal cluster core remained intact only on  $\gamma\text{-Al}_2\text{O}_3$  and decreased in Pt-Ru contributions were observed on the adsorption on MgO and  $\text{TiO}_2$ . It was possible that loss of hydrides took place during adsorption. The precursor adsorbed on  $\gamma\text{-Al}_2\text{O}_3$  support by interactions between cluster metal and surface oxygen as well as with oxygen of CO ligands and surface hydroxyl groups and/or  $\text{Al}^{3+}$  acid sites. Interactions on MgO and  $\text{TiO}_2$  also occurred via oxygen of CO ligands of precursor and surface hydroxyl groups forming adsorbed carbonates and carboxylates species. Hydrogen bonding was observed on MgO and partial decarbonylation from Ru atoms was observed on  $\text{TiO}_2$ . Carbonyl ligands of adsorbed precursor could be completely removed in He flow at  $300^\circ\text{C}$  for 2 hours resulting in high dispersion of supported bimetallic PtRu

particles. The average metal-metal bond distances of catalysts supported on  $\gamma$ -Al<sub>2</sub>O<sub>3</sub>, MgO and TiO<sub>2</sub> were: Pt-Pt, 2.64, 2.69 and 2.65 Å; Pt-Ru, 2.68, 2.69 and 2.69 Å; Ru-Ru, 2.62, 2.63 and 2.65 Å, respectively. The average metal-metal coordination numbers for PtRu catalysts supported on  $\gamma$ -Al<sub>2</sub>O<sub>3</sub>, MgO and TiO<sub>2</sub> were: Pt-Pt, 1.7, 1.3 and 1.8; Pt-Ru 2.2, 0.9 and 1.9; Ru-Ru, 2.1, 2.6 and 2.4; Ru-Pt, 1.0, 1.1 and 0.9, respectively.

Supported PtRu catalysts prepared from Pt<sub>3</sub>Ru<sub>6</sub>(CO)<sub>21</sub>( $\mu$ <sub>3</sub>-H)( $\mu$ -H)<sub>3</sub> were active for both ethylene hydrogenation and *n*-butane hydrogenolysis. The apparent activation energies for ethylene hydrogenation for catalysts on  $\gamma$ -Al<sub>2</sub>O<sub>3</sub>, MgO and TiO<sub>2</sub> were 8.4, 7.6 and 8.1 kcal/mol, while the apparent activation energies for *n*-butane hydrogenolysis were 30.9, 15.5 and 28.2 kcal/mol.

Supported PtRu catalysts prepared from Pt<sub>3</sub>Ru<sub>6</sub>(CO)<sub>21</sub>( $\mu$ <sub>3</sub>-H)( $\mu$ -H)<sub>3</sub> supported on  $\gamma$ -Al<sub>2</sub>O<sub>3</sub> and MgO were compared with those prepared from a mixture of Pt(acac)<sub>2</sub> and Ru(acac)<sub>3</sub>. Although this was the first report for supported PtRu catalysts prepared from Pt(acac)<sub>2</sub> and Ru(acac)<sub>3</sub>, the resulting materials did not contain any Pt-Ru bonds after treatment in H<sub>2</sub> flow at 300°C. The catalysts prepared from the mixture of organometallic precursors were also active for ethylene hydrogenation with similar range of apparent activation energies.

School of Chemistry

Academic Year 2004

Student's Signature.....

Advisor's Signature.....

Co-advisor's Signature.....

## **ACKNOWLEDGEMENTS**

I would like to express my gratefulness to all those who have helped me throughout my study. First and foremost, I would like to thank Asst. Prof. Dr. Jatuporn Wittayakun and Prof. Dr. Bruce C. Gates for their invaluable supervision, advice, kind guidance, and continual encouragement during my study. It has been a pleasure to work under their supervision. I would like to thank Assoc. Prof. Dr. Nurak Grisdanurak from Department of Chemical Engineering at the Thammasart University- Rungsit Campus. I would also like to thank all lecturers at the School of Chemistry, Suranaree University of Technology for their good attitude and advice.

I would like to thank Prof. Neil E. Schore at Department of Chemistry, University of California, Davis, for UV facility and kind guidance for organometallic synthesis and also thank the members of the Department of Chemical Engineering at the University of California, Davis.

Special thanks go to Stanford Synchrotron Radiation Laboratory (SSRL) at the Stanford Linear Accelerator Center (SLAC), Stanford, CA and Brookhaven National Laboratory (BNL) at the National Synchrotron Light Source (NSLS), Upton, NY for X-ray absorption experiment. The EXAFS data were processed by ATHENA software developed by Bruce Ravel and analyzed by EXAFSPAK software developed by Graham. N. George including FEFF7.0 developed by John J. Rehr and co-workers.

I would also like to thank all of my good friends in the Catalysis Research Group at the University of California, Davis, and the School of Chemistry, Suranaree University of Technology and other friends for their friendship and all the help they

have provided, especially Guzman, Stefan, Vinesh, Juan Carlos, Fen, Ann, Sailu, Netnapid, Narumol, Tipawan, Montra, Supaporn, Nuttinee and Kittipong.

I am grateful to the Ministry of University Affairs of the Thai Government for the full scholarship throughout my study. I also thank Suranaree University of Technology, Prince of Songkla University, Pattani campus and the University of California, Davis, for their support.

Finally, I want to thank my parents, my sister and my brother for their love and continual encouragement during my education.

Saowapa Chotisuwan

# CONTENTS

	<b>Page</b>
ABSTRACT IN THAI.....	I
ABSTRACT IN ENGLISH.....	III
ACKNOWLEDGEMENTS.....	V
CONTENTS.....	VII
LIST OF TABLES.....	XX
LIST OF FIGURES.....	XXII
LIST OF ABBREVIATIONS.....	XLVIII

## CHAPTER

### I GENERAL INTRODUCTION

1.1 Supported bimetallic catalysts.....	1
1.1.1 Preparation methods of supported bimetallic catalysts.....	2
1.1.2 Supported Pt catalysts incorporating with oxophillic metal.....	3
1.1.3 Supported Pt catalysts incorporating with noble metal.....	4
1.1.3.1 Supported PtRu catalyst prepared from two salts.....	4

## CONTENTS (CONTINUED)

	<b>Page</b>
1.1.3.2 Supported PtRu catalyst prepared from a molecular cluster .....	5
1.2 Catalyst characterization techniques.....	8
1.2.1 Temperature-programmed reductive decomposition (TPRD).....	8
1.2.2 Infrared (IR) spectroscopy.....	9
1.2.3 X-ray absorption spectroscopy.....	9
1.2.3.1 EXAFS spectroscopy.....	10
1.2.3.2 XANES spectroscopy.....	11
1.3 Catalytic activity test .....	11
1.3.1 Ethylene hydrogenation test.....	12
1.3.2 <i>n</i> -Butane hydrogenolysis test.....	13
1.4 Research objectives.....	14
1.5 Scope and limitations of study.....	15
<b>II CHARACTERIZATION AND TESTING OF Pt-Ru/<math>\gamma</math>-Al<sub>2</sub>O<sub>3</sub></b>	
<b>CATALYST PREPARED FROM Pt<sub>3</sub>Ru<sub>6</sub>(CO)<sub>21</sub>(<math>\mu</math><sub>3</sub>-H)(<math>\mu</math>-H)<sub>3</sub></b>	
2.1 Introduction.....	16
2.1.1 Supported Pt catalysts incorporating another noble metal on $\gamma$ -Al <sub>2</sub> O <sub>3</sub> .....	17
2.1.2 $\gamma$ -Al <sub>2</sub> O <sub>3</sub> -supported Pt-Ru catalysts.....	17

## CONTENTS (CONTINUED)

	<b>Page</b>
2.1.3 Research goals.....	18
2.2 Experimental.....	18
2.2.1 Chemicals and materials.....	18
2.2.2 Synthesis of organometallic precursor.....	19
2.2.2.1 Synthesis of starting material, Pt <sub>2</sub> Ru <sub>4</sub> (CO) <sub>18</sub>	19
2.2.2.2 Synthesis of Pt <sub>3</sub> Ru <sub>6</sub> (CO) <sub>21</sub> (μ <sub>3</sub> -H)(μ-H) <sub>3</sub> .....	20
2.2.3 Preparation of supported catalyst.....	21
2.2.4 Extraction of adsorbed species.....	21
2.2.5 PtRu catalyst activation.....	22
2.2.6 Precursor and catalyst characterization.....	22
2.2.6.1 IR spectroscopy.....	22
2.2.6.2 <sup>1</sup> H, and <sup>13</sup> C NMR spectroscopy.....	22
2.2.6.3 EXAFS spectroscopy.....	23
2.2.7 EXAFS data analysis.....	23
2.2.8 Catalytic activity of PtRu/γ-Al <sub>2</sub> O <sub>3</sub> for ethylene hydrogenation.....	24
2.2.9 Catalytic activity of PtRu/γ-Al <sub>2</sub> O <sub>3</sub> for <i>n</i> -butane hydrogenolysis.....	25
2.3 Results and discussion.....	26
2.3.1 Characterization of Pt <sub>3</sub> Ru <sub>6</sub> (CO) <sub>21</sub> (μ <sub>3</sub> -H)(μ-H) <sub>3</sub> .....	26

## CONTENTS (CONTINUED)

	<b>Page</b>
2.3.2 IR and EXAFS evidence of interactions between cluster precursor and $\gamma$ -Al <sub>2</sub> O <sub>3</sub> .....	28
2.3.3 Structural changes of metal framework after adsorption.....	42
2.3.4 Stability of metal framework in supported sample after ligand removal.....	43
2.3.5 High dispersion of bimetallic particles on supported sample after ligand removal.....	51
2.3.6 Effect of strong Pt-Ru interactions on ethylene hydrogenation.....	52
2.3.6.1 Catalytic activity and time on stream (TOS)..	52
2.3.6.2 Kinetics of ethylene hydrogenation catalyzed by PtRu/ $\gamma$ -Al <sub>2</sub> O <sub>3</sub> .....	55
2.3.6.3 Rate expression for ethylene hydrogenation catalyzed by PtRu/ $\gamma$ -Al <sub>2</sub> O <sub>3</sub> .....	57
2.3.6.4 IR during ethylene hydrogenation catalyzed by PtRu/ $\gamma$ -Al <sub>2</sub> O <sub>3</sub> .....	63
2.3.7 Effect of strong Pt-Ru interactions on <i>n</i> -butane hydrogenolysis.....	67
2.3.7.1 Catalytic activity and TOS.....	67

## CONTENTS (CONTINUED)

	<b>Page</b>
2.3.7.2 Apparent activation energy of <i>n</i> -butane hydrogenolysis catalyzed by PtRu/ $\gamma$ -Al <sub>2</sub> O <sub>3</sub> ....	71
2.3.7.3 Evidence of catalyst deactivation at high reaction temperature.....	73
2.4 Conclusions.....	73
<b>III EXAFS CHARACTERATION AND CATALYTIC ACTIVITY OF Pt-Ru/MgO CATALYST PREPARED FROM Pt<sub>3</sub>Ru<sub>6</sub>(CO)<sub>21</sub>(<math>\mu</math><sub>3</sub>-H)(<math>\mu</math>-H)<sub>3</sub></b>	
3.1 Background of MgO, metal supported on MgO and objectives.....	75
3.1.1 Nature of MgO.....	75
3.1.2 MgO-supported Pt catalysts incorporating second metal.....	76
3.1.3 Research goals.....	76
3.2 Experimental.....	77
3.2.1 Chemicals and materials.....	77
3.2.2 Synthesis of organometallic precursor.....	77
3.2.3 Preparation of supported catalyst.....	78
3.2.4 Extraction of adsorbed species on MgO.....	78
3.2.5 PtRu catalyst activation.....	78

## CONTENTS (CONTINUED)

	<b>Page</b>
3.2.6 Characterization techniques.....	78
3.2.6.1 IR spectroscopy.....	78
3.2.6.2 EXAFS spectroscopy.....	79
3.2.7 EXAFS data analysis.....	79
3.2.8 Catalytic activity of PtRu/MgO for ethylene hydrogenation.....	80
3.2.9 Catalytic activity of PtRu/MgO for <i>n</i> -butane hydrogenolysis.....	81
3.3 Results and discussion .....	81
3.3.1 IR evidence of interaction between cluster precursor and MgO.....	81
3.3.2 Strong interaction between cluster precursor and MgO.....	84
3.3.3 EXAFS evidence for structural changes of adsorbed precursor on MgO.....	85
3.3.4 Pt-Ru interaction in supported sample after ligand removal.....	93
3.3.5 Effect of chemistry of support on cluster-support interaction.....	100
3.3.6 Effect of Pt-Ru interactions on ethylene hydrogenation.....	101

**CONTENTS (CONTINUED)**

	<b>Page</b>
3.3.6.1 Catalytic activity and time on stream (TOS)..	101
3.3.6.2 Kinetics of ethylene hydrogenation catalyzed by PtRu/MgO.....	103
3.3.6.3 Rate expression for ethylene hydrogenation catalyzed by PtRu/MgO.....	105
3.3.6.4 Change of IR spectrum during ethylene hydrogenation catalyzed by PtRu/MgO.....	110
3.3.7 Effect of Pt-Ru interactions on <i>n</i> -butane hydrogenolysis catalyzed by PtRu/MgO.....	114
3.3.7.1 Catalytic activity and TOS.....	114
3.3.7.2 Apparent activation energy of <i>n</i> -butane hydrogenolysis catalyzed by PtRu/MgO.....	118
3.3.7.3 Evidence of catalyst deactivation at high reaction temperature.....	120
3.4 Conclusions.....	120
 <b>IV CHARACTERIZATION AND CATALYTIC ACTIVITY OF Pt-Ru/TiO<sub>2</sub> CATALYST PREPARED FROM Pt<sub>3</sub>Ru<sub>6</sub>(CO)<sub>21</sub>(μ<sub>3</sub>-H)(μ-H)<sub>3</sub></b>	
4.1 Introduction.....	122

## CONTENTS (CONTINUED)

	<b>Page</b>
4.1.1 Supported Pt catalysts incorporating second metal on TiO <sub>2</sub> .....	122
4.1.2 Research goals.....	123
4.2 Experimental.....	123
4.2.1 Chemicals and materials.....	123
4.2.2 Synthesis of organometallic precursor.....	124
4.2.3 Preparation of supported catalyst.....	124
4.2.4 Extraction of adsorbed species on TiO <sub>2</sub> .....	124
4.2.5 PtRu catalyst activation.....	125
4.2.6 Characterization techniques.....	125
4.2.6.1 IR spectroscopy.....	125
4.2.6.2 EXAFS spectroscopy.....	125
4.2.7 EXAFS data analysis.....	125
4.2.8 Catalytic activity of PtRu/TiO <sub>2</sub> for ethylene hydrogenation.....	127
4.2.9 Catalytic activity of PtRu/TiO <sub>2</sub> for <i>n</i> -butane hydrogenolysis.....	127
4.3 Results and discussion.....	128
4.3.1 IR evidence of interaction between adsorbed precursor and TiO <sub>2</sub> surface.....	128

## CONTENTS (CONTINUED)

	<b>Page</b>
4.3.2 Strong interaction between cluster precursor and TiO <sub>2</sub> .....	131
4.3.3 EXAFS evidence of structural changes of adsorbed precursor on TiO <sub>2</sub> .....	134
4.3.4 EXAFS evidence of Pt-Ru contribution after ligand removal.....	143
4.3.5 Effect of chemistry of support on cluster-support interaction.....	149
4.3.6 Catalytic activity of ethylene hydrogenation catalyzed by PtRu/TiO <sub>2</sub> .....	150
4.3.6.1 Catalytic activity and time on stream (TOS)..	150
4.3.6.2 Kinetics of ethylene hydrogenation catalyzed by PtRu/TiO <sub>2</sub> .....	152
4.3.6.3 Rate expression for ethylene hydrogenation catalyzed by PtRu/TiO <sub>2</sub> .....	154
4.3.7 Catalytic activity of <i>n</i> -butane hydrogenolysis catalyzed by PtRu/TiO <sub>2</sub> .....	160
4.3.7.1 Catalytic activity and TOS.....	160
4.3.7.2 Apparent activation energy of <i>n</i> -butane hydrogenolysis catalyzed by PtRu/TiO <sub>2</sub> .....	165

## CONTENTS (CONTINUED)

	<b>Page</b>
4.3.7.3 Evidence of catalyst deactivation at high reaction temperature.....	166
4.4 Conclusions.....	167
<b>V SUPPORTED Pt-Ru CATALYSTS PREPARED FROM A MIXTURE OF PLATINUM AND RUTHENIUM ACETYLACETONATE AND ACTIVITIES FOR ETHYLENE HYDROGENATION</b>	
5.1 Introduction.....	169
5.1.1 Supported Pt and Ru catalysts prepared from acetylacetonate complexes.....	170
5.1.2 Research goals.....	171
5.2 Experimental.....	171
5.2.1 Chemicals and materials.....	171
5.2.2 Preparation of supported Pt-Ru catalysts from a mixture solution of Pt(acac) <sub>2</sub> and Ru(acac) <sub>3</sub> .....	172
5.2.3 PtRu catalyst activation.....	172
5.2.4 Characterization techniques.....	172
5.2.4.1 IR spectroscopy.....	172
5.2.4.2 Temperature-programmed reductive decomposition (TPRD).....	173

**CONTENTS (CONTINUED)**

	<b>Page</b>
5.2.4.3 XANES spectroscopy.....	173
5.2.4.4 EXAFS spectroscopy.....	174
5.2.5 EXAFS data analysis .....	174
5.2.6 Catalytic activity of ethylene hydrogenation of supported PtRu catalysts prepared from a mixture of Pt(acac) <sub>2</sub> and Ru(acac) <sub>3</sub> .....	175
5.3 Results and discussion.....	176
5.3.1 IR evidence of interaction between precursors and support after adsorption.....	176
5.3.1.1 PtRu/ $\gamma$ -Al <sub>2</sub> O <sub>3</sub> catalyst prepared from a mixture of Pt(acac) <sub>2</sub> and Ru(acac) <sub>3</sub> .....	176
5.3.1.2 PtRu/MgO catalyst prepared from a mixture of Pt(acac) <sub>2</sub> and Ru(acac) <sub>3</sub> .....	179
5.3.2 TPRD of supported PtRu samples.....	182
5.3.2.1 TPRD of Pt(acac) <sub>2</sub> and/or Ru(acac) <sub>3</sub> supported on $\gamma$ -Al <sub>2</sub> O <sub>3</sub> .....	182
5.3.2.2 TPRD of Pt(acac) <sub>2</sub> and/or Ru(acac) <sub>3</sub> supported on MgO.....	184
5.3.3 XANES spectra of dry supported Pt(acac) <sub>2</sub> and Ru(acac) <sub>3</sub> on $\gamma$ -Al <sub>2</sub> O <sub>3</sub> .....	185
5.3.4 EXAFS spectroscopy results.....	187

**CONTENTS (CONTINUED)**

	<b>Page</b>
5.3.4.1 EXAFS evidence for PtRu/ $\gamma$ -Al <sub>2</sub> O <sub>3</sub> catalyst prepared from a mixture of Pt(acac) <sub>2</sub> and Ru(acac) <sub>3</sub> .....	187
5.3.4.2 EXAFS evidence for PtRu/MgO catalyst prepared from a mixture of Pt(acac) <sub>2</sub> and Ru(acac) <sub>3</sub> .....	193
5.3.5 Catalytic activity of ethylene hydrogenation catalyzed by PtRu/ $\gamma$ -Al <sub>2</sub> O <sub>3</sub> and PtRu/MgO prepared from a mixture of Pt(acac) <sub>2</sub> and Ru(acac) <sub>3</sub> .....	200
5.3.5.1 Time on stream (TOS) for ethylene hydrogenation catalyzed by PtRu/ $\gamma$ -Al <sub>2</sub> O <sub>3</sub> and PtRu/MgO prepared from a mixture of Pt(acac) <sub>2</sub> and Ru(acac) <sub>3</sub> .....	200
5.3.5.2 Apparent activation energy of ethylene hydrogenation catalyzed by PtRu/ $\gamma$ -Al <sub>2</sub> O <sub>3</sub> and PtRu/MgO prepared from a mixture solution of Pt(acac) <sub>2</sub> and Ru(acac) <sub>3</sub> .....	201
5.4 Conclusions.....	204
<b>VI CONCLUSIONS</b> .....	<b>206</b>

**CONTENTS (CONTINUED)**

	<b>Page</b>
REFERENCES.....	209
APPENDICES.....	226
Appendix A    SYNTHESIS AND CHARACTERIZATION OF Bis[1,2,5,6- $\eta$ -(1,5 CYCLOOCTADIENE)] PLATINUM.....	227
Appendix B    Article in proceeding of an oral presentation at the 10 <sup>th</sup> Asian Pacific Confederation of Chemical Engineering (APCChE) Congress 2004.....	231
Appendix C    Article in proceeding of an oral presentation at the 14 <sup>th</sup> Regional Symposium on Chemical Engineering (RSCE) 2004.....	240
CURRICULUM VITAE.....	247

## LIST OF TABLES

<b>Table</b>	<b>Page</b>
<b>2.1</b> Summary of EXAFS data of sample formed by adsorption of $\text{Pt}_3\text{Ru}_6(\text{CO})_{21}(\mu_3\text{-H})(\mu\text{-H})_3$ on $\gamma\text{-Al}_2\text{O}_3$ before ligand removal.....	35
<b>2.2</b> Comparison XRD data of crystalline $\text{Pt}_3\text{Ru}_6(\text{CO})_{21}(\mu_3\text{-H})(\mu\text{-H})_3$ (Adams et al., 1994) and EXAFS of this cluster adsorbed on $\gamma\text{-Al}_2\text{O}_3$ .....	41
<b>2.3</b> Summary of EXAFS data of $\text{PtRu}/\gamma\text{-Al}_2\text{O}_3$ prepared by decarbonylation of adsorbed $\text{Pt}_3\text{Ru}_6(\text{CO})_{21}(\mu_3\text{-H})(\mu\text{-H})_3$ on $\gamma\text{-Al}_2\text{O}_3$ .....	45
<b>2.4</b> Apparent activation energy of ethylene hydrogenation catalyzed by supported Pt, Ru and PtRu catalysts.....	56
<b>3.1</b> Summary of EXAFS data of sample formed by adsorption of $\text{Pt}_3\text{Ru}_6(\text{CO})_{21}(\mu_3\text{-H})(\mu\text{-H})_3$ on MgO before ligand removal.....	86
<b>3.2</b> Comparison XRD data of crystalline $\text{Pt}_3\text{Ru}_6(\text{CO})_{21}(\mu_3\text{-H})(\mu\text{-H})_3$ (Adams et al., 1994) and EXAFS of supported species formed from this cluster on MgO.....	92
<b>3.3</b> Summary of EXAFS data of sample prepared by adsorption of $\text{Pt}_3\text{Ru}_6(\text{CO})_{21}(\mu_3\text{-H})(\mu\text{-H})_3$ on MgO after ligand removal in He flow at 300°C for 2 h.....	94

## LIST OF TABLES (CONTINUED)

<b>Table</b>	<b>Page</b>
<b>4.1</b> Summary of EXAFS data of sample formed by adsorption of $\text{Pt}_3\text{Ru}_6(\text{CO})_{21}(\mu_3\text{-H})(\mu\text{-H})_3$ on $\text{TiO}_2$ before ligand removal.....	135
<b>4.2</b> Comparison XRD data of crystalline $\text{Pt}_3\text{Ru}_6(\text{CO})_{21}(\mu_3\text{-H})(\mu\text{-H})_3$ (Adams et al., 1994) and EXAFS of supported species formed from this cluster on $\text{TiO}_2$ .....	141
<b>4.3</b> Summary of EXAFS data of sample prepared by adsorption of $\text{Pt}_3\text{Ru}_6(\text{CO})_{21}(\mu_3\text{-H})(\mu\text{-H})_3$ on $\text{TiO}_2$ after ligand removal in He flow at 300°C for 2 h.....	144
<b>4.4</b> Rate expression of ethylene hydrogenation catalyzed by supported PtRu catalysts prepared from adsorption of $\text{Pt}_3\text{Ru}_6(\text{CO})_{21}(\mu_3\text{-H})(\mu\text{-H})_3$ on $\gamma\text{-Al}_2\text{O}_3$ , MgO and $\text{TiO}_2$ .....	160
<b>5.1</b> Summary of EXAFS data of PtRu/ $\gamma\text{-Al}_2\text{O}_3$ prepared from a mixture of $\text{Pt}(\text{acac})_2$ and $\text{Ru}(\text{acac})_3$ after ligand removal in $\text{H}_2$ flow at 300°C for 2 h	188
<b>5.2</b> Summary of EXAFS data of PtRu/MgO prepared from a mixture of $\text{Pt}(\text{acac})_2$ and $\text{Ru}(\text{acac})_3$ after ligand removal in $\text{H}_2$ flow at 300°C for 2 h	194
<b>5.3</b> Apparent activation energy for ethylene hydrogenation catalyzed by PtRu catalysts prepared from mixture solution of Pt and Ru compounds and ligand removal in $\text{H}_2$ flow at 300°C for 2 h.....	203

## LIST OF FIGURES

Figure	Page
1.1 Structure of crystalline $\text{Pt}_3\text{Ru}_6(\text{CO})_{21}(\mu_3\text{-H})(\mu\text{-H})_3$ (reproduced from Adams, Barnard et al., 1994 by Weblab ViewerPro software).....	7
1.2 Absorption of X-ray as a function of photon energy $E=h\nu$ by atoms in a lattice (a) and the fine structure represents the EXAFS function and energy at near edge absorption representing XANES (b).....	10
1.3 The three surface structures of adsorbed ethylene on metal surface: (a) $\pi$ -bonded ethylene; (b) di- $\sigma$ -bonded ethylene; and (c) ethylidyne.....	13
1.4 Proposed mechanisms of <i>n</i> -butane hydrogenolysis reaction.....	14
1.5 Proposed mechanisms of <i>n</i> -butane isomerization reaction.....	14
2.1 IR spectrum of $\text{Pt}_3\text{Ru}_6(\text{CO})_{21}(\mu_3\text{-H})(\mu\text{-H})_3$ dissolved in $\text{CH}_2\text{Cl}_2$ .....	26
2.2 $^1\text{H}$ NMR spectrum of $\text{Pt}_3\text{Ru}_6(\text{CO})_{21}(\mu_3\text{-H})(\mu\text{-H})_3$ dissolved in acetone- $\text{d}_6$ recorded at $-88^\circ\text{C}$ : (A) $\delta = 15$ to $17$ ppm; (B) $\delta = -18$ to $-20$ ppm.....	27
2.3 $^{13}\text{C}$ NMR spectrum of $\text{Pt}_3\text{Ru}_6(\text{CO})_{21}(\mu_3\text{-H})(\mu\text{-H})_3$ dissolved in acetone- $\text{d}_6$ recorded at $20^\circ\text{C}$ .....	27

## LIST OF FIGURES (CONTINUED)

Figure	Page
<p><b>2.4</b> (A) IR spectrum in <math>\nu_{\text{OH}}</math> region: (1) Calcined <math>\gamma\text{-Al}_2\text{O}_3</math>; (2) dry sample prepared from <math>\text{Pt}_3\text{Ru}_6(\text{CO})_{21}(\mu_3\text{-H})(\mu\text{-H})_3</math> on <math>\gamma\text{-Al}_2\text{O}_3</math>; (3) sample after ligand removal in He flow at <math>300^\circ\text{C}</math> for 2 h. (B) Infrared in <math>\nu_{\text{CO}}</math> regions: (1) <math>\text{Pt}_3\text{Ru}_6(\text{CO})_{21}(\mu_3\text{-H})(\mu\text{-H})_3</math> adsorbed on <math>\gamma\text{-Al}_2\text{O}_3</math> after removal of solvent; (2) dry supported sample after extracted with <math>\text{CH}_2\text{Cl}_2</math>; (3) sample after ligand removal in He flow at <math>300^\circ\text{C}</math> for 2 h.....</p>	29
<p><b>2.5</b> IR spectrum in <math>\nu_{\text{CO}}</math> region of <math>\text{CH}_2\text{Cl}_2</math> extract solution from the supported sample .....</p>	32
<p><b>2.6</b> EXAFS results scanned at the Pt <math>L_{\text{III}}</math> edge characterizing the adsorbed <math>\text{Pt}_3\text{Ru}_6(\text{CO})_{21}(\mu_3\text{-H})(\mu\text{-H})_3</math> on <math>\gamma\text{-Al}_2\text{O}_3</math>: (A) Experimental EXAFS function (solid line) and sum of the calculated Pt-Pt, Pt-Ru, Pt-C, Pt-O*, Pt-O<sub>s</sub>, and Pt-O<sub>l</sub> contributions (dotted line). (B) Magnitude of uncorrected Fourier transform (<math>k^0</math> weighted) of experimental EXAFS function (solid line) and sum of the calculated Pt-Pt, Pt-Ru, Pt-C, Pt-O*, Pt-O<sub>s</sub>, and Pt-O<sub>l</sub> contributions (dotted line).....</p>	36

## LIST OF FIGURES (CONTINUED)

Figure	Page
<p><b>2.6</b> (continued) EXAFS results scanned at the Pt L<sub>III</sub> edge characterizing the adsorbed Pt<sub>3</sub>Ru<sub>6</sub>(CO)<sub>21</sub>(μ<sub>3</sub>-H)(μ-H)<sub>3</sub> on γ-Al<sub>2</sub>O<sub>3</sub>: (C) Magnitude of uncorrected Fourier transform (<math>k^1</math> weighted) of experimental EXAFS function (solid line) and sum of the calculated Pt-Pt, Pt-Ru, Pt-C, Pt-O*, Pt-O<sub>s</sub>, and Pt-O<sub>1</sub> contributions (dotted line). (D) Magnitude of uncorrected Fourier transform (<math>k^3</math> weighted) of experimental EXAFS function (solid line) and sum of the calculated Pt-Pt, Pt-Ru, Pt-C, Pt-O*, Pt-O<sub>s</sub>, and Pt-O<sub>1</sub> contributions (dotted line).....</p>	37
<p><b>2.7</b> EXAFS results scanned at the Ru K edge characterizing adsorbed Pt<sub>3</sub>Ru<sub>6</sub>(CO)<sub>21</sub>(μ<sub>3</sub>-H)(μ-H)<sub>3</sub> on γ-Al<sub>2</sub>O<sub>3</sub>: (A) Experimental EXAFS function (solid line) and sum of the calculated Ru-Ru, Ru-Pt, Ru-C, Ru-O*, Ru-O<sub>s</sub>, and Ru-O<sub>1</sub> contributions (dotted line). (B) Magnitude of uncorrected Fourier transform (<math>k^0</math> weighted) of experimental EXAFS function (solid line) and sum of the calculated Ru-Ru, Ru-Pt, Ru-C, Ru-O*, Ru-O<sub>s</sub>, and Ru-O<sub>1</sub> contributions (dotted line).....</p>	38

## LIST OF FIGURES (CONTINUED)

Figure	Page
<p><b>2.7</b> (continued) EXAFS results scanned at the Ru K edge characterizing the adsorbed <math>\text{Pt}_3\text{Ru}_6(\text{CO})_{21}(\mu_3\text{-H})(\mu\text{-H})_3</math> on <math>\gamma\text{-Al}_2\text{O}_3</math>: (C) Magnitude of uncorrected Fourier transform (<math>k^1</math> weighted) of experimental EXAFS function (solid line) and sum of the calculated Ru-Ru, Ru-Pt, Ru-C, Ru-O*, Ru-O<sub>s</sub>, and Ru-O<sub>l</sub> contributions (dotted line). (D) Magnitude of uncorrected Fourier transform (<math>k^3</math> weighted) of experimental EXAFS function (solid line) and sum of the calculated Ru-Ru, Ru-Pt, Ru-C, Ru-O*, Ru-O<sub>s</sub>, and Ru-O<sub>l</sub> contributions (dotted line).....</p>	39
<p><b>2.8</b> EXAFS results scanned at the Pt L<sub>III</sub> edge characterizing the PtRu/<math>\gamma\text{-Al}_2\text{O}_3</math> sample prepared by adsorption of <math>\text{Pt}_3\text{Ru}_6(\text{CO})_{21}(\mu_3\text{-H})(\mu\text{-H})_3</math> after ligand removal: (A) Experimental EXAFS function (solid line) and sum of the calculated Pt-Pt, Pt-Ru, Pt-C, Pt-O*, Pt-O<sub>s</sub>, and Pt-O<sub>l</sub> contributions (dotted line). (B) Magnitude of uncorrected Fourier transform (<math>k^0</math> weighted) of experimental EXAFS function (solid line) and sum of the calculated Pt-Pt, Pt-Ru, Pt-C, Pt-O*, Pt-O<sub>s</sub>, and Pt-O<sub>l</sub> contributions (dotted line).....</p>	46

## LIST OF FIGURES (CONTINUED)

Figure	Page
<p><b>2.8</b> (continued) EXAFS results scanned at the Pt L<sub>III</sub> edge characterizing the PtRu/<math>\gamma</math>-Al<sub>2</sub>O<sub>3</sub> sample prepared by adsorption of Pt<sub>3</sub>Ru<sub>6</sub>(CO)<sub>21</sub>(<math>\mu_3</math>-H)(<math>\mu</math>-H)<sub>3</sub> after ligand removal: (C) Magnitude of uncorrected Fourier transform (<math>k^1</math> weighted) of experimental EXAFS function (solid line) and sum of the calculated Pt-Pt, Pt-Ru, Pt-C, Pt-O*, Pt-O<sub>s</sub>, and Pt-O<sub>l</sub> contributions (dotted line). (D) Magnitude of uncorrected Fourier transform (<math>k^3</math> weighted) of experimental EXAFS function (solid line) and sum of the calculated Pt-Pt, Pt-Ru, Pt-C, Pt-O*, Pt-O<sub>s</sub>, and Pt-O<sub>l</sub> contributions (dotted line).....</p>	47
<p><b>2.9</b> EXAFS results scanned at the Ru K edge characterizing the PtRu/<math>\gamma</math>-Al<sub>2</sub>O<sub>3</sub> sample prepared by adsorption of Pt<sub>3</sub>Ru<sub>6</sub>(CO)<sub>21</sub>(<math>\mu_3</math>-H)(<math>\mu</math>-H)<sub>3</sub> after ligand removal: (A) Experimental EXAFS function (solid line) and sum of the calculated Ru-Ru, Ru-Pt, Ru-C, Ru-O*, Ru-O<sub>s</sub>, and Ru-O<sub>l</sub> contributions (dotted line). (B) Magnitude of uncorrected Fourier transform (<math>k^0</math> weighted) of experimental EXAFS function (solid line) and sum of the calculated Ru-Ru, Ru-Pt, Ru-C, Ru-O*, Ru-O<sub>s</sub>, and Ru-O<sub>l</sub> contributions (dotted line).....</p>	48

## LIST OF FIGURES (CONTINUED)

Figure	Page
<p><b>2.9</b> (continued) EXAFS results scanned at the Ru K edge characterizing the PtRu/<math>\gamma</math>-Al<sub>2</sub>O<sub>3</sub> sample prepared by adsorption of Pt<sub>3</sub>Ru<sub>6</sub>(CO)<sub>21</sub>(<math>\mu_3</math>-H)(<math>\mu</math>-H)<sub>3</sub> after ligand removal: (C) Magnitude of uncorrected Fourier transform (<math>k^1</math> weighted) of experimental EXAFS function (solid line) and sum of the calculated Ru-Ru, Ru-Pt, Ru-C, Ru-O*, Ru-O<sub>s</sub>, and Ru-O<sub>l</sub> contributions (dotted line). (D) Magnitude of uncorrected Fourier transform (<math>k^3</math> weighted) of experimental EXAFS function (solid line) and sum of the calculated Ru-Ru, Ru-Pt, Ru-C, Ru-O*, Ru-O<sub>s</sub>, and Ru-O<sub>l</sub> contributions (dotted line).....</p>	49
<p><b>2.10</b> Demonstration of differential reactor operation at -75°C, <math>P_{C_2H_4} = 40</math> Torr, <math>P_{H_2} = 80</math> Torr, balanced with He, total feed flow rate = 200 ml (NTP)/min catalyzed by PtRu/<math>\gamma</math>-Al<sub>2</sub>O<sub>3</sub>.....</p>	53
<p><b>2.11</b> Activity of ethylene hydrogenation with time on stream (TOS) catalyzed by PtRu/<math>\gamma</math>-Al<sub>2</sub>O<sub>3</sub> at reaction condition: <math>P_{C_2H_4} = 40</math> Torr, <math>P_{H_2} = 80</math> Torr, balanced He with total feed flow rate 200 ml (NTP)/min, catalyst mass 0.013 mg, and temperature -75°C.....</p>	54
<p><b>2.12</b> Arrhenius plot for ethylene hydrogenation catalyzed by PtRu/<math>\gamma</math>-Al<sub>2</sub>O<sub>3</sub> at condition: <math>P_{C_2H_4} = 40</math> Torr, <math>P_{H_2} = 80</math> Torr, balanced with He, total feed flow rate = 200 ml (NTP)/min, catalyst mass 0.013 g.....</p>	55

## LIST OF FIGURES (CONTINUED)

<b>Figure</b>	<b>Page</b>
<b>2.13</b> Effect of hydrogen pressure on ethylene hydrogenation catalyzed by PtRu/ $\gamma$ -Al <sub>2</sub> O <sub>3</sub> at 40 Torr ethylene.....	58
<b>2.14</b> The plot between TOF in a natural log scale as a function of hydrogen pressure in a natural log scale for ethylene hydrogenation catalyzed by PtRu/ $\gamma$ -Al <sub>2</sub> O <sub>3</sub> at 40 Torr ethylene and 80 to 200 Torr hydrogen.....	59
<b>2.15</b> Effect of ethylene pressure on ethylene hydrogenation catalyzed by PtRu/ $\gamma$ -Al <sub>2</sub> O <sub>3</sub> at 80 Torr hydrogen.....	60
<b>2.16</b> The plot in a natural log scale between TOF and ethylene pressure for ethylene hydrogenation catalyzed by PtRu/ $\gamma$ -Al <sub>2</sub> O <sub>3</sub> at -75°C, 80 Torr hydrogen and 80 to 200 Torr ethylene.....	61
<b>2.17</b> Proposed mechanism for ethylene hydrogenation on Pt (111) and Rh (111) (reproduced from Hwang et al., 2003).....	63
<b>2.18</b> IR spectra during ethylene flow over PtRu/ $\gamma$ -Al <sub>2</sub> O <sub>3</sub> at 30°C in the IR ranges of (A) 2700-3700 cm <sup>-1</sup> ; and (B) 2200-1000 cm <sup>-1</sup> at ethylene pressure (1) 20 Torr; (2) 40 Torr; (3) 80 Torr; (4) 120 Torr; 150 Torr; and 200 Torr.....	65

## LIST OF FIGURES (CONTINUED)

Figure	Page
<p><b>2.19</b> IR spectra during catalysis of ethylene hydrogenation in a flow reactor at 30°C catalyzed by PtRu/<math>\gamma</math>-Al<sub>2</sub>O<sub>3</sub> in IR ranges of 2700-3500 cm<sup>-1</sup> and (B) 1300-2100 cm<sup>-1</sup> at condition (1) flowing He; (2) He with 40 Torr C<sub>2</sub>H<sub>4</sub>; (3) He, 40 Torr C<sub>2</sub>H<sub>4</sub> and 80 Torr H<sub>2</sub>; (4) at 120 s after flowing He, 40 Torr C<sub>2</sub>H<sub>4</sub> and 80 Torr H<sub>2</sub>; (5) purging with He after reaction.....</p>	66
<p><b>2.20</b> Demonstration of differential reactor operation at 220°C, <math>P_{\text{H}_2} = 540</math> Torr, <math>P_{n\text{-C}_4\text{H}_{10}} = 60</math> Torr with 100 ml (NTP)/min flow rate catalyzed by PtRu/<math>\gamma</math>-Al<sub>2</sub>O<sub>3</sub>.....</p>	68
<p><b>2.21</b> Selectivity varied with inv. WHSV for ethylene hydrogenation at 220°C, <math>P_{\text{H}_2} = 540</math> Torr, <math>P_{n\text{-C}_4\text{H}_{10}} = 60</math> Torr with 100 ml (NTP)/min flow rate catalyzed by PtRu/<math>\gamma</math>-Al<sub>2</sub>O<sub>3</sub>.....</p>	68
<p><b>2.22</b> Activity varied with time on stream (TOS) for <i>n</i>-butane hydrogenolysis catalyzed by PtRu/<math>\gamma</math>-Al<sub>2</sub>O<sub>3</sub>.....</p>	69
<p><b>2.23</b> Selectivity varied with reaction temperature of <i>n</i>-butane hydrogenolysis catalyzed by PtRu/<math>\gamma</math>-Al<sub>2</sub>O<sub>3</sub>.....</p>	70
<p><b>2.24</b> Arrhenius plot of <i>n</i>-butane hydrogenolysis catalyzed by PtRu/<math>\gamma</math>-Al<sub>2</sub>O<sub>3</sub>...</p>	71
<p><b>3.1</b> IR spectrum in <math>\nu_{\text{OH}}</math> region: (1) Calcined MgO; (2) dry sample prepared from Pt<sub>3</sub>Ru<sub>6</sub>(CO)<sub>21</sub>(<math>\mu_3</math>-H)(<math>\mu</math>-H)<sub>3</sub> on MgO.....</p>	82

## LIST OF FIGURES (CONTINUED)

Figure	Page
<p><b>3.2</b> IR spectrum in <math>\nu_{\text{CO}}</math> regions: (1) Dry sample prepared from <math>\text{Pt}_3\text{Ru}_6(\text{CO})_{21}(\mu_3\text{-H})(\mu\text{-H})_3</math> on MgO; (2) dry supported sample after extraction with <math>\text{CH}_2\text{Cl}_2</math>; (3) sample after ligand removal in He flow at <math>300^\circ\text{C}</math> for 2 h; (4) calcined MgO.....</p>	83
<p><b>3.3</b> EXAFS results scanned at the Pt <math>L_{\text{III}}</math> edge characterizing the adsorbed <math>\text{Pt}_3\text{Ru}_6(\text{CO})_{21}(\mu_3\text{-H})(\mu\text{-H})_3</math> on MgO: (A) Experimental EXAFS function (solid line) and sum of the calculated Pt-Pt, Pt-Ru, Pt-C, Pt-O*, Pt-O<sub>s</sub>, and Pt-O<sub>l</sub> contributions (dotted line). (B) Magnitude of uncorrected Fourier transform (<math>k^0</math> weighted) of experimental EXAFS function (solid line) and sum of the calculated Pt-Pt, Pt-Ru, Pt-C, Pt-O*, Pt-O<sub>s</sub>, and Pt-O<sub>l</sub> contributions (dotted line).....</p>	87
<p><b>3.3</b> (continued) EXAFS results scanned at the Pt <math>L_{\text{III}}</math> edge characterizing the adsorbed <math>\text{Pt}_3\text{Ru}_6(\text{CO})_{21}(\mu_3\text{-H})(\mu\text{-H})_3</math> on MgO: (C) Magnitude of uncorrected Fourier transform (<math>k^1</math> weighted) of experimental EXAFS function (solid line) and sum of the calculated Pt-Pt, Pt-Ru, Pt-C, Pt-O*, Pt-O<sub>s</sub>, and Pt-O<sub>l</sub> contributions (dotted line). (D) Magnitude of uncorrected Fourier transform (<math>k^3</math> weighted) of experimental EXAFS function (solid line) and sum of the calculated Pt-Pt, Pt-Ru, Pt-C, Pt-O*, Pt-O<sub>s</sub>, and Pt-O<sub>l</sub> contributions (dotted line).....</p>	88

## LIST OF FIGURES (CONTINUED)

Figure	Page
<p><b>3.4</b> EXAFS results scanned at the Ru K edge characterizing the adsorbed <math>\text{Pt}_3\text{Ru}_6(\text{CO})_{21}(\mu_3\text{-H})(\mu\text{-H})_3</math> on MgO: (A) Experimental EXAFS function (solid line) and sum of the calculated Ru-Ru, Ru-Pt, Ru-C, Ru-O*, Ru-O<sub>s</sub>, and Ru-O<sub>l</sub> contributions (dotted line). (B) Magnitude of uncorrected Fourier transform (<math>k^0</math> weighted) of experimental EXAFS function (solid line) and sum of the calculated Ru-Ru, Ru-Pt, Ru-C, Ru-O*, Ru-O<sub>s</sub>, and Ru-O<sub>l</sub> contributions (dotted line).....</p>	89
<p><b>3.4</b> (continued) EXAFS results scanned at Ru K edge characterizing the adsorbed <math>\text{Pt}_3\text{Ru}_6(\text{CO})_{21}(\mu_3\text{-H})(\mu\text{-H})_3</math> on MgO: (C) Magnitude of uncorrected Fourier transform (<math>k^1</math> weighted) of experimental EXAFS function (solid line) and sum of the calculated Ru-Ru, Ru-Pt, Ru-C, Ru-O*, Ru-O<sub>s</sub>, and Ru-O<sub>l</sub> contributions (dotted line). (D) Magnitude of uncorrected Fourier transform (<math>k^3</math> weighted) of experimental EXAFS function (solid line) and sum of the calculated Ru-Ru, Ru-Pt, Ru-C, Ru-O*, Ru-O<sub>s</sub>, and Ru-O<sub>l</sub> contributions (dotted line).....</p>	90

## LIST OF FIGURES (CONTINUED)

Figure	Page
<p><b>3.5</b> EXAFS results scanned at the Pt L<sub>III</sub> edge characterizing the PtRu/MgO sample prepared by adsorption of Pt<sub>3</sub>Ru<sub>6</sub>(CO)<sub>21</sub>(μ<sub>3</sub>-H)(μ-H)<sub>3</sub> after ligand removal: (A) Experimental EXAFS function (solid line) and sum of the calculated Pt-Pt, Pt-Ru, Pt-C, Pt-O*, Pt-O<sub>s</sub>, and Pt-O<sub>l</sub> contributions (dotted line). (B) Magnitude of uncorrected Fourier transform (<math>k^0</math> weighted) of experimental EXAFS function (solid line) and sum of the calculated Pt-Pt, Pt-Ru, Pt-C, Pt-O*, Pt-O<sub>s</sub>, and Pt-O<sub>l</sub> contributions (dotted line).....</p>	95
<p><b>3.5</b> (continued) EXAFS results scanned at the Pt L<sub>III</sub> edge characterizing the PtRu/MgO sample prepared by adsorption of Pt<sub>3</sub>Ru<sub>6</sub>(CO)<sub>21</sub>(μ<sub>3</sub>-H)(μ-H)<sub>3</sub> after ligand removal: (C) Magnitude of uncorrected Fourier transform (<math>k^1</math> weighted) of experimental EXAFS function (solid line) and sum of the calculated Pt-Pt, Pt-Ru, Pt-C, Pt-O*, Pt-O<sub>s</sub>, and Pt-O<sub>l</sub> contributions (dotted line). (D) Magnitude of uncorrected Fourier transform (<math>k^3</math> weighted) of experimental EXAFS function (solid line) and sum of the calculated Pt-Pt, Pt-Ru, Pt-C, Pt-O*, Pt-O<sub>s</sub>, and Pt-O<sub>l</sub> contributions (dotted line).....</p>	96

## LIST OF FIGURES (CONTINUED)

Figure	Page
<p><b>3.6</b> EXAFS results scanned at the Ru K edge characterizing the PtRu/MgO sample prepared by adsorption of <math>\text{Pt}_3\text{Ru}_6(\text{CO})_{21}(\mu_3\text{-H})(\mu\text{-H})_3</math> after ligand removal: (A) Experimental EXAFS function (solid line) and sum of the calculated Ru-Ru, Ru-Pt, Ru-C, Ru-O*, Ru-O<sub>s</sub>, and Ru-O<sub>l</sub> contributions (dotted line). (B) Magnitude of uncorrected Fourier transform (<math>k^0</math> weighted) of experimental EXAFS function (solid line) and sum of the calculated Ru-Ru, Ru-Pt, Ru-C, Ru-O*, Ru-O<sub>s</sub>, and Ru-O<sub>l</sub> contributions (dotted line).....</p>	97
<p><b>3.6</b> (continued) EXAFS results scanned at the Ru K edge characterizing the PtRu/MgO sample prepared by adsorption of <math>\text{Pt}_3\text{Ru}_6(\text{CO})_{21}(\mu_3\text{-H})(\mu\text{-H})_3</math> after ligand removal: (C) Magnitude of uncorrected Fourier transform (<math>k^1</math> weighted) of experimental EXAFS function (solid line) and sum of the calculated Ru-Ru, Ru-Pt, Ru-C, Ru-O*, Ru-O<sub>s</sub>, and Ru-O<sub>l</sub> contributions (dotted line). (D) Magnitude of uncorrected Fourier transform (<math>k^3</math> weighted) of experimental EXAFS function (solid line) and sum of the calculated Ru-Ru, Ru-Pt, Ru-C, Ru-O*, Ru-O<sub>s</sub>, and Ru-O<sub>l</sub> contributions (dotted line).....</p>	98
<p><b>3.7</b> Demonstration of differential reactor operation at <math>-75^\circ\text{C}</math>, <math>P_{\text{C}_2\text{H}_4} = 40</math> Torr, <math>P_{\text{H}_2} = 80</math> Torr, balanced with He, total feed flow rate = 200 ml (NTP)/min catalyzed by PtRu/MgO.....</p>	101

## LIST OF FIGURES (CONTINUED)

Figure	Page
<b>3.8</b> Activity plot with TOS of ethylene hydrogenation catalyzed by PtRu/MgO at reaction condition: $P_{C_2H_4} = 40$ Torr, $P_{H_2} = 80$ Torr, balanced He with total feed flow rate 200 ml (NTP)/min, catalyst mass 0.012 mg, and temperature $-75^\circ\text{C}$ .....	102
<b>3.9</b> Stainless steel U-tube reactor cooling with liquid nitrogen.....	103
<b>3.10</b> Arrhenius plot of ethylene hydrogenation catalyzed by PtRu/MgO at reaction condition: $P_{C_2H_4} = 40$ Torr, $P_{H_2} = 80$ Torr, balanced He with total feed flow rate 200 ml (NTP)/min, catalyst mass 0.012 g.....	104
<b>3.11</b> Effect of pressure of hydrogen on ethylene hydrogenation catalyzed by PtRu/MgO.....	106
<b>3.12</b> The plot in a natural log scale between TOF and pressure of hydrogen for ethylene hydrogenation catalyzed by PtRu/MgO at $-75^\circ\text{C}$ , 40 Torr ethylene and 80 to 200 Torr hydrogen.....	107
<b>3.13</b> Effect of pressure of ethylene on ethylene hydrogenation catalyzed by PtRu/MgO.....	108
<b>3.14</b> The plot in a natural log scale between TOF and pressure of ethylene for ethylene hydrogenation catalyzed by PtRu/MgO at $-75^\circ\text{C}$ , 80 Torr hydrogen and ( $\blacktriangle$ ) 20 to 40 Torr ethylene; and ( $\bullet$ ) 120 to 200 Torr ethylene.....	109

## LIST OF FIGURES (CONTINUED)

Figure	Page
<p><b>3.15</b> The difference IR spectra during ethylene flow over PtRu/MgO at 30°C in the IR ranges of (A) 2700-3300 cm<sup>-1</sup>; and (B) 2200-1000 cm<sup>-1</sup> at ethylene pressure (1) 20 Torr; (2) 40 Torr; (3) 80 Torr; (4) 120 Torr; 150 Torr; and 200 Torr.....</p>	112
<p><b>3.16</b> IR spectra during catalysis of ethylene hydrogenation in a flow reactor at 30°C catalyzed by PtRu/MgO in IR ranges of (A) 2700-3200 cm<sup>-1</sup> and (B) 1200-2200 cm<sup>-1</sup> at conditions (1) He, 40 Torr C<sub>2</sub>H<sub>4</sub> and 80 Torr H<sub>2</sub>; (2) at 240 s after flowing reactant gas; (3) at 480 s after flowing reactant gas; (4) at 38 min after flowing reactant gas.....</p>	113
<p><b>3.17</b> Demonstration of differential reactor operation at 220°C, <math>P_{H_2} = 540</math> Torr, <math>P_{n-C_4H_{10}} = 60</math> Torr with 100 ml (NTP)/min flow rate catalyzed by PtRu/MgO.....</p>	114
<p><b>3.18</b> Selectivity varied with inv. WHSV at 220°C, <math>P_{H_2} = 540</math> Torr, <math>P_{n-C_4H_{10}} = 60</math> Torr with 100 ml (NTP)/min flow rate catalyzed by PtRu/MgO.....</p>	115
<p><b>3.19</b> Activity varied with time on stream (TOS) for <i>n</i>-butane hydrogenolysis catalyzed by PtRu/MgO (■) 200°C; (○) 210°C; (▲) 220°C; (*) 240°C; and (◆) 260°C.....</p>	116
<p><b>3.20</b> Selectivity varied with reaction temperature of <i>n</i>-butane hydrogenolysis catalyzed by PtRu/MgO.....</p>	117

## LIST OF FIGURES (CONTINUED)

Figure	Page
3.21 Arrhenius plot of <i>n</i> -butane hydrogenolysis catalyzed by PtRu/MgO.....	119
4.1 IR spectra in $\nu_{\text{OH}}$ region of: (1) Dry sample prepared from Pt <sub>3</sub> Ru <sub>6</sub> (CO) <sub>21</sub> ( $\mu_3$ -H)( $\mu$ -H) <sub>3</sub> on TiO <sub>2</sub> ; (2) sample after ligand removal in He flow at 300°C for 2 h; (3) calcined TiO <sub>2</sub> .....	129
4.2 IR spectra in $\nu_{\text{CO}}$ region of: (1) Dry sample prepared from Pt <sub>3</sub> Ru <sub>6</sub> (CO) <sub>21</sub> ( $\mu_3$ -H)( $\mu$ -H) <sub>3</sub> on TiO <sub>2</sub> ; (2) sample after ligand removal in He flow at 300 °C for 2 h; (3) calcined TiO <sub>2</sub> .....	130
4.3 IR spectrum in $\nu_{\text{CO}}$ region of extract solution after extraction of the supported sample on TiO <sub>2</sub> with CH <sub>2</sub> Cl <sub>2</sub> .....	132
4.4 IR spectrum of dry supported sample on TiO <sub>2</sub> after extraction with CH <sub>2</sub> Cl <sub>2</sub> in (A) $\nu_{\text{OH}}$ , and (B) $\nu_{\text{CO}}$ region.....	133
4.5 EXAFS results scanned at the Pt L <sub>III</sub> edge characterizing the adsorbed Pt <sub>3</sub> Ru <sub>6</sub> (CO) <sub>21</sub> ( $\mu_3$ -H)( $\mu$ -H) <sub>3</sub> on TiO <sub>2</sub> : (A) Experimental EXAFS function (solid line) and sum of the calculated Pt-Pt, Pt-Ru, Pt-C, Pt-O*, Pt-O <sub>s</sub> , and Pt-O <sub>l</sub> contributions (dotted line). (B) Magnitude of uncorrected Fourier transform ( $k^0$ weighted) of experimental EXAFS function (solid line) and sum of the calculated Pt-Pt, Pt-Ru, Pt-C, Pt-O*, Pt-O <sub>s</sub> , and Pt-O <sub>l</sub> contributions (dotted line).....	136

## LIST OF FIGURES (CONTINUED)

Figure	Page
<p><b>4.5</b> (continued) EXAFS results scanned at the Pt L<sub>III</sub> edge characterizing the adsorbed Pt<sub>3</sub>Ru<sub>6</sub>(CO)<sub>21</sub>(μ<sub>3</sub>-H)(μ-H)<sub>3</sub> on TiO<sub>2</sub>: (C) Magnitude of uncorrected Fourier transform (<math>k^1</math> weighted) of experimental EXAFS function (solid line) and sum of the calculated Pt-Pt, Pt-Ru, Pt-C, Pt-O*, Pt-O<sub>s</sub>, and Pt-O<sub>1</sub> contributions (dotted line). (D) Magnitude of uncorrected Fourier transform (<math>k^3</math> weighted) of experimental EXAFS function (solid line) and sum of the calculated Pt-Pt, Pt-Ru, Pt-C, Pt-O*, Pt-O<sub>s</sub>, and Pt-O<sub>1</sub> contributions (dotted line).....</p>	137
<p><b>4.6</b> EXAFS results scanned at the Ru K edge characterizing the adsorbed Pt<sub>3</sub>Ru<sub>6</sub>(CO)<sub>21</sub>(μ<sub>3</sub>-H)(μ-H)<sub>3</sub> on TiO<sub>2</sub>: (A) Experimental EXAFS function (solid line) and sum of the calculated Ru-Ru, Ru-Pt, Ru-C, Ru-O*, Ru-O<sub>s</sub>, and Ru-O<sub>1</sub> contributions (dotted line). (B) Magnitude of uncorrected Fourier transform (<math>k^0</math> weighted) of experimental EXAFS function (solid line) and sum of the calculated Ru-Ru, Ru-Pt, Ru-C, Ru-O*, Ru-O<sub>s</sub>, and Ru-O<sub>1</sub> contributions (dotted line).....</p>	138

## LIST OF FIGURES (CONTINUED)

Figure	Page
<p><b>4.6</b> (continued) EXAFS results scanned at the Ru K edge characterizing the adsorbed <math>\text{Pt}_3\text{Ru}_6(\text{CO})_{21}(\mu_3\text{-H})(\mu\text{-H})_3</math> on <math>\text{TiO}_2</math>: (C) Magnitude of uncorrected Fourier transform (<math>k^1</math> weighted) of experimental EXAFS function (solid line) and sum of the calculated Ru-Ru, Ru-Pt, Ru-C, Ru-O*, Ru-O<sub>s</sub>, and Ru-O<sub>l</sub> contributions (dotted line). (D) Magnitude of uncorrected Fourier transform (<math>k^3</math> weighted) of experimental EXAFS function (solid line) and sum of the calculated Ru-Ru, Ru-Pt, Ru-C, Ru-O*, Ru-O<sub>s</sub>, and Ru-O<sub>l</sub> contributions (dotted line).....</p>	139
<p><b>4.7</b> EXAFS results scanned at the Pt L<sub>III</sub> edge characterizing the PtRu/TiO<sub>2</sub> sample prepared by adsorption of <math>\text{Pt}_3\text{Ru}_6(\text{CO})_{21}(\mu_3\text{-H})(\mu\text{-H})_3</math> after ligand removal: (A) Experimental EXAFS function (solid line) and sum of the calculated Pt-Pt, Pt-Ru, Pt-C, Pt-O*, Pt-O<sub>s</sub>, and Pt-O<sub>l</sub> contributions (dotted line). (B) Magnitude of uncorrected Fourier transform (<math>k^0</math> weighted) of experimental EXAFS function (solid line) and sum of the calculated Pt-Pt, Pt-Ru, Pt-C, Pt-O*, Pt-O<sub>s</sub>, and Pt-O<sub>l</sub> contributions (dotted line).....</p>	145

## LIST OF FIGURES (CONTINUED)

Figure	Page
<p><b>4.7</b> (continued) EXAFS results scanned at the Pt L<sub>III</sub> edge characterizing the PtRu/TiO<sub>2</sub> sample prepared by adsorption of Pt<sub>3</sub>Ru<sub>6</sub>(CO)<sub>21</sub>(μ<sub>3</sub>-H)(μ-H)<sub>3</sub> after ligand removal: (C) Magnitude of uncorrected Fourier transform (<math>k^1</math> weighted) of experimental EXAFS function (solid line) and sum of the calculated Pt-Pt, Pt-Ru, Pt-C, Pt-O*, Pt-O<sub>s</sub>, and Pt-O<sub>l</sub> contributions (dotted line). (D) Magnitude of uncorrected Fourier transform (<math>k^3</math> weighted) of experimental EXAFS function (solid line) and sum of the calculated Pt-Pt, Pt-Ru, Pt-C, Pt-O*, Pt-O<sub>s</sub>, and Pt-O<sub>l</sub> contributions (dotted line).....</p>	146
<p><b>4.8</b> EXAFS results scanned at the Ru K edge characterizing the PtRu/TiO<sub>2</sub> sample prepared by adsorption of Pt<sub>3</sub>Ru<sub>6</sub>(CO)<sub>21</sub>(μ<sub>3</sub>-H)(μ-H)<sub>3</sub> after ligand removal: (A) Experimental EXAFS function (solid line) and sum of the calculated Ru-Ru, Ru-Pt, Ru-C, Ru-O*, Ru-O<sub>s</sub>, and Ru-O<sub>l</sub> contributions (dotted line). (B) Magnitude of uncorrected Fourier transform (<math>k^0</math> weighted) of experimental EXAFS function (solid line) and sum of the calculated Ru-Ru, Ru-Pt, Ru-C, Ru-O*, Ru-O<sub>s</sub>, and Ru-O<sub>l</sub> contributions (dotted line).....</p>	147

## LIST OF FIGURES (CONTINUED)

Figure	Page
<p><b>4.8</b> (continued) EXAFS results scanned at the Ru K edge characterizing the PtRu/TiO<sub>2</sub> sample prepared by adsorption of Pt<sub>3</sub>Ru<sub>6</sub>(CO)<sub>21</sub>(μ<sub>3</sub>-H)(μ-H)<sub>3</sub> after ligand removal: (C) Magnitude of uncorrected Fourier transform (<math>k^l</math> weighted) of experimental EXAFS function (solid line) and sum of the calculated Ru-Ru, Ru-Pt, Ru-C, Ru-O*, Ru-O<sub>s</sub>, and Ru-O<sub>l</sub> contributions (dotted line). (D) Magnitude of uncorrected Fourier transform (<math>k^3</math> weighted) of experimental EXAFS function (solid line) and sum of the calculated Ru-Ru, Ru-Pt, Ru-C, Ru-O*, Ru-O<sub>s</sub>, and Ru-O<sub>l</sub> contributions (dotted line).....</p>	148
<p><b>4.9</b> Demonstration of differential reactor operation at -75°C, <math>P_{C_2H_4} = 40</math> Torr, <math>P_{H_2} = 80</math> Torr, balanced with He, total feed flow rate = 200 ml (NTP)/min catalyzed by PtRu/TiO<sub>2</sub>.....</p>	151
<p><b>4.10</b> Activity of ethylene hydrogenation with time on stream (TOS) catalyzed by PtRu/TiO<sub>2</sub> at reaction condition: <math>P_{C_2H_4} = 40</math> Torr, <math>P_{H_2} = 80</math> Torr, balance He with total feed flow rate 200 ml (NTP)/min, catalyst mass 0.013 mg, and temperature -75°C.....</p>	152
<p><b>4.11</b> Arrhenius plot of ethylene hydrogenation catalyzed by PtRu/TiO<sub>2</sub> at reaction condition: <math>P_{C_2H_4} = 40</math> Torr, <math>P_{H_2} = 80</math> Torr, balance He with total feed flow rate 200 ml (NTP)/min, catalyst mass 0.013 g.....</p>	153

## LIST OF FIGURES (CONTINUED)

Figure	Page
<b>4.12</b> Effect of pressure of hydrogen on ethylene hydrogenation catalyzed by PtRu/TiO <sub>2</sub> at 40 torr ethylene at -75°C.....	155
<b>4.13</b> The plot in a natural log scale between TOF and pressure of hydrogen for ethylene hydrogenation catalyzed by PtRu/TiO <sub>2</sub> at -75°C, 40 Torr ethylene and 20 to 200 Torr hydrogen.....	156
<b>4.14</b> Effect of pressure of ethylene on ethylene hydrogenation catalyzed by PtRu/TiO <sub>2</sub> at 80 Torr hydrogen.....	157
<b>4.15</b> The plot in a natural log scale between TOF and pressure of ethylene for ethylene hydrogenation catalyzed by PtRu/TiO <sub>2</sub> at -75°C, 80 Torr hydrogen and 80 to 200 Torr ethylene.....	159
<b>4.16</b> Demonstration of differential reactor operation at 220°C, $P_{H_2} = 540$ Torr, $P_{n-C_4H_{10}} = 60$ Torr with 100 ml (NTP)/min flow rate catalyzed by PtRu/TiO <sub>2</sub> .....	161
<b>4.19</b> Selectivity varied with inv. WHSV at 220°C, $P_{H_2} = 540$ Torr, $P_{n-C_4H_{10}} = 60$ Torr with 100 ml (NTP)/min flow rate catalyzed by PtRu/TiO <sub>2</sub> .....	162
<b>4.18</b> Activity varied with time on stream (TOS) for <i>n</i> -butane hydrogenolysis catalyzed by PtRu/TiO <sub>2</sub> (◇) 200°C; (▲) 220°C; (*) 240°C; (■) 260°C; and (□) 280°C.....	163
<b>4.19</b> Selectivity varied with various reaction temperature of <i>n</i> -butane hydrogenolysis catalyzed by PtRu/TiO <sub>2</sub> .....	164

## LIST OF FIGURES (CONTINUED)

Figure	Page
4.20 Arrhenius plot of <i>n</i> -butane hydrogenolysis catalyzed by PtRu/TiO <sub>2</sub> .....	165
5.1 IR spectra in $\nu_{OH}$ region of (1) calcined $\gamma$ -Al <sub>2</sub> O <sub>3</sub> ; (2) dry supported Pt(acac) <sub>2</sub> and Ru(acac) <sub>3</sub> on $\gamma$ -Al <sub>2</sub> O <sub>3</sub> ; (3) PtRu/ $\gamma$ -Al <sub>2</sub> O <sub>3</sub> after treated in H <sub>2</sub> flow at 300°C for 2 h.....	177
5.2 IR spectra in $\nu_{C-C}$ and $\nu_{C-H}$ regions of (1) calcined $\gamma$ -Al <sub>2</sub> O <sub>3</sub> ; (2) PtRu/ $\gamma$ -Al <sub>2</sub> O <sub>3</sub> after treated in H <sub>2</sub> flow at 300°C for 2 h; (3) dry supported Pt(acac) <sub>2</sub> and Ru(acac) <sub>3</sub> on $\gamma$ -Al <sub>2</sub> O <sub>3</sub> .....	178
5.3 IR spectra in $\nu_{OH}$ region of (1) dry supported Pt(acac) <sub>2</sub> and Ru(acac) <sub>3</sub> on MgO; (2) PtRu/MgO after ligand removal in H <sub>2</sub> flow at 300°C for 2 h; (3) calcined MgO.....	180
5.4 IR spectra $\nu_{C-C}$ and $\nu_{C-H}$ regions of (1) dry supported Pt(acac) <sub>2</sub> and Ru(acac) <sub>3</sub> on MgO; (2) PtRu/MgO after ligand removal in H <sub>2</sub> flow at 300°C for 2 h.....	181
5.5 TPRD profiles of (1) Pt(acac) <sub>2</sub> and Ru(acac) <sub>3</sub> adsorbed on $\gamma$ -Al <sub>2</sub> O <sub>3</sub> ; (2) Pt(acac) <sub>2</sub> adsorbed on $\gamma$ -Al <sub>2</sub> O <sub>3</sub> ; (3) Ru(acac) <sub>3</sub> adsorbed on $\gamma$ -Al <sub>2</sub> O <sub>3</sub> .....	183
5.6 TPRD profiles of (1) Pt(acac) <sub>2</sub> adsorbed on MgO; (2) Pt(acac) <sub>2</sub> and Ru(acac) <sub>3</sub> adsorbed on MgO; (3) Ru(acac) <sub>3</sub> adsorbed on MgO; (4) calcined MgO.....	184
5.7 XANES spectra of Pt(acac) <sub>2</sub> and Ru(acac) <sub>3</sub> supported on $\gamma$ -Al <sub>2</sub> O <sub>3</sub> during H <sub>2</sub> flow from room temperature to 100°C. (A) Scanned at the Pt L <sub>III</sub> edge; (B) the Ru K edge at temperature (1) 25°C and (2) 100°C.....	186

## LIST OF FIGURES (CONTINUED)

Figure	Page
<p><b>5.8</b> EXAFS results scanned at the Pt L<sub>III</sub> edge characterizing the PtRu/<math>\gamma</math>-Al<sub>2</sub>O<sub>3</sub> sample prepared by adsorption of a mixture of Pt(acac)<sub>2</sub> and Ru(acac)<sub>3</sub> after ligand removal in H<sub>2</sub> flow at 300°C: (A) Experimental EXAFS function (solid line) and sum of the calculated Pt-Pt, Pt-O<sub>s</sub>, and Pt-O<sub>1</sub> contributions (dotted line). (B) Magnitude of uncorrected Fourier transform (<math>k^0</math> weighted) of experimental EXAFS function (solid line) and sum of the calculated Pt-Pt, Pt-O<sub>s</sub>, and Pt-O<sub>1</sub> contributions (dotted line).....</p>	189
<p><b>5.8</b> (continued) EXAFS results scanned at the Pt L<sub>III</sub> edge characterizing the PtRu/<math>\gamma</math>-Al<sub>2</sub>O<sub>3</sub> sample prepared by adsorption of a mixture of Pt(acac)<sub>2</sub> and Ru(acac)<sub>3</sub> after ligand removal in H<sub>2</sub> flow at 300°C: (C) Magnitude of uncorrected Fourier transform (<math>k^1</math> weighted) of experimental EXAFS function (solid line) and sum of the calculated Pt-Pt, Pt-O<sub>s</sub>, and Pt-O<sub>1</sub> contributions (dotted line). (D) Magnitude of uncorrected Fourier transform (<math>k^3</math> weighted) of experimental EXAFS function (solid line) and sum of the calculated Pt-Pt, Pt-O<sub>s</sub>, and Pt-O<sub>1</sub> contributions (dotted line).....</p>	190

## LIST OF FIGURES (CONTINUED)

Figure	Page
<p><b>5.9</b> EXAFS results scanned at the Ru K edge characterizing the PtRu/<math>\gamma</math>-Al<sub>2</sub>O<sub>3</sub> sample prepared by adsorption of a mixture of Pt(acac)<sub>2</sub> and Ru(acac)<sub>3</sub> after ligand removal in H<sub>2</sub> flow at 300°C: (A) Experimental EXAFS function (solid line) and sum of the calculated Pt-Pt, Pt-O<sub>s</sub>, and Pt-O<sub>l</sub> contributions (dotted line). (B) Magnitude of uncorrected Fourier transform (<math>k^0</math> weighted) of experimental EXAFS function (solid line) and sum of the calculated Pt-Pt, Pt-O<sub>s</sub>, and Pt-O<sub>l</sub> contributions (dotted line).....</p>	191
<p><b>5.9</b> (continued) EXAFS results scanned at the Ru K edge characterizing the PtRu/<math>\gamma</math>-Al<sub>2</sub>O<sub>3</sub> sample prepared by adsorption of a mixture of Pt(acac)<sub>2</sub> and Ru(acac)<sub>3</sub> after ligand removal in H<sub>2</sub> flow at 300°C: (C) Magnitude of uncorrected Fourier transform (<math>k^1</math> weighted) of experimental EXAFS function (solid line) and sum of the calculated Pt-Pt, Pt-O<sub>s</sub>, and Pt-O<sub>l</sub> contributions (dotted line). (D) Magnitude of uncorrected Fourier transform (<math>k^3</math> weighted) of experimental EXAFS function (solid line) and sum of the calculated Pt-Pt, Pt-O<sub>s</sub>, and Pt-O<sub>l</sub> contributions (dotted line).....</p>	192

## LIST OF FIGURES (CONTINUED)

Figure	Page
<p><b>5.10</b> EXAFS results scanned at the Pt L<sub>III</sub> edge characterizing the PtRu/MgO sample prepared by adsorption of a mixture of Pt(acac)<sub>2</sub> and Ru(acac)<sub>3</sub> after ligand removal in H<sub>2</sub> flow at 300°C: (A) Experimental EXAFS function (solid line) and sum of the calculated Pt-Pt, Pt-O<sub>s</sub>, and Pt-O<sub>l</sub> contributions (dotted line). (B) Magnitude of uncorrected Fourier transform (<math>k^0</math> weighted) of experimental EXAFS function (solid line) and sum of the calculated Pt-Pt, Pt-O<sub>s</sub>, and Pt-O<sub>l</sub> contributions (dotted line).....</p>	195
<p><b>5.10</b> (continued) EXAFS results scanned at the Pt L<sub>III</sub> edge characterizing the PtRu/MgO sample prepared by adsorption of a mixture of Pt(acac)<sub>2</sub> and Ru(acac)<sub>3</sub> after ligand removal in H<sub>2</sub> flow at 300°C: (C) Magnitude of uncorrected Fourier transform (<math>k^1</math> weighted) of experimental EXAFS function (solid line) and sum of the calculated Pt-Pt, Pt-O<sub>s</sub>, and Pt-O<sub>l</sub> contributions (dotted line). (D) Magnitude of uncorrected Fourier transform (<math>k^3</math> weighted) of experimental EXAFS function (solid line) and sum of the calculated Pt-Pt, Pt-O<sub>s</sub>, and Pt-O<sub>l</sub> contributions (dotted line).....</p>	196

## LIST OF FIGURES (CONTINUED)

Figure	Page
<p><b>5.11</b> EXAFS results scanned at the Ru K edge characterizing the PtRu/MgO sample prepared by adsorption of a mixture of Pt(acac)<sub>2</sub> and Ru(acac)<sub>3</sub> after ligand removal in H<sub>2</sub> flow at 300°C: (A) Experimental EXAFS function (solid line) and sum of the calculated Pt-Pt, Pt-O<sub>s</sub>, and Pt-O<sub>l</sub> contributions (dotted line). (B) Magnitude of uncorrected Fourier transform (<math>k^0</math> weighted) of experimental EXAFS function (solid line) and sum of the calculated Pt-Pt, Pt-O<sub>s</sub>, and Pt-O<sub>l</sub> contributions (dotted line).....</p>	197
<p><b>5.11</b> (continued) EXAFS results scanned at the Ru K edge characterizing the PtRu/MgO sample prepared by adsorption of a mixture of Pt(acac)<sub>2</sub> and Ru(acac)<sub>3</sub> after ligand removal in H<sub>2</sub> flow at 300°C: (C) Magnitude of uncorrected Fourier transform (<math>k^1</math> weighted) of experimental EXAFS function (solid line) and sum of the calculated Pt-Pt, Pt-O<sub>s</sub>, and Pt-O<sub>l</sub> contributions (dotted line). (D) Magnitude of uncorrected Fourier transform (<math>k^3</math> weighted) of experimental EXAFS function (solid line) and sum of the calculated Pt-Pt, Pt-O<sub>s</sub>, and Pt-O<sub>l</sub> contributions (dotted line).....</p>	198
<p><b>5.12</b> Activity for ethylene hydrogenation catalyzed by (■) PtRu/MgO; (▲) PtRu/<math>\gamma</math>-Al<sub>2</sub>O<sub>3</sub>, prepared from a mixture solution of Pt(acac)<sub>2</sub> and Ru(acac)<sub>3</sub> at temperature -50°C.....</p>	201

**LIST OF FIGURES (CONTINUED)**

<b>Figure</b>	<b>Page</b>
<b>5.13</b> Arrhenius plot for ethylene hydrogenation catalyzed by (■) PtRu/MgO; (▲) PtRu/ $\gamma$ -Al <sub>2</sub> O <sub>3</sub> , prepared from a mixture solution of Pt(acac) <sub>2</sub> and Ru(acac) <sub>3</sub> .....	202

## LIST OF ABBREVIATIONS

Å	Angstrom
acac	Acetylacetonate (C <sub>5</sub> H <sub>7</sub> O <sub>2</sub> <sup>-</sup> )
a.u.	Arbitrary unit
°C	Degree celcius
cm <sup>-1</sup>	Per centimeter
cod	1,5-Cyclooctadiene
$\Delta E_o$	Inner potential correction
$\Delta\sigma^2$	Debye-Waller factor
$E_{app}$	Apparent activation energy (kcal/mol)
EXAFS	Extended X-ray absorption fine structure
g cat/mol/h	Grams of catalyst per mole of reactant per hour
inv. WHSV	Inverse weight hourly space velocity
IR	Infrared
K	Kelvin
$k$	Wave vector; reaction rate
kcal/mol	Kilocalorie per mole
min	Minute
$P$	Pressure (Torr)
$r$	Distance between absorber atom and neighbor atom (Å)
$R$	Interatomic distance (Å)

**LIST OF ABBREVIATIONS (CONTINUED)**

s	Second
T	Temperature (K)
TOF	Turn over frequency ( $s^{-1}$ )
TOS	Time on stream
TPRD	Temperature-programmed reductive decomposition
vol%	Percentage by volume
wt%	Percentage by weight
XANES	X-ray absorption near edge structure
XRD	X-ray diffraction
$\nu$	wavenumber ( $cm^{-1}$ )
$\chi$	EXAFS function

# **CHAPTER I**

## **GENERAL INTRODUCTION**

Heterogeneous catalysis plays an important role in many industrial applications, for example, in fine chemical, pharmaceutical industry, or even in environmental protection such as automobile catalysts. In general, heterogeneous catalysts are comprised of active catalytic phase, promoter which increases activity and/or stability of the catalyst, and high-surface area support which facilitates good dispersion and stability of the active catalytic phase. When an active phase such as metal or metal oxide in the form of microcrystallites of 1-50 nm in diameter is dispersed on surface of support, the catalyst surface area is maximized because the number of active sites upon which chemisorption and catalytic reaction is enhanced (Farrauto and Bartholomew, 1997).

### **1.1 Supported bimetallic catalysts**

Platinum (Pt) is a noble metal which is widely used in both homogeneous and heterogeneous catalysis. Pt monometallic catalysts are effective for reactions of hydrocarbons such as hydrogenation, dehydrogenation and oxidation reactions. In addition, Pt can form bimetallic catalysts by incorporation with other metal such as Rh, Ru, and other oxophilic metals to improve catalytic performance.

### 1.1.1 Preparation methods of supported bimetallic catalysts

There are many preparation methods for supported bimetallic catalysts and the method selection depends on the metal precursors and type of support. As the selection of precursors, supporting materials and method of preparation is a part of catalyst design to control dispersion and morphology of supported bimetallic catalysts (Ichikawa, 2000).

The conventional precursors for supported Pt-Ru bimetallic catalyst are mixed metal salts of desired metals such as  $\text{H}_2\text{PtCl}_6$  and  $\text{RuCl}_3$ . However, the conventional precursors do not allow ability to control particle size, structure, composition, and stoichiometry of bimetallic catalysts (Shirai, Yang, Weber, and Gates, 1999). Moreover, nonuniform materials with large metal particles and broad particle size distribution could be formed after a high-temperature reduction.

To avoid difficulties caused by conventional precursors, preformed bimetallic precursors are alternatives for impregnation and/or adsorption. The unconventional precursors are organometallic or molecular compounds or a solution of mixed-metal clusters. Metal cluster is defined as two or more metal atoms of group held together by direct and substantial metal-metal bonding (Cotton, Wilkinson, Murillo, and Bochmann, 1999). Mixed-metal cluster precursors are suitable for the preparation of supported bimetallic catalysts with well-defined and highly dispersed metallic species (Alexeev, Shelef, and Gates, 1996). In addition, bimetal particles with nanometer-sized, uniform, and precise stoichiometry can lead to unique physical and chemical properties, which are important for catalysts.

Advantages expected from heterogeneous supported catalysts from cluster precursors can be summarized below (Braunstein and Rose, 1998, 1999).

1. Decomposition of preformed cluster complexes on support gives particles with particularly small, uniform and well-defined stoichiometry because metal frameworks do not change significantly upon activation, and they allow systematic variation in particle stoichiometry by changing precursors.
2. Metal atoms in cluster precursors are easy to activate because they have low initial oxidation states and cluster ligands such as CO can be removed under mild condition.
3. Metal particles are highly dispersed on support because of strong interaction between metal cluster and oxide supports. For example, neutral cluster favors on acidic support like alumina and silica, and anionic clusters favors on basic support like magnesia.
4. Contaminating anions such as  $\text{Cl}^-$  on the surface are avoidable. Those ions usually affect catalytic properties. Other ligands containing phosphorus or sulfur may not be innocent during the activation step of catalyst and may also affect its properties in either a beneficial or a detrimental manner.

### **1.1.2 Supported Pt catalysts incorporating with oxophilic metal**

Supported bimetallic catalysts incorporating oxophilic metal-noble metal combinations and the roles of the two metals (e.g., rhenium in RePt) are important in technology (e.g., reforming of naphtha) and show greater resistance to deactivation than single Pt catalyst (Antos, Aitani, and Parera, 1995; Sinfelt, 1983; Fung, Kelley, Koningsberger, and Gates, 1997).

Bimetallic catalysts such as WPt, MoPt and RePt which were made from bimetallic precursors demonstrated how the oxophilic metal helped to stabilize the

dispersion of the noble metal. The incorporation of oxophilic metal led to changes in electronic property of noble metal and perhaps stabilizing dispersion (Alexeev, Graham, Kim, Shelef, and Gates, 1999; Alexeev, Graham, Shelef, and Gates, 2000; Alexeev, Kawi, Shelef, and Gates, 1996; Alexeev, Shelef, and Gates, 1996; Lai et al., 2000).

### **1.1.3 Supported Pt catalysts incorporating with noble metal**

Supported bimetallic catalysts incorporating two noble metals are also important in technology. The most evident examples are in reforming of naphtha and automotive three-way catalysis (Shelef and Graham, 1994). The incorporation of second noble metal such as Ir in IrPt catalyst can improve thermal stability and resistance to deactivation (Sinfelt, 1983).

Ruthenium (Ru), also one of platinum group metals, is employed as monometallic catalyst in reactions such as Fischer-Tropsch reaction and ethane hydrogenolysis. It can also be found in Pt-Ru bimetallic catalysts for proton exchange membrane (PEM) and direct methanol fuel cells (DMFCs) (Boxall, Deluga, Kenik, King, and Lukehart, 2001; Braccini, Indovina, De Rossi, and Giorgi, 2000; Chrzanowski and Wieckowski, 1998; Hamnett, Kennedy, and Wagner, 1990; Tess et al., 2000). The incorporation of Ru in supported platinum catalysts could prevent the formation of strong Pt-CO or CO poisons of Pt (Braccini et al., 2000).

#### **1.1.3.1 Supported PtRu catalyst prepared from two salts**

Some supported Pt-Ru catalysts prepared from a conventional method by deposition of a mixture of platinum chloride and ruthenium chloride on a support,

after reduction in H<sub>2</sub>, typically around 400°C, were found to form separate monometallic particles rather than bimetallic particles on metal oxide support (Alerasool, Boecker, Rejai, and Gonzalez, 1988; Diaz, Garin, and Maine, 1983; Diaz, Garin, Maine, Alerasool, and Gonzalez, 1995; Miura, Osawa, Suzuki, Sugiyama, and Matsuda, 1982).

### **1.1.3.2 Supported PtRu catalyst prepared from a molecular cluster**

In contrast to the conventional method, highly dispersed bimetallic particles on oxide support could be prepared from metal cluster precursors containing heterometallic bonds (Alexeev and Gates, 2003; Alexeev, Grahem, Shelef, Adams, and Gates, 2002; Bergmeister and Hanson, 1989). Because metal atoms in molecular bimetallic precursors are in low oxidation states, catalyst activation by ligand removal can be accomplished at mild conditions, namely, low temperature. This preparation method provided highly dispersed and uniform supported bimetallic particles containing desired bimetallic metal-metal bonds on support. Those catalysts were reported to be more selective than catalysts from conventional preparation (Alexeev and Gates, 2003; Bergmeister and Hanson, 1989).

For supported PtRu catalysts, there is a family of PtRu carbonyl clusters made by Adams and coworkers that can be used as molecular catalyst precursors (Adams, Alexander, Arafa, and Wu, 1991; Adams, Barnard, Li, Wu, and Yamamoto, 1994; Adams, Chen, and Wu, 1993; Adams and Wu, 1991). Pt-Ru carbonyl cluster family without phosphine ligands were prepared with various metal compositions and ligands including Pt<sub>2</sub>Ru<sub>4</sub>(CO)<sub>18</sub>, PtRu<sub>5</sub>C(CO)<sub>16</sub> and Pt<sub>3</sub>Ru<sub>6</sub>(CO)<sub>21</sub>(μ<sub>3</sub>-H)(μ-H)<sub>3</sub> (Adams, Barnard et al., 1994; Adams, Chen et al., 1993; Adams and Wu, 1991). The last

cluster, which contains hydride ligands bonded to ruthenium, was of interest as a catalyst precursor for this work because it had not yet been utilized as a catalyst precursor. Related work was the preparation and characterization of Pt-Ru/ $\gamma$ -Al<sub>2</sub>O<sub>3</sub> from a smaller cluster precursor, Pt<sub>2</sub>Ru<sub>4</sub>(CO)<sub>18</sub> to give highly dispersed and extremely small Pt-Ru particles (Alexeev, Grahem et al., 2002). IR and EXAFS spectroscopy showed that Pt<sub>2</sub>Ru<sub>4</sub>(CO)<sub>18</sub> adsorbed intact on  $\gamma$ -Al<sub>2</sub>O<sub>3</sub> and the metal core remained on support after decarbonylation (in He or H<sub>2</sub>) at 300-400°C. It was believed that strong Pt-Ru interactions led to highly dispersed Pt-Ru on  $\gamma$ -Al<sub>2</sub>O<sub>3</sub>.

Moreover, the chemistry of support was important to cluster-support interaction and metal dispersion (Alexeev, Grahem et al., 2002). The data obtained from  $\gamma$ -Al<sub>2</sub>O<sub>3</sub>-supported PtRu prepared from Pt<sub>2</sub>Ru<sub>4</sub>(CO)<sub>18</sub> were in contrast with carbon-supported PtRu prepared from that precursor (Nasher, Frenkel, Adler, Shapley, and Nuzzo, 1997; Nasher, Frenkel et al., 1998; Hills, Nasher, Frenkel, Shapley, and Nuzzo, 1999). The decarbonylated sample in H<sub>2</sub> at 400°C showed larger PtRu particles (around tens of Pt and Ru atoms) on carbon than those on  $\gamma$ -Al<sub>2</sub>O<sub>3</sub>. Because carbon support was nonpolar resulting in weaker cluster-support interactions than that on  $\gamma$ -Al<sub>2</sub>O<sub>3</sub>. To obtain PtRu catalyst with high metal dispersion,  $\gamma$ -Al<sub>2</sub>O<sub>3</sub> was one type of oxide supports chosen in this work along with MgO and TiO<sub>2</sub>.

A molecular cluster precursor chosen to study in this work was Pt<sub>3</sub>Ru<sub>6</sub>(CO)<sub>21</sub>( $\mu_3$ -H)( $\mu$ -H)<sub>3</sub>, which contains preformed Pt-Ru bonds with 1:2 of Pt:Ru ratio. Its crystalline structure is shown in Figure 1.1.

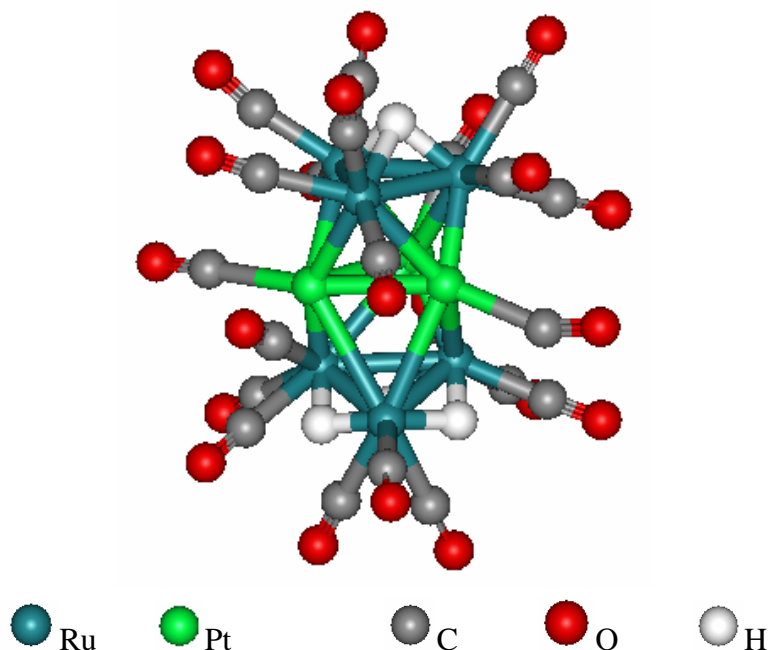


**Figure 1.1** Structure of crystalline  $\text{Pt}_3\text{Ru}_6(\text{CO})_{21}(\mu_3\text{-H})(\mu\text{-H})_3$  (reproduced from Adams, Barnard et al., 1994 by Weblab ViewerPro software)

$\text{Pt}_3\text{Ru}_6(\text{CO})_{21}(\mu_3\text{-H})(\mu\text{-H})_3$  has a face-shared bi-octahedron structure containing central layer of three platinum atoms connected with outer triangular layers of ruthenium triangles. Each edge of one  $\text{Ru}_3$  triangular face was bridged with three hydride ligands while another  $\text{Ru}_3$  face contains a triply-bridged hydride. Valence electrons of the cluster metal core were 124 and identical to the value predicted by the polyhedral skeletal electron pair theory (Adams, Barnard et al., 1994) indicating that the metal atoms were coordinatively saturated.

Other cluster which has been utilized as a precursor for supported Pt-Ru catalyst was  $\text{Ru}_3\text{Pt}(\text{CO})_{12}\text{Py}_3$  which was impregnated onto inorganic oxides or carbon to produce a very active and selective catalyst for hydrocarbon conversion. The performance of the resulting  $[\text{Ru}_3\text{Pt}]$  catalyst was governed by high activity in

hydrogenolysis by Ru with enhanced hydrogenation activity by Pt (Braunstein and Rose, 1999).

Several supports that have been used for Pt-Ru catalysts included various types of carbon, silica and zeolite. Because those supports provide weak cluster-support interaction, supports with stronger interaction including  $\gamma$ -Al<sub>2</sub>O<sub>3</sub>, MgO and TiO<sub>2</sub> were selected for this work.

## **1.2 Catalyst characterization techniques**

Techniques that were utilized for characterization of supported bimetallic catalysts in this work included thermal methods and spectroscopy. A brief background of each technique is described below.

### **1.2.1 Temperature-programmed reductive decomposition (TPRD)**

Decomposition of organometallic precursor adsorbed on supports to supported metals by H<sub>2</sub> flow can be investigated by temperature-programmed reductive decomposition (TPRD) (Dossi et al., 1998). TPRD results show the ranges and peaks of reductive decomposition temperature as well as the number of steps in decomposition. TPRD can indicate whether the two metals in bimetallic catalyst contact each other or not. If two metals such as Pt and Ru are in contact, the decomposition of the metal complex which is harder to decompose could shift to lower temperature. Suppose that a Pt complex was decomposed first and provided new adsorption sites for hydrogen atoms. Hydrogen could then adsorb there and migrate to accelerate the decomposition of the adjacent ruthenium complex.

The TPRD technique is discussed only in Chapter V of this thesis in which  $\text{Pt}(\text{acac})_2$  and  $\text{Ru}(\text{acac})_3$  (acac is acetylacetonate,  $\text{C}_5\text{H}_7\text{O}_2^-$ ) were used as catalyst precursors and their decomposition could give products such as methane or acetone. For the cluster precursor of interest, hydride and carbonyl ligands could be simply removed by heating in He flow.

### **1.2.2 Infrared (IR) spectroscopy**

Infrared spectroscopy (IR) is a useful vibrational technique to investigate the behavior of “probe” adsorbates, such as CO and/or NO, on the chemistry of surface functional groups (particularly on oxides). IR is also used to determine the binding nature of adsorbates and number of the active sites. In this work it was used to study the vibrational behavior of the cluster-precursor ligands, especially carbonyl, as well as the hydroxyl groups of oxide supports during catalyst preparation.

### **1.2.3 X-ray absorption spectroscopy**

Even though IR spectroscopy and TPRD provide information about the nature of adsorption of the precursor and sometimes can indicate whether bimetallic particles are formed or not, such information is not quantitative. Techniques that can provide additional insightful information are X-ray absorption spectroscopy technique such as extended X-ray absorption fine structure (EXAFS) and X-ray absorption near edge structure (XANES) spectroscopy.

### 1.2.3.1 EXAFS spectroscopy

EXAFS refers to oscillatory structures which appear in the high energy side of characteristic X-ray absorption edges of elements (Koningsberger, Mojet, Dorssen, and Ramaker, 2000; Rehr and Albers, 2000; Vaarkamp and Koningsberger, 1997). It appears only when the absorbing atoms are in a condensed phase, and reflects the local structure around the atoms. Each element has its characteristic absorption energy in the X-ray region. When an atom absorbs an X-ray photon, a photoelectron emanates from the atom as an outgoing wave. If the atom is in a condensed phase, the photoelectron will be backscattered by surrounding atoms and interfere with the original wave (Figure 1.2a) (Niemantsverdriet, 2000). Constructive interference increases the wave amplitudes while destructive interference causes the amplitude to disappear as in Figure 1.2b.

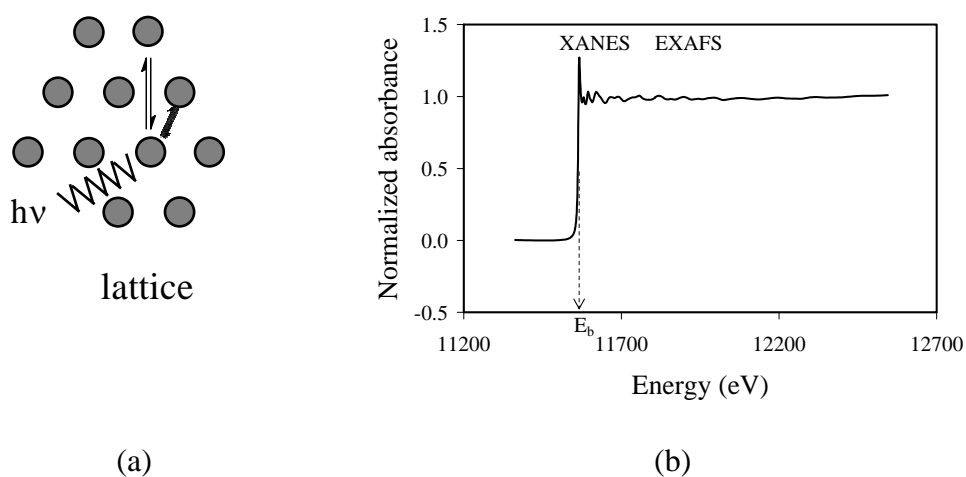


**Figure 1.2** Absorption of X-ray as a function of photon energy  $E = h\nu$  by atoms in a lattice (a) and the fine structure represents the EXAFS function and energy at near edge absorption representing XANES (b).

EXAFS as a tool for structural determination of various physical state including gases, liquids, solutions, amorphous solids, and crystalline solids (Zhang et al., 1999) has been used to determine the local structure of supported metal catalysts indicating whether metal-metal interactions occur or not after precursor is supported on a support. The data obtained from EXAFS are distance between absorbing atom and its surrounding coordination sphere, coordination number, identities of the absorber and its neighbors, and the dynamic and static disorder in the internuclear distances.

### **1.2.3.2 XANES spectroscopy**

XANES is another technique of X-ray absorption spectroscopy. When an atom is bombarded with high-energy photon beam at increasing energies until the energy of this incident beam nears the ionization energy of target atom, the absorption occurs and one electron is emitted. The energy of the absorption edge and the presence of “pre-edge features” from XANES provide information about the oxidation state and coordination geometry of the absorbing atom.

For example, the structure of Pt-Ru/carbon determined by XANES was predominant in the form of Pt and Ru oxides in their as-prepared state, and Pt/Ru had very different structure. After it had been utilized for methanol oxidation catalysis, XANES data indicated that the metal oxides were reduced to metals (O’Grady, Hagans, Pandya, and Maricle, 2001).

## **1.3 Catalytic activity test**

Catalytic performances of supported bimetallic catalysts depend on the state of the dispersion, structure, shape, composition and morphology of the metal particles,

as well as the metal-support interactions, which in many cases are not clearly understood. Supported bimetallic catalysts have been used in many catalytic reactions (e.g. naphtha reforming, alkene hydrogenation and CO hydrogenation, NO<sub>x</sub> conversion and alkane conversion). In this work, ethylene hydrogenation and *n*-butane hydrogenolysis were used to test catalytic activities of supported PtRu catalysts.

### 1.3.1 Ethylene hydrogenation test

Ethylene hydrogenation has been used for many years as a classical model reaction to understand the hydrogenation of olefins and aromatics (Neurock and van Santen, 2000). Hydrogenation of ethylene is a relatively simple and structural-insensitive reaction in which catalytic activity does not depend on particle size of active metals. There are at least three reaction mechanisms for ethylene hydrogenation that have been proposed, but much of the experimental evidence strongly supports the Horiuti-Polanyi mechanism (Neurock and van Santen, 2000). In the Horiuti-Polanyi mechanism that was proposed in 1934 by Polanyi and Horiuti, a hydrogen molecule dissociates on the metal surface and sequentially hydrogenates C<sub>2</sub>H<sub>4</sub> to C<sub>2</sub>H<sub>5</sub> and then C<sub>2</sub>H<sub>5</sub> to C<sub>2</sub>H<sub>6</sub> (Hwang, Yang, Zhu, Grunes, and Somorjai, 2003). It has been known that an ethylene molecule can adsorb on a metal surface, possibly forming three adsorbed species: (a)  $\pi$ -bonded ethylene; (b) di- $\sigma$ -bonded ethylene; and (c) ethylidyne, as shown in Figure 1.3 (Hwang et al., 2003).

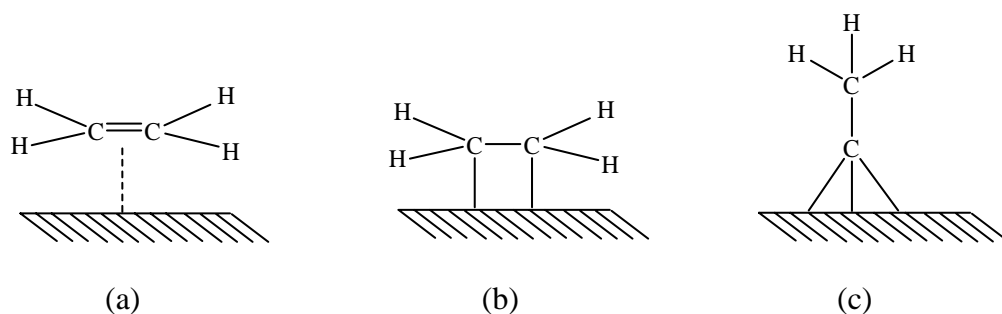


**Figure 1.3** The three surface structures of adsorbed ethylene on a metal surface: (a)  $\pi$ -bonded ethylene; (b) di- $\sigma$ -bonded ethylene; and (c) ethylidyne.

### 1.3.2 *n*-Butane hydrogenolysis test

Hydrogenolysis of light alkanes or rupture of C-C bonds by  $H_2$  such as in cyclopentane and *n*-butane is sensitive to the surface structure of metal particles, at least Pt particles on alumina; or in the other words, it is structure-sensitive (Leclercq, Leclercq, and Maurel, 1976; Passos, Schmal, and Vannice, 1996). Thus, hydrogenolysis of saturated hydrocarbons can be used as a test reaction to study the influence of surface structure of such catalysts. The single *n*-butane hydrogenolysis on supported catalysts can be expressed by the following two reactions:



However, in some cases, multiple hydrogenolysis can occur, giving high yields of methane product, and isomerization of *n*-butane can also take place giving *iso*-butane product (Jackson, Kelly, and Webb, 1998). *n*-Butane hydrogenolysis and

isomerization mechanisms on supported catalysts were proposed as in Figures 1.4 and 1.5, respectively (Bond and Lin, 1997).

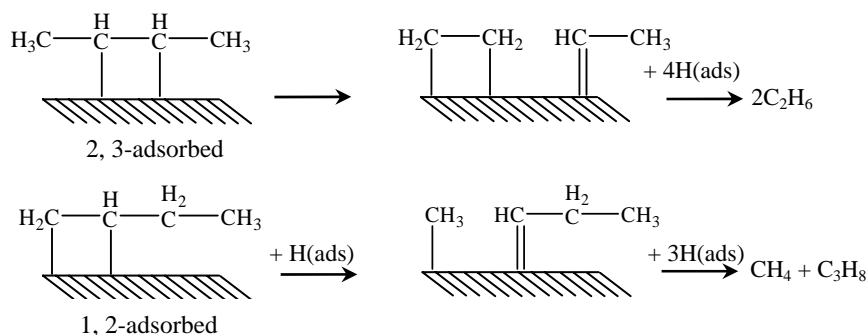


**Figure 1.4** Proposed mechanisms of *n*-butane hydrogenolysis reaction.

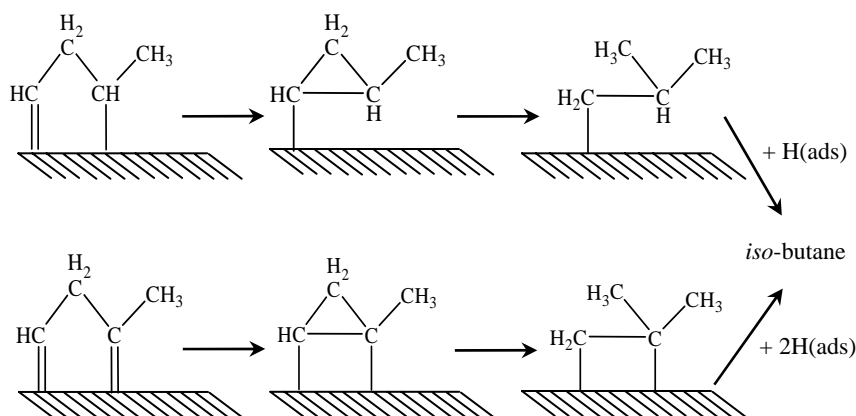


**Figure 1.5** Proposed mechanisms of *n*-butane isomerization reaction.

## 1.4 Research objectives

- 1.4.1 To prepared supported Pt-Ru catalysts from  $\text{Pt}_3\text{Ru}_6(\text{CO})_{21}(\mu_3\text{-H})(\mu\text{-H})_3$  and alternatively from a mixture of Pt and Ru compounds on oxide supports such as  $\gamma\text{-Al}_2\text{O}_3$ , MgO, and  $\text{TiO}_2$ .
- 1.4.2 To characterize the supported PtRu catalyst by IR and EXAFS spectroscopies.

- 1.4.3 To study the catalyst reduction temperature of supported Pt-Ru catalysts prepared from a mixture of metal salts by temperature-programmed reductive decomposition (TPRD).
- 1.4.4 To compare the catalytic performance of these catalysts for hydrogenation of ethylene and hydrogenolysis of *n*-butane.

## 1.5 Scope and limitations of study

The broad goals were to understand how to make extremely highly dispersed bimetallics in which two noble metals were bonded to each other and to understand how the catalytic properties of these material were different from those of conventional supported bimetallic catalysts.

Supported Pt-Ru catalysts were prepared by adsorption of  $\text{Pt}_3\text{Ru}_6(\text{CO})_{21}(\mu_3\text{-H})(\mu\text{-H})_3$  onto  $\gamma\text{-Al}_2\text{O}_3$ , MgO, and  $\text{TiO}_2$  and compared with those prepared from a mixed solution of Pt and Ru compounds supported on  $\gamma\text{-Al}_2\text{O}_3$  and MgO. The catalysts were characterized by techniques including TPRD and IR spectroscopy. Metal environments such as metal-metal and metal-support interaction including bond distances and coordination numbers were determined by EXAFS spectroscopy.

Catalytic performance of these catalysts was investigated in hydrogenation of ethylene and hydrogenolysis of *n*-butane. The results from catalytic characterization and catalytic performance obtained from each support were compared.

## CHAPTER II

# CHARACTERIZATION AND TESTING OF Pt-Ru/ $\gamma$ -Al<sub>2</sub>O<sub>3</sub> CATALYST PREPARED FROM Pt<sub>3</sub>Ru<sub>6</sub>(CO)<sub>21</sub>( $\mu$ -H)( $\mu$ -H)<sub>3</sub>

### 2.1 Introduction

This chapter is focused on preparation of supported PtRu catalyst on  $\gamma$ -Al<sub>2</sub>O<sub>3</sub> (PtRu/ $\gamma$ -Al<sub>2</sub>O<sub>3</sub>) by adsorption of Pt<sub>3</sub>Ru<sub>6</sub>(CO)<sub>21</sub>( $\mu$ -H)( $\mu$ -H)<sub>3</sub> on the alumina. Characterization of the initially adsorbed and the activated sample was intended to lead to a good understanding about the interactions between the cluster precursor and the support or between the resulting metal clusters and the support. The characterization results for PtRu/ $\gamma$ -Al<sub>2</sub>O<sub>3</sub> are compared with those for supported PtRu catalysts on MgO and on TiO<sub>2</sub> in Chapters III and IV, respectively. In addition, the catalytic activity of the catalyst was tested for ethylene hydrogenation and *n*-butane hydrogenolysis.

The  $\gamma$ -Al<sub>2</sub>O<sub>3</sub> powder is commercially available and widely used to support active metals in solid catalysts. It is inexpensive, has high surface area and high stability.  $\gamma$ -Al<sub>2</sub>O<sub>3</sub> is acid support consisting of Brønsted acid sites (-OH groups), Lewis acid sites (Al<sup>3+</sup>) and Lewis basic sites (O<sup>2-</sup>) on the surface.

### 2.1.1 Supported Pt catalysts incorporating another noble metal on $\gamma$ -Al<sub>2</sub>O<sub>3</sub>

Supported bimetallic Pt incorporating noble metal on  $\gamma$ -Al<sub>2</sub>O<sub>3</sub> has been prepared and tested for many applications. For instance, Pt-Rh/ $\gamma$ -Al<sub>2</sub>O<sub>3</sub> catalysts prepared by conventional incipient wetness impregnation were active for the reduction of NO by CO (Granger, Lecomte, Dathy, Leclercq, and Leclercq, 1998). For clean-fuel environment legislation, supported Pt-Pd/ $\gamma$ -Al<sub>2</sub>O<sub>3</sub> catalysts were also prepared by conventional incipient wetness impregnation and tested for hydrogenation of tetralin, naphthalene, and phenanthrene (Jongpatiwut et al., 2004).

### 2.1.2 $\gamma$ -Al<sub>2</sub>O<sub>3</sub>-supported Pt-Ru catalysts

Supported PtRu/ $\gamma$ -Al<sub>2</sub>O<sub>3</sub> catalysts could be prepared from conventional impregnation method by using a mixture of metal compounds such as H<sub>2</sub>PtCl<sub>6</sub> and RuCl<sub>3</sub> hydrate as precursors. Those were found to be active for methylcyclopentane hydrogenolysis and 2-methylpentane isomerization (Diaz, Garin, and Maire, 1983), and for dehydrogenation of cyclohexane (Miura, Osawa, Suzuki, Sugiyama, and Matsuda, 1982).

Recently, PtRu catalysts with high metal dispersion could be prepared from a metal carbonyl cluster as precursor. Alexeev et al. (2002) prepared supported PtRu/ $\gamma$ -Al<sub>2</sub>O<sub>3</sub> by adsorption of Pt<sub>2</sub>Ru<sub>4</sub>(CO)<sub>18</sub> from CH<sub>2</sub>Cl<sub>2</sub> onto  $\gamma$ -Al<sub>2</sub>O<sub>3</sub> and studied the cluster-support interaction. Results from IR and EXAFS spectroscopy indicated that the cluster precursor adsorbed intact on  $\gamma$ -Al<sub>2</sub>O<sub>3</sub> by hydrogen bonding. The metal core changed slightly on the  $\gamma$ -Al<sub>2</sub>O<sub>3</sub> after treatment in He flow at 300°C for 2 h to remove CO ligands. However, the cluster framework expanded as a result of the treatment.

### 2.1.3 Research goals

The goal of this work was to prepare highly dispersed supported PtRu catalyst on  $\gamma$ -Al<sub>2</sub>O<sub>3</sub> by adsorption of Pt<sub>3</sub>Ru<sub>6</sub>(CO)<sub>21</sub>( $\mu$ <sub>3</sub>-H)( $\mu$ -H)<sub>3</sub> from CH<sub>2</sub>Cl<sub>2</sub> onto  $\gamma$ -Al<sub>2</sub>O<sub>3</sub>. Properties of the supported bimetallic samples, especially the interactions between the cluster and support surface before and after ligand removal, were studied by IR and EXAFS spectroscopy. The nature of the adsorbed species and structural changes of the cluster precursor were also investigated. Activities of the bimetallic catalyst were tested for ethylene hydrogenation and *n*-butane hydrogenolysis. Results were compared with those of PtRu/ $\gamma$ -Al<sub>2</sub>O<sub>3</sub> catalysts prepared conventionally.

## 2.2 Experimental

### 2.2.1 Chemicals and materials

Organometallic syntheses, supported catalyst preparations and sample handling were performed under dry N<sub>2</sub> or Ar and samples were stored in an Ar drybox to minimize contact with moisture and air. Traces of O<sub>2</sub> and moisture in He, N<sub>2</sub> (Airgas, 99.99%), H<sub>2</sub> (Matheson, 99.999% or from a Balston H<sub>2</sub> generator, 99.99%), C<sub>2</sub>H<sub>4</sub> (Matheson, 99.5%), and *n*-C<sub>4</sub>H<sub>10</sub> (Airgas, 99.5%) used in catalyst treatment and testing were removed by passing each gas through traps containing reduced Cu/Al<sub>2</sub>O<sub>3</sub> and molecular sieve particles.

Powder  $\gamma$ -Al<sub>2</sub>O<sub>3</sub> (Degussa, BET surface area 100 m<sup>2</sup>/g) was mixed with deionized water to form a paste before drying overnight at 120°C. Prior to use, it was calcined or partially dehydroxylated in flowing O<sub>2</sub> at 400°C for 2 h followed by evacuation (pressure  $\approx 10^{-3}$  Torr) for 14 h at the same temperature. Organic solvents

for catalyst preparation such as *n*-hexane, *n*-pentane and toluene (Fisher Scientific) were distilled individually over Na/benzophenone and purged with dry N<sub>2</sub> to remove O<sub>2</sub>. Traces of moisture in dichloromethane (EMD, 99.96% purity) were removed by molecular sieve 4A, and O<sub>2</sub> was removed by purging with dry N<sub>2</sub> prior to use.

## 2.2.2 Synthesis of organometallic precursor

Pt<sub>3</sub>Ru<sub>6</sub>(CO)<sub>21</sub>(μ<sub>3</sub>-H)(μ-H)<sub>3</sub> was synthesized under dry N<sub>2</sub> and/or Ar by a procedure described by Adams and co-workers (1994) from a reaction between Pt<sub>2</sub>Ru<sub>4</sub>(CO)<sub>18</sub> and H<sub>2</sub> at 97°C and purified by washing with cold *n*-pentane. The cluster structure in CH<sub>2</sub>Cl<sub>2</sub> solution was confirmed by IR, <sup>1</sup>H and <sup>13</sup>C NMR spectroscopy. The detail of synthesis method is as follow.

### 2.2.2.1 Synthesis of starting material, Pt<sub>2</sub>Ru<sub>4</sub>(CO)<sub>18</sub>

Pt<sub>2</sub>Ru<sub>4</sub>(CO)<sub>18</sub> was prepared from a reaction between Ru(CO)<sub>5</sub> and Pt(cod)<sub>2</sub> in *n*-hexane (reaction 2.1). Ru(CO)<sub>5</sub> was obtained from photo degradation of Ru<sub>3</sub>(CO)<sub>12</sub>.



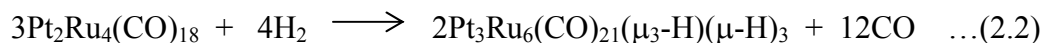
A 250 mg of Ru<sub>3</sub>(CO)<sub>12</sub> (Strem, 99%) was stirred until dissolved completely in 500 mL of *n*-hexane. The solution was then irradiated with medium-pressure mercury UV lamp (Hanovia, 450W medium pressure mercury lamp) under a slow flowing of carbon monoxide at room temperature. After the reaction was completed, the solution

color changed from orange to colorless (ca. 3 h). The colorless solution mainly contain  $\text{Ru}(\text{CO})_5$ .

The  $\text{Ru}(\text{CO})_5$  solution was cooled to  $0^\circ\text{C}$ , evacuated, and refilled with Ar three times to removed excess CO. The reaction flask was covered with aluminium foil to avoid light exposure during reaction. A solution of 75 mg of  $\text{Pt}(\text{cod})_2$  in 10 mL of  $\text{CH}_2\text{Cl}_2$  was quickly added in  $\text{Ru}(\text{CO})_5$  solution, and the solution mixture was stirred at  $0^\circ\text{C}$  for 30 min. During this period, the reaction flask was evacuated and refilled with Ar three more times. After 30 min, an additional solution of 50 mg  $\text{Pt}(\text{cod})_2$  in 10 mL of  $\text{CH}_2\text{Cl}_2$  was quickly added. The solution was stirred overnight and the temperature was allowed to increase to room temperature. When the solution color changed to purple, its volume was reduced to about 100 mL by evacuation. The bimetallic product was separated by column chromatography containing silica gel (Whatman) in a column dimension 25 mm x 500 mm. The first yellow band of unreacted  $\text{Ru}_3(\text{CO})_{12}$  was eluted by hexane while the purple band of  $\text{Pt}_2\text{Ru}_4(\text{CO})_{18}$  was eluted by a  $\text{CH}_2\text{Cl}_2$ /hexane (1/4 ratio) solvent mixture. After drying by evacuation,  $\text{Pt}_2\text{Ru}_4(\text{CO})_{18}$  product was dissolved in  $\text{CH}_2\text{Cl}_2$ /hexane (2/1 ratio) solvent mixture and crystallized by slow evaporation at  $10^\circ\text{C}$  to yield air-stable purple crystals. It was dissolved in  $\text{CH}_2\text{Cl}_2$  to characterize by IR spectroscopy.

#### 2.2.2.2 Synthesis of $\text{Pt}_3\text{Ru}_6(\text{CO})_{21}(\mu_3\text{-H})(\mu\text{-H})_3$

$\text{Pt}_3\text{Ru}_6(\text{CO})_{21}(\mu_3\text{-H})(\mu\text{-H})_3$  was synthesized from a reaction between  $\text{Pt}_2\text{Ru}_4(\text{CO})_{18}$  in *n*-heptane and  $\text{H}_2$  as described in reaction 2.2.



The  $\text{Pt}_2\text{Ru}_4(\text{CO})_{18}$  (25.0 mg) was dissolved in 140 mL of *n*-heptane and purged with  $\text{H}_2$  for 5 min. The mixture was slowly refluxed at  $97^\circ\text{C}$  and a slow flow of  $\text{H}_2$  (ca. 3-4 bubbles per second) was continued for about 15 min until the solution color changed from deep purple to black brown. Then the  $\text{H}_2$  flow was stopped and the mixture was cooled to  $50^\circ\text{C}$  in a water bath. The solution was filtered and the solvent was removed by evacuation. The solid product was scraped from the flask side by a spatula and washed many times with 5-mL portions of cold *n*-pentane until the washing solvent was colorless. The black solid product,  $\text{Pt}_3\text{Ru}_6(\text{CO})_{21}(\mu_3\text{-H})(\mu\text{-H})_3$ , was characterized by IR,  $^1\text{H}$ , and  $^{13}\text{C}$  NMR spectroscopy.

### 2.2.3 Preparation of supported catalyst

The supported Pt-Ru catalysts on  $\gamma\text{-Al}_2\text{O}_3$  were prepared by slurring  $\gamma\text{-Al}_2\text{O}_3$  with a solution of  $\text{Pt}_3\text{Ru}_6(\text{CO})_{21}(\mu_3\text{-H})(\mu\text{-H})_3$  in  $\text{CH}_2\text{Cl}_2$  for 1 day followed by evacuation ( $\approx 10^{-3}$  bar) for an additional 1 day to ensure complete uptake of the precursor by the support. The amount of chosen precursor gave sample containing 1.0 wt% Pt and 1.0 wt% Ru after ligand removal from precursor.

### 2.2.4 Extraction of adsorbed species

After the sample was dried by evacuation, recovery of the precursor was tested by extraction with  $\text{CH}_2\text{Cl}_2$  for approximately 30 min with stirring. The extract solution and extracted dry sample were characterized by IR spectroscopy.

## 2.2.5 PtRu catalyst activation

Dry sample containing adsorbed precursor was heated in He flow at 300°C for 2 h to remove ligands from the metal core. The process to remove carbonyl ligands is called decarbonylation. The resulting sample was characterized again by IR and EXAFS. Note that inert gas such as He was chosen for ligand removal to minimize cluster decomposition.

## 2.2.6 Precursor and catalyst characterization

### 2.2.6.1 IR spectroscopy

IR spectra of  $\text{Pt}_3\text{Ru}_6(\text{CO})_{21}(\mu_3\text{-H})(\mu\text{-H})_3$  in  $\text{CH}_2\text{Cl}_2$  and the dry supported sample, before and after ligand removal were recorded with a Bruker IFS-66v spectrometer with a resolution of  $4\text{ cm}^{-1}$ . Each sample was scanned 64 times and the signals were averaged. For the dry supported, a small amount of powder was pressed into a semitransparent wafer between KBr pellets placed in a cell in a glovebox. The liquid sample was transferred by a syringe into an IR cell equipped with valves to prevent contact with air and moisture.

### 2.2.6.2 $^1\text{H}$ , and $^{13}\text{C}$ NMR spectroscopy

$\text{Pt}_3\text{Ru}_6(\text{CO})_{21}(\mu_3\text{-H})(\mu\text{-H})_3$  was dissolved in acetone- $d_6$  and filtered to remove any precipitates. The clear, brown solution (6 ml) was transferred into an NMR tube and placed in an NMR spectrometer (Avance-500 spectrometer with proton frequency 500 MHz). The  $^1\text{H}$  NMR spectrum was recorded at  $-88^\circ\text{C}$ . Because this sample was not  $^{13}\text{C}$ -enriched, the  $^{13}\text{C}$  NMR spectrum was recorded at  $20^\circ\text{C}$  for 14 h.

### 2.2.6.3 EXAFS spectroscopy

EXAFS experiments were performed at the X-ray beamline X18B at the National Synchrotron Light Source (NSLS), Brookhaven National Laboratory (BNL), Upton, New York, USA. The storage ring energy was 2.5 GeV and the ring current was in the range 110-250 mA. For transmission EXAFS spectroscopy, 0.3 g of sample was pressed into self-supporting wafer in the Ar-filled glovebox at the synchrotron laboratory, and placed in a special designed XAS holder (Jentoft, Deutsch, and Gates, 1996). The cell was evacuated, installed at the beamline, and cooled to nearly liquid nitrogen temperature. The sample was scanned at the Pt L<sub>III</sub> edge (11564 eV) and at the Ru K edge (22117 eV) in transmission mode, with integration for 1 s at each energy in the range from 200 eV below each absorption edge to 975 eV beyond the edge. A double crystal monochromator Si(111) was used.

### 2.2.7 EXAFS data analysis

Because of the large difference in energy between the Pt L<sub>III</sub> edge (11564 eV) and the Ru K edge (22117 eV), EXAFS data were collected at individual Pt L<sub>III</sub> and Ru K absorption edge and analyzed with theoretical reference files. The EXAFS data processing was carried out with ATHENA software (Raval, computer program, 2003). The final normalized EXAFS function from ATHENA software for each edge of each sample was obtained from the average of four scans. Phase shift and backscattering amplitudes of Pt-Pt, Pt-Ru, Pt-O<sub>support</sub>, Ru-Ru, Ru-Pt, and Ru-O<sub>support</sub> interactions were calculated by FEFF7.0 software (Rehr, Mustre de leon, Zabinsky, and Albers, 1991). The EXAFS data fitting done by EXAFSPAK software (George, George, and Pickering, computer program, 2000) were accomplished with

single and multiple scattering paths calculated by FEFF7.0, and the EXAFS parameters were extracted from the raw data with the EXAFSPAK software. The fittings were done both in  $r$  space ( $r$  is interatomic distance from the absorber atom) and  $k$  space ( $k$  is the wave vector) with application of  $k^0$ ,  $k^1$ , and  $k^3$  weightings.

The EXAFS data of the dry supported sample scanned at the Pt L<sub>III</sub> edge were Fourier transformed over the ranges  $3.56 < k < 12.85$  with  $k^3$  weighting without phase correction and  $0.0 < r < 5.0$  Å.

The EXAFS data characterizing Pt<sub>3</sub>Ru<sub>6</sub>(CO)<sub>21</sub>(μ<sub>3</sub>-H)(μ-H)<sub>3</sub>/γ-Al<sub>2</sub>O<sub>3</sub> scanned at the Ru K edge were Fourier transformed over the ranges  $4.25 < k < 14.50$  and  $0.0 < r < 4.0$  Å. The statistically justified numbers of free parameters estimated from Nyquist theorem (Stern, 1993),  $n = (2\Delta k\Delta r/\pi) + 1$ , for the Pt L<sub>III</sub> and the Ru K edges of sample before ligand removal were about 31 and 27, respectively.

The EXAFS data characterizing the Pt-Ru/γ-Al<sub>2</sub>O<sub>3</sub> sample after treatment in He and scanned at the Pt L<sub>III</sub> edge were Fourier transformed over the ranges  $3.25 < k < 14.25$  and  $0.0 < r < 5.0$  Å. The EXAFS data characterizing this sample scanned at the Ru K edge were Fourier transformed over the ranges  $3.40 < k < 14.45$  and  $0.0 < r < 4.0$  Å. The statistically justified number of free parameters estimated from Nyquist theorem for the Pt L<sub>III</sub> and the Ru K edges of this sample were about 36 and 29, respectively.

### 2.2.8 Catalytic activity of PtRu/γ-Al<sub>2</sub>O<sub>3</sub> for ethylene hydrogenation

This study was carried out in a stainless steel U-tube flow reactor at atmospheric pressure. Prior to reaction testing, the sample was pretreated in He flow at 300°C for 2 h. The reactor held 10 to 20 mg of pretreated catalyst that was diluted

with 600 mg of inert nonporous  $\alpha$ -Al<sub>2</sub>O<sub>3</sub> and loaded into the reactor in an Ar-filled glovebox. The reactor was isolated from air and moisture and then moved to the catalytic testing apparatus. The reactor was cooled to the desired temperature with He flowing through it before a gas mixture of H<sub>2</sub>, C<sub>2</sub>H<sub>4</sub>, and the balance He was allowed to flow into it at a rate of 200 ml (NTP)/min. The effluent gas mixture was analyzed with an online gas chromatograph (Hewlett-Packard HP 6890) equipped with an Al<sub>2</sub>O<sub>3</sub> capillary column (50 m x 0.53 mm x 15.0 micron film thickness), and a flame ionization detector. The conditions in the reactor were as follow:  $P_{\text{H}_2} = 80$  Torr,  $P_{\text{C}_2\text{H}_4} = 40$  Torr, and temperature varied from -75 to -20°C.

### 2.2.9 Catalytic activity of PtRu/ $\gamma$ -Al<sub>2</sub>O<sub>3</sub> for *n*-butane hydrogenolysis

This test was performed with a quartz tube flow reactor at atmospheric pressure. Prior to reaction testing, sample was pretreated in He flow at 300°C for 2 h. In an Ar-filled glovebox, 25 to 30 mg of treated sample was diluted with inert nonporous  $\alpha$ -Al<sub>2</sub>O<sub>3</sub>, loaded into the reactor and isolated from air and moisture before being moved to the catalyst testing apparatus. The reactor was heated to the desired temperature with He flowing through it before the start of a flow of a gas mixture containing H<sub>2</sub>, *n*-C<sub>4</sub>H<sub>10</sub>, and balance He at a rate of 100 ml (NTP)/min. The effluent gas mixture was analyzed with the online gas chromatograph equipped with an Al<sub>2</sub>O<sub>3</sub> capillary column (50 m x 0.53 mm x 15.0 micron film thickness) and a flame ionization detector. Testing conditions were as follow:  $P_{\text{H}_2} = 540$  Torr,  $P_{n\text{-C}_4\text{H}_{10}} = 60$  Torr, and temperature varied from 190 to 260°C.

## 2.3 Results and discussion

### 2.3.1 Characterization of $\text{Pt}_3\text{Ru}_6(\text{CO})_{21}(\mu_3\text{-H})(\mu\text{-H})_3$

A solution of  $\text{Pt}_3\text{Ru}_6(\text{CO})_{21}(\mu_3\text{-H})(\mu\text{-H})_3$  in  $\text{CH}_2\text{Cl}_2$  showed IR peaks in the  $\nu_{\text{CO}}$  range at 2106 (w, sh), 2081 (m), 2065 (s), 2048 (m), and 2023 (w)  $\text{cm}^{-1}$ , similar to values from literature (Adams et al., 1994) which were 2081 (w, sh), 2066 (vs), 2052 (m, sh), 2026 (w)  $\text{cm}^{-1}$ .

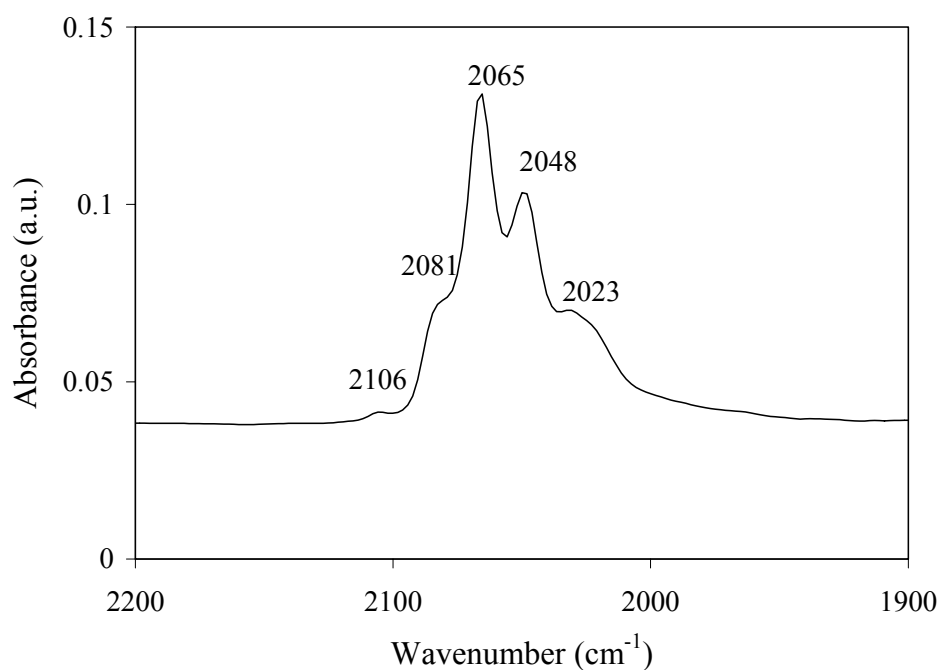


**Figure 2.1** IR spectrum of  $\text{Pt}_3\text{Ru}_6(\text{CO})_{21}(\mu_3\text{-H})(\mu\text{-H})_3$  dissolved in  $\text{CH}_2\text{Cl}_2$ .

The  $^1\text{H}$  NMR spectrum of  $\text{Pt}_3\text{Ru}_6(\text{CO})_{21}(\mu_3\text{-H})(\mu\text{-H})_3$  dissolved in acetone- $d_6$  was recorded at  $-88^\circ\text{C}$  to slow down a facile exchange process of hydride ligands. According to Adams's work, the resonances of bridging hydride ligands are not observed at  $25^\circ\text{C}$  in the  $^1\text{H}$  NMR spectrum. The  $^1\text{H}$  NMR spectrum at  $-88^\circ\text{C}$  in Figure 2.2 shows resonances at  $\delta$  -15.84 and -19.28 ppm corresponding to three ligands

$\mu$ -H and one  $\mu_3$ -H ligand, respectively. The ratio of  $^1\text{H}$  NMR intensity at  $\delta$  -15.84 and -19.28 ppm was 3/1 as expected for  $\mu$ -H and  $\mu_3$ -H. The  $^{13}\text{C}$  NMR spectrum of  $\text{Pt}_3\text{Ru}_6(\text{CO})_{21}(\mu_3\text{-H})(\mu\text{-H})_3$  dissolved in acetone- $d_6$  was measured at  $20^\circ\text{C}$  for 16 h. Because this compound was not prepared from enriched  $^{13}\text{C}$ O, the measurement period was longer than that of the sample prepared from enriched  $^{13}\text{C}$ O. Figure 2.3 indicates CO ligands at  $\delta$  190.28 ppm. According to Adams's work, the  $^{13}\text{C}$  NMR spectrum at  $\delta$  190.28 ppm corresponded to dynamically averaged CO ligands in  $\text{Pt}_3\text{Ru}_6(\text{CO})_{21}(\mu_3\text{-H})(\mu\text{-H})_3$ .

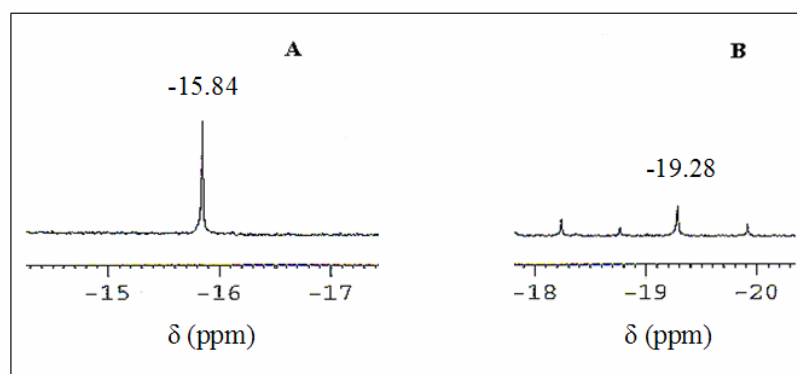


**Figure 2.2**  $^1\text{H}$  NMR spectrum of  $\text{Pt}_3\text{Ru}_6(\text{CO})_{21}(\mu_3\text{-H})(\mu\text{-H})_3$  dissolved in acetone- $d_6$  recorded at  $-88^\circ\text{C}$ : (A)  $\delta = 15$  to  $17$  ppm; (B)  $\delta = -18$  to  $-20$  ppm.

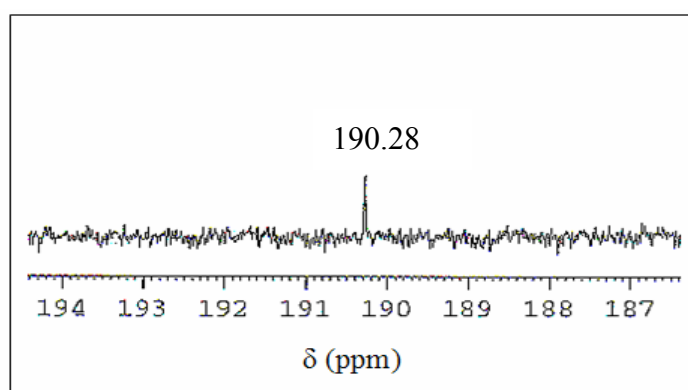


**Figure 2.3**  $^{13}\text{C}$  NMR spectrum of  $\text{Pt}_3\text{Ru}_6(\text{CO})_{21}(\mu_3\text{-H})(\mu\text{-H})_3$  dissolved in acetone- $d_6$  recorded at  $20^\circ\text{C}$ .

### 2.3.2 IR and EXAFS evidence of interactions between cluster precursor and $\gamma\text{-Al}_2\text{O}_3$

The chemistry of interactions between metal carbonyl clusters and  $\gamma\text{-Al}_2\text{O}_3$  is complex and depends on nature of the metal cluster and the chemistry of the support (Alexeev et al., 2002; Guzzi and Beck, 1988). The cluster-support interaction can be characterized by IR and EXAFS spectroscopy by observing the shift of  $\nu_{\text{OH}}$  of the support and  $\nu_{\text{CO}}$  of the precursor.

IR bands of bare  $\gamma\text{-Al}_2\text{O}_3$  in the  $\nu_{\text{OH}}$  region were observed at 3786 (w), 3728 (m), 3672 (m), and 3575 (s)  $\text{cm}^{-1}$  (spectrum 1 in Figure 2.4A). The first three IR bands were assigned to different types of isolated hydroxyl groups and the peak at 3575  $\text{cm}^{-1}$  represents hydrogen-bonded OH groups (Knözinger and Ratnasamy, 1978; Mestl and Knözinger 1997). The bands of alumina containing adsorbed species in the  $\nu_{\text{OH}}$  region were observed at 3679 (m) and 3587 (m)  $\text{cm}^{-1}$  (spectrum 2 in Figure 2.4A). The broad peak at 3587  $\text{cm}^{-1}$  also represents hydrogen-bonded OH groups.

After adsorption of  $\text{Pt}_3\text{Ru}_6(\text{CO})_{21}(\mu_3\text{-H})(\mu\text{-H})_3$  (confirmed by IR and  $^1\text{H}$  NMR spectroscopy) from  $\text{CH}_2\text{Cl}_2$ , onto  $\gamma\text{-Al}_2\text{O}_3$  and drying by evacuation, the IR band characterizing hydrogen-bonded OH group at 3575  $\text{cm}^{-1}$  shifted to 3587  $\text{cm}^{-1}$  and its intensity decreased, as shown in Figure 2.4A. The changes in intensity of hydroxyl peaks in the  $\nu_{\text{OH}}$  region indicated that these groups were involved in the interaction with the cluster.

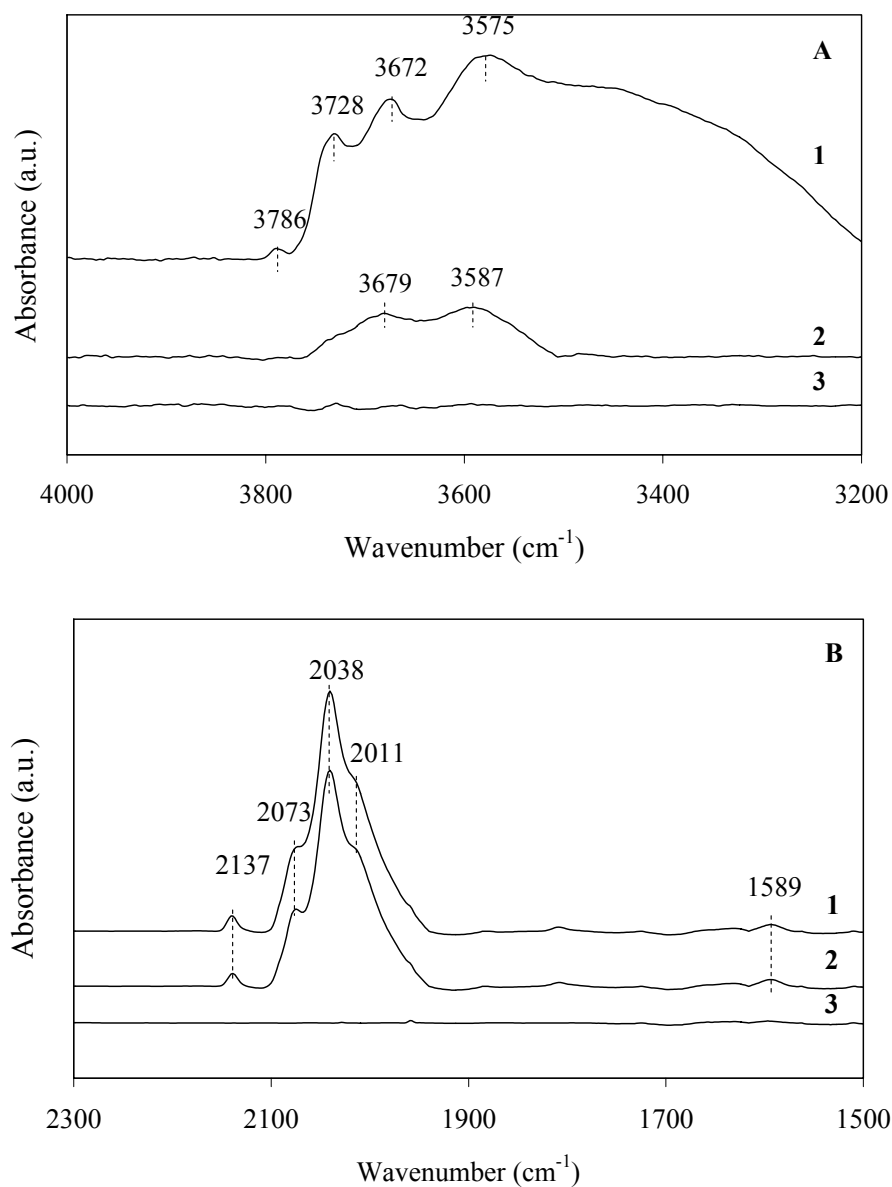


**Figure 2.4** (A) IR spectrum in  $\nu_{\text{OH}}$  region: (1) Calcined  $\gamma\text{-Al}_2\text{O}_3$ ; (2) dry sample prepared from  $\text{Pt}_3\text{Ru}_6(\text{CO})_{21}(\mu_3\text{-H})(\mu\text{-H})_3$  on  $\gamma\text{-Al}_2\text{O}_3$ ; (3) sample after ligand removal in He flow at 300°C for 2 h. (B) IR spectra in  $\nu_{\text{CO}}$  region: (1)  $\text{Pt}_3\text{Ru}_6(\text{CO})_{21}(\mu_3\text{-H})(\mu\text{-H})_3$  adsorbed on  $\gamma\text{-Al}_2\text{O}_3$  after removal of solvent; (2) dry supported sample after extraction with  $\text{CH}_2\text{Cl}_2$ ; (3) sample after ligand removal in He flow at 300°C for 2 h.

In general, IR bands of carbonyl ligands of supported metal carbonyl clusters differ from those of the cluster in solid or solution due to cluster-support interactions (Alexeev et al., 2002). Bands in  $\nu_{\text{CO}}$  region which were characteristic of the precursor in  $\text{CH}_2\text{Cl}_2$  at 2081 (w, sh), 2065 (vs), 2048 (m), and 2023 (sh)  $\text{cm}^{-1}$  shifted to 2073 (w, sh), 2038 (vs) and 2011 (w, sh)  $\text{cm}^{-1}$ , respectively. A small broad IR band at 1589  $\text{cm}^{-1}$  was detected (spectrum 1 in Figure 2B). The band at 2073 (w, sh)  $\text{cm}^{-1}$  is assigned to  $\text{Pt}^0\text{-CO}$  which was reported at 2100-2060  $\text{cm}^{-1}$  (Hadjiivanov and Vayssilov, 2002). The strong band at 2038  $\text{cm}^{-1}$  was assigned to linear M-CO species (where M in this work are Pt or Ru). There was no bridging CO band, which typically occurs at about 1850  $\text{cm}^{-1}$  for CO adsorbed on metal platinum (Hadjiivanov, 1998). The band at 2137  $\text{cm}^{-1}$  was observed in the supported sample both before and after extraction, possibly from carbonyl ligands of bimetallic carbonyl clusters. This peak could be assigned to  $\text{Pt}^{2+}\text{-CO}$  or  $\text{Pt}^+\text{-CO}$  which was observed at 2135-2110  $\text{cm}^{-1}$ . In addition, these four peaks could also be assigned to  $\text{Ru}^{n+}(\text{CO})_3$  on  $\text{Al}_2\text{O}_3$  (Hadjiivanov and Vayssilov, 2002; Asakura et al., 1990).

Comparing with IR spectrum of cluster solution in  $\text{CH}_2\text{Cl}_2$ , the IR bands of CO ligands of the adsorbed precursor on  $\gamma\text{-Al}_2\text{O}_3$  shifted to lower frequency (spectrum 1 in Figure 2.4B), indicating that carbonyl ligands were involved in the cluster-support interaction. The shifts to lower frequency implied that C-O bonds became weaker due to interactions between carbonyl oxygen with support, possibly by hydrogen bonding with alumina hydroxyl groups and bonding with  $\text{Al}^{3+}$  Lewis acid sites. A small, broad IR band was observed at 1589  $\text{cm}^{-1}$  indicating coordination between metal-bound CO ligands of the precursor and surface  $\text{Al}^{3+}$  ions on  $\gamma\text{-Al}_2\text{O}_3$ .

Therefore, IR data in Figure 2.4 imply that the interaction between precursor and support occurred through CO ligands and the support surface. Although the cluster  $\text{Pt}_3\text{Ru}_6(\text{CO})_{21}(\mu_3\text{-H})(\mu\text{-H})_3$  was probably not intact after the adsorption on  $\gamma\text{-Al}_2\text{O}_3$ , the IR evidence from IR data indicated that adsorbed species was still in the form of metal carbonyl cluster. However, hydrides could not be detected by IR spectroscopy. The loss of hydrides possibly took place during adsorption and drying resulting in changes in average Ru-Ru bond distance (see EXAFS results and discussion).

After adsorption and drying, only a small amount of the adsorbed precursor could be extracted back with  $\text{CH}_2\text{Cl}_2$  solvent. Only trace of the IR spectrum of metal carbonyl species in  $\nu_{\text{CO}}$  region at 2065 (s), 2046 (sh) and 2031 (sh)  $\text{cm}^{-1}$  (Figure 2.5) which was similar to that of the cluster precursor was observed in the extract solution. This result indicated that some of the cluster did not decompose on the alumina support after adsorption. In addition, the IR spectrum of dry sample was similar to that of fresh sample before the extraction (Figure 2.4B), which confirmed that the cluster precursor chemisorbed and was stable on this support.

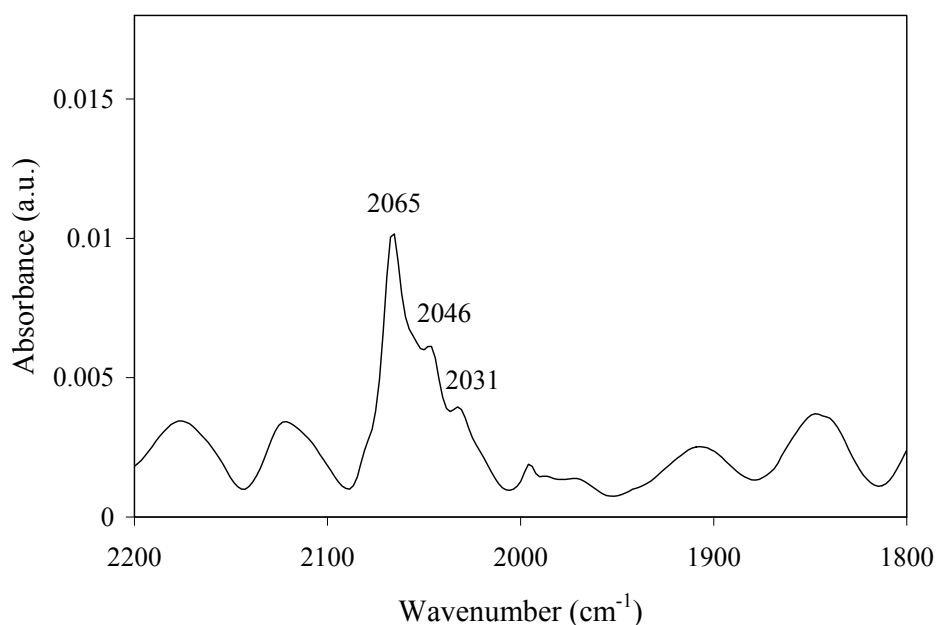


**Figure 2.5** IR spectrum in  $\nu_{\text{CO}}$  region of  $\text{CH}_2\text{Cl}_2$  extract solution from the supported sample.

After adsorption and extraction with  $\text{CH}_2\text{Cl}_2$  and drying, IR peak of the solvent were not observed, indicating that adsorbed  $\text{CH}_2\text{Cl}_2$  was negligible and should not compete with the cluster adsorption. Note that  $\text{CH}_2\text{Cl}_2$  was chosen for extraction because it was a good solvent for the cluster. These results also suggested that the interaction of the adsorbed surface species with the solvent was weaker than that of adsorbed species with the surface of the support. This result indicated strong cluster-support interaction which was probably responsible to changes observed in the precursor structure after adsorption.

Furthermore, the IR spectrum of the dried sample after extraction by slurry the freshly prepared sample with  $\text{CH}_2\text{Cl}_2$  for approximately 30 minutes showed peak positions similar to those of the freshly prepared sample, indicating that the adsorbed species were stable upon extraction, it was not possible to extract the adsorbed species

by this solvent. Only low absorbance of  $\nu_{\text{CO}}$  band of adsorbed species in extract solution was observed at 2065 (s), 2046 (m, sh), and 2031 (w, sh)  $\text{cm}^{-1}$  (Figure 2.5), indicating that only a small amount of adsorbed species was presented in the extract solution. This observation was a good sign for preparation of supported Pt-Ru because strong cluster-support interaction would lead to good dispersion of metal particles after ligand removal. Strong cluster-support interaction could also prevent aggregation of metal particles. This evidence could be further elaborated in the EXAFS results, as described below.

In conclusion, upon adsorption,  $\text{Pt}_3\text{Ru}_6(\text{CO})_{21}(\mu_3\text{-H})(\mu\text{-H})_3$  or related species interacted strongly with the  $\gamma\text{-Al}_2\text{O}_3$  support. The adsorbed species were still metal carbonyls and were stable during the studied period.

The extraction of the adsorbed cluster species was easier when the smaller cluster  $\text{Pt}_2\text{Ru}_4(\text{CO})_{18}$  was used as a precursor (Alexeev et al., 2002). The majority of  $\text{Pt}_2\text{Ru}_4(\text{CO})_{18}$  could be extracted intact from the  $\gamma\text{-Al}_2\text{O}_3$  support by  $\text{CH}_2\text{Cl}_2$ , and only trace of the cluster remained on the support. Thus, the cluster only adsorbed physically on alumina and its interaction with  $\text{CH}_2\text{Cl}_2$  was stronger than that with the alumina support. This might be the reason of the aggregation tendency of metal particles observed after ligand removal.

To determine the strength of interaction between the cluster metal core with oxygen atom of the support, it would be worthwhile to find out whether the cluster metal core is saturated or not in term of coordination. This could be done by considering number of valence electrons in the metal core. Although  $\text{Pt}_2\text{Ru}_4(\text{CO})_{18}$  and  $\text{Pt}_3\text{Ru}_6(\text{CO})_{21}(\mu_3\text{-H})(\mu\text{-H})_3$  have the same Pt:Ru ratio, they are different in the degree of saturation of the metal core. The metal core of the former has 88 valence

electrons, lower than the value predicted by the polyhedral skeletal electron pair theory (i.e., 90 electrons) (Adams et al., 1993). The lower number of electrons indicates that the metal core of  $\text{Pt}_2\text{Ru}_4(\text{CO})_{18}$  is not coordinatively saturated and can interact with electron donor groups. However, the metal-oxygen interaction is still presented by carbonyl ligands.

On the other hand, the metal core of the latter cluster, mainly used in this work, has 124 valence electrons, identical to the predicted number from the polyhedral skeletal electron pair theory (Adams et al., 1994). Thus, the metal core of  $\text{Pt}_3\text{Ru}_6(\text{CO})_{21}(\mu_3\text{-H})(\mu\text{-H})_3$  is coordinatively saturated and was expected to have weaker interaction with oxygen of  $\gamma\text{-Al}_2\text{O}_3$  than the former cluster. The interaction between the metal core of the precursor and oxygen atoms of support could be confirmed by EXAFS spectroscopy, as described below.

The EXAFS data were averaged by ATHENA software and analyzed by EXAFSPAK software with phase shift and backscattering amplitudes calculated by FEFF7.0. The EXAFS spectra of sample formed by adsorption of  $\text{Pt}_3\text{Ru}_6(\text{CO})_{21}(\mu_3\text{-H})(\mu\text{-H})_3$  on  $\gamma\text{-Al}_2\text{O}_3$  scanned at the Pt  $L_{\text{III}}$  and the Ru K edge are shown in Figures 2.6 and 2.7, respectively. The EXAFS parameters determined in the fit are summarized in Table 2.1. The estimated accuracies of coordination number ( $N$ ), distance ( $R$ ), Debye-Waller factor ( $\Delta\sigma^2$ ), and inner potential correction ( $\Delta E_0$ ) are as follows:  $\pm 20\%$ ,  $\pm 1\%$ ,  $\pm 30\%$ ,  $\pm 10\%$ , respectively.

**Table 2.1** Summary of EXAFS data of sample formed by adsorption of  $\text{Pt}_3\text{Ru}_6(\text{CO})_{21}(\mu_3\text{-H})(\mu\text{-H})_3$  on  $\gamma\text{-Al}_2\text{O}_3$  before ligand removal

Edge	Shell	$N$	$R$ (Å)	$10^3 \times \Delta\sigma^2$ (Å <sup>2</sup> )	$\Delta E_o$ (eV)
Pt L <sub>III</sub>	Pt-Pt	$2.2 \pm 0.1$	$2.68 \pm 0.01$	$6.4 \pm 0.3$	$2.7 \pm 0.1$
	Pt-Ru	$3.9 \pm 0.1$	$2.95 \pm 0.01$	$6.9 \pm 0.1$	$-8.2 \pm 0.1$
	Pt-CO				
	Pt-C	$0.8 \pm 0.1$	$1.85 \pm 0.01$	$-0.1 \pm 0.4$	$6.2 \pm 0.3$
	Pt-O*	$0.8 \pm 0.1$	$3.09 \pm 0.01$	$-10.9 \pm 0.1$	$10.6 \pm 0.2$
	Pt-O <sub>support</sub>				
	Pt-O <sub>s</sub>	$1.8 \pm 0.1$	$2.55 \pm 0.01$	$0.7 \pm 0.2$	$-0.6 \pm 0.1$
	Pt-O <sub>l</sub>	$2.3 \pm 0.1$	$3.05 \pm 0.01$	$-7.3 \pm 0.1$	$19.2 \pm 0.1$
Ru K	Ru-Ru	$1.9 \pm 0.1$	$2.83 \pm 0.01$	$12.5 \pm 0.6$	$7.1 \pm 0.2$
	Ru-Pt	$2.0 \pm 0.1$	$2.95 \pm 0.01$	$7.0 \pm 0.5$	$9.9 \pm 0.3$
	Ru-CO				
	Ru-C	$3.1 \pm 0.1$	$1.88 \pm 0.01$	$3.8 \pm 0.2$	$-4.3 \pm 0.3$
	Ru-O*	$3.1 \pm 0.1$	$3.00 \pm 0.01$	$1.6 \pm 0.3$	$-1.4 \pm 0.2$
	Ru-O <sub>support</sub>				
	Ru-O <sub>s</sub>	$1.4 \pm 0.1$	$2.34 \pm 0.01$	$9.3 \pm 0.7$	$12.3 \pm 0.2$
	Ru-O <sub>l</sub>	$0.6 \pm 0.1$	$3.40 \pm 0.01$	$-2.1 \pm 1.2$	$16.2 \pm 0.5$

Notation: subscript s and l refer to short and long, respectively.

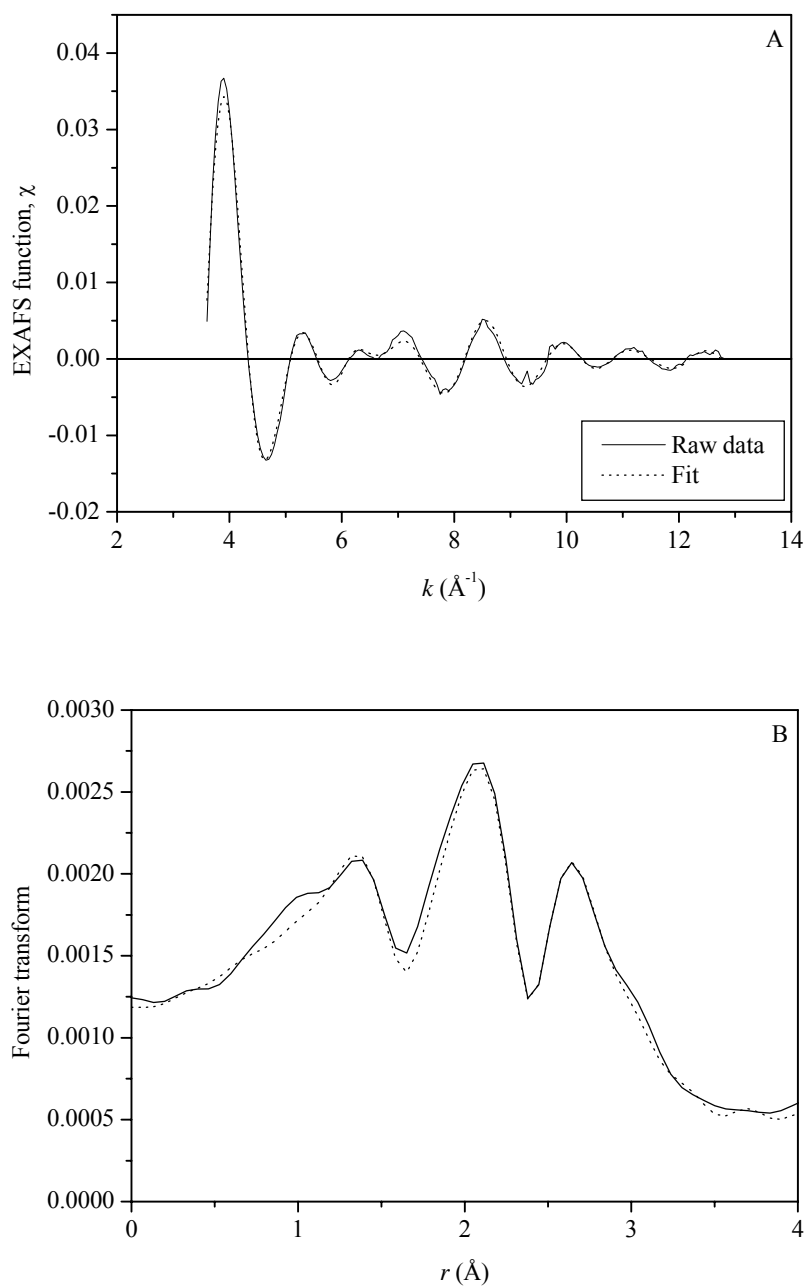


**Figure 2.6** EXAFS results scanned at the Pt  $L_{III}$  edge characterizing the adsorbed  $\text{Pt}_3\text{Ru}_6(\text{CO})_{21}(\mu_3\text{-H})(\mu\text{-H})_3$  on  $\gamma\text{-Al}_2\text{O}_3$ : (A) Experimental EXAFS function (solid line) and sum of the calculated Pt-Pt, Pt-Ru, Pt-C, Pt-O\*, Pt-O<sub>s</sub>, and Pt-O<sub>l</sub> contributions (dotted line). (B) Magnitude of uncorrected Fourier transform ( $k^0$  weighted) of experimental EXAFS function (solid line) and sum of the calculated Pt-Pt, Pt-Ru, Pt-C, Pt-O\*, Pt-O<sub>s</sub>, and Pt-O<sub>l</sub> contributions (dotted line).

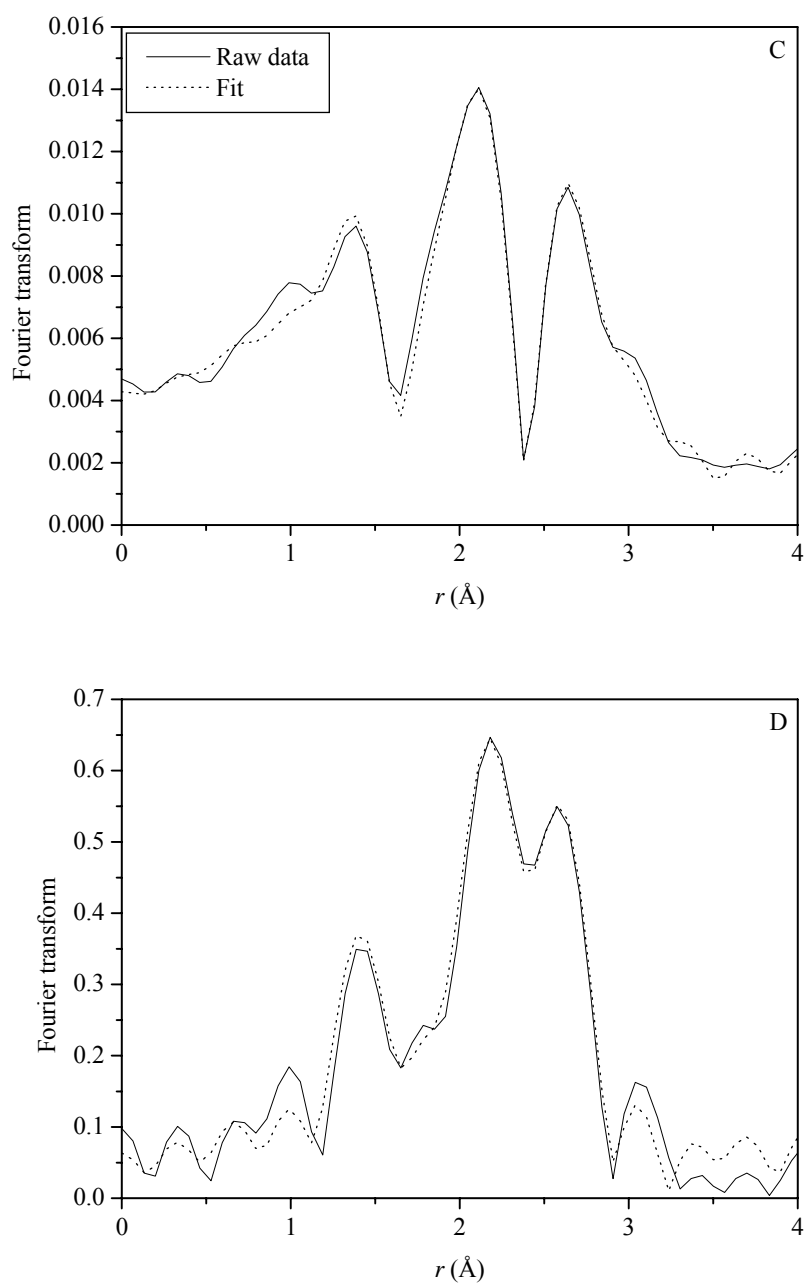


**Figure 2.6** (continued) EXAFS results scanned at the Pt  $L_{III}$  edge characterizing the adsorbed  $\text{Pt}_3\text{Ru}_6(\text{CO})_{21}(\mu_3\text{-H})(\mu\text{-H})_3$  on  $\gamma\text{-Al}_2\text{O}_3$ : (C) Magnitude of uncorrected Fourier transform ( $k^l$  weighted) of experimental EXAFS function (solid line) and sum of the calculated Pt-Pt, Pt-Ru, Pt-C, Pt-O\*, Pt-O<sub>s</sub>, and Pt-O<sub>l</sub> contributions (dotted line). (D) Magnitude of uncorrected Fourier transform ( $k^3$  weighted) of experimental EXAFS function (solid line) and sum of the calculated Pt-Pt, Pt-Ru, Pt-C, Pt-O\*, Pt-O<sub>s</sub>, and Pt-O<sub>l</sub> contributions (dotted line).

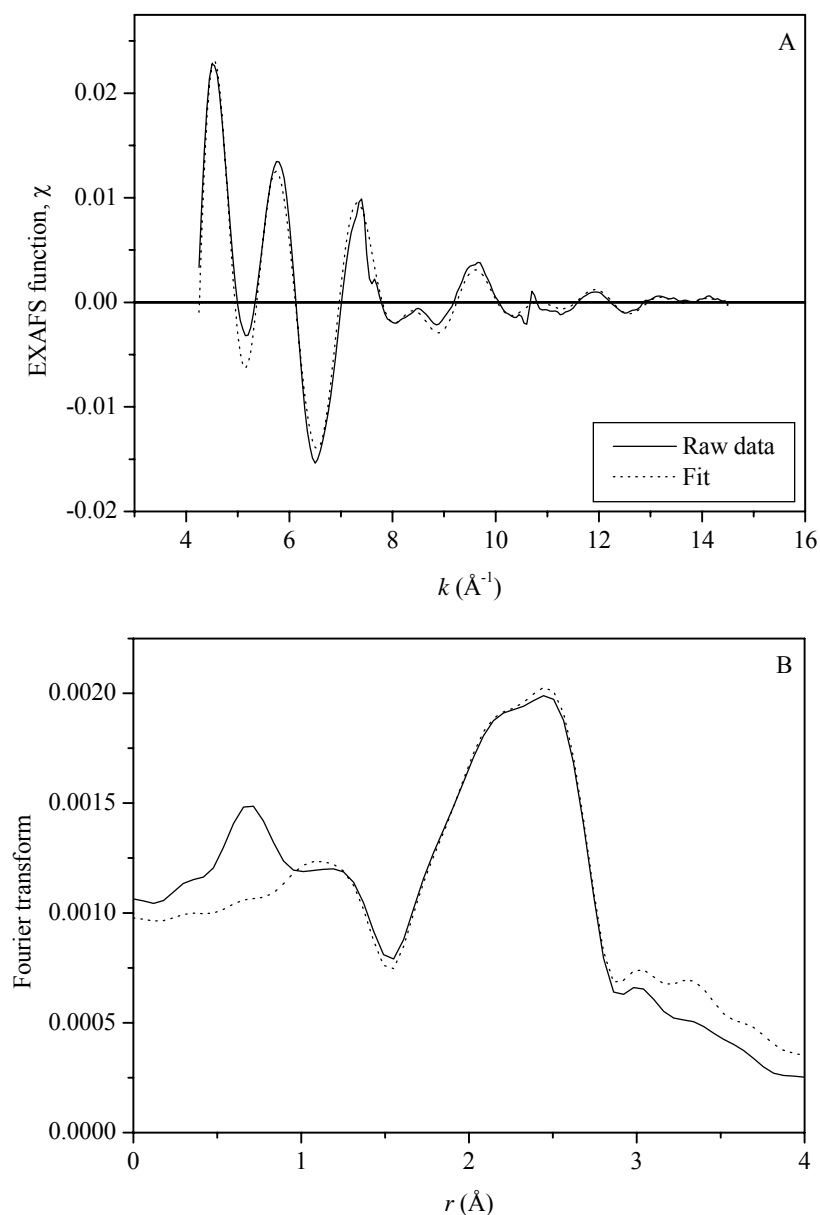


**Figure 2.7** EXAFS results scanned at the Ru K edge characterizing the adsorbed Pt<sub>3</sub>Ru<sub>6</sub>(CO)<sub>21</sub>(μ<sub>3</sub>-H)(μ-H)<sub>3</sub> on γ-Al<sub>2</sub>O<sub>3</sub>: (A) Experimental EXAFS function (solid line) and sum of the calculated Ru-Ru, Ru-Pt, Ru-C, Ru-O\*, Ru-O<sub>s</sub>, and Ru-O<sub>l</sub> contributions (dotted line). (B) Magnitude of uncorrected Fourier transform ( $k^0$  weighted) of experimental EXAFS function (solid line) and sum of the calculated Ru-Ru, Ru-Pt, Ru-C, Ru-O\*, Ru-O<sub>s</sub>, and Ru-O<sub>l</sub> contributions (dotted line).

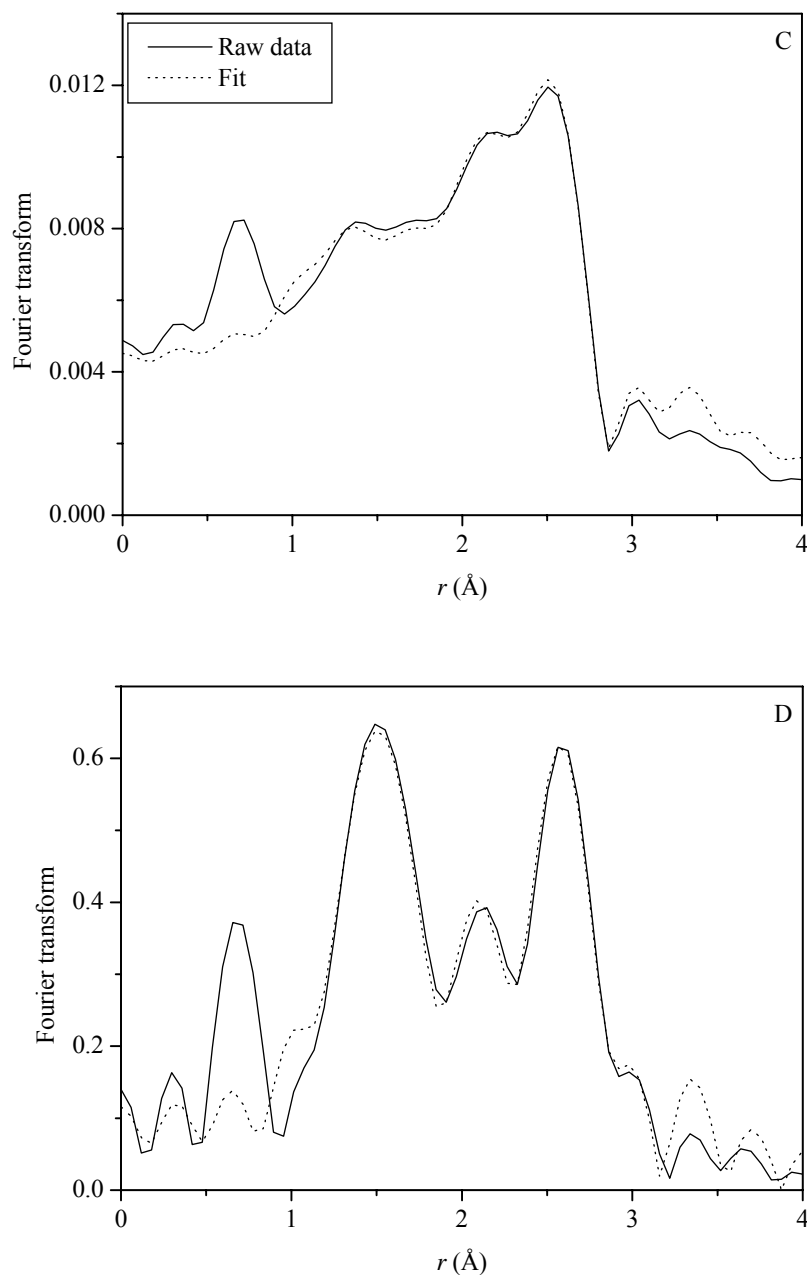


**Figure 2.7** (continued) EXAFS results scanned at the Ru K edge characterizing the adsorbed  $\text{Pt}_3\text{Ru}_6(\text{CO})_{21}(\mu_3\text{-H})(\mu\text{-H})_3$  on  $\gamma\text{-Al}_2\text{O}_3$ : (C) Magnitude of uncorrected Fourier transform ( $k^1$  weighted) of experimental EXAFS function (solid line) and sum of the calculated Ru-Ru, Ru-Pt, Ru-C, Ru-O\*, Ru-O<sub>s</sub>, and Ru-O<sub>l</sub> contributions (dotted line). (D) Magnitude of uncorrected Fourier transform ( $k^3$  weighted) of experimental EXAFS function (solid line) and sum of the calculated Ru-Ru, Ru-Pt, Ru-C, Ru-O\*, Ru-O<sub>s</sub>, and Ru-O<sub>l</sub> contributions (dotted line).

The EXAFS fitting parameters of adsorbed  $\text{Pt}_3\text{Ru}_6(\text{CO})_{21}(\mu_3\text{-H})(\mu\text{-H})_3$  on  $\gamma\text{-Al}_2\text{O}_3$  after evacuation (Table 2.1) indicate average distances and coordination number of  $\text{M-O}_{\text{support}}$  ( $\text{M-O}_s$  and  $\text{M-O}_l$ ) (M in this work refer to Pt and Ru) and changes in average distances and coordination numbers of M-CO bond. The interactions between metal and oxygen on support lead to structural change of adsorbed clusters.

For interaction with the nearest oxygen atom of alumina support when  $\text{Pt}_3\text{Ru}_6(\text{CO})_{21}(\mu_3\text{-H})(\mu\text{-H})_3$  was a precursor, the average Pt- $\text{O}_s$  distance was  $2.55 \pm 0.01$  Å with coordination number  $1.8 \pm 0.1$  and the average Ru- $\text{O}_s$  distance was  $2.34 \pm 0.01$  Å with coordination number  $1.4 \pm 0.1$ . Both average distances are longer than  $2.26 \pm 0.01$  and  $2.13 \pm 0.01$  Å for Pt- $\text{O}_s$  and Ru- $\text{O}_s$  reported when  $\text{Pt}_2\text{Ru}_4(\text{CO})_{18}$  was a precursor. This observation agreed with the degree of saturation of metal core based on electron counting, namely, coordinatively saturated metal core had weaker interaction with alumina oxygen. In addition, the distances between metal and the support oxygen were long because metal atoms were still stabilized and blocked by carbonyl ligands. By removal of blocking carbonyls, the M- $\text{O}_s$  distances were expected to become shorter.

Moreover, the average Pt- $\text{O}_s$  and Ru- $\text{O}_s$  distances when  $\text{Pt}_3\text{Ru}_6(\text{CO})_{21}(\mu_3\text{-H})(\mu\text{-H})_3$  was a precursor were longer than that on other supported catalysts which were found in the range 2.1-2.2 Å (Koningsberger and Gates, 1992). Although the  $\text{M-O}_{\text{support}}$  interaction was not strong, the precursor could also interact with  $\gamma\text{-Al}_2\text{O}_3$  support through carbonyl groups when the carbonyl oxygen interact with either hydroxyl protons or  $\text{Al}^{3+}$  acid sites of  $\gamma\text{-Al}_2\text{O}_3$ . The expansion of C-O bonds were expected and this would result in long distance of Pt-O\*.

Comparison XRD data of crystalline precursor (Adams et al., 1994) and EXAFS data of adsorbed  $\text{Pt}_3\text{Ru}_6(\text{CO})_{21}(\mu_3\text{-H})(\mu\text{-H})_3$  on  $\gamma\text{-Al}_2\text{O}_3$  was shown in Table 2.2.

**Table 2.2** Comparison XRD data of crystalline  $\text{Pt}_3\text{Ru}_6(\text{CO})_{21}(\mu_3\text{-H})(\mu\text{-H})_3$  (Adams et al., 1994) and EXAFS data of this cluster adsorbed on  $\gamma\text{-Al}_2\text{O}_3$

Shell	XRD data of		EXAFS data of adsorbed	
	$\text{Pt}_3\text{Ru}_6(\text{CO})_{21}(\mu_3\text{-H})(\mu\text{-H})_3$		$\text{Pt}_3\text{Ru}_6(\text{CO})_{21}(\mu_3\text{-H})(\mu\text{-H})_3$ on $\gamma\text{-Al}_2\text{O}_3$	
	$N$	$R$ (Å)	$N$	$R$ (Å)
Pt-Pt	2.0	2.64	$2.2 \pm 0.1$	$2.68 \pm 0.01$
Pt-Ru	4.0	2.80	$3.9 \pm 0.1$	$2.95 \pm 0.01$
Pt-CO				
Pt-C	1.0	1.85	$0.8 \pm 0.1$	$1.85 \pm 0.01$
Pt-O*	1.0	2.99	$0.8 \pm 0.1$	$3.09 \pm 0.01$
Ru-Ru	2.0	3.04	$1.9 \pm 0.1$	$2.83 \pm 0.01$
Ru-Pt	2.0	2.80	$2.0 \pm 0.1$	$2.95 \pm 0.01$
Ru-CO				
Ru-C	3.0	1.89	$3.1 \pm 0.1$	$1.88 \pm 0.01$
Ru-O*	3.0	3.03	$3.1 \pm 0.1$	$3.00 \pm 0.01$

From Table 2.2, the distances Pt-C and Ru-C from carbonyl carbon and coordination numbers in the adsorbed species on alumina were the same within error as those in crystal form, which were 1.85 and 1.89 Å, respectively. This confirmed the existence of metal carbonyl species adsorbed on the alumina support. The average Pt-O\* distance in the adsorbed species was  $3.09 \pm 0.01$  Å, slightly longer than the distance in unsupported crystal form (i.e., 2.99 Å in Table 2) and  $2.92 \pm 0.01$  Å reported by Alexeev for  $\text{Pt}_2\text{Ru}_4(\text{CO})_{18}$  precursor. However, Ru-CO contributions did

not change significantly after adsorption. Ru-C and Ru-O\* interactions were observed at  $1.88 \pm 0.01$  and  $3.00 \pm 0.01$  Å, respectively with coordination number  $3.1 \pm 0.1$ .

Consequently, it could be concluded from IR and EXAFS data that metal framework of  $\text{Pt}_3\text{Ru}_6(\text{CO})_{21}(\mu_3\text{-H})(\mu\text{-H})_3$  remained intact after adsorption and the cluster structure was only slightly changed. Furthermore, the adsorbed surface species were still metal carbonyl which could not be re-extracted by  $\text{CH}_2\text{Cl}_2$ .

### 2.3.3 Structural changes of metal framework after adsorption

For the EXAFS fitting parameters of bimetallic contributions, the reliability and consistence of parameters were determined. The bond distances and Debye-Waller factors must be equivalent for each edge of Pt-Ru interactions, the coordination numbers  $N_{\text{PtRu}}$  related to  $N_{\text{RuPt}}$  by this equation:  $N_{\text{PtRu}}/N_{\text{RuPt}} = n_{\text{Ru}}/n_{\text{Pt}}$ , where  $n_{\text{Ru}}$  and  $n_{\text{Pt}}$  are the total numbers of Ru and Pt atoms in sample.

Table 2.2 shows comparison between bond distances and coordination numbers of  $\text{Pt}_3\text{Ru}_6(\text{CO})_{21}(\mu_3\text{-H})(\mu\text{-H})_3$  from crystallography (Adams et al., 1994) and cluster supported on  $\gamma\text{-Al}_2\text{O}_3$  from EXAFS. The average Pt-Pt and Pt-Ru distances of impregnated sample increased from 2.64 to  $2.68 \pm 0.01$  Å and from 2.80 to  $2.95 \pm 0.01$  Å, respectively, while average Ru-Ru distance decreased from 3.04 to  $2.83 \pm 0.01$  Å. The shorter Ru-Ru distance was most likely due to the loss of hydride ligands attached to one  $\text{Ru}_3$  face and Ru-Ru edges. The new Ru-Ru distance was close to the average distance of hydride-free  $\text{Ru}_3$  face of  $\text{Pt}_3\text{Ru}_6(\text{CO})_{21}(\mu\text{-CPhCHPh})(\mu\text{-H})$  which was 2.81 Å (Adams et al., 1994). Note that there are 9 terminal and 1 bridging carbonyl ligands at one of  $\text{Ru}_3$  face.

Coordination number of metal-metal bonds did not change significantly after adsorption. The coordination numbers of Pt-Ru and Ru-Pt were still the same to that of the precursor,  $3.9 \pm 0.4$  and  $2.0 \pm 0.1$ , respectively. These results indicate that the metal core of the precursor remained the same during adsorption and drying process. Reasons for the expansion of Pt-Pt and Pt-Ru distances were still obscure. It might be caused by the contraction of  $\text{Ru}_3$  faces due to loss of electron-rich hydrides.

The changes in average metal-metal distances were different from that observed in  $\text{Pt}_2\text{Ru}_4(\text{CO})_{18}$  in which physical adsorption occurred, all metal-metal distances of impregnated sample were nearly the same distances found in XRD data. Thus, cluster precursor in this work which contains hydrides tends to have more change of metal core upon hydride loss during adsorption. Fortunately, the distortion did not cause the cleavage of metal framework of adsorbed precursor.

Therefore, structural changes of precursor were observed after impregnation and loss of hydride ligands were expected to cause distortion of metal core of adsorbed bimetallic carbonyl species.

#### **2.3.4 Stability of metal framework in supported sample after ligand removal**

Some supported Pt-Ru catalysts prepared by conventional methods, using mixed-metal chlorides, platinum chloride and ruthenium chloride, usually gave monometallic particles rather than bimetallic particles on metal oxide support after reduction in  $\text{H}_2$ , typically at about  $400^\circ\text{C}$  (Alerasool et al., 1988; Diaz et al., 1983; Diaz, Garin, Maire, Alerasool, and Gonzalez, 1995; Miura et al., 1982). In contrast, the preparation of supported bimetallic catalysts from metal cluster precursors

containing metal-metal bonds gave highly dispersed bimetallic particles on oxide supports (Alexeev et al., 2002, 2003; Bergmeister and Hanson, 1989). Because the metal atoms in molecular bimetallic precursor are generally in low oxidation states, the activation step to remove ligands from precursor can be done at low temperature. Thus, the metal-metal bonds may remain intact in the cluster on the support, resulting in highly dispersed and uniform supported bimetallic particles (Alexeev and Gates, 2003; Bergmeister and Hanson, 1989).

After treatment in He at 300°C for 2 h to remove ligands from the adsorbed precursor, the IR bands in the  $\nu_{\text{CO}}$  region disappeared, indicating complete CO removal (spectrum 3 in Figure 2.4B). Although hydrides could not be detected, they should be removed at these conditions as well because their adsorption bond energy is less than that of carbonyl. For example, bond energy of Pt-H and Ru-H are 80.1 and 55.9 kcal/mol whereas those of Pt-C and Ru-C are 143 and 154.9 kcal/mol (Lide, 1993-1994). The PtRu sample treated in He flow was characterized by EXAFS spectroscopy. The EXAFS spectra of PtRu/ $\gamma$ -Al<sub>2</sub>O<sub>3</sub> after ligand removal scanned at both the Pt L<sub>III</sub> and the Ru K edges are shown in Figures 2.8 and 2.9. The EXAFS fitting parameters are summarized in Table 2.3. The estimated accuracies of coordination number ( $N$ ), distance ( $R$ ), Debye-Waller factor ( $\Delta\sigma^2$ ), and inner potential correction ( $\Delta E_0$ ) are as follows:  $\pm 20\%$ ,  $\pm 1\%$ ,  $\pm 30\%$ ,  $\pm 10\%$ , respectively.

**Table 2.3** Summary of EXAFS data of PtRu/ $\gamma$ -Al<sub>2</sub>O<sub>3</sub> prepared by decarbonylation of adsorbed Pt<sub>3</sub>Ru<sub>6</sub>(CO)<sub>21</sub>( $\mu_3$ -H)( $\mu$ -H)<sub>3</sub> on  $\gamma$ -Al<sub>2</sub>O<sub>3</sub>

Edge	Shell	$N$	$R$ (Å)	$10^3 \times \Delta\sigma^2$ (Å <sup>2</sup> )	$\Delta E_o$ (eV)
Pt L <sub>III</sub>	Pt-Pt	$1.7 \pm 0.2$	$2.64 \pm 0.01$	$3.0 \pm 0.7$	$-4.5 \pm 0.8$
	Pt-Ru	$2.2 \pm 0.1$	$2.68 \pm 0.01$	$4.2 \pm 0.5$	$6.0 \pm 0.3$
	Pt-O <sub>support</sub>				
	Pt-O <sub>s</sub>	$2.2 \pm 0.1$	$2.08 \pm 0.01$	$11.3 \pm 1.4$	$8.7 \pm 0.6$
	Pt-O <sub>l</sub>	$0.8 \pm 0.1$	$2.99 \pm 0.02$	$-2.3 \pm 2.0$	$-7.6 \pm 1.4$
Ru K	Ru-Ru	$2.1 \pm 0.1$	$2.62 \pm 0.01$	$4.1 \pm 0.3$	$-13.3 \pm 0.3$
	Ru-Pt	$1.0 \pm 0.1$	$2.68 \pm 0.01$	$4.5 \pm 0.7$	$-11.5 \pm 1.0$
	Ru-O <sub>support</sub>				
	Ru-O <sub>s</sub>	$1.2 \pm 0.1$	$2.06 \pm 0.01$	$10.9 \pm 1.7$	$4.1 \pm 0.7$
	Ru-O <sub>l</sub>	$2.1 \pm 0.1$	$2.89 \pm 0.01$	$0.1 \pm 0.7$	$11.8 \pm 0.2$
	Ru-O <sub>l2</sub>	$1.4 \pm 0.2$	$3.32 \pm 0.02$	$5.2 \pm 2.8$	$6.2 \pm 0.6$

Notation: subscript s and l refer to short and long, respectively.

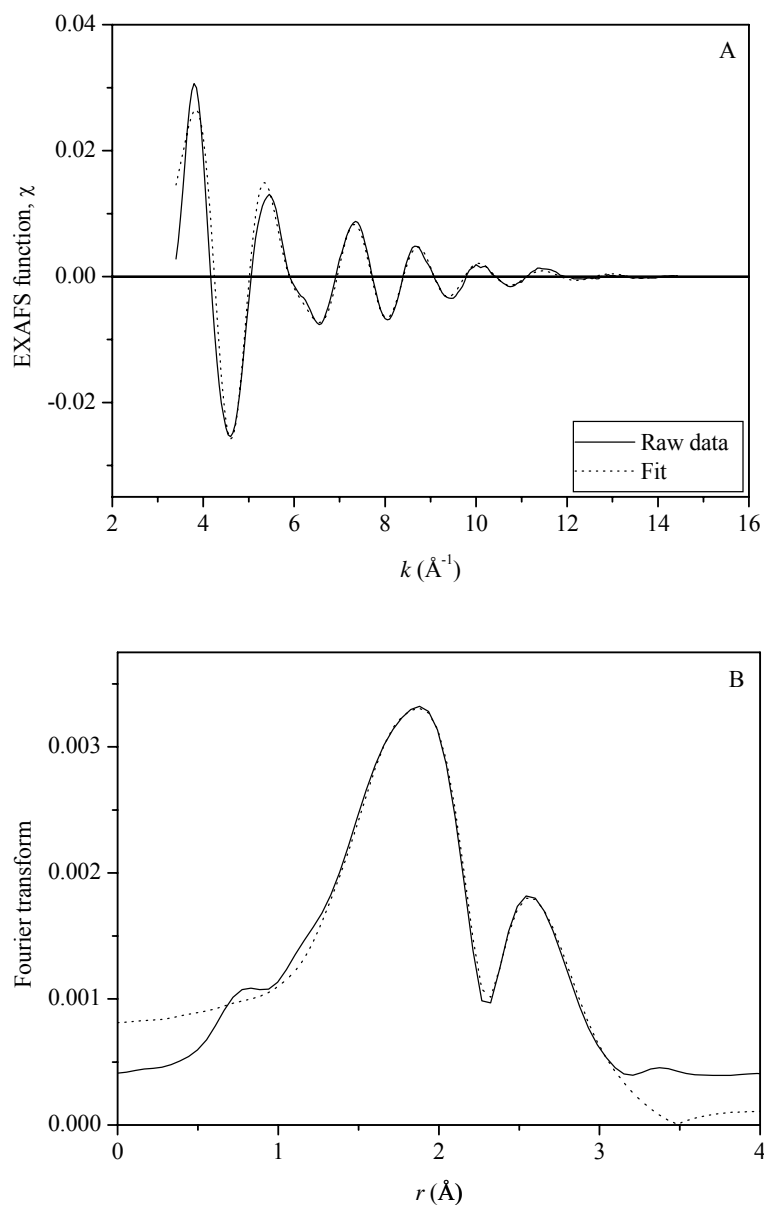


**Figure 2.8** EXAFS results scanned at the Pt L<sub>III</sub> edge characterizing the PtRu/ $\gamma$ -Al<sub>2</sub>O<sub>3</sub> sample prepared by adsorption of Pt<sub>3</sub>Ru<sub>6</sub>(CO)<sub>21</sub>( $\mu_3$ -H)( $\mu$ -H)<sub>3</sub> after ligand removal: (A) Experimental EXAFS function (solid line) and sum of the calculated Pt-Pt, Pt-Ru, Pt-C, Pt-O\*, Pt-O<sub>s</sub>, and Pt-O<sub>l</sub> contributions (dotted line). (B) Magnitude of uncorrected Fourier transform ( $k^0$  weighted) of experimental EXAFS function (solid line) and sum of the calculated Pt-Pt, Pt-Ru, Pt-C, Pt-O\*, Pt-O<sub>s</sub>, and Pt-O<sub>l</sub> contributions (dotted line).

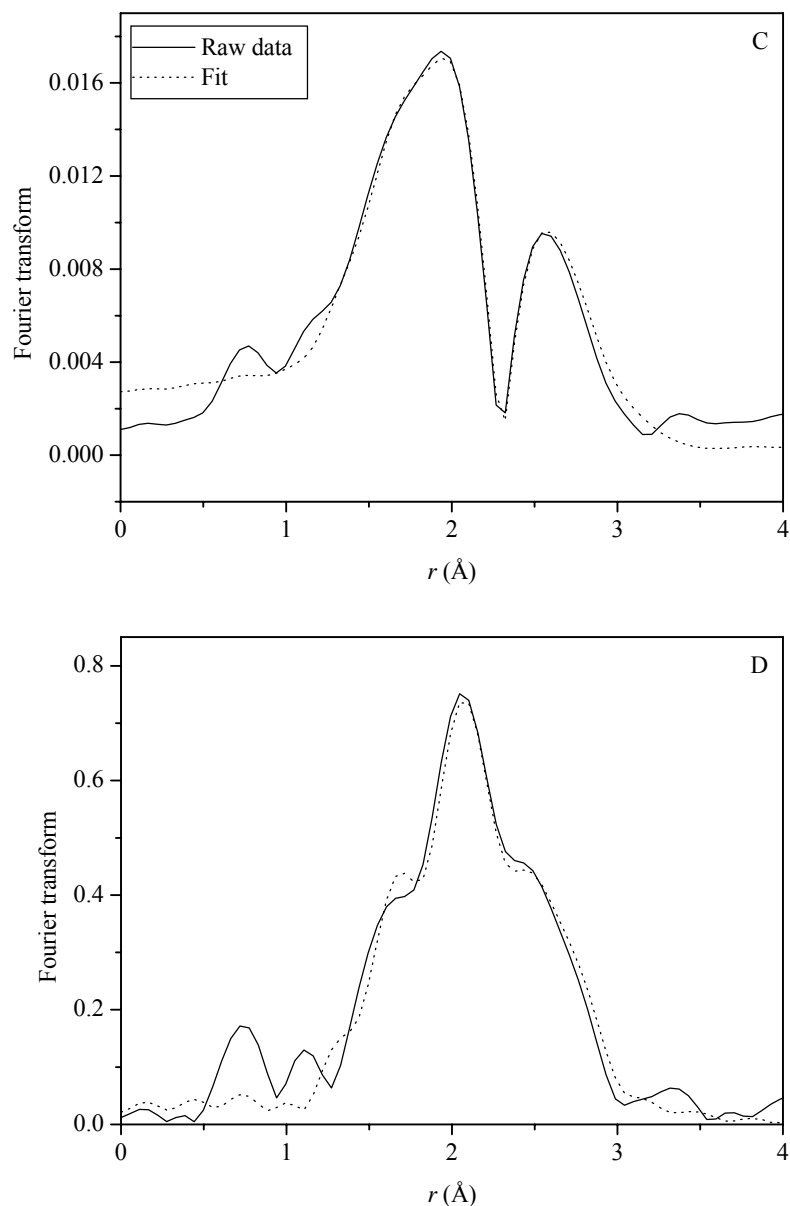


**Figure 2.8** (continued) EXAFS results scanned at the Pt L<sub>III</sub> edge characterizing the PtRu/ $\gamma$ -Al<sub>2</sub>O<sub>3</sub> sample prepared by adsorption of Pt<sub>3</sub>Ru<sub>6</sub>(CO)<sub>21</sub>( $\mu$ -H)<sub>3</sub> after ligand removal: (C) Magnitude of uncorrected Fourier transform ( $k^1$  weighted) of experimental EXAFS function (solid line) and sum of the calculated Pt-Pt, Pt-Ru, Pt-C, Pt-O\*, Pt-O<sub>s</sub>, and Pt-O<sub>l</sub> contributions (dotted line). (D) Magnitude of uncorrected Fourier transform ( $k^3$  weighted) of experimental EXAFS function (solid line) and sum of the calculated Pt-Pt, Pt-Ru, Pt-C, Pt-O\*, Pt-O<sub>s</sub>, and Pt-O<sub>l</sub> contributions (dotted line).

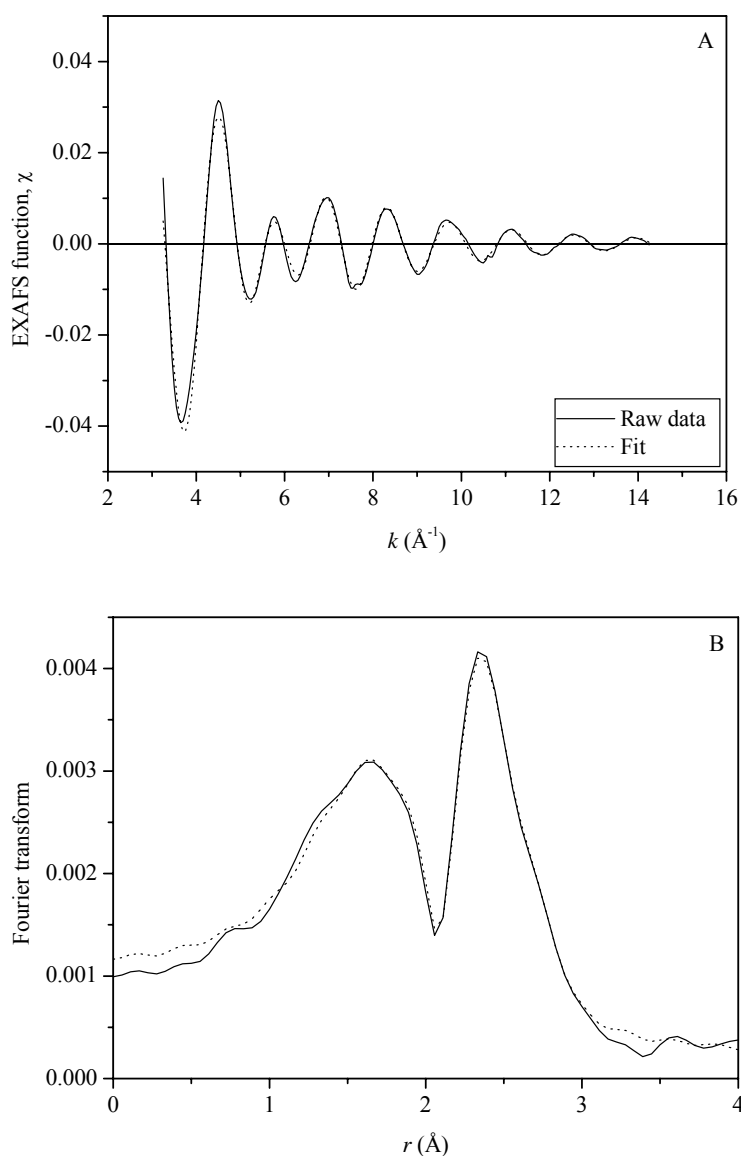


**Figure 2.9** EXAFS results scanned at the Ru K edge characterizing the PtRu/ $\gamma$ -Al<sub>2</sub>O<sub>3</sub> sample prepared by adsorption of Pt<sub>3</sub>Ru<sub>6</sub>(CO)<sub>21</sub>( $\mu_3$ -H)( $\mu$ -H)<sub>3</sub> after ligand removal: (A) Experimental EXAFS function (solid line) and sum of the calculated Ru-Ru, Ru-Pt, Ru-C, Ru-O\*, Ru-O<sub>s</sub>, and Ru-O<sub>l</sub> contributions (dotted line). (B) Magnitude of uncorrected Fourier transform ( $k^0$  weighted) of experimental EXAFS function (solid line) and sum of the calculated Ru-Ru, Ru-Pt, Ru-C, Ru-O\*, Ru-O<sub>s</sub>, and Ru-O<sub>l</sub> contributions (dotted line).

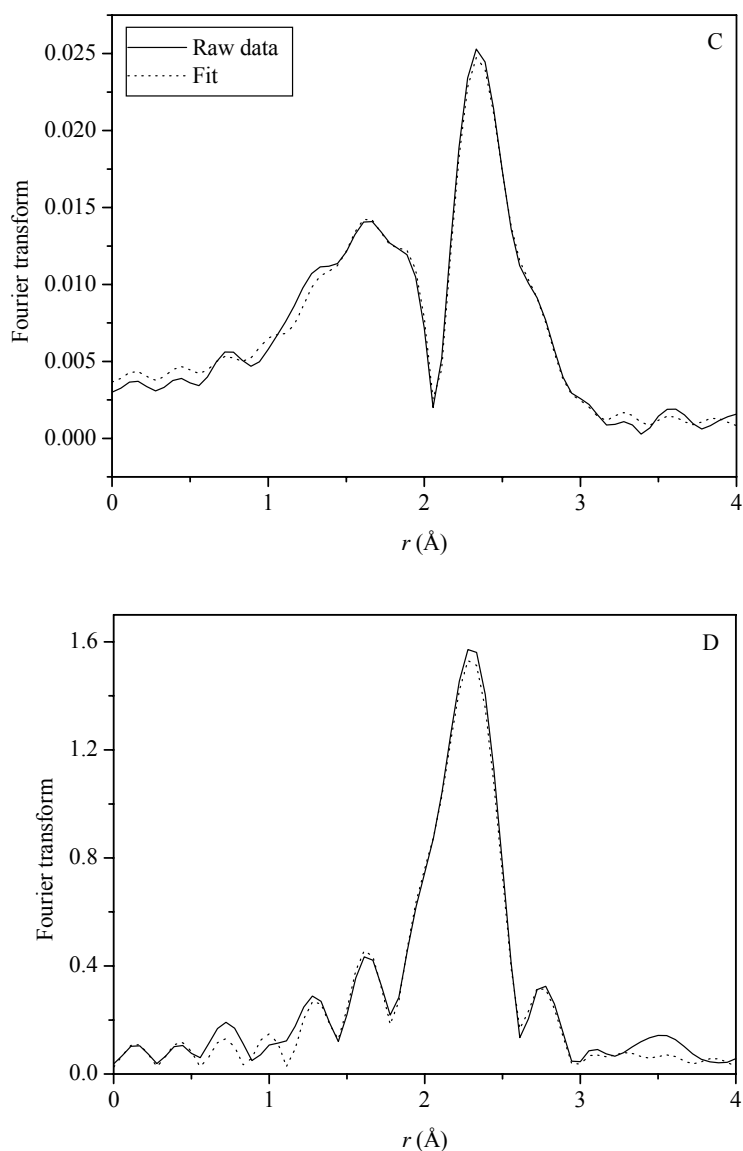


**Figure 2.9** (continued) EXAFS results scanned at the Ru K edge characterizing the PtRu/ $\gamma$ -Al<sub>2</sub>O<sub>3</sub> sample prepared by adsorption of Pt<sub>3</sub>Ru<sub>6</sub>(CO)<sub>21</sub>( $\mu_3$ -H)( $\mu$ -H)<sub>3</sub> after ligand removal: (C) Magnitude of uncorrected Fourier transform ( $k^1$  weighted) of experimental EXAFS function (solid line) and sum of the calculated Ru-Ru, Ru-Pt, Ru-C, Ru-O\*, Ru-O<sub>s</sub>, and Ru-O<sub>l</sub> contributions (dotted line). (D) Magnitude of uncorrected Fourier transform ( $k^3$  weighted) of experimental EXAFS function (solid line) and sum of the calculated Ru-Ru, Ru-Pt, Ru-C, Ru-O\*, Ru-O<sub>s</sub>, and Ru-O<sub>l</sub> contributions (dotted line).

From EXAFS data of decarbonylated PtRu sample in He, the reliable and consistent of the EXAFS fitting parameters of bimetallic contributions were also determined. The bond distances and Debye-Waller factors must be equivalent for each edge of Pt-Ru interactions, the coordination numbers  $N_{\text{PtRu}}$  related to  $N_{\text{RuPt}}$  by this equation:  $N_{\text{PtRu}}/N_{\text{RuPt}} = n_{\text{Ru}}/n_{\text{Pt}}$ , where  $n_{\text{Ru}}$  and  $n_{\text{Pt}}$  are the total numbers of Ru and Pt atoms in the sample. These constraints were applied to get good fits of the data. As shown in Table 2.3, the average Pt-Ru and Ru-Pt distances and Debye-Waller factors obtained from both Pt L<sub>III</sub> and Ru K edge data match with each other. The values of  $N_{\text{PtRu}}/N_{\text{RuPt}}$  match the value of  $n_{\text{Ru}}/n_{\text{Pt}}$  of 2 which was calculated from precursor stoichiometry.

Table 2.3 displays the interaction and coordination number of metal-metal bonds (Pt-Pt, Pt-Ru, Ru-Pt and Ru-Ru) and metal-support bonds (Pt-O<sub>support</sub> and Ru-O<sub>support</sub>). After ligand removal Pt-Pt bond distance decreased from  $2.78 \pm 0.01$  to  $2.64 \pm 0.01$  Å and Ru-Ru distance decreased from  $2.83 \pm 0.01$  to  $2.62 \pm 0.01$  Å. The average Pt-Ru and Ru-Pt bond distance also decreased from  $2.95 \pm 0.01$  to  $2.68 \pm 0.01$  Å. After carbonyl ligands were removed, steric repulsion among them was removed resulting in shorter metal-metal bonds.

The coordination number in Pt-Pt and Ru-Ru did not significantly changed, i.e., from  $1.6 \pm 0.2$  to  $1.7 \pm 0.2$  and from  $1.9 \pm 0.1$  to  $2.1 \pm 0.1$ , respectively. In contrast, the coordination number of Pt-Ru and Ru-Pt decreased from  $3.9 \pm 0.1$  to  $2.2 \pm 0.1$  and from  $2.0 \pm 0.1$  to  $1.0 \pm 0.1$ , respectively indicating that some bimetallic bonds were broken during treatment in He. The changes in Pt-Pt, Ru-Ru, Pt-Ru and Ru-Pt coordination numbers might indicate that both metals tend to segregate from one another during ligand removal. This change might be minimized by lowering the

ligand removal temperature. After carbonyl ligands were removed, all metal atoms had more empty coordination sites and the EXAFS results indicated the stronger bond between metal and oxygen of surface which is electronegative atoms.

The average Pt-O<sub>s</sub> distances decreased from  $2.52 \pm 0.01$  in the adsorbed species to  $2.08 \pm 0.01$  Å with coordination number  $2.2 \pm 0.1$  in the sample after ligand removal indicating strong Pt-O<sub>s</sub> interaction. The average Ru-O<sub>s</sub> bond distances also decreased from  $2.34 \pm 0.01$  to  $2.06 \pm 0.01$  Å and Ru-O<sub>l2</sub> was also found at  $3.32 \pm 0.02$  Å indicating strong Ru-O<sub>support</sub> interaction. Coordination number of Ru-O<sub>s</sub> contribution did not significantly changed, namely, from  $1.4 \pm 0.1$  to  $1.2 \pm 0.1$ .

Therefore, bimetallic core of adsorbed species was stable on  $\gamma$ -Al<sub>2</sub>O<sub>3</sub> upon treatment in He flow at 300°C to remove ligands indicating strong interaction of metal-metal on support meanwhile metal-support interaction increased.

### **2.3.5 High dispersion of bimetallic particles on supported sample after ligand removal**

The average coordination numbers of Pt-Pt and Ru-Ru contributions after decarbonylation (Table 2.3) were found to  $1.7 \pm 0.1$  and  $2.1 \pm 0.1$ , respectively, indicating high dispersion of metal particles. These values were not much different from the values of supported PtRu sample before treatment (within error) indicating that metal core was stable upon ligand removal. Strong metal-support interaction in this work resulted in high dispersion of metal on support.

Compared with EXAFS results of PtRu/ $\gamma$ -Al<sub>2</sub>O<sub>3</sub> prepared from impregnation of Pt<sub>2</sub>Ru<sub>4</sub>(CO)<sub>18</sub> after ligand removal, the tendency for aggregation of Ru atoms was greater than Pt even though the degree of aggregation was extremely low in this

ligand removal condition (Alexeev et al., 2002). The average coordination numbers of Pt-Pt and Ru-Ru were 2.0 and 4.0 which were higher than that before ligand removal, 1.0 and 1.0 respectively, and that of Ru-Ru contribution also higher than that when  $\text{Pt}_3\text{Ru}_6(\text{CO})_{21}(\mu_3\text{-H})(\mu\text{-H})_3$  was used as precursor.

Thus, highly dispersed bimetallic PtRu/ $\gamma\text{-Al}_2\text{O}_3$  sample could be prepared by decarbonylation of adsorbed  $\text{Pt}_3\text{Ru}_6(\text{CO})_{21}(\mu_3\text{-H})(\mu\text{-H})_3$  on  $\gamma\text{-Al}_2\text{O}_3$  in He flow at 300°C for 2 h.

### **2.3.6 Effect of strong Pt-Ru interactions on ethylene hydrogenation**

#### **2.3.6.1 Catalytic activity and time on stream (TOS)**

A blank test for ethylene hydrogenation was performed with stainless U-tube reactor containing  $\alpha\text{-Al}_2\text{O}_3$ . A plot between activity and inversed weight hourly space velocity (inv. WHSV, g cat/mol/h) at -75°C was in Figure 2.10 showing straight line from the origin and the data determine rate of the catalytic reaction could be obtained directly from the slope. This plot implied that stainless U-tube reactor testing within inv. WHSV ranges of 0-4.11 g cat/mol/h with conversion < 5% was a differential reactor.

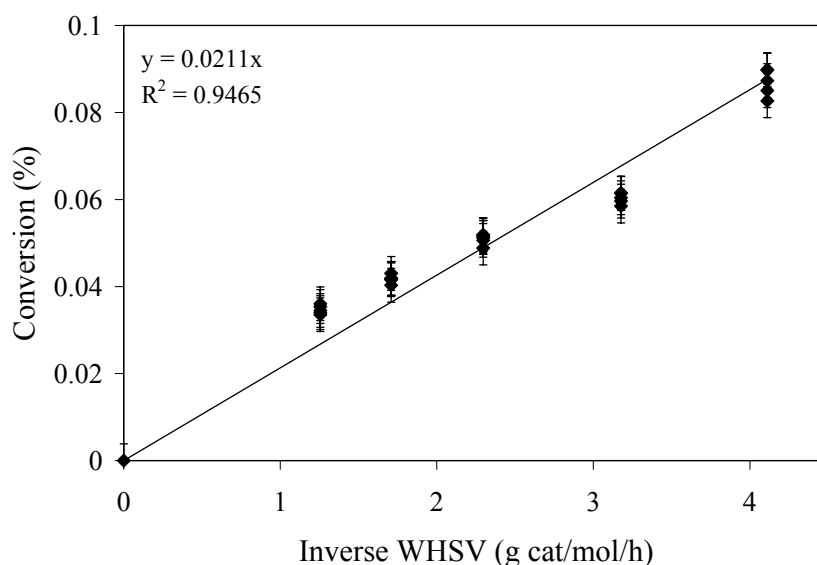


**Figure 2.10** Demonstration of differential reactor operation at  $-75^{\circ}\text{C}$ ,  $P_{\text{C}_2\text{H}_4} = 40$  Torr,  $P_{\text{H}_2} = 80$  Torr, balanced with He, total feed flow rate = 200 ml (NTP)/min catalyzed by PtRu/ $\gamma$ -Al<sub>2</sub>O<sub>3</sub>.

The catalytic activity of ethylene hydrogenation in terms of the turnover frequency (TOF) was represented the number of molecules reacting per active sites per second (Fogler, 1999). It was assumed that all metal particles were accessible to reactants, so that TOF was defined as the following equation

$$\text{TOF (s}^{-1}\text{)} = \frac{\text{Conversion (\%)} \times (\text{Mol of input C}_2\text{H}_4)}{(\text{Catalyst weight}) \times [\text{Metal loading (\%)/MW}_{\text{metal}}] \times \text{Dispersion (\%)}} \quad \dots(2.3)$$

Ethylene hydrogenation reaction started as soon as reactant gas arrived the catalyst bed. The plot between activity and time on stream (TOS) is in Figure 2.11.

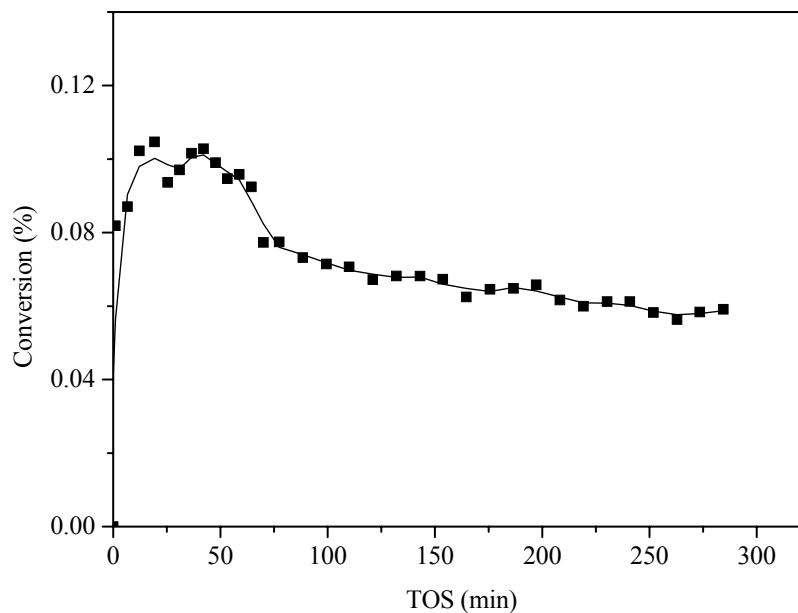


**Figure 2.11** Activity of ethylene hydrogenation with time on stream (TOS) catalyzed by PtRu/ $\gamma$ -Al<sub>2</sub>O<sub>3</sub> at reaction condition:  $P_{\text{C}_2\text{H}_4} = 40$  Torr,  $P_{\text{H}_2} = 80$  Torr, balanced He with total feed flow rate 200 ml (NTP)/min, catalyst mass 0.013 mg, and temperature -75°C.

The initial deactivation was observed, reaction conversion increased fast at the beginning and then slightly decreased with increasing TOS and then reached steady state. It has been known that coking on supported Pt particles easily occurred during reaction at low temperature due to strong interaction between Pt and C atom. Coking leads to catalyst deactivation and shorten catalyst lifetime. However, in this work, the plot between activity and TOS in Figure 2.11 indicated that the PtRu/ $\gamma$ -Al<sub>2</sub>O<sub>3</sub> catalyst slightly deactivated during 280 minutes TOS.

### 2.3.6.2 Kinetics of ethylene hydrogenation catalyzed by PtRu/ $\gamma$ -Al<sub>2</sub>O<sub>3</sub>

The apparent activation energy of ethylene hydrogenation was carried out over supported PtRu/ $\gamma$ -Al<sub>2</sub>O<sub>3</sub> with metal loading 1%wt Pt and 1%wt Ru. Reaction was performed during temperature -75 to -20°C at condition:  $P_{C_2H_4} = 40$  Torr,  $P_{H_2} = 80$  Torr, balanced with He, total feed flow rate = 200 ml (NTP)/min in stainless U-tube flow reactor. The Arrhenius plot between TOF in a natural log scale and (1/T) is in Figure 2.12.

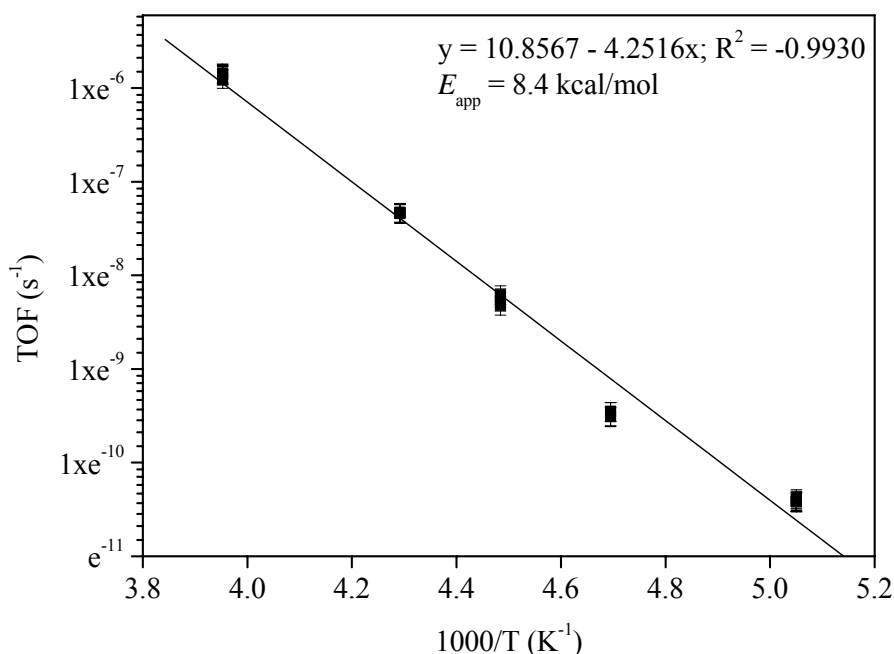


**Figure 2.12** Arrhenius plot for ethylene hydrogenation catalyzed by PtRu/ $\gamma$ -Al<sub>2</sub>O<sub>3</sub> at condition:  $P_{C_2H_4} = 40$  Torr,  $P_{H_2} = 80$  Torr, balanced with He, total feed flow rate = 200 ml (NTP)/min, catalyst mass 0.013 g.

From slope of linear plot in Figure 2.12, the calculated apparent activation energy from temperature dependence of rate of ethylene hydrogenation reaction for

this catalyst was  $8.4 \pm 0.1$  kcal/mol. This apparent activation energy was comparable to those reported for ethylene hydrogenation catalyzed by Pt catalysts supported on oxides supports, ranged from 8.6 to 11.7 kcal/mol, obtained at various conditions as shown in Table 2.4. The apparent activation energy obtained from this work was near the value for supported Pt/SiO<sub>2</sub> (Cortright, Goddard, Rekoske, and Dumesic, 1991; Schlatter and Boudart, 1972) but significantly lower than that for Pt/Al<sub>2</sub>O<sub>3</sub> near the value obtained from polymer-supported Pt-Ru catalysts prepared from [RuPt<sub>2</sub>(CO)<sub>5</sub>(Ph<sub>2</sub>P- $\Phi$ )<sub>3</sub>],  $7.8 \pm 1.2$  kcal/mol obtained at  $P_{\text{H}_2} = 555$  Torr and  $P_{\text{C}_2\text{H}_4} = 152$  Torr, temperature ranges 73 to 98°C (Pierantozzi et al., 1979).

**Table 2.4** Apparent activation energy of ethylene hydrogenation catalyzed by supported Pt, Ru and PtRu catalysts

Catalysts	Apparent activation energy (kcal/mol)	Temperature range (°C)	References
PtRu/ $\gamma$ -Al <sub>2</sub> O <sub>3</sub>	8.4	-75 to -20	This work
RuPt <sub>2</sub> /polymer	7.8	73 to 98	Pierantozzi et al., 1979
Pt/Al <sub>2</sub> O <sub>3</sub>	10.2	40 to 150	Hwang et al., 2003; Grunes et al., 2003
Pt/SiO <sub>2</sub>	8.6	-50 to 63	Cortright et al., 1991
Pt/SiO <sub>2</sub>	8.9	-60 to 0	Schlatter et al., 1972
Pt/SiO <sub>2</sub>	11.7	-78 to -60	Dorling et al., 1969

The apparent activation energy obtained from this work was less than that for nanoparticles Pt adsorbed on Al<sub>2</sub>O<sub>3</sub>,  $10.2 \pm 0.2$  kcal/mol at condition:  $P_{\text{H}_2} = 100$  Torr

and  $P_{\text{C}_2\text{H}_4} = 10$  Torr, temperature range 40 to 150°C (Grunes et al., 2003; Hwang et al., 2003).

In this work, catalytic activity (TOF) of ethylene hydrogenation catalyzed by PtRu/ $\gamma$ -Al<sub>2</sub>O<sub>3</sub> at -40°C was  $(6.5 \pm 0.1) \times 10^{-4}$  (s<sup>-1</sup>).

In conclusion, Pt-Ru/ $\gamma$ -Al<sub>2</sub>O<sub>3</sub> catalyst prepared from Pt<sub>3</sub>Ru<sub>6</sub>(CO)<sub>21</sub>( $\mu_3$ -H)( $\mu$ -H)<sub>3</sub> was active for ethylene hydrogenation giving apparent activation energy  $8.4 \pm 0.1$  kcal/mol at the studied conditions.

### **2.3.6.3 Rate expression for ethylene hydrogenation catalyzed by PtRu/ $\gamma$ -Al<sub>2</sub>O<sub>3</sub>**

Kinetics experiment to determine ethylene and hydrogen kinetic orders for ethylene hydrogenation catalyzed by supported PtRu/ $\gamma$ -Al<sub>2</sub>O<sub>3</sub> was performed at temperature -75°C with conversion < 5% at steady-state operation. Pressure of hydrogen was varied from 20 to 200 Torr and ethylene pressure was kept constant at 40 Torr. TOF and pressure of hydrogen is plotted in Figure 2.13.

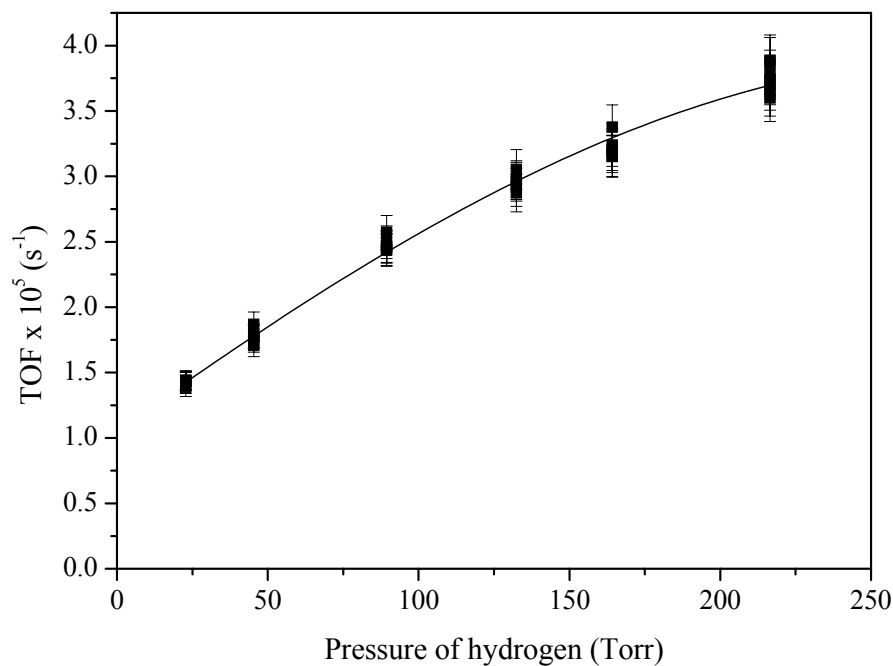


**Figure 2.13** Effect of hydrogen pressure on ethylene hydrogenation catalyzed by PtRu/ $\gamma$ -Al<sub>2</sub>O<sub>3</sub> at 40 Torr ethylene.

Orders of hydrogen and ethylene were determined in the form of rate expression in equation 2.4.

$$\text{rate} = k P_{\text{H}_2}^a P_{\text{C}_2\text{H}_4}^b \quad \dots(2.4)$$

Where  $k$  = reaction rate

$a$  = hydrogen order

$b$  = ethylene order

Hydrogen order could be obtained from excess method in which excess ethylene amount was used and the rate expression could be written as equation 2.5

$$\text{rate} = k' P_{\text{H}_2}^a \quad \dots(2.5)$$

where  $k' = k P_{C_2H_4}^b$

After taking the natural logarithm of equation (2.5), equation 2.6 was obtained.

$$\ln(\text{rate}) = \ln k' + a \ln P_{H_2} \quad \dots(2.6)$$

The slope of a plot of rate in a natural log scale as a function of  $P_{H_2}$  in a natural log scale is the hydrogen order as in Figure 2.14 in which rate of reaction was presented in term of TOF.

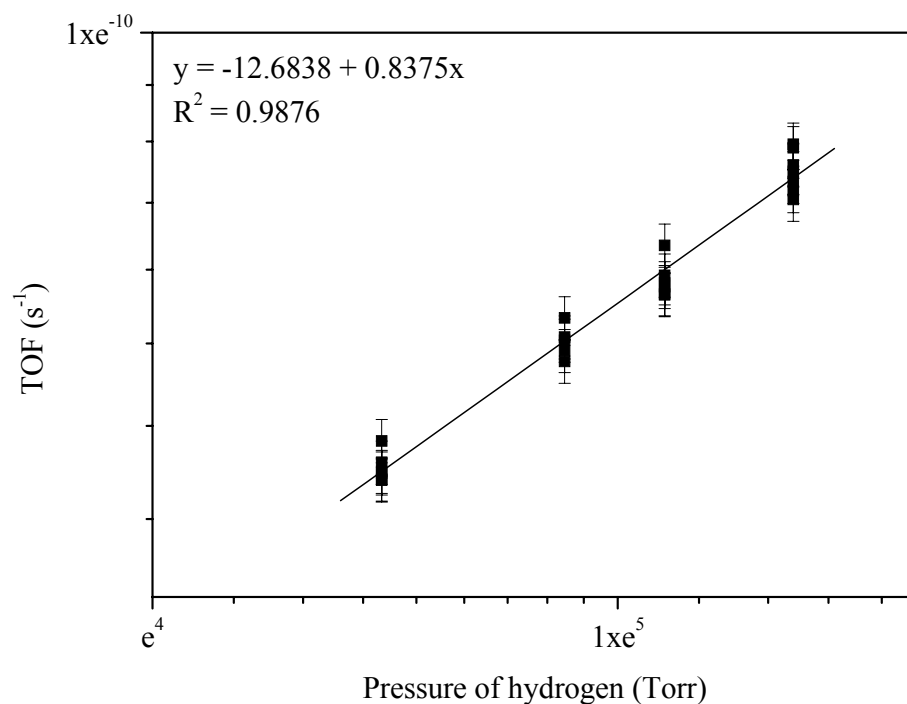


**Figure 2.14** The plot between TOF in a natural log scale as a function of hydrogen pressure in a natural log scale for ethylene hydrogenation catalyzed by PtRu/ $\gamma$ -Al<sub>2</sub>O<sub>3</sub> at 40 Torr ethylene and 80 to 200 Torr hydrogen.

Hydrogen order obtained from slope in Figure 2.14 was 0.46 at reaction temperature  $-75^{\circ}\text{C}$ . Similarly, ethylene order could be obtained from the same method by varying pressure of ethylene.

The effect of pressure of ethylene on catalytic activity was studied by varied pressure of ethylene from 20 to 200 Torr whereas pressure of hydrogen was constant at 80 Torr. The plot between activity in terms of TOF and pressure of ethylene is in Figure 2.15.

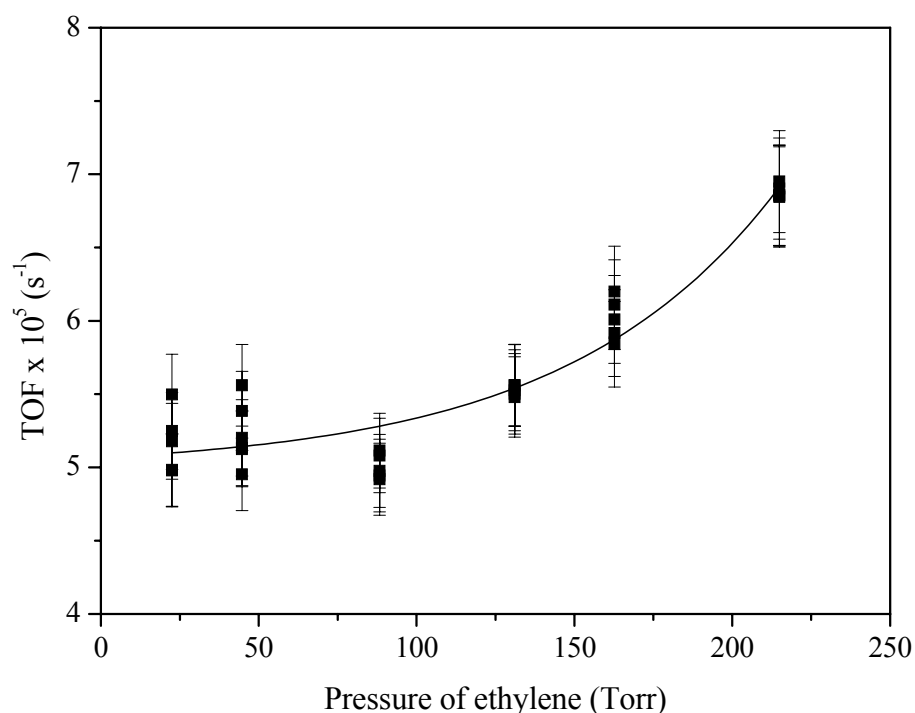


**Figure 2.15** Effect of ethylene pressure on ethylene hydrogenation catalyzed by PtRu/ $\gamma$ -Al<sub>2</sub>O<sub>3</sub> at 80 Torr hydrogen.

Figure 2.15 indicated that catalytic activity did not change much with pressure of ethylene at low pressure of ethylene,  $< 100$  Torr. Catalytic activities increased with excess of ethylene when pressure of ethylene  $> 100$  Torr.

In addition, ethylene order could be obtained from the rate expression in equation 2.6.

$$\text{rate} = k'' P_{\text{C}_2\text{H}_4}^b \quad \dots(2.6)$$

Where  $k'' = k P_{\text{H}_2}^a$

The slope of a plot in a natural log scale between TOF and  $P_{\text{C}_2\text{H}_4}$  is ethylene order as plotted in Figure 2.16.

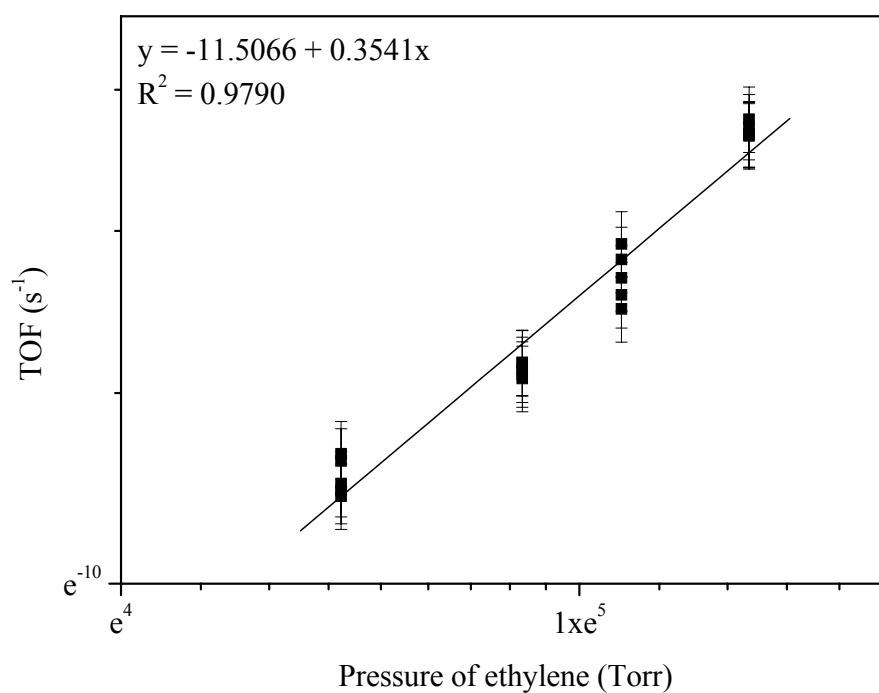


**Figure 2.16** The plot in a natural log scale between TOF and ethylene pressure for ethylene hydrogenation catalyzed by PtRu/ $\gamma$ -Al<sub>2</sub>O<sub>3</sub> at -75°C, 80 Torr hydrogen and 80 to 200 Torr ethylene.

The slope from Figure 2.16 was found to be 0.35 at ethylene hydrogenation reaction temperature  $-75^{\circ}\text{C}$ . Therefore, rate expression for ethylene hydrogenation catalyzed by PtRu/ $\gamma$ - $\text{Al}_2\text{O}_3$  at  $-75^{\circ}\text{C}$  could be written as in equation 2.7.

$$\text{rate} = k P_{\text{H}_2}^{0.46} P_{\text{C}_2\text{H}_4}^{0.35} \quad \dots(2.7)$$

From orders of hydrogen and ethylene, the reaction was nearly half order on both hydrogen and ethylene pressure. The hydrogen order value in this work was in the same range with that from other work at various conditions. For example, Cortright and co-workers (1991) reported rate expression for ethylene hydrogenation catalyzed by 0.04 wt% Pt/Cab-O-Sil as

$$\text{rate} = k P_{\text{H}_2}^{0.48} P_{\text{C}_2\text{H}_4}^{-0.17} \quad \dots(2.8)$$

when obtained data for hydrogen order at condition: temperature  $-50^{\circ}\text{C}$ ; 25 Torr  $P_{\text{C}_2\text{H}_4}$ ; and 50-650 Torr  $P_{\text{H}_2}$  in flow reactor. The kinetic experiment in Cortright's work for ethylene order was performed at condition: 5-75 Torr  $P_{\text{C}_2\text{H}_4}$ ; 150 Torr  $P_{\text{H}_2}$  at temperature  $-50^{\circ}\text{C}$ . When ethylene pressure was low,  $< 100$  Torr, ethylene order became negative value.

In contrast, ethylene order for reaction catalyzed by PtRu/ $\gamma$ - $\text{Al}_2\text{O}_3$  was 0.35 at high ethylene pressure, 80-200 Torr. It could be suggested that reaction mechanism for ethylene hydrogenation at low ethylene pressure was different from that at high ethylene pressure. Due to three different types of adsorbed species of ethylene on metal surface;  $\pi$ -bonded ethylene, di- $\sigma$ -bonded ethylene and ethylidyne,  $\pi$ -bonded ethylene is weakly bound and occurred at high pressure of hydrogen and ethylene in reaction. Ethylene hydrogenation mechanism proposed by Hwang et al. (2003) on Pt(111) and Rh (111) (Figure 2.17) was started by dissociative adsorption of hydrogen

molecules on an ethynyl-covered metal surface. Hydrogenation then occurred through an ethyl intermediate to ethane. They found that ethynyl was a spectator by isotope exchange while most of ethane products were from  $\pi$ -bonded ethylene hydrogenation. Therefore, it implied that in this study that, ethylene order at high ethylene pressure represented  $\pi$ -bonded ethylene hydrogenation.

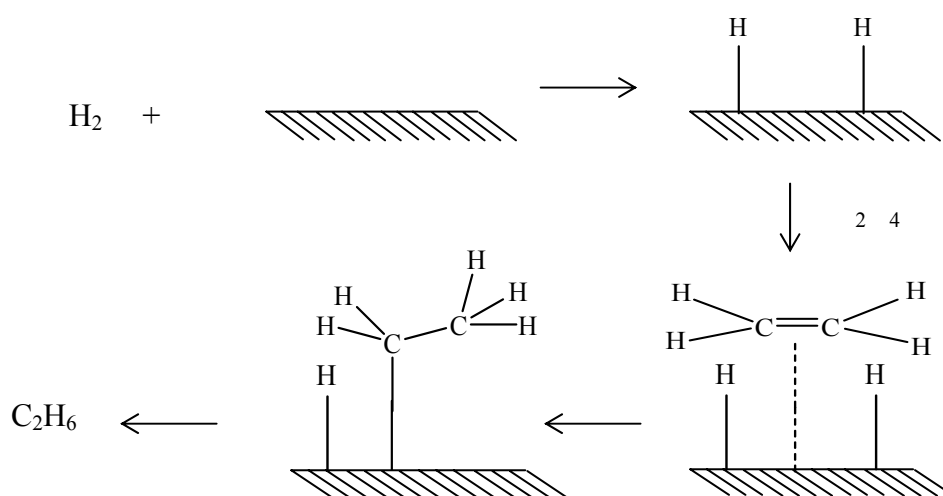


**Figure 2.17** Proposed mechanism for ethylene hydrogenation on Pt (111) and Rh (111) (reproduced from Hwang et al., 2003).

#### 2.3.6.4 IR during ethylene hydrogenation catalyzed by

##### **PtRu/ $\gamma$ - $\text{Al}_2\text{O}_3$**

The adsorption of ethylene on PtRu/ $\gamma$ - $\text{Al}_2\text{O}_3$  was investigated by IR spectroscopy during ethylene flow at various ethylene pressure balanced with He at room temperature. In the dry box, approximately 30 mg of pretreated sample was pressed into a self-supporting wafer (diameter approximately 1 cm) before transferring into an IR cell equipped with KBr windows and valves to isolate sample from air and moisture. The cell was mounted in the IR spectrometer and purged with

He before starting flow of a mixture of ethylene and He. The IR signal was scanned at the rate of 128 scan/min every 120 s. The IR spectra of adsorbed ethylene subtracted from that of gas phase ethylene during flowing ethylene are in Figure 2.18.

Figures 2.18A and 2.18B represent IR spectra in the  $\nu_{C-H}$  stretching and angle-deformation ranges, 2700-3300  $\text{cm}^{-1}$  and 1000-2200  $\text{cm}^{-1}$ . It has been well established that three adsorbed ethylene-derived species on Pt/SiO<sub>2</sub> catalysts at room temperature were: (i) the ethylidyne  $\text{CH}_3\text{CM}_3$  (M = metal) showing strong IR bands in bond-stretching and angle-deformation regions at 2885 and 1340  $\text{cm}^{-1}$ ; (ii) di  $\sigma$ -adsorbed species give medium absorptions at 2920 and 1420  $\text{cm}^{-1}$ ; and (iii)  $\pi$ -bonded species showing weak absorptions at around 3105 and 1500  $\text{cm}^{-1}$  (Shahid and Sheppard, 1990). Therefore, it was inferred that the IR bands occurring at 3122 and 3076  $\text{cm}^{-1}$  in this work represent  $\pi$ -bonded ethylene, that at 3010  $\text{cm}^{-1}$  represents di- $\sigma$ -bonded ethylene, and those at 2987 and 2966  $\text{cm}^{-1}$  represent ethylidyne adsorbed on the cluster.

Furthermore, IR spectra during ethylene hydrogenation catalysis were collected as shown in Figure 2.19 in which IR spectra were not subtracted with gas phase ethane due to high conversion of ethylene at room temperature. The IR band representing ethane at 2968  $\text{cm}^{-1}$  appeared immediately after reactant gas arrived the sample wafer, showing that catalytic hydrogenation took place.

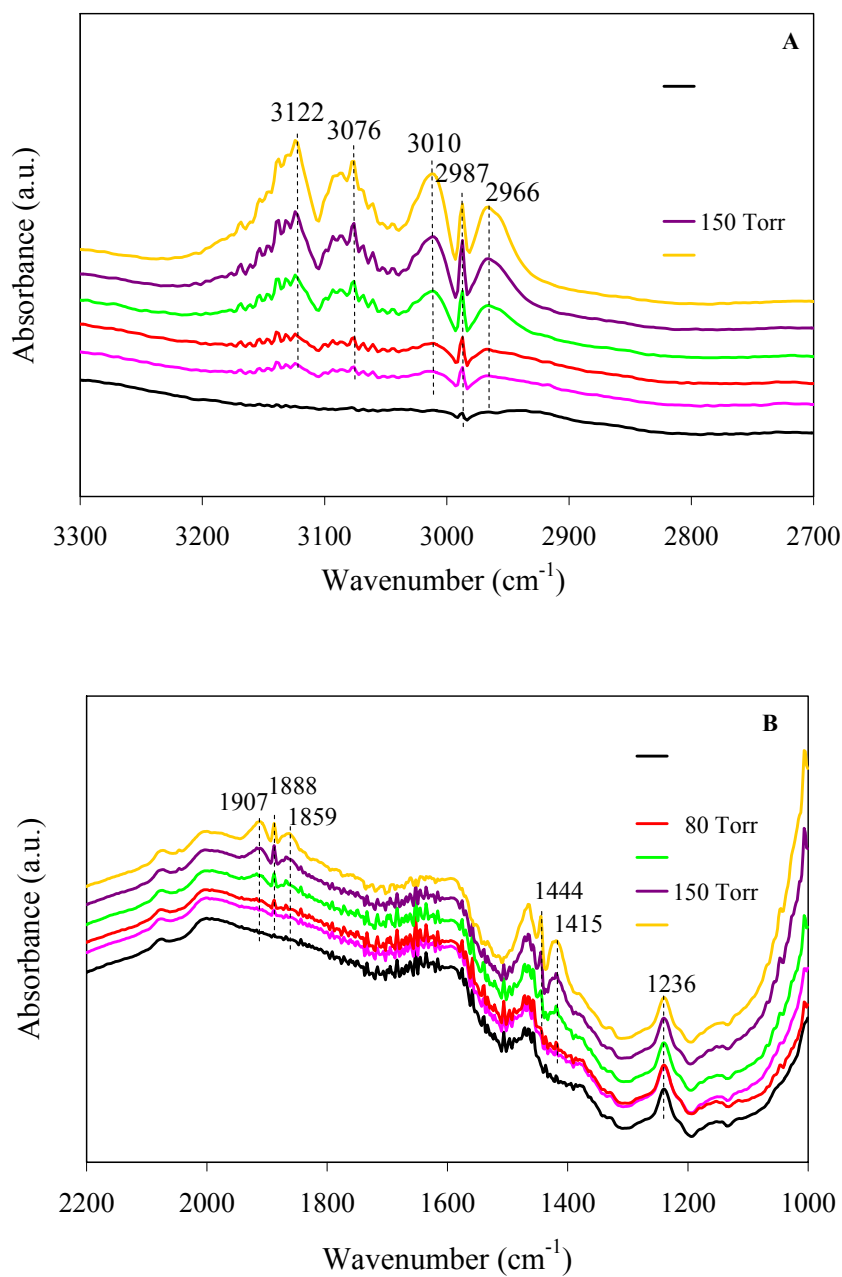


**Figure 2.18** IR spectra during ethylene flow over PtRu/ $\gamma$ -Al<sub>2</sub>O<sub>3</sub> at 30°C in the IR ranges of (A) 2700-3700  $\text{cm}^{-1}$ ; and (B) 2200-1000  $\text{cm}^{-1}$  at ethylene pressure (1) 20 Torr; (2) 40 Torr; (3) 80 Torr; (4) 120 Torr; 150 Torr; and 200 Torr.

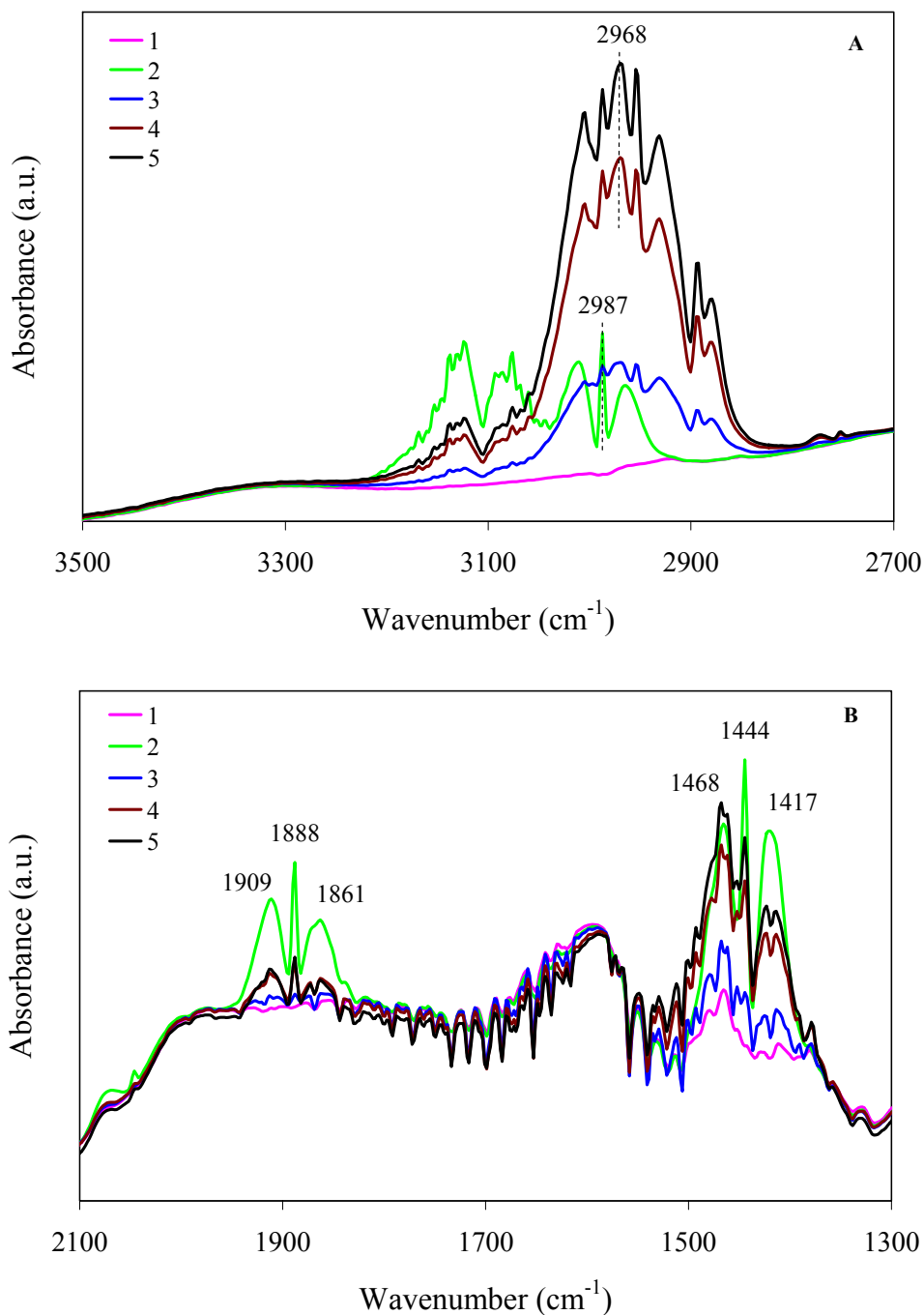


**Figure 2.19** IR spectra during catalysis of ethylene hydrogenation in a flow reactor at 30°C catalyzed by PtRu/ $\gamma$ -Al<sub>2</sub>O<sub>3</sub> in IR ranges of 2700-3500  $\text{cm}^{-1}$  and (B) 1300-2100  $\text{cm}^{-1}$  at condition (1) flowing He; (2) He with 40 Torr C<sub>2</sub>H<sub>4</sub>; (3) He, 40 Torr C<sub>2</sub>H<sub>4</sub> and 80 Torr H<sub>2</sub>; (4) at 120 s after flowing He, 40 Torr C<sub>2</sub>H<sub>4</sub> and 80 Torr H<sub>2</sub>; (5) purging with He after reaction.

## 2.3.7 Effect of strong Pt-Ru interactions on *n*-butane hydrogenolysis

### 2.3.7.1 Catalytic activity and TOS

Catalytic activity of *n*-butane hydrogenolysis reaction which is structural-sensitive reaction was tested for PtRu/ $\gamma$ -Al<sub>2</sub>O<sub>3</sub> prepared from adsorption of Pt<sub>3</sub>Ru<sub>6</sub>(CO)<sub>21</sub>( $\mu_3$ -H)( $\mu$ -H)<sub>3</sub> on  $\gamma$ -Al<sub>2</sub>O<sub>3</sub>. A blank test for *n*-butane hydrogenolysis was carried out in quartz-tube reactor with inert  $\alpha$ -Al<sub>2</sub>O<sub>3</sub> at the following reaction conditions;  $P_{\text{H}_2} = 540$  Torr,  $P_{n\text{-C}_4\text{H}_{10}} = 60$  Torr with 100 ml (NTP)/min flow rate, and at temperature 220°C. The quartz reactor was then tested for differential reactor at this reaction condition. Pretreated PtRu catalyst around 25-30 mg mixed with inert  $\alpha$ -Al<sub>2</sub>O<sub>3</sub> was loaded into reactor in inert atmosphere. The reactor under He flow was heated to desired temperature before an exposure to a gas mixture of H<sub>2</sub>, *n*-C<sub>4</sub>H<sub>10</sub>, and balance He with 100 ml (NTP)/min flow rate. The effluent gas mixture was analyzed with the online gas chromatograph.

A plot of conversion of *n*-butane and inverse weight hourly space velocity (inv. WHSV, g cat/mol/h) at steady-state operation with conversion < 5%, is in Figure 2.20. Linear plot during 0-24.9 g cat/mol/h of inv. WHSV in Figure 2.19 indicated that this quartz-tubed reactor tested at this condition was a differential reactor. A plot of selectivity varied with inv. WHSV for this reaction is also shown in Figure 2.21.

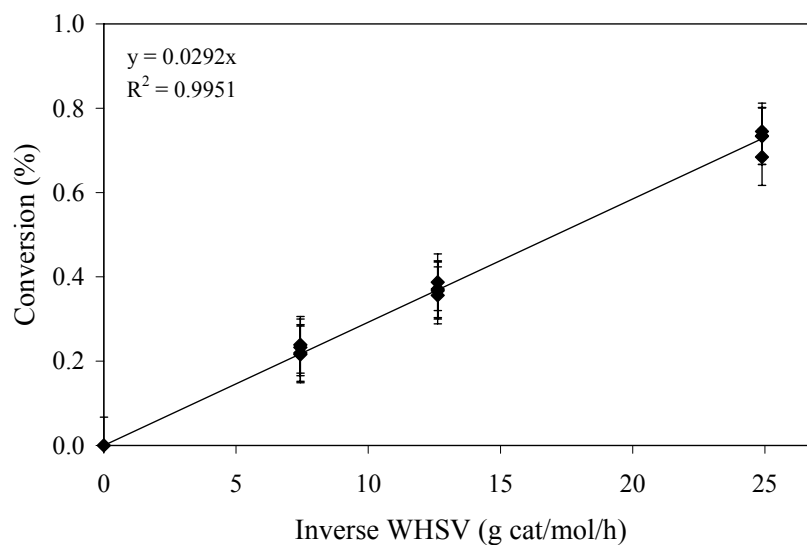


**Figure 2.20** Demonstration of differential reactor operation at 220°C,  $P_{\text{H}_2} = 540$  Torr,  $P_{n\text{-C}_4\text{H}_{10}} = 60$  Torr with 100 ml (NTP)/min flow rate catalyzed by PtRu/ $\gamma\text{-Al}_2\text{O}_3$ .

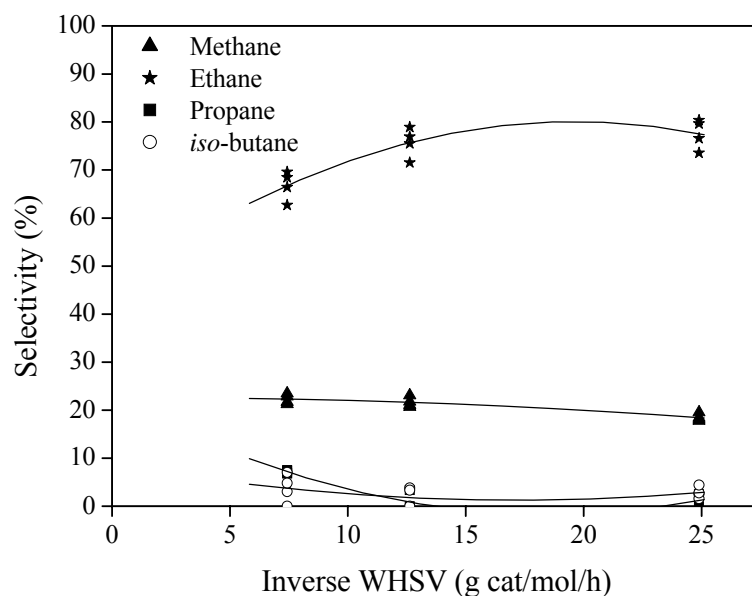


**Figure 2.21** Selectivity varied with inv. WHSV for ethylene hydrogenation at 220°C,  $P_{\text{H}_2} = 540$  Torr,  $P_{n\text{-C}_4\text{H}_{10}} = 60$  Torr with 100 ml (NTP)/min flow rate catalyzed by PtRu/ $\gamma\text{-Al}_2\text{O}_3$ .

From Figure 2.21, selectivity at the initial conversion obtained at the zero inv. WHSV from *n*-butane hydrogenolysis was 23, 45, 23, and 9% for methane, ethane, propane and *iso*-butane, respectively.

*n*-Butane hydrogenolysis reaction catalyzed by supported PtRu/ $\gamma$ -Al<sub>2</sub>O<sub>3</sub> at various reaction temperature was carried out and percent conversion versus TOS are shown in Figure 2.22.

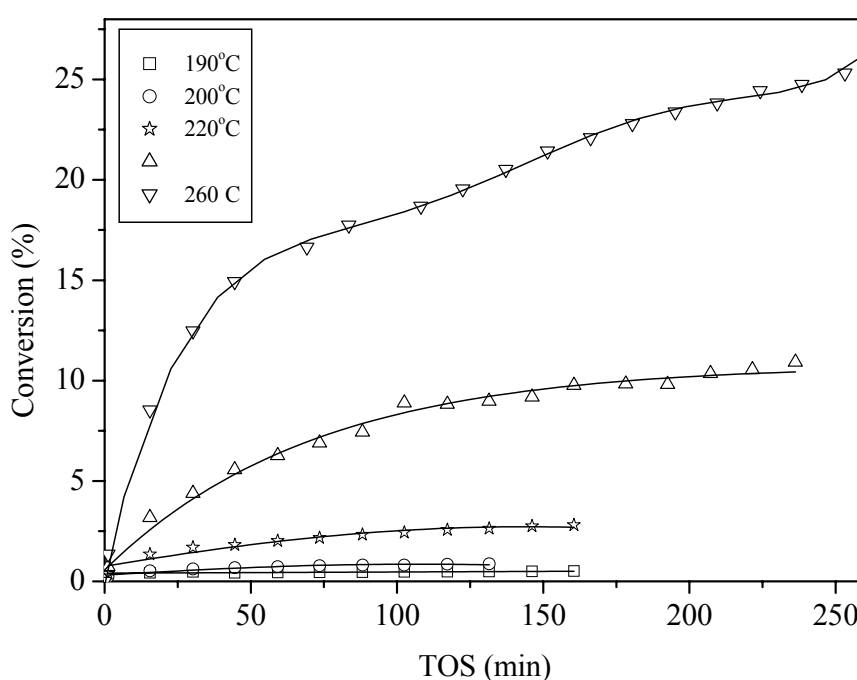


**Figure 2.22** Activity varied with time on stream (TOS) for *n*-butane hydrogenolysis catalyzed by PtRu/ $\gamma$ -Al<sub>2</sub>O<sub>3</sub>.

Figure 2.22 shows that *n*-butane hydrogenolysis activity increased fast at the beginning of TOS, and then slightly increased after 50 min TOS. There was no sign of deactivation during 250 min TOS during reaction temperature of 190-260°C implying that aggregation of metal particles or coking might not occur significantly during the test at each temperature within 250 min.

The catalytic activity in terms of TOF at 220°C of this Pt-Ru/ $\gamma$ -Al<sub>2</sub>O<sub>3</sub> catalyst was found to be  $(5.2 \pm 0.2) \times 10^{-4}$  (s<sup>-1</sup>). Percent product distribution (selectivity) from 190 to 260°C included 33% methane, 63% ethane, 4% propane and less than 0.3% *iso*-butane. The plot of selectivity as a function of reaction temperature in the ranges 190-260°C is shown in Figure 2.23.

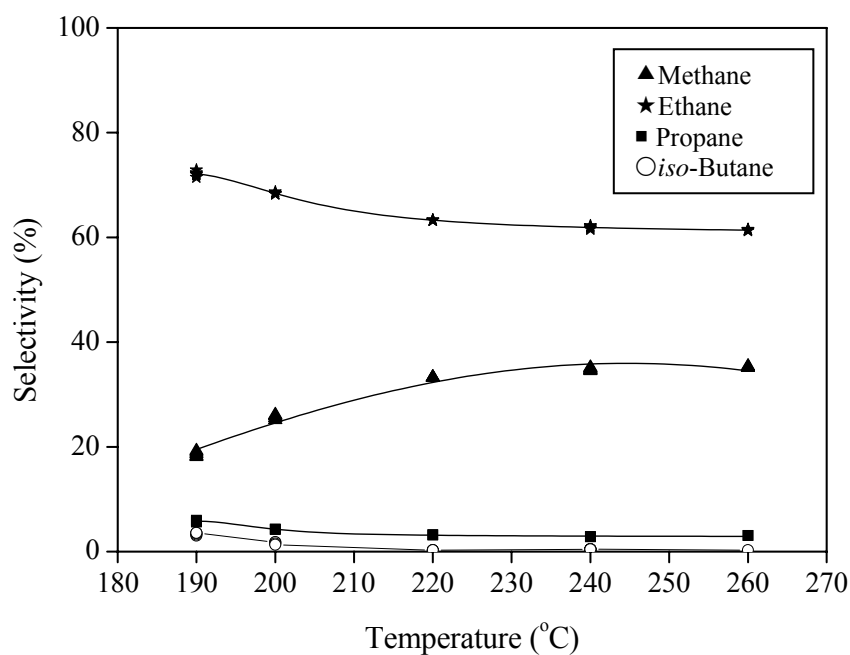


**Figure 2.23** Selectivity varied with reaction temperature of *n*-butane hydrogenolysis catalyzed by PtRu/ $\gamma$ -Al<sub>2</sub>O<sub>3</sub>.

It was found that selectivity of ethane, propane and *iso*-butane slightly decreased with reaction temperature whereas that of methane slightly increased indicating a tendency of multiple hydrogenolysis at high temperature.

### 2.3.7.2 Apparent activation energy of *n*-butane hydrogenolysis catalyzed by PtRu/ $\gamma$ -Al<sub>2</sub>O<sub>3</sub>

*n*-Butane hydrogenolysis reaction catalyzed by PtRu/ $\gamma$ -Al<sub>2</sub>O<sub>3</sub> was performed at temperature range 190-260°C at  $P_{\text{H}_2} = 540$  Torr,  $P_{n\text{-C}_4\text{H}_{10}} = 60$  Torr and 100 ml (NTP)/min flow rate. A plot of TOF in a natural log scale as a function of 1/T is shown in Figure 2.24.

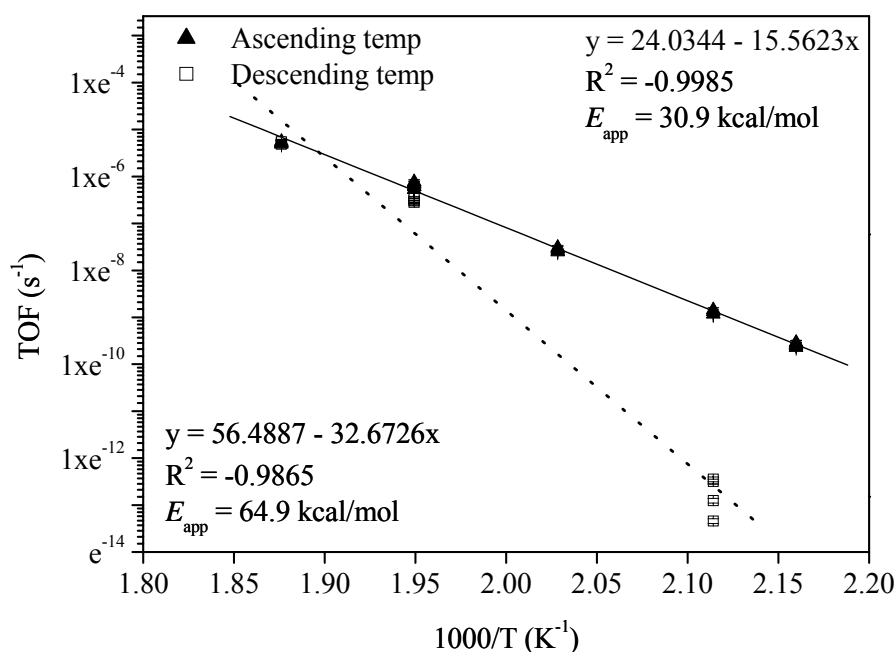


**Figure 2.24** Arrhenius plot of *n*-butane hydrogenolysis catalyzed by PtRu/ $\gamma$ -Al<sub>2</sub>O<sub>3</sub>.

From temperature dependence linear plot in Figure 2.24, the apparent activation energy obtained from a slope of ascending temperature line during 190 to 260°C was  $30.9 \pm 0.1$  kcal/mol. The apparent activation energy in this work was similar to that of reaction catalyzed by Pt on alumina at various reaction conditions (Bond and Cunningham, 1996; Leclercq, Leclercq, and Maurel, 1976; Passos, Schmal, and Vannice, 1996). For example, the apparent activation energy over Pt/Al<sub>2</sub>O<sub>3</sub> was

30 kcal/mol obtained at  $P_{n-C_4H_{10}} = 75$  Torr,  $P_{H_2} = 675$  Torr and temperature ranges 266 to 379°C giving methane and propane products whereas reaction giving only ethane showed higher apparent activation energy which was 38 kcal/mol (Leclercq et al.).

The selectivity from this work suggested that *n*-butane hydrogenolysis over Pt-Ru/ $\gamma$ -Al<sub>2</sub>O<sub>3</sub> preferred to give ethane more than methane and propane and small amount of *iso*-butane (less than 0.3%) was detected at 220°C. It was possibly that isomerization reaction was suppressed when Pt atoms are incorporated with Ru on Pt-Ru/ $\gamma$ -Al<sub>2</sub>O<sub>3</sub> similarly with that over supported bimetallic RhPt catalysts on mesoporous FSM-16 and HMM-1, which gave 82% ethane selectivity at 200°C, gas flow H<sub>2</sub>:*n*-C<sub>4</sub>H<sub>10</sub> = 9:1 (Dhepe, Fukuoka and Ichikawa, 2003). An addition of Pt to Rh helped facilitate the central C-C bond cleavage. High selectivity of ethane indicated that adsorption of *n*-butane on surface mainly occurred through 2, 3-adsorbed the same as reported for RhPt/SiO<sub>2</sub> (Wong et al., 1984). The main *n*-butane hydrogenolysis reaction on RhPt/SiO<sub>2</sub> catalyst was central-bond cleavage to form ethane while methane and propane products resulting from terminal-bond cleavage or 1, 2-adsorbed (see Figure 1.4 of Chapter I).

Thus, it could be concluded from this work that most of *n*-butane molecules adsorbed on active site through 2, 3-adsorbed rather than 1, 2-adsorbed species giving ethane as a main product.

However, data in this work showed that selectivity for methane was higher than that for propane suggesting multiple hydrogenolysis occurred over this bimetallic catalyst in *n*-butane hydrogenolysis. Moreover, the apparent activation energy obtained from this work was in the same range with that from Ru supported on

alumina prepared from different types of Ru precursors, 26-36 kcal/mol at various conditions reported by Bond and Slaa (1995). The data were obtained at  $P_{n-C_4H_{10}} = 54$  Torr,  $P_{H_2} = 543$  Torr and temperature ranges 110-181°C and selectivity for ethane was much higher than that for propane.

### 2.3.7.3 Evidence of catalyst deactivation at high reaction temperature

In this work, there was no sign of catalyst deactivation during the test period at each temperature for ascending temperature testing as in Figure 2.24. Nonetheless, the apparent activation energy obtained from descending temperature testing (Figure 2.24), 64.9 kcal/mol, was double the value of that from ascending temperature. Thus, deactivation occurred after testing reaction at higher temperature. Causes of deactivation might be coking or aggregation of metals on support.

The catalytic data demonstrated that strong Pt-Ru interaction on  $\gamma$ -Al<sub>2</sub>O<sub>3</sub> might affect ethylene hydrogenation and *n*-butane hydrogenolysis. Although the effect was not investigated, one would suggest that Pt-Ru interactions lead to change electronic and chemisorptive properties of Pt, and then its catalytic properties as it was suggested for  $\gamma$ -Al<sub>2</sub>O<sub>3</sub>-supported Pt-W catalyst prepared from bimetallic precursor for H<sub>2</sub> or CO chemisorption and toluene hydrogenation (Alexeev et al., 2000).

## 2.4 Conclusions

Supported bimetallic PtRu/ $\gamma$ -Al<sub>2</sub>O<sub>3</sub> with Pt-Ru connection and high dispersion could be prepared successfully from Pt-Ru carbonyl hydride cluster, Pt<sub>3</sub>Ru<sub>6</sub>(CO)<sub>21</sub>

$(\mu_3\text{-H})(\mu\text{-H})_3$  which is coordinatively saturated and has preformed Pt-Ru bonds. Characterization by IR and EXAFS spectroscopy indicated that the adsorbed species from  $\text{Pt}_3\text{Ru}_6(\text{CO})_{21}(\mu_3\text{-H})(\mu\text{-H})_3$  could bound to  $\gamma\text{-Al}_2\text{O}_3$  support by the interactions between metal and surface oxygen, oxygen of CO ligands and surface hydroxyl groups and  $\text{Al}^{3+}$  acid sites. The adsorbed species was still in the form of bimetallic Pt-Ru carbonyl cluster but the structure was slightly changed possibly due to loss of hydrides during adsorption and interaction with the support. The cluster metal core was remained intact. The adsorbed species could not be extracted from support by  $\text{CH}_2\text{Cl}_2$ . Coordination number of metal core after adsorption was unchanged from the crystal structure. Carbonyl ligands of adsorbed precursor could be completely removed in He flow at  $300^\circ\text{C}$  for 2 h resulting in supported bimetallic Pt-Ru particles with high dispersion. EXAFS data showed structural changes in bond distances and coordination number of Pt-Ru contribution due to partial segregation but the bimetallic frame remained on support. However, Pt-Pt and Ru-Ru contributions were stable upon ligand removal with the average coordination numbers of  $1.7 \pm 0.1$  and  $2.1 \pm 0.1$ , respectively. Strong Pt-Ru and cluster-support interactions might lead to high dispersion bimetallic species on  $\gamma\text{-Al}_2\text{O}_3$ . PtRu/ $\gamma\text{-Al}_2\text{O}_3$  catalyst was active for both ethylene hydrogenation and *n*-butane hydrogenolysis with apparent activation energy  $8.4 \pm 0.1$  and  $30.9 \pm 0.1$  kcal/mol, respectively. Catalytic activity (TOF) of ethylene hydrogenation catalyzed by PtRu/ $\gamma\text{-Al}_2\text{O}_3$  at temperature  $-75^\circ\text{C}$  was  $(3.0 \pm 0.1) \times 10^{-5}$  ( $\text{s}^{-1}$ ). TOF of *n*-butane hydrogenolysis catalyzed by PtRu/ $\gamma\text{-Al}_2\text{O}_3$  at temperature  $220^\circ\text{C}$  was  $(5.2 \pm 0.2) \times 10^{-4}$  ( $\text{s}^{-1}$ ) and products included 33% methane, 63% ethane, 4% propane and less than 0.3% *iso*-butane.

**CHAPTER III**

**EXAFS CHARACTERIZATION AND CATALYTIC  
ACTIVITY OF Pt-Ru/MgO CATALYST PREPARED  
FROM  $\text{Pt}_3\text{Ru}_6(\text{CO})_{21}(\mu_3\text{-H})(\mu\text{-H})_3$**

**3.1 Background of MgO, metal supported on MgO and objectives**

**3.1.1 Nature of MgO**

Magnesium oxide or magnesia (MgO) is the most basic support in heterogeneous catalyst. It has the simplest structure, i.e. rock-salt (Serp, Kalck, and Feurer, 2002) and widely used as model support (001 plane). The reasons that MgO can be used as a support are: (1) its structure is predominantly (100) faces which may give relatively uniform structure at the metal-support interface and (2)  $\text{Mg}^{2+}$  is on the surface layer of this (001) face, thus it was expected to be located near metal that metal- $\text{Mg}^{2+}$  interactions can be characterized (Purnell, Sanchez, Patrini, Chang, and Gates, 1994). MgO can also be prepared to have high surface area ( $> 100 \text{ m}^2/\text{g}$ ). Surface of MgO contains two types of sites such as Mg-O-Mg and -OH groups. The latter types are very weakly acidic in character (Serp et al., 2002).

### 3.1.2 MgO-supported Pt catalysts incorporating second metal

MgO-supported Pt incorporating second metal catalysts have been reported. Supported Pt incorporating with Sn on MgO was prepared from organometallic precursors without preformed Pt-Sn (Stievano et al., 2000), MgO-supported PtW and PtMo catalysts with and without preformed Pt-W and Pt-Mo were prepared (Alexeev, Shelef et al., 1996; Alexeev, Kawi et al., 1996; Kondarides, Tomishige, Nagasawa, Lee, and Iwasawa, 1996). However, Pt-W and Pt-Mo contributions were only observed by EXAFS spectroscopy when using preformed bimetallic precursors. (Alexeev, Shelef et al., 1996; Alexeev, Kawi et al., 1996). However, none of Pt-Ru/MgO prepared from a cluster precursor has been previously reported.

Supported Pt incorporating noble metal on MgO catalysts were also reported. From precursors without preformed Pt-Rh bonds, PtRh/MgO catalysts for toluene hydrogenation were prepared with high yield from  $\text{RhCl}_3 \cdot x\text{H}_2\text{O}$ ,  $\text{Na}_2\text{PtCl}_6$  and CO slurry with MgO to form  $[\text{PtRh}_5(\text{CO})_{15}]^-$  on MgO (Shirai, Yang, Weber, and Gates, 1999; Weber, Yang, Shirai, and Gates, 1999; Yang, Shirai, Weber, and Gates, 1998; Xu, Kawi, Rheingold, and Gates, 1994). PtPd/MgO catalysts were prepared by chemical vapor deposition (CVD) of organometallic precursors, i.e.  $\text{Pt}(\text{acac})_2$  and  $\text{Pd}(\text{acac})_2$  in  $\text{CH}_2\text{Cl}_2$  and were expected to form bimetallic particles as observed by temperature-programmed reductive decomposition (TPRD) (Dossi et al., 2003).

### 3.1.3 Research goals

The goal of this work was to prepare highly dispersed supported PtRu catalyst on MgO by adsorption of  $\text{Pt}_3\text{Ru}_6(\text{CO})_{21}(\mu_3\text{-H})(\mu\text{-H})_3$  from  $\text{CH}_2\text{Cl}_2$  onto MgO

support. Properties of supported bimetallic samples, especially the interactions between cluster and surface of support before and after ligand removal, were studied by IR and EXAFS spectroscopy. The nature of adsorbed species and structural changes of the cluster precursor were also investigated. Catalytic activities of the bimetallic catalyst were tested for ethylene hydrogenation and *n*-butane hydrogenation reactions. Results were compared with those of bimetallic catalysts prepared conventionally.

## 3.2 Experimental

### 3.2.1 Chemicals and materials

Organometallic syntheses, solvent purification, supported catalyst preparations and samples handling were performed similarly to those in section 2.2.1 of Chapter II (page 18).

MgO (EM Science, 97%) was mixed with deionized water to form a paste before drying overnight at 120°C. Prior to use, it was calcined or partially dehydroxylated in O<sub>2</sub> flow at 400°C for 2 h followed by evacuation (pressure  $\approx 10^{-3}$  Torr) at this temperature for an additional 14 h.

### 3.2.2 Synthesis of organometallic precursor

Pt<sub>3</sub>Ru<sub>6</sub>(CO)<sub>21</sub>( $\mu_3$ -H)( $\mu$ -H)<sub>3</sub> was synthesized by a procedure described by Adams and his group (1994). The detail of synthesis and characterization are in section 2.2.2 of Chapter II (page 19). Briefly, Pt<sub>3</sub>Ru<sub>6</sub>(CO)<sub>21</sub>( $\mu_3$ -H)( $\mu$ -H)<sub>3</sub> was synthesized from the reaction between Pt<sub>2</sub>Ru<sub>4</sub>(CO)<sub>18</sub> and H<sub>2</sub> and purified by washing

with cold *n*-pentane several times before characterized by IR,  $^1\text{H}$  and  $^{13}\text{C}$  NMR spectroscopy.

### 3.2.3 Preparation of supported catalyst

Supported Pt-Ru catalysts on MgO was prepared by slurring MgO with a solution of  $\text{Pt}_3\text{Ru}_6(\text{CO})_{21}(\mu_3\text{-H})(\mu\text{-H})_3$  in  $\text{CH}_2\text{Cl}_2$  for 1 day followed by evacuation ( $\approx 10^{-3}$  bar) for an additional 1 day to ensure complete uptake of the precursor by the support. The amount of chosen precursor gave sample containing 1.0 wt% Pt and 1.0 wt% Ru after ligand removal from precursor.

### 3.2.4 Extraction of adsorbed species on MgO

Adsorbed species on MgO after adsorption with  $\text{Pt}_3\text{Ru}_6(\text{CO})_{21}(\mu_3\text{-H})(\mu\text{-H})_3$  was recovered by extraction with  $\text{CH}_2\text{Cl}_2$  for approximately 30 min with stirring. The extract solution and extracted dry sample were characterized by IR spectroscopy.

### 3.2.5 PtRu catalyst activation

Fresh supported sample was heated in He flow at  $300^\circ\text{C}$  for 2 h to remove ligands from adsorbed precursor.

### 3.2.6 Characterization techniques

#### 3.2.6.1 IR spectroscopy

IR spectra of the dry supported samples supported with  $\text{Pt}_3\text{Ru}_6(\text{CO})_{21}(\mu_3\text{-H})(\mu\text{-H})_3$  were recorded before and after ligand removal with a

Bruker IFS-66v spectrometer with a resolution of  $4 \text{ cm}^{-1}$ . Each sample was scanned 64 times and the signals were averaged. Details for sample preparation and measurement are in section 2.2.6.1 of Chapter II (page 22).

### 3.2.6.2 EXAFS spectroscopy

EXAFS experiments were performed at the X-ray beamline X18B at the National Synchrotron Light Source (NSLS), Brookhaven National Laboratory (BNL), Upton, New York, USA. EXAFS instrument, sample preparation and measurement were described in section 2.2.6.3 of Chapter II (page 23).

### 3.2.7 EXAFS data analysis

Details of EXAFS data analysis were in section 2.2.7 of Chapter II (page 23). Briefly, EXAFS data were collected at the individual Pt L<sub>III</sub> (11564 eV) and the Ru K (22117 eV) absorption edge and analyzed with theoretical reference files. The EXAFS data processing was carried out with ATHENA software (Raval, 2003). Phase shift and backscattering amplitudes of metal-metal and metal-surface oxygen interactions were calculated by FEFF7.0 software (Rehr et al., 1991). EXAFSPAK software (George et al., 2000) was used to fit the EXAFS data with single and multiple scattering paths calculated by FEFF7.0 and the EXAFS parameters were extracted from the raw data with the EXAFSPAK software. The fittings were done both in  $r$  space and  $k$  space with application of  $k^0$ ,  $k^1$ , and  $k^3$  weightings.

Raw EXAFS data of sample prepared by adsorption of Pt<sub>3</sub>Ru<sub>6</sub>(CO)<sub>21</sub>( $\mu_3$ -H)( $\mu$ -H)<sub>3</sub> onto MgO obtained at the Pt L<sub>III</sub> edge were Fourier transformed over the ranges  $3.35 < k < 13.25$  with  $k^3$  weighting without phase correction and  $0.0 < r < 4.0 \text{ \AA}$ .

The EXAFS data of this sample scanned at the Ru K edge were Fourier transformed over the ranges  $4.14 < k < 14.52$  and  $0.0 < r < 5.0$  Å. The statistically justified numbers of free parameters estimated from Nyquist theorem (Stern, 1993),  $n = (2\Delta k\Delta r/\pi) + 1$ , for the Pt L<sub>III</sub> and the Ru K edge of this sample were about 26 and 34, respectively.

The EXAFS data of the Pt-Ru/MgO treated in He scanned at the Pt L<sub>III</sub> edge were Fourier transformed over the ranges  $3.00 < k < 13.40$  and  $0.0 < r < 4.0$  Å. The EXAFS data of this Pt-Ru/MgO scanned at the Ru K edge were Fourier transformed over the ranges  $4.25 < k < 14.35$  and  $0.0 < r < 4.0$  Å. The statistically justified number of free parameters estimated from Nyquist theorem for the Pt L<sub>III</sub> and the Ru K edge of this sample were about 28 and 27, respectively.

### 3.2.8 Catalytic activity of PtRu/MgO for ethylene hydrogenation

Ethylene hydrogenation was carried out with the procedure described in section 2.2.8 of Chapter II (page 24). Briefly, 10 to 20 mg of pretreated catalyst in He flow (300°C, 2 h) diluted with inert nonporous  $\alpha$ -Al<sub>2</sub>O<sub>3</sub> in a stainless steel U-tube flow reactor was cooled to desired temperature under He flow before a gas mixture of H<sub>2</sub>, C<sub>2</sub>H<sub>4</sub> and balance He was flowed into reactor with 200 ml (NTP)/min flow rate. The effluent gas mixture was analyzed with an online gas chromatograph (Hewlett-Packard HP 6890) equipped with an Al<sub>2</sub>O<sub>3</sub> capillary column (50 m x 0.53 mm x 15.0 micron film thickness) and a flame ionization detector. Testing conditions were as followed:  $P_{\text{H}_2} = 80$  Torr,  $P_{\text{C}_2\text{H}_4} = 40$  Torr and temperature varied from -75 to -20°C.

### 3.2.9 Catalytic activity of PtRu/MgO for *n*-butane hydrogenolysis

The procedure to test *n*-Butane hydrogenolysis on PtRu/MgO was similar to that on PtRu/ $\gamma$ -Al<sub>2</sub>O<sub>3</sub> described in section 2.2.9 of Chapter II (page 25). Briefly, 25-30 mg of catalyst was diluted with inert nonporous  $\alpha$ -Al<sub>2</sub>O<sub>3</sub> in quartz-tube flow reactor and heated to the desired temperature with He flowing through it before a gas mixture of H<sub>2</sub>, *n*-C<sub>4</sub>H<sub>10</sub>, and the balance He was introduced into the reactor at a rate of 100 ml (NTP)/min. The effluent gas mixture was analyzed with the online gas chromatograph (Hewlett-Packard HP 6890) equipped with an Al<sub>2</sub>O<sub>3</sub> capillary column (50 m x 0.53 mm x 15.0 micron film thickness) and a flame ionization detector. Testing conditions were as followed:  $P_{\text{H}_2} = 540$  Torr,  $P_{n\text{-C}_4\text{H}_{10}} = 60$  Torr and temperature varied from 190 to 260°C.

## 3.3 Results and discussion

### 3.3.1 IR evidence of interaction between cluster precursor and MgO

The interaction between a metal carbonyl cluster and surface of support could occur through oxygen of CO ligands with hydroxyl groups or surface oxygen or Mg<sup>2+</sup> on MgO forming hydrogen bonds, exchange between CO and -OH or surface oxygen (partial decarbonylation), oxidation of metal atoms or CO by -OH group resulting in hydrido anions species (Guczi and Beck, 1988) and carbonates or carboxylates may formed (Alexeev, Kawi et al., 1996; Rethwisch and Dumesic 1986). IR and EXAFS spectroscopy are useful techniques to investigate the interaction between metal carbonyl precursor and support surface.

Partially dehydroxylated MgO was prepared by calcination in O<sub>2</sub> flow at 400°C for 2 h and evacuation to remove trace of water for an additional 14 h. The  $\nu_{\text{OH}}$  spectrum of bare MgO after calcination (spectrum 1 in Figure 3.1) gave strong band at 3766 cm<sup>-1</sup> representing isolate surface hydroxyls and broad band at 3583 cm<sup>-1</sup> indicating hydrogen-bonded hydroxyls (Alexeev et al., 1996).

Dry sample after adsorption of Pt<sub>3</sub>Ru<sub>6</sub>(CO)<sub>21</sub>( $\mu_3$ -H)( $\mu$ -H)<sub>3</sub> shows strong IR band in  $\nu_{\text{OH}}$  region at 3766 cm<sup>-1</sup> but intensity significantly decreased and small broad IR band characterizing traces of hydrogen-bonded hydroxyl groups occurred at 3583 cm<sup>-1</sup> (spectrum 2 in Figure 3.1).

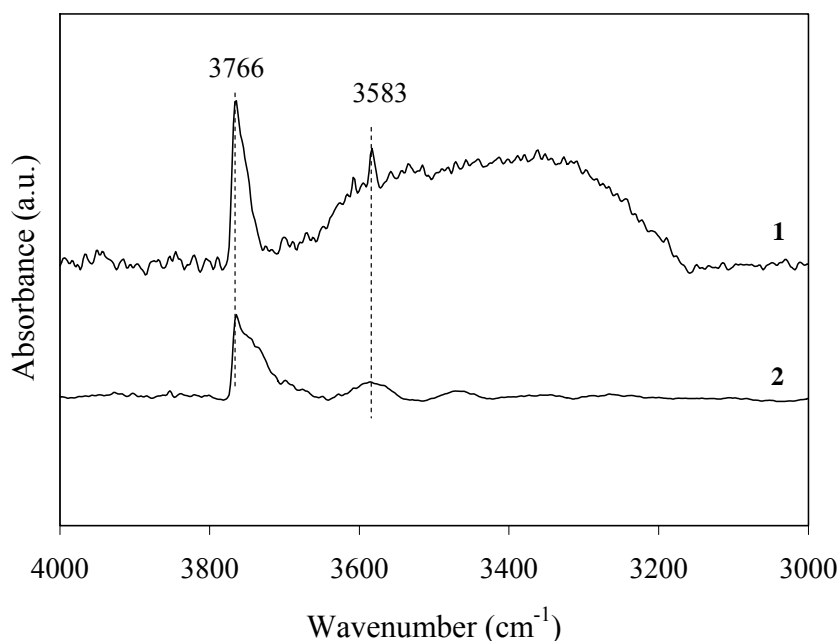


**Figure 3.1** IR spectrum in  $\nu_{\text{OH}}$  region: (1) Calcined MgO; (2) dry sample prepared from Pt<sub>3</sub>Ru<sub>6</sub>(CO)<sub>21</sub>( $\mu_3$ -H)( $\mu$ -H)<sub>3</sub> on MgO.

The decrease in relative intensity of IR band at 3766 cm<sup>-1</sup> and 3583 cm<sup>-1</sup> after Pt<sub>3</sub>Ru<sub>6</sub>(CO)<sub>21</sub>( $\mu_3$ -H)( $\mu$ -H)<sub>3</sub> adsorbed on MgO imply that hydroxyl groups involved in

interaction between cluster precursor and surface of MgO. The interaction could occur through oxygen of CO ligands with OH groups and  $O^{2-}$  sites on MgO forming hydrogen bonding and carbonates or carboxylates resulting in shift of IR in  $\nu_{CO}$  region to lower frequency. The IR spectrum in  $\nu_{CO}$  region of sample after adsorption with  $Pt_3Ru_6(CO)_{21}(\mu_3-H)(\mu-H)_3$  (spectrum 1 in Figure 3.2) shifted to lower wavenumber compared with those of  $Pt_3Ru_6(CO)_{21}(\mu_3-H)(\mu-H)_3$  dissolved in  $CH_2Cl_2$  [Figure 2.4 of Chapter II: 2081 (w, sh), 2066 (vs), 2052 (m, sh), and 2026 (w)]. The IR band in  $\nu_{CO}$  region of MgO-supported sample contained adsorbed species was observed at 2019 (vs) and 1595 (m)  $cm^{-1}$  (spectrum 1 in Figure 3.2).

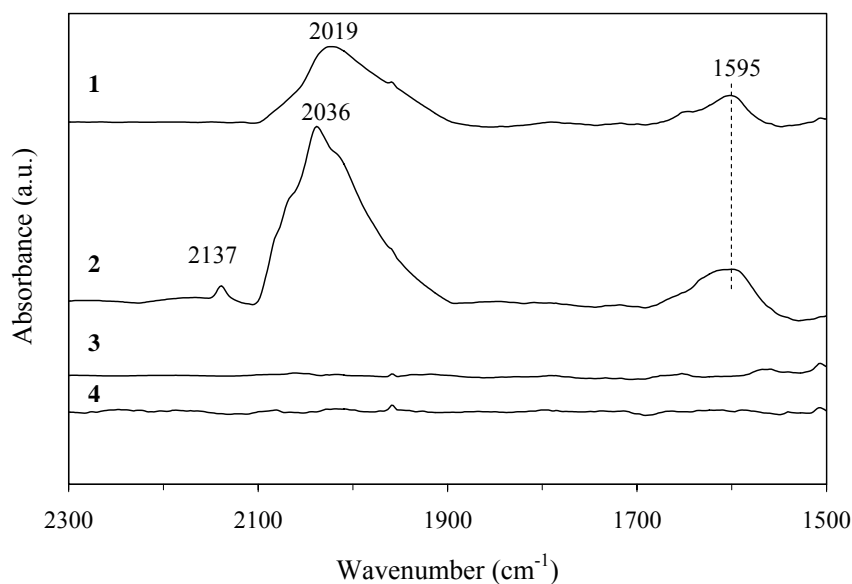


**Figure 3.2** IR spectrum in  $\nu_{CO}$  regions: (1) Dry sample prepared from  $Pt_3Ru_6(CO)_{21}(\mu_3-H)(\mu-H)_3$  on MgO; (2) dry supported sample after extraction with  $CH_2Cl_2$ ; (3) sample after ligand removal in He flow at  $300^\circ C$  for 2 h; (4) calcined MgO.

The strong IR band at  $2019\text{ cm}^{-1}$  was CO stretching from CO ligands of adsorbed species while the latter band was from carbonates or carboxylates on MgO surface which occur in the range  $1700\text{-}1200\text{ cm}^{-1}$  (Busca and Lorenzelli 1982; Rethwisch and Dumesic 1986). The strong IR band at  $2019\text{ cm}^{-1}$  was assigned to be linear M-CO species (where M in this work is Pt or Ru). There was no bridging CO ligand which typically occurred at about  $1850\text{ cm}^{-1}$  for CO adsorbed on metal platinum (Hadjivanov, 1998).

Therefore, the shift of CO and OH bands indicated that  $\text{Pt}_3\text{Ru}_6(\text{CO})_{21}(\mu_3\text{-H})(\mu\text{-H})_3$  was not adsorbed intact on MgO but still in the form of metal carbonyl species. Moreover, the interaction between bimetallic cluster precursor, and MgO surface occurred through oxygen of CO ligands with hydroxyls or  $\text{O}^{2-}$  on MgO forming carbonates or carboxylates on MgO and traces of hydrogen bonding.

### **3.3.2 Strong interaction between cluster precursor and MgO**

There was an attempt to extract adsorbed species on MgO by slurry with  $\text{CH}_2\text{Cl}_2$  for 30 min. The extract solution was characterized by IR spectroscopy but IR band in  $\nu_{\text{CO}}$  region was not detected implying that extraction was not successful and there was a strong precursor-support interaction. The solid sample after extraction was dried under vacuum and characterized with IR spectrometer again. As in spectrum 2 in Figure 3.2, the spectrum was more or less similar to that before extraction indicating that adsorbed metal carbonyl remained on MgO.

In addition, new bands occurred at  $2137\text{ (w)}\text{ cm}^{-1}$  and  $2036\text{ (s)}\text{ cm}^{-1}$  while IR band at  $1595\text{ (m)}\text{ cm}^{-1}$  representing carbonates and carboxylates on MgO did not change in position. The new band at  $2137\text{ cm}^{-1}$  also observed when  $\text{Pt}_3\text{Ru}_6(\text{CO})_{21}$

$(\mu_3\text{-H})(\mu\text{-H})_3$  adsorbed on  $\gamma\text{-Al}_2\text{O}_3$  in Chapter II. This band was assigned to stretching mode of CO ligands from supported bimetallic PtRu on support or from unknown species of metal carbonyl cluster (Hadjiivanov and Vayssilov, 2002). The strong band at  $2036\text{ cm}^{-1}$  was likely shifted from  $2019\text{ cm}^{-1}$  which occurred after adsorption of  $\text{Pt}_3\text{Ru}_6(\text{CO})_{21}(\mu_3\text{-H})(\mu\text{-H})_3$  on MgO. The change of IR peaks after extraction with  $\text{CH}_2\text{Cl}_2$  suggested that  $\text{CH}_2\text{Cl}_2$  affected to precursor-support interaction.

Thus, adsorbed precursor in the form of metal carbonyl species remained on support after extraction implies strong interaction between cluster precursor and MgO surface.

### 3.3.3 EXAFS evidence for structural changes of adsorbed precursor on MgO

The interactions between the precursor and MgO surface were observed by EXAFS spectroscopy. The changes in IR position and occurring of new bands of fresh sample containing adsorbed cluster species agreed well with EXAFS fitting parameters.

The EXAFS fitting parameters of fresh sample of adsorbed  $\text{Pt}_3\text{Ru}_6(\text{CO})_{21}(\mu_3\text{-H})(\mu\text{-H})_3$  on MgO scanned at the Pt  $L_{\text{III}}$  and the Ru K edge at nearly liquid nitrogen temperature are summarized in Table 3.1. The EXAFS fitting results in  $k$  and  $r$  space with  $k^0$ ,  $k^1$  and  $k^3$  weighted are in Figures 3.3 and 3.4. The estimated accuracies of coordination number ( $N$ ), distance ( $R$ ), Debye-Waller factor ( $\Delta\sigma^2$ ), and inner potential correction ( $\Delta E_0$ ) are as follows:  $\pm 20\%$ ,  $\pm 1\%$ ,  $\pm 30\%$ , and  $\pm 10\%$ , respectively.

**Table 3.1** Summary of EXAFS data of sample formed by adsorption of  $\text{Pt}_3\text{Ru}_6(\text{CO})_{21}(\mu_3\text{-H})(\mu\text{-H})_3$  on MgO before ligand removal

Edge	Shell	$N$	$R$ (Å)	$10^3 \times \Delta\sigma^2$ (Å <sup>2</sup> )	$\Delta E_0$ (eV)
Pt L <sub>III</sub>	Pt-Pt	$1.8 \pm 0.1$	$2.53 \pm 0.01$	$3.8 \pm 0.3$	$-8.2 \pm 0.3$
	Pt-Ru	$1.8 \pm 0.1$	$2.89 \pm 0.01$	$7.6 \pm 0.8$	$9.9 \pm 0.1$
	Pt-CO				
	Pt-C	$0.9 \pm 0.1$	$1.88 \pm 0.01$	$-0.2 \pm 0.5$	$-9.2 \pm 0.5$
	Pt-O*	$0.9 \pm 0.1$	$3.02 \pm 0.01$	$-5.0 \pm 0.4$	$11.3 \pm 0.3$
	Pt-O <sub>support</sub>				
	Pt-O <sub>s</sub>	$0.7 \pm 0.1$	$2.03 \pm 0.01$	$-1.2 \pm 0.4$	$7.5 \pm 0.2$
	Pt-O <sub>l</sub>	$1.0 \pm 0.1$	$2.92 \pm 0.01$	$-6.6 \pm 0.2$	$-12.0 \pm 0.3$
Ru K	Ru-Ru	$1.4 \pm 0.1$	$2.83 \pm 0.01$	$14.0 \pm 1.6$	$8.3 \pm 0.6$
	Ru-Pt	$1.2 \pm 0.1$	$2.89 \pm 0.01$	$7.5 \pm 0.7$	$-5.3 \pm 0.8$
	Ru-CO				
	Ru-C	$3.1 \pm 0.3$	$1.91 \pm 0.01$	$7.0 \pm 1.1$	$-1.9 \pm 0.9$
	Ru-O*	$3.1 \pm 0.1$	$2.93 \pm 0.01$	$6.4 \pm 0.5$	$-6.5 \pm 0.2$
	Ru-O <sub>support</sub>				
	Ru-O <sub>s</sub>	$2.1 \pm 0.1$	$2.07 \pm 0.01$	$3.9 \pm 0.5$	$-5.9 \pm 0.7$
	Ru-O <sub>l</sub>	$0.2 \pm 0.1$	$3.35 \pm 0.03$	$-6.1 \pm 0.2$	$6.6 \pm 3.0$

Notation: subscript s and l refer to short and long, respectively

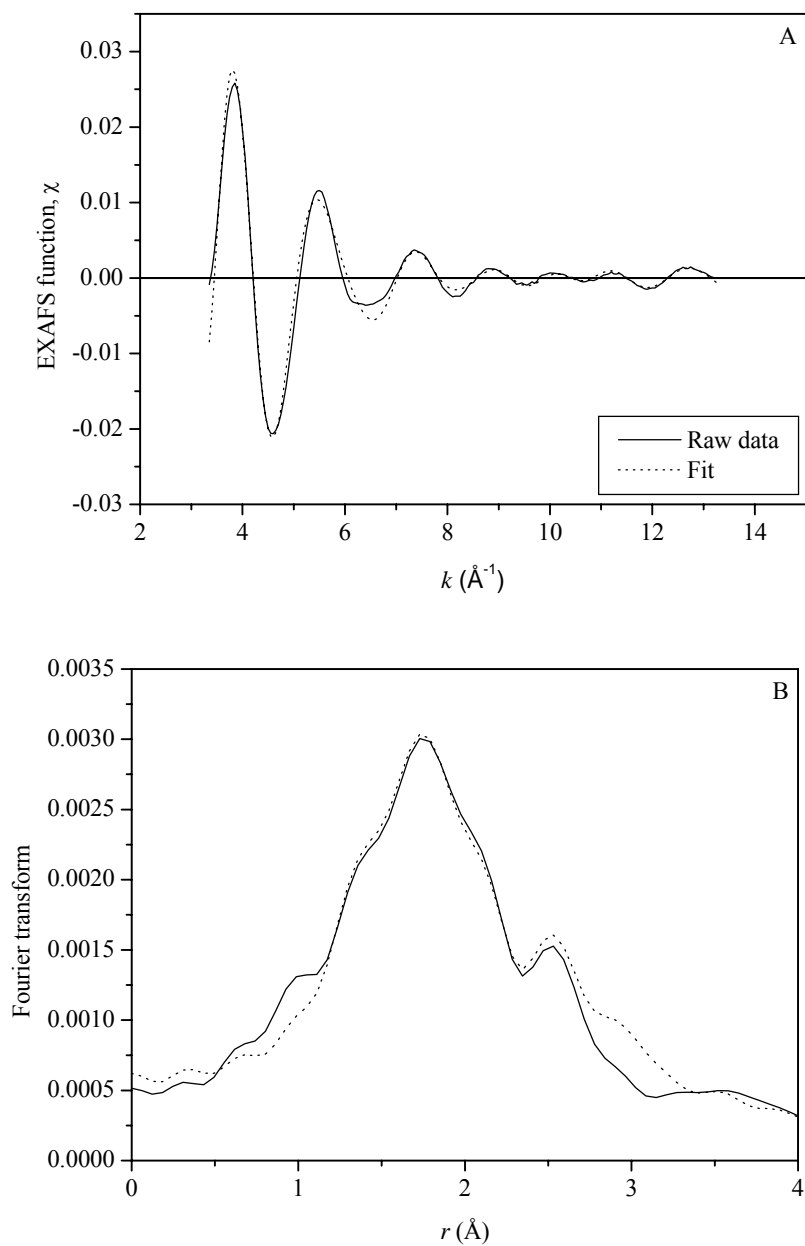


**Figure 3.3** EXAFS results scanned at the Pt L<sub>III</sub> edge characterizing the adsorbed Pt<sub>3</sub>Ru<sub>6</sub>(CO)<sub>21</sub>( $\mu_3$ -H)( $\mu$ -H)<sub>3</sub> on MgO: (A) Experimental EXAFS function (solid line) and sum of the calculated Pt-Pt, Pt-Ru, Pt-C, Pt-O\*, Pt-O<sub>s</sub>, and Pt-O<sub>l</sub> contributions (dotted line). (B) Magnitude of uncorrected Fourier transform ( $k^0$  weighted) of experimental EXAFS function (solid line) and sum of the calculated Pt-Pt, Pt-Ru, Pt-C, Pt-O\*, Pt-O<sub>s</sub>, and Pt-O<sub>l</sub> contributions (dotted line).

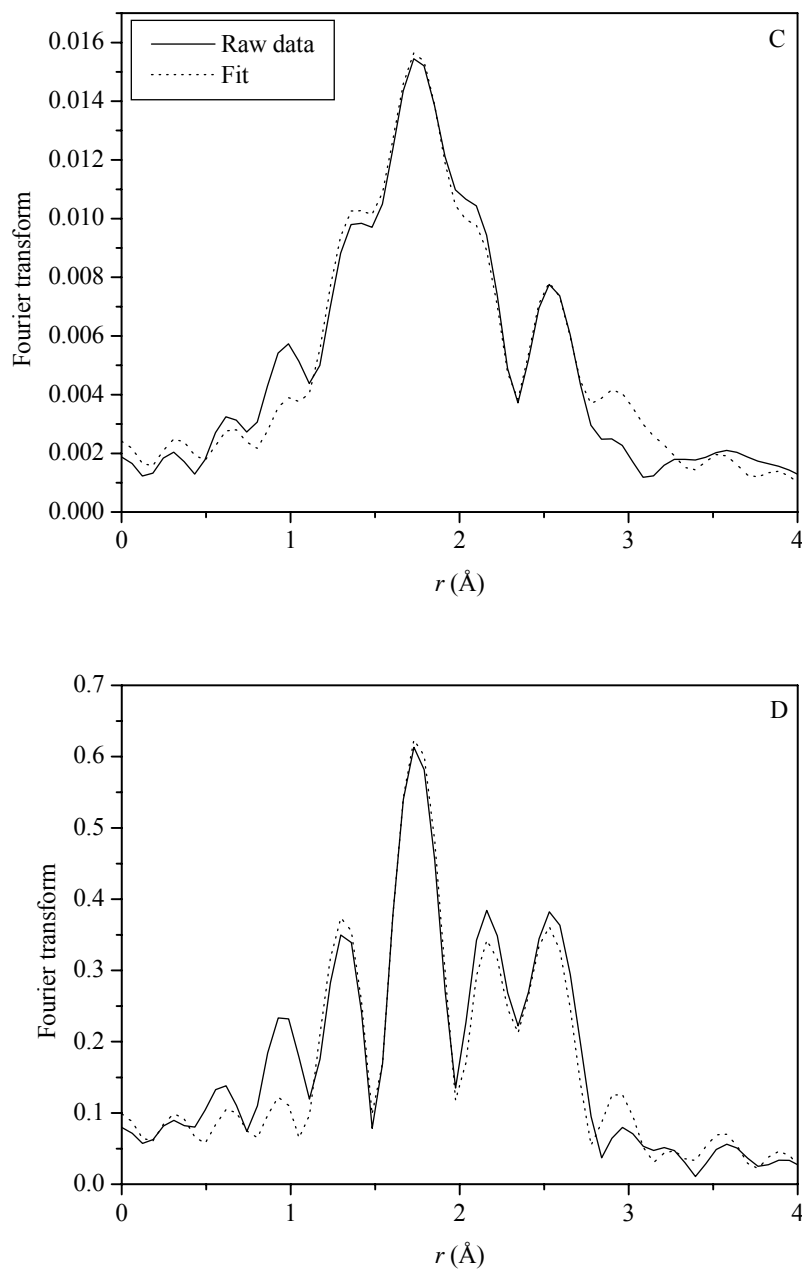


**Figure 3.3** (continued) EXAFS results scanned at the Pt L<sub>III</sub> edge characterizing the adsorbed Pt<sub>3</sub>Ru<sub>6</sub>(CO)<sub>21</sub>(μ<sub>3</sub>-H)(μ-H)<sub>3</sub> on MgO: (C) Magnitude of uncorrected Fourier transform ( $k^1$  weighted) of experimental EXAFS function (solid line) and sum of the calculated Pt-Pt, Pt-Ru, Pt-C, Pt-O\*, Pt-O<sub>s</sub>, and Pt-O<sub>l</sub> contributions (dotted line). (D) Magnitude of uncorrected Fourier transform ( $k^3$  weighted) of experimental EXAFS function (solid line) and sum of the calculated Pt-Pt, Pt-Ru, Pt-C, Pt-O\*, Pt-O<sub>s</sub>, and Pt-O<sub>l</sub> contributions (dotted line).

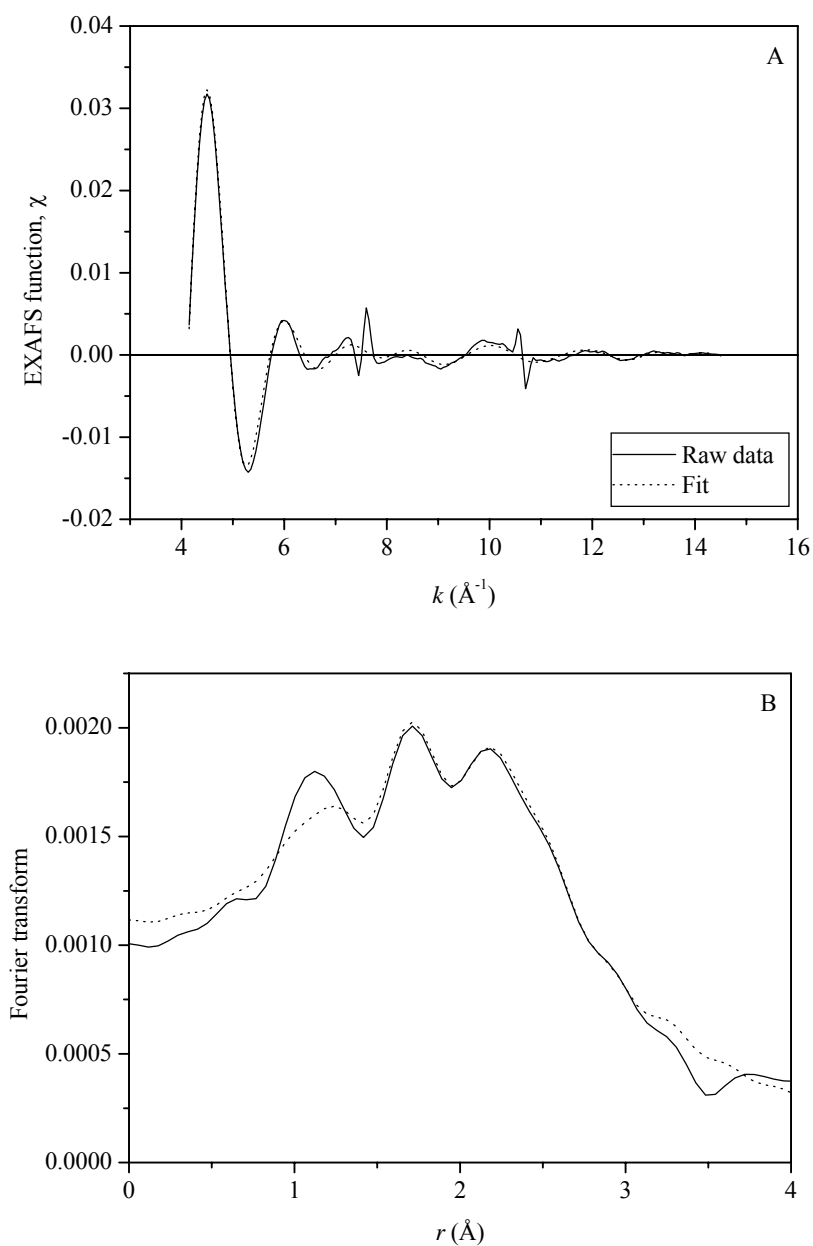


**Figure 3.4** EXAFS results scanned at the Ru K edge characterizing the adsorbed  $\text{Pt}_3\text{Ru}_6(\text{CO})_{21}(\mu_3\text{-H})(\mu\text{-H})_3$  on MgO: (A) Experimental EXAFS function (solid line) and sum of the calculated Ru-Ru, Ru-Pt, Ru-C, Ru-O\*, Ru-O<sub>s</sub>, and Ru-O<sub>l</sub> contributions (dotted line). (B) Magnitude of uncorrected Fourier transform ( $k^0$  weighted) of experimental EXAFS function (solid line) and sum of the calculated Ru-Ru, Ru-Pt, Ru-C, Ru-O\*, Ru-O<sub>s</sub>, and Ru-O<sub>l</sub> contributions (dotted line).

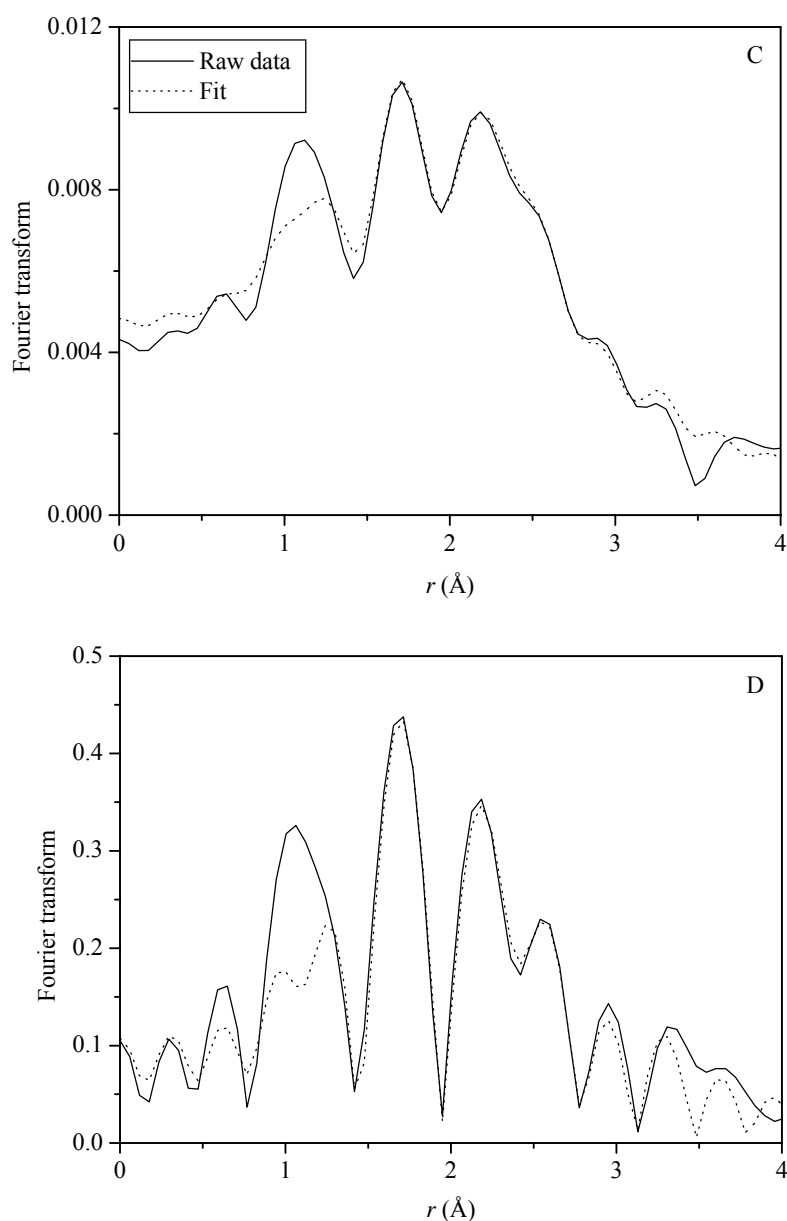


**Figure 3.4** (continued) EXAFS results scanned at the Ru K edge characterizing the adsorbed  $\text{Pt}_3\text{Ru}_6(\text{CO})_{21}(\mu_3\text{-H})(\mu\text{-H})_3$  on MgO: (C) Magnitude of uncorrected Fourier transform ( $k^1$  weighted) of experimental EXAFS function (solid line) and sum of the calculated Ru-Ru, Ru-Pt, Ru-C, Ru-O\*, Ru-O<sub>s</sub>, and Ru-O<sub>l</sub> contributions (dotted line). (D) Magnitude of uncorrected Fourier transform ( $k^3$  weighted) of experimental EXAFS function (solid line) and sum of the calculated Ru-Ru, Ru-Pt, Ru-C, Ru-O\*, Ru-O<sub>s</sub>, and Ru-O<sub>l</sub> contributions (dotted line).

The reliability and consistency of parameters from EXAFS fitting were determined. For each edge of Pt-Ru contributions, the bond distances and Debye-Waller factors must be equivalent and the coordination numbers  $N_{\text{PtRu}}$  related to  $N_{\text{RuPt}}$  by this equation:  $N_{\text{PtRu}}/N_{\text{RuPt}} = n_{\text{Ru}}/n_{\text{Pt}}$ , where  $n_{\text{Ru}}$  and  $n_{\text{Pt}}$  are the total numbers of Ru and Pt atoms in sample.

The EXAFS parameters in Table 3.1 showed Pt-O<sub>support</sub> and Ru-O<sub>support</sub> interactions on MgO surface and changes in bond distance of CO ligands indicating structural changes of adsorbed precursor on MgO. Table 3.1 presents average Pt-O<sub>s</sub> interatomic distance at  $2.03 \pm 0.01 \text{ \AA}$  with coordination number  $0.7 \pm 0.1$  and Pt-O<sub>l</sub> contributions was also detected at average distance  $2.92 \pm 0.01 \text{ \AA}$  with coordination number  $1.0 \pm 0.1$ . These EXAFS data indicated that Pt atom could interact with surface oxygen on MgO resulting in Pt-O bonding. In addition, changes in average Pt-C and Pt-O\* bond distances were observed. The average coordination number of Pt-C was  $0.9 \pm 0.1$  and average Pt-C bond distance did not significantly change, namely from 1.85 to  $1.88 \pm 0.01 \text{ \AA}$ , compared to that of precursor in crystalline form (Table 3.2).

Table 3.2 compared XRD data of precursor in crystalline form (Adams, Barnard et al., 1994) with EXAFS data of adsorbed precursor on MgO. No significant change in both distances and coordination number of Pt-C and Pt-O\* indicating that partial decarbonylation from Pt did not take place after adsorption.

The EXAFS data scanned at Ru K edge in Table 3.1 also indicate Ru-O<sub>support</sub> contributions. The average Ru-O<sub>s</sub> bond distance was detected at  $2.07 \pm 0.01 \text{ \AA}$  with  $2.1 \pm 0.1$  coordination numbers. The Ru-O<sub>l</sub> contribution was observed at longer distance,  $3.35 \pm 0.03 \text{ \AA}$  with small number of coordination number,  $0.2 \pm 0.1$ . These

data indicated that Ru interact strongly with surface oxygen on MgO. The Pt-O<sub>support</sub> and Ru-O<sub>support</sub> interactions might be the causes of structural changes of adsorbed precursor on MgO.

**Table 3.2** Comparison XRD data of crystalline Pt<sub>3</sub>Ru<sub>6</sub>(CO)<sub>21</sub>(μ<sub>3</sub>-H)(μ-H)<sub>3</sub> (Adams et al., 1994) and EXAFS of supported species formed from this cluster on MgO

Shell	XRD data of		EXAFS data of adsorbed	
	Pt <sub>3</sub> Ru <sub>6</sub> (CO) <sub>21</sub> (μ <sub>3</sub> -H)(μ-H) <sub>3</sub>		Pt <sub>3</sub> Ru <sub>6</sub> (CO) <sub>21</sub> (μ <sub>3</sub> -H)(μ-H) <sub>3</sub> on MgO	
	<i>N</i>	<i>R</i> (Å)	<i>N</i>	<i>R</i> (Å)
Pt-Pt	2.0	2.64	1.8 ± 0.1	2.53 ± 0.01
Pt-Ru	4.0	2.80	1.8 ± 0.1	2.89 ± 0.01
Pt-CO				
Pt-C	1.0	1.85	0.9 ± 0.1	1.88 ± 0.01
Pt-O*	1.0	2.99	0.9 ± 0.1	3.02 ± 0.01
Ru-Ru	2.0	3.04	1.4 ± 0.1	2.83 ± 0.01
Ru-Pt	2.0	2.80	1.2 ± 0.1	2.88 ± 0.01
Ru-CO				
Ru-C	3.0	1.89	3.1 ± 0.3	1.91 ± 0.01
Ru-O*	3.0	3.03	3.1 ± 0.1	2.93 ± 0.01

Partial decarbonylation from Ru atom was not observed because no significant changes on Ru-C and Ru-O\* contributions.

The changes in metal cluster core were also observed. The average Pt-Pt coordination number did not change much compared to XRD data of precursor in crystalline form (Table 3.2), from 2.0 to 1.8 ± 0.1, whereas average distance decreased from 2.64 to 2.53 ± 0.01 Å. The stronger in Pt-Pt interaction resulted from

interaction between precursor and support through CO ligands with hydroxyl groups or  $O^{2-}$  basic sites. The decreasing of coordination number of Pt-Ru from 4.0 to  $1.8 \pm 0.1$  indicated segregation of some Pt-Ru contribution implies strong precursor-support interaction. This behavior was different from that on  $\gamma\text{-Al}_2\text{O}_3$  support. The average Pt-Ru bond distance changed to  $2.89 \pm 0.01 \text{ \AA}$  compared to that of precursor in crystalline form,  $2.80 \text{ \AA}$ .

The EXAFS fitting parameters obtained at Ru K edge show that average Ru-Ru bond distance significantly decreased from  $3.04 \text{ \AA}$  to  $2.83 \text{ \AA}$  and coordination number was  $1.4 \pm 0.1$ , lower than that of crystalline  $\text{Pt}_3\text{Ru}_6(\text{CO})_{21}(\mu_3\text{-H})(\mu\text{-H})_3$ . The decrease in Ru-Ru interatomic distance might due to loss of electron-rich hydride ligands resulting in stronger Ru-Ru bonding. In addition, the coordination number of Ru-Pt decreased from 2.0 to  $1.2 \pm 0.1$  whereas the interatomic distance increase from  $2.80$  to  $2.89 \pm 0.01 \text{ \AA}$ .

From IR and EXAFS data, it can be conclude that  $\text{Pt}_3\text{Ru}_6(\text{CO})_{21}(\mu_3\text{-H})(\mu\text{-H})_3$  did not adsorb intact on MgO and interaction of adsorbed bimetallic carbonyl species and MgO occurred through oxygen-bound CO ligands and hydroxyls or surface oxygen on MgO surface forming carbonates and carboxylates rather than hydrogen bonding imply strong precursor-support interaction.

### 3.3.4 Pt-Ru interaction in supported sample after ligand removal

MgO-supported PtRu sample prepared by adsorption of  $\text{Pt}_3\text{Ru}_6(\text{CO})_{21}(\mu_3\text{-H})(\mu\text{-H})_3$  was heated in He flow at  $300^\circ\text{C}$  for 2 h to remove ligands and characterized by IR and EXAFS spectroscopy. No IR bands in  $\nu_{\text{CO}}$  region were

observed (spectrum 3 in Figure 3.2) indicating that all carbonyl ligands were removed from adsorbed precursor on MgO.

The EXAFS data scanned at the Pt L<sub>III</sub> and the Ru K edges of decarbonylated PtRu sample at nearly liquid nitrogen temperature were analyzed with ATHENA software for data processing and then fitted with EXAFSPAK software. The EXAFS fitting parameters were summarized in Table 3.3. The EXAFS fitting results in  $k$  and  $r$  space with  $k^0$ ,  $k^1$  and  $k^3$  weighted scanned at the Pt L<sub>III</sub> and the Ru K edges are in Figures 3.5 and 3.6. The estimated accuracies of coordination number ( $N$ ), distance ( $R$ ), Debye-Waller factor ( $\Delta\sigma^2$ ), and inner potential correction ( $\Delta E_0$ ) are as follows:  $\pm 20\%$ ,  $\pm 1\%$ ,  $\pm 30\%$ , and  $\pm 10\%$ , respectively.

**Table 3.3** Summary of EXAFS data of sample prepared by adsorption of Pt<sub>3</sub>Ru<sub>6</sub>(CO)<sub>21</sub>( $\mu_3$ -H)( $\mu$ -H)<sub>3</sub> on MgO after ligand removal in He flow at 300°C for 2 h

Edge	Shell	$N$	$R$ (Å)	$10^3 \times \Delta\sigma^2$ (Å <sup>2</sup> )	$\Delta E_0$ (eV)
Pt L <sub>III</sub>	Pt-Pt	$1.3 \pm 0.2$	$2.69 \pm 0.02$	$5.1 \pm 2.2$	$8.7 \pm 1.4$
	Pt-Ru	$0.9 \pm 0.1$	$2.69 \pm 0.01$	$3.4 \pm 1.5$	$3.6 \pm 1.2$
	Pt-O <sub>support</sub>				
	Pt-O <sub>s</sub>	$2.3 \pm 0.1$	$2.03 \pm 0.01$	$4.8 \pm 1.1$	$7.1 \pm 0.3$
	Pt-O <sub>l</sub>	$0.4 \pm 0.1$	$3.09 \pm 0.05$	$12.1 \pm 12.5$	$-3.1 \pm 2.5$
Ru K	Ru-Ru	$2.6 \pm 0.1$	$2.63 \pm 0.01$	$4.8 \pm 0.1$	$-5.2 \pm 0.1$
	Ru-Pt	$1.1 \pm 0.1$	$2.69 \pm 0.01$	$3.7 \pm 0.2$	$-4.0 \pm 0.3$
	Ru-O <sub>support</sub>				
	Ru-O <sub>s</sub>	$1.4 \pm 0.1$	$2.09 \pm 0.01$	$12.0 \pm 0.3$	$7.4 \pm 0.2$
	Ru-O <sub>l</sub>	$0.2 \pm 0.1$	$2.87 \pm 0.01$	$-6.3 \pm 0.9$	$6.4 \pm 1.3$

Notation: subscript s and l refer to short and long, respectively

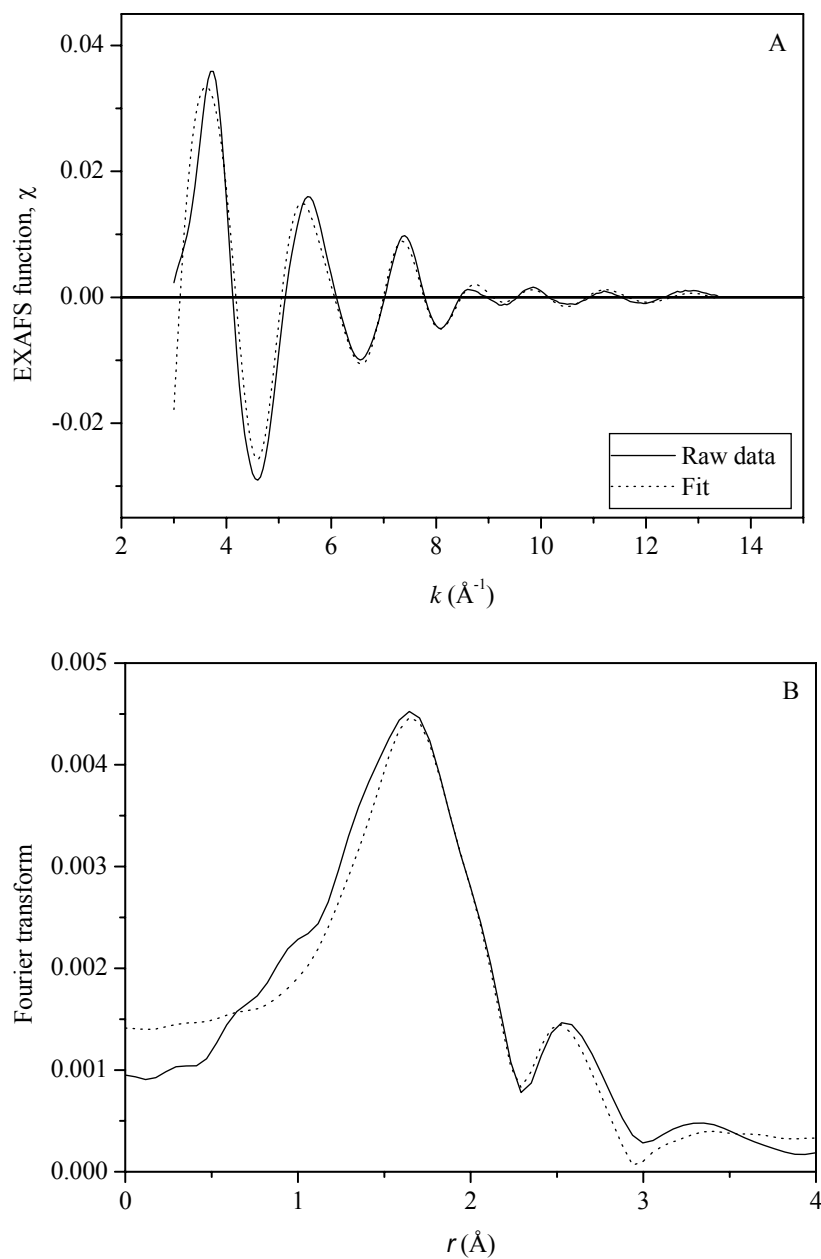


**Figure 3.5** EXAFS results scanned at the Pt L<sub>III</sub> edge characterizing the PtRu/MgO sample prepared by adsorption of Pt<sub>3</sub>Ru<sub>6</sub>(CO)<sub>21</sub>( $\mu_3$ -H)( $\mu$ -H)<sub>3</sub> after ligand removal: (A) Experimental EXAFS function (solid line) and sum of the calculated Pt-Pt, Pt-Ru, Pt-C, Pt-O\*, Pt-O<sub>s</sub>, and Pt-O<sub>l</sub> contributions (dotted line). (B) Magnitude of uncorrected Fourier transform ( $k^0$  weighted) of experimental EXAFS function (solid line) and sum of the calculated Pt-Pt, Pt-Ru, Pt-C, Pt-O\*, Pt-O<sub>s</sub>, and Pt-O<sub>l</sub> contributions (dotted line).

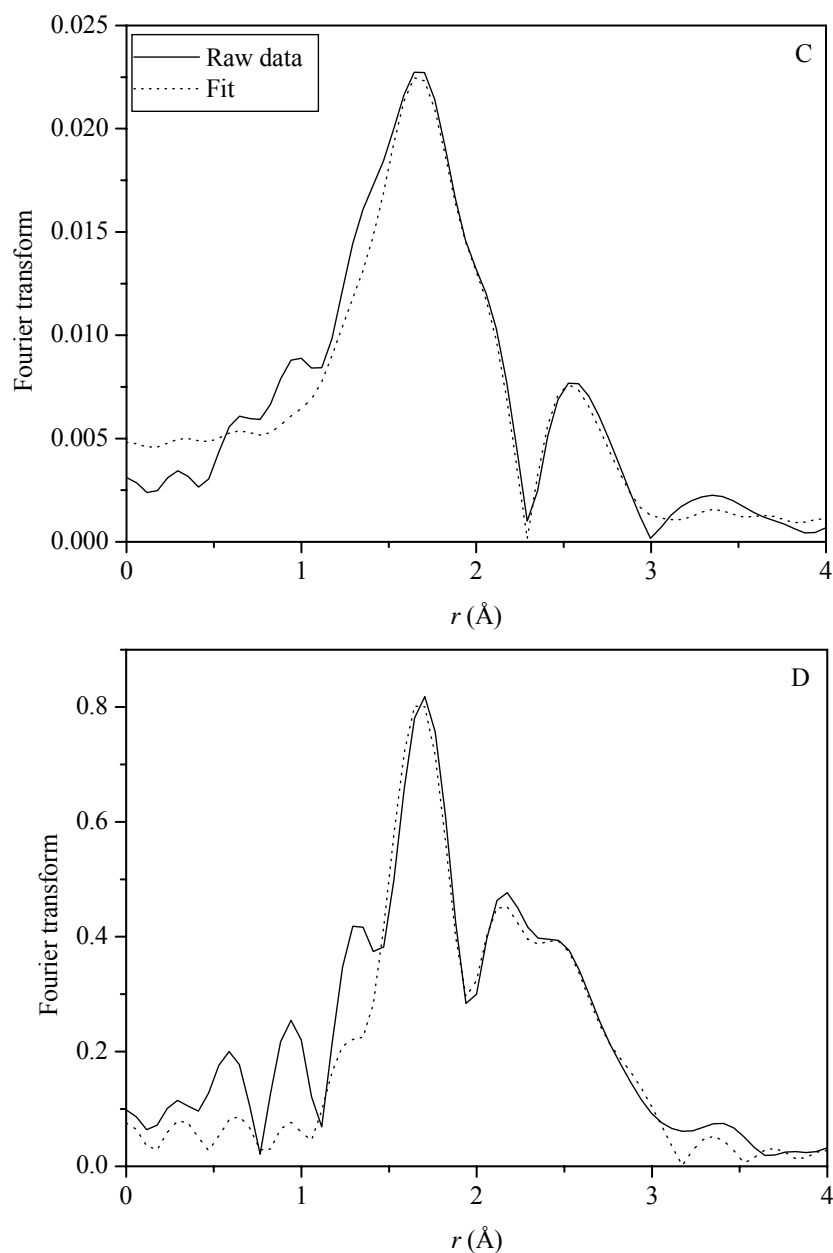


**Figure 3.5** (continued) EXAFS results scanned at the Pt L<sub>III</sub> edge characterizing the PtRu/MgO sample prepared by adsorption of Pt<sub>3</sub>Ru<sub>6</sub>(CO)<sub>21</sub>(μ<sub>3</sub>-H)(μ-H)<sub>3</sub> after ligands removal: (C) Magnitude of uncorrected Fourier transform ( $k^1$  weighted) of experimental EXAFS function (solid line) and sum of the calculated Pt-Pt, Pt-Ru, Pt-C, Pt-O\*, Pt-O<sub>s</sub>, and Pt-O<sub>l</sub> contributions (dotted line). (D) Magnitude of uncorrected Fourier transform ( $k^3$  weighted) of experimental EXAFS function (solid line) and sum of the calculated Pt-Pt, Pt-Ru, Pt-C, Pt-O\*, Pt-O<sub>s</sub>, and Pt-O<sub>l</sub> contributions (dotted line).

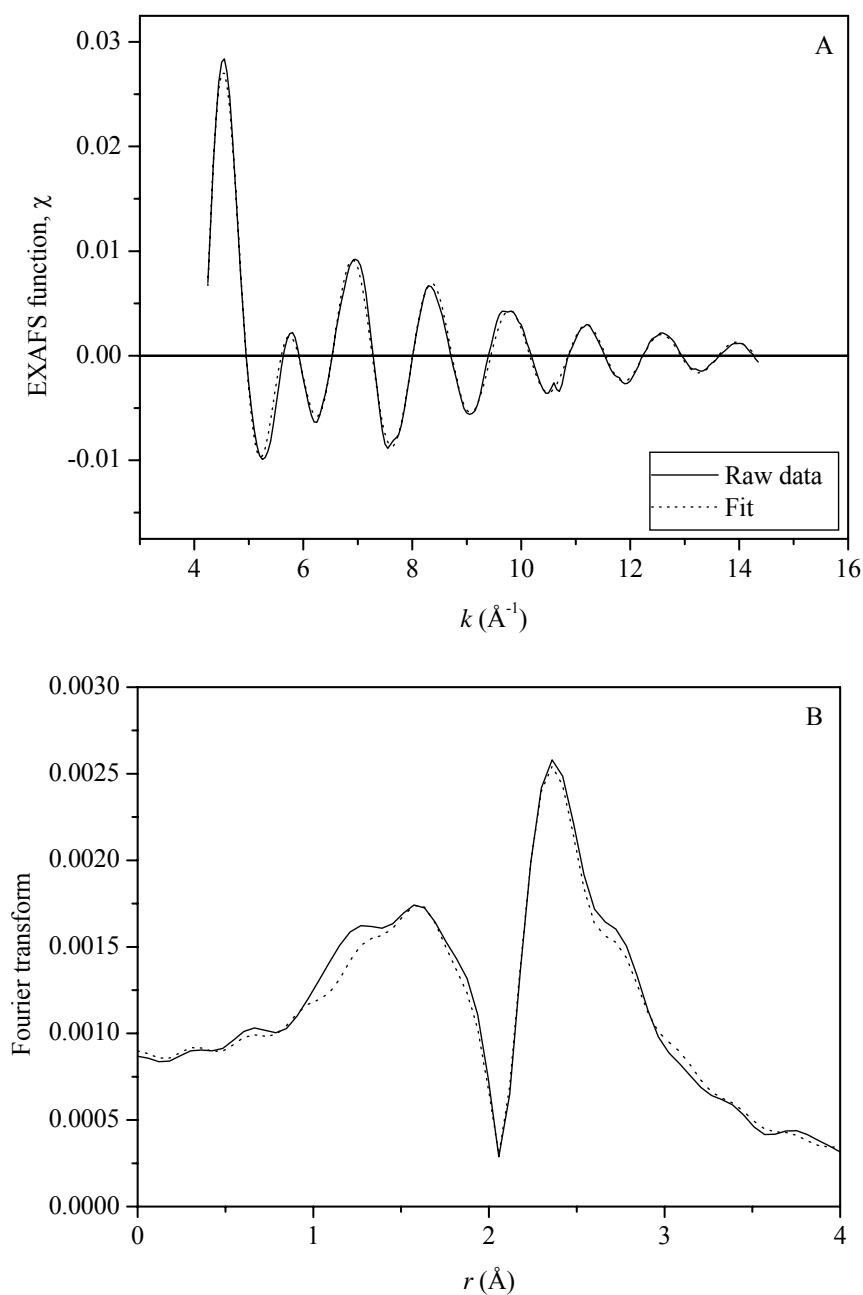


**Figure 3.6** EXAFS results scanned at the Ru K edge characterizing the PtRu/MgO sample prepared by adsorption of  $\text{Pt}_3\text{Ru}_6(\text{CO})_{21}(\mu_3\text{-H})(\mu\text{-H})_3$  after ligands removal: (A) Experimental EXAFS function (solid line) and sum of the calculated Ru-Ru, Ru-Pt, Ru-C, Ru-O\*, Ru-O<sub>s</sub>, and Ru-O<sub>l</sub> contributions (dotted line). (B) Magnitude of uncorrected Fourier transform ( $k^0$  weighted) of experimental EXAFS function (solid line) and sum of the calculated Ru-Ru, Ru-Pt, Ru-C, Ru-O\*, Ru-O<sub>s</sub>, and Ru-O<sub>l</sub> contributions (dotted line).

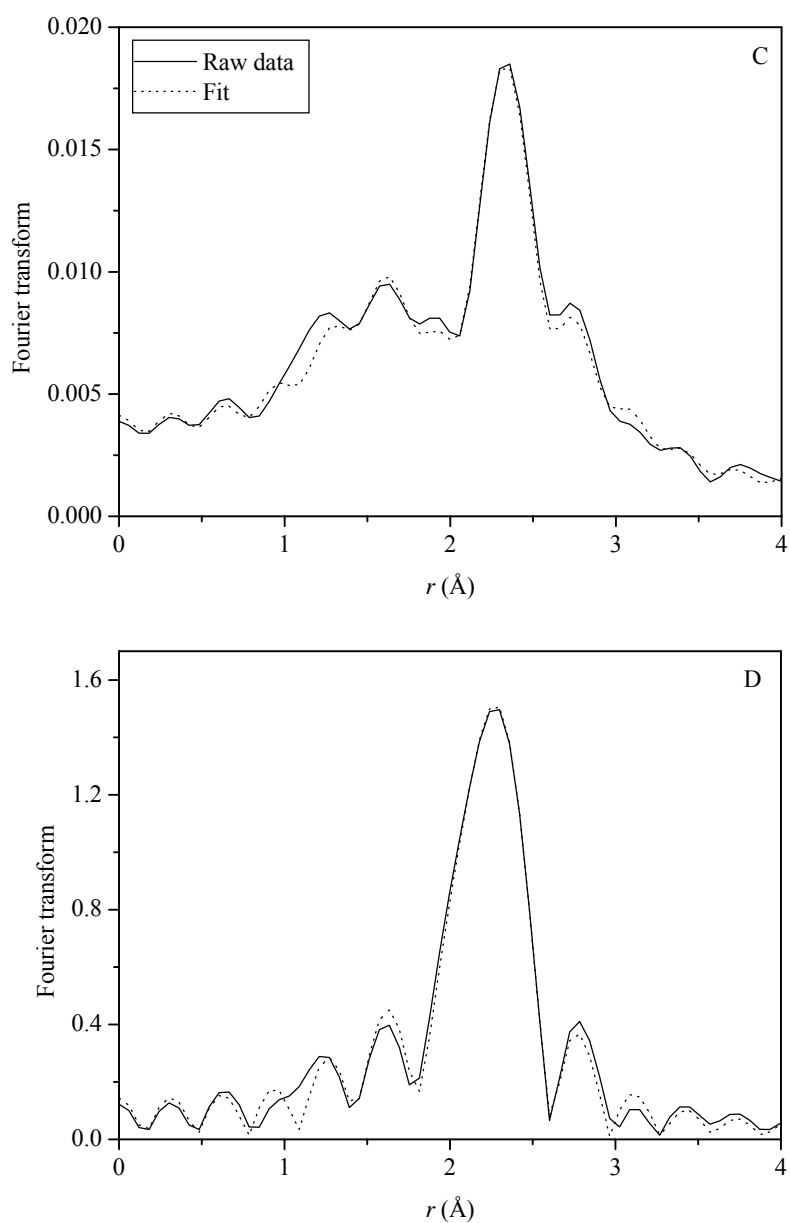


**Figure 3.6** (continued) EXAFS results scanned at the Ru K edge characterizing the PtRu/MgO sample prepared by adsorption of  $\text{Pt}_3\text{Ru}_6(\text{CO})_{21}(\mu_3\text{-H})(\mu\text{-H})_3$  after ligands removal: (C) Magnitude of uncorrected Fourier transform ( $k^1$  weighted) of experimental EXAFS function (solid line) and sum of the calculated Ru-Ru, Ru-Pt, Ru-C, Ru-O\*, Ru-O<sub>s</sub>, and Ru-O<sub>l</sub> contributions (dotted line). (D) Magnitude of uncorrected Fourier transform ( $k^3$  weighted) of experimental EXAFS function (solid line) and sum of the calculated Ru-Ru, Ru-Pt, Ru-C, Ru-O\*, Ru-O<sub>s</sub>, and Ru-O<sub>l</sub> contributions (dotted line).

The EXAFS fitting parameters show changes of the metal core after ligand removal in He flow at 300°C for 2 h. Comparing with data before the treatment, the average Pt-Pt interatomic distance increased from  $2.54 \pm 0.01 \text{ \AA}$  to  $2.69 \pm 0.02 \text{ \AA}$  and coordination number slightly changed to  $1.3 \pm 0.2$ . Moreover, the coordination number of Pt-Ru contribution significantly decreased from  $2.0 \pm 0.1$  to  $0.9 \pm 0.1$  with average Pt-Ru bond distance  $2.69 \pm 0.01 \text{ \AA}$  indicating a tendency of Pt and Ru to segregate from each other. Removal of CO ligands leads to stronger interaction between Pt and surface oxygen on support. The interaction of Pt-O<sub>support</sub> increased as shown by coordination number of Pt-O<sub>s</sub> increased to  $2.3 \pm 0.1$  at interatomic distance  $2.03 \pm 0.01 \text{ \AA}$ . The Pt-O<sub>l</sub> contribution was found at  $3.09 \pm 0.05 \text{ \AA}$  with coordination number  $0.4 \pm 0.1$ .

The EXAFS fitting parameters obtained at Ru K edge of sample after ligand removal also show changes in Ru-Ru interaction. The average distance of Ru-Ru contribution decreased from  $2.83 \pm 0.01 \text{ \AA}$  to  $2.63 \pm 0.01 \text{ \AA}$  while coordination number increased to  $2.6 \pm 0.1$  indicating stronger Ru-Ru interaction and confirming Ru segregation from Pt. The high dispersion of Pt-Ru contribution was observed with coordination number  $1.1 \pm 0.1$  at average interatomic distance  $2.69 \pm 0.01 \text{ \AA}$ . In addition, Ru-O<sub>s</sub> coordination number slightly decreased from  $2.1 \pm 0.1$  to  $1.4 \pm 0.1$  while average bond distance did not significantly change,  $2.09 \pm 0.01 \text{ \AA}$ . Small number of Ru-O<sub>l</sub> contribution was detected at  $2.87 \pm 0.01 \text{ \AA}$  with coordination number only  $0.2 \pm 0.1$ .

The EXAFS fitting parameters at Ru K edge suggested that Ru particles on MgO likely have greater tendency to aggregate during ligand removal under He flow

at 300°C than Pt particles. However, the aggregation at this condition did not cause Pt-Ru bonds to break completely.

Consequently, preparation of PtRu/MgO by adsorption of  $\text{Pt}_3\text{Ru}_6(\text{CO})_{21}(\mu_3\text{-H})(\mu\text{-H})_3$  on MgO gave bimetallic PtRu particles with high dispersion.

### 3.3.5 Effect of chemistry of support on cluster-support interaction

Cluster-support interactions depend not only on nature of precursor, but also on the chemistry of support. MgO was a basic support containing basic sites such as hydroxyls and  $\text{O}^{2-}$ , and unsaturated  $\text{Mg}^{2+}$  sites. Comparing with  $\gamma\text{-Al}_2\text{O}_3$  which is slightly acidic, MgO is basic. It was found that precursor-support and cluster-support interactions on MgO were stronger than that on  $\gamma\text{-Al}_2\text{O}_3$ . The metal framework of adsorbed precursor remained intact on  $\gamma\text{-Al}_2\text{O}_3$  whereas bimetallic Pt-Ru contributions adsorbed on MgO were partially broken upon adsorption and strong Pt- $\text{O}_{\text{support}}$  on MgO were detected. Although, adsorption of precursor on MgO was not intact, it was still in the form of bimetallic carbonyl species which could not be extracted by  $\text{CH}_2\text{Cl}_2$ . After decarbonylation, some of Pt-Ru contributions were partially broken for both supported samples. Only  $0.9 \pm 0.1$  coordination number of Pt-Ru contributions were found on MgO while  $2.2 \pm 0.1$  were found for that on  $\gamma\text{-Al}_2\text{O}_3$ . The Ru-Pt contribution on MgO and  $\gamma\text{-Al}_2\text{O}_3$  was not different,  $1.0 \pm 0.1$  and  $1.1 \pm 0.1$ , respectively.

Consequently, this precursor has stronger interaction with basic support MgO than that with  $\gamma\text{-Al}_2\text{O}_3$  resulting in greater tendency to segregate and also extremely high dispersion of bimetallic particles on MgO.

### 3.3.6 Effect of Pt-Ru interactions on ethylene hydrogenation

#### 3.3.6.1 Catalytic activity and time on stream (TOS)

A blank test for ethylene hydrogenation was performed with stainless U-tube reactor containing  $\alpha$ -Al<sub>2</sub>O<sub>3</sub>. A plot between activity and inversed weight hourly space velocity (inv. WHSV, g cat/mol/h) at -75°C was in Figure 3.7 showing straight line from the origin and the data determine rate of the catalytic reaction could be obtained directly from the slope. This plot implies that stainless U-tube reactor testing within inv. WHSV ranges of 0-4.56 g cat/mol/h with conversion < 5% was a differential reactor.

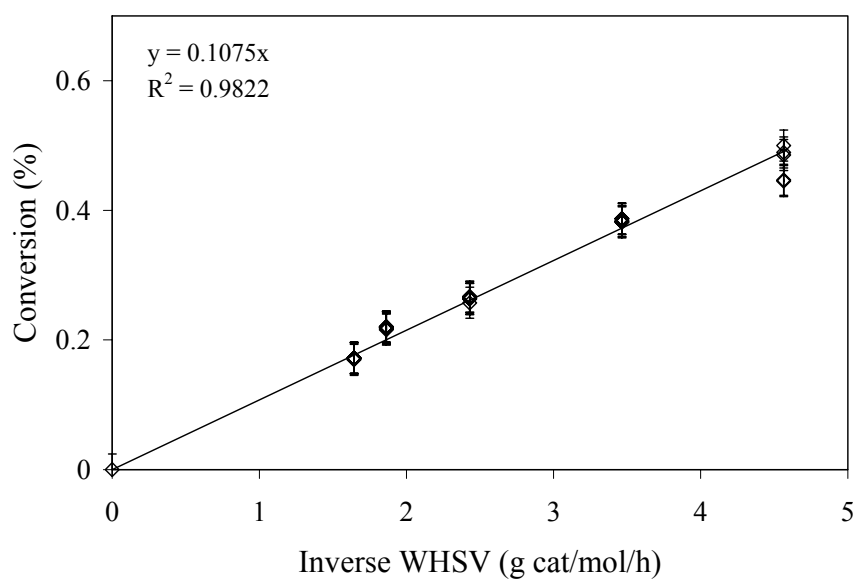


**Figure 3.7** Demonstration of differential reactor operation at -75°C,  $P_{\text{C}_2\text{H}_4} = 40$  Torr,  $P_{\text{H}_2} = 80$  Torr, balanced with He, total feed flow rate = 200 ml (NTP)/min catalyzed by PtRu/MgO.

The catalytic activity of reaction was calculated in terms of the turnover frequency (TOF) representing the number of molecules reacting per active sites per

second (Fogler, 1999). It was assumed that all metal particles were accessible for reactant gas, thus TOF was defined in equation 2.3 (Chapter II, page 53)

The plot between activity and time on stream (TOS) of ethylene hydrogenation on PtRu/MgO is in Figure 3.8. Ethylene hydrogenation reaction occurred as soon as reactant gas flowed to catalyst bed with conversion around 0.3% at reaction condition:  $P_{C_2H_4} = 40$  Torr,  $P_{H_2} = 80$  Torr, balanced He with total feed flow rate 200 ml (NTP)/min, catalyst mass 0.012 mg, 1.0 wt% Pt and 1.0 wt% Ru, and temperature  $-75^\circ\text{C}$ . The catalytic activities slightly decreased during 270 min.

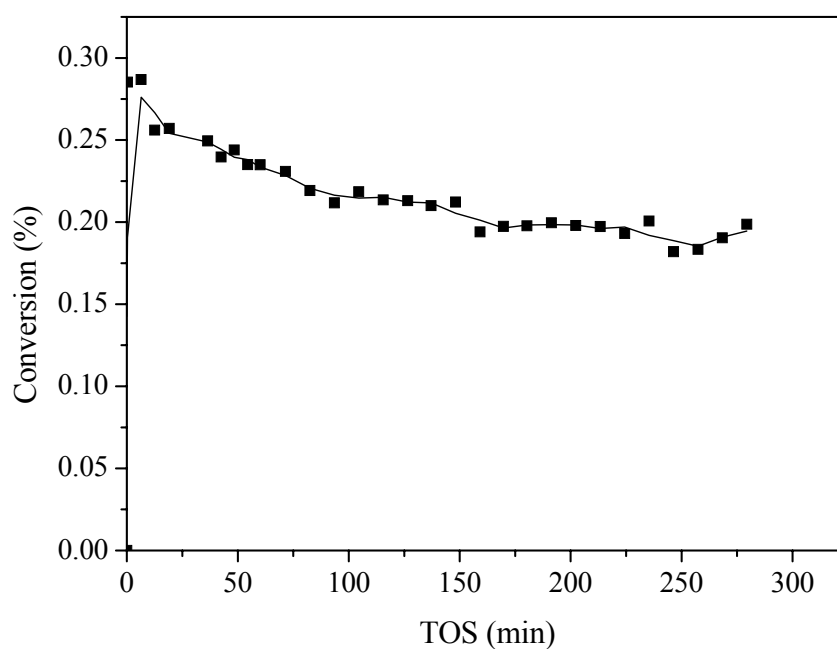


**Figure 3.8** Activity plot with TOS of ethylene hydrogenation catalyzed by PtRu/MgO at reaction condition:  $P_{C_2H_4} = 40$  Torr,  $P_{H_2} = 80$  Torr, balanced He with total feed flow rate 200 ml (NTP)/min, catalyst mass 0.012 mg, and temperature  $-75^\circ\text{C}$ .

### 3.3.6.2 Kinetics of ethylene hydrogenation catalyzed by PtRu/MgO

Kinetic data of ethylene hydrogenation catalyzed by MgO-supported Pt-Ru sample after ligand removal in flowing He at 300°C for 2 h was investigated. The apparent activation energy of ethylene hydrogenation catalyzed by Pt-Ru/MgO was collected at around 50 min TOS at reaction condition:  $P_{\text{C}_2\text{H}_4} = 40$  Torr,  $P_{\text{H}_2} = 80$  Torr, balanced He with total feed flow rate 200 ml (NTP)/min, catalyst mass 0.010-0.020 mg, 1.0 wt% Pt and 1.0 wt% Ru, and temperature from -75 to -30°C. Reaction temperature was controlled within  $\pm 1^\circ\text{C}$  with heater connected to temperature controller as shown in Figure 3.9. The Arrhenius plot of a natural log of TOF as a function of inversed temperature was in Figure 3.10.

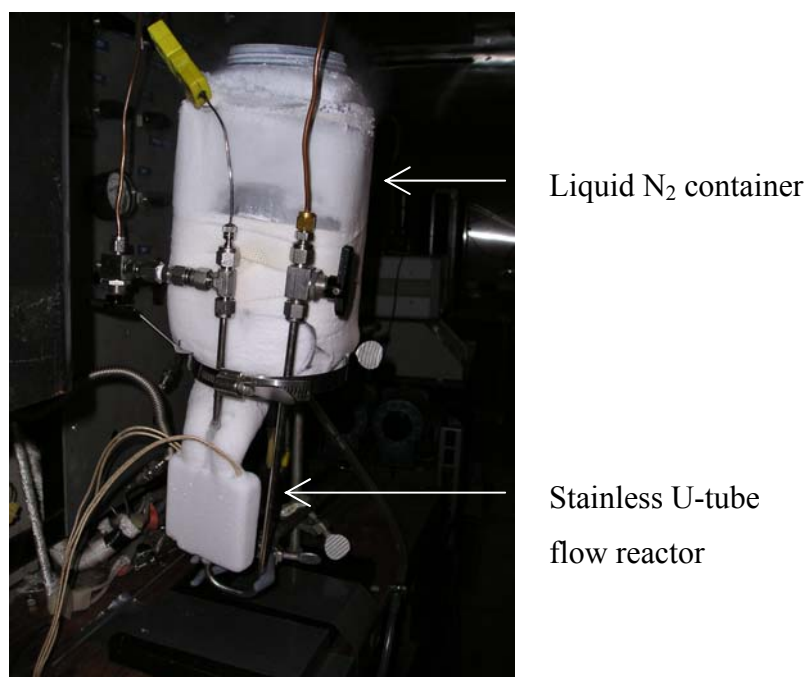


**Figure 3.9** Stainless steel U-tube reactor cooling with liquid nitrogen.

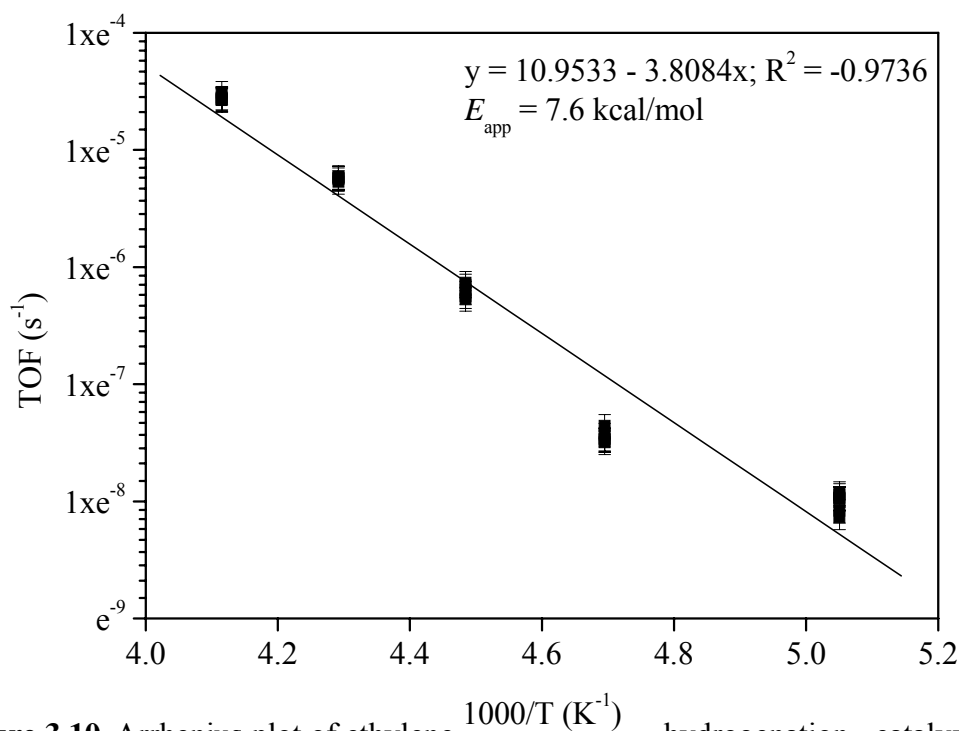


**Figure 3.10** Arrhenius plot of ethylene  $1000/T$  ( $K^{-1}$ ) hydrogenation catalyzed by PtRu/MgO at reaction condition:  $P_{C_2H_4} = 40$  Torr,  $P_{H_2} = 80$  Torr, balanced He with total feed flow rate 200 ml (NTP)/min, catalyst mass 0.012 g.

The apparent activation energy obtained from temperature dependence of rate of ethylene hydrogenation reaction of Pt-Ru/MgO was  $7.6 \pm 0.1$  kcal/mol, slightly lower than that of Pt-Ru/ $\gamma$ -Al<sub>2</sub>O<sub>3</sub> which was  $8.4 \pm 0.1$  kcal/mol. The value was lower than those reported for ethylene hydrogenation catalyzed by Pt catalysts supported on oxides supports that were in the range of 8.6-11.7 kcal/mol obtained at various conditions as in Table 2.4 (Chapter II). Moreover, Table 2.4 shows that apparent activation energy obtained from this work is near the valued obtained from polymer-supported Pt-Ru catalysts prepared from bimetallic cluster, [RuPt<sub>2</sub>(CO)<sub>5</sub>(Ph<sub>2</sub>P- $\text{C}$ )<sub>3</sub>],

$7.8 \pm 1.2$  kcal/mol obtained at  $P_{\text{H}_2} = 555$  Torr and  $P_{\text{C}_2\text{H}_4} = 152$  Torr, and temperature range 73 to 98°C (Pierantozzi, McQuade, and Gates, 1979).

Catalytic activity (TOF) of ethylene hydrogenation catalyzed by PtRu/MgO at temperature -75°C was  $(3.4 \pm 0.2) \times 10^{-4}$  (s<sup>-1</sup>). However, reports of catalytic activity of ethylene hydrogenation catalyzed by MgO-supported Pt or Ru catalysts were not found from literature review from ScienceDirect and ACS database upto October 2004.

Therefore, it could be concluded that MgO-supported Pt-Ru catalyst prepared from  $\text{Pt}_3\text{Ru}_6(\text{CO})_{21}(\mu_3\text{-H})(\mu\text{-H})_3$  was active for ethylene hydrogenation giving apparent activation energy  $7.6 \pm 0.1$  kcal/mol at the studied conditions. The catalytic data demonstrated that strong cluster-support interaction might affect catalytic property of ethylene hydrogenation and also metal dispersion.

### **3.3.6.3 Rate expression for ethylene hydrogenation catalyzed by PtRu/MgO**

The effect of pressure of hydrogen on Pt-Ru/MgO catalyst was investigated on 0.01-0.020 mg catalyst at -75°C with conversion < 5% at  $P_{\text{C}_2\text{H}_4} = 40$  Torr,  $P_{\text{H}_2}$  varied from 20 to 200 Torr, balanced He with total feed flow rate 200 ml (NTP)/min. Catalytic activities of ethylene hydrogenation in terms of TOF was plotted as a function of hydrogen pressure in Figure 3.11.

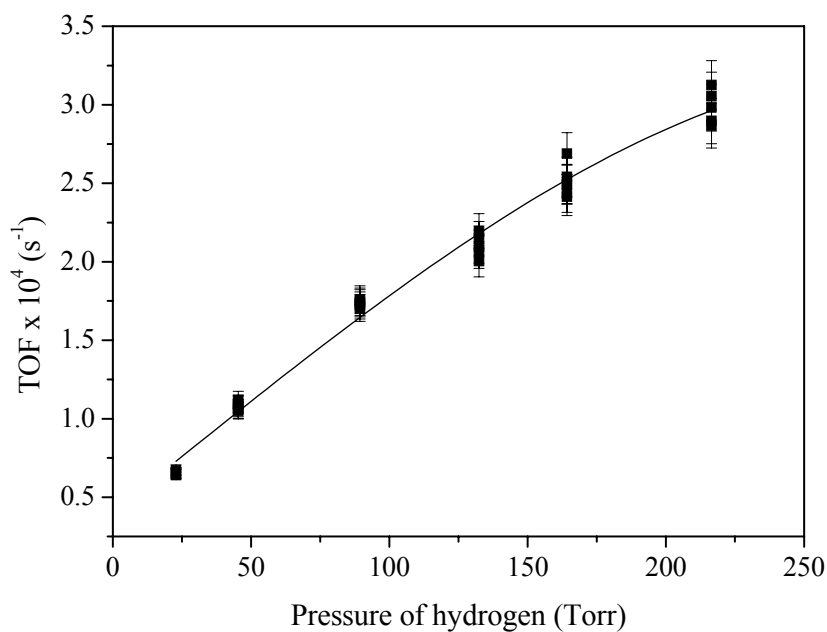


**Figure 3.11** Effect of pressure of hydrogen on ethylene hydrogenation catalyzed by PtRu/MgO.

The catalytic activities of ethylene hydrogenation catalyzed by Pt-Ru/MgO catalyst at 40 Torr ethylene pressure increased with hydrogen pressure.

Reaction orders of hydrogen and ethylene can be determined in the form of rate expression in equation 3.1.

$$\text{rate} = k P_{\text{H}_2}^a P_{\text{C}_2\text{H}_4}^b \quad \dots(3.1)$$

Where  $k$  = reaction rate

$a$  = hydrogen order

$b$  = ethylene order

In this work, rate of reaction was presented in term of turn over frequencies (TOF) and plot in a natural log scale of TOF versus  $P_{H_2}$  were shown in Figure 3.12 with excess hydrogen, 80 to 200 Torr while ethylene pressure was constant at 40 Torr.

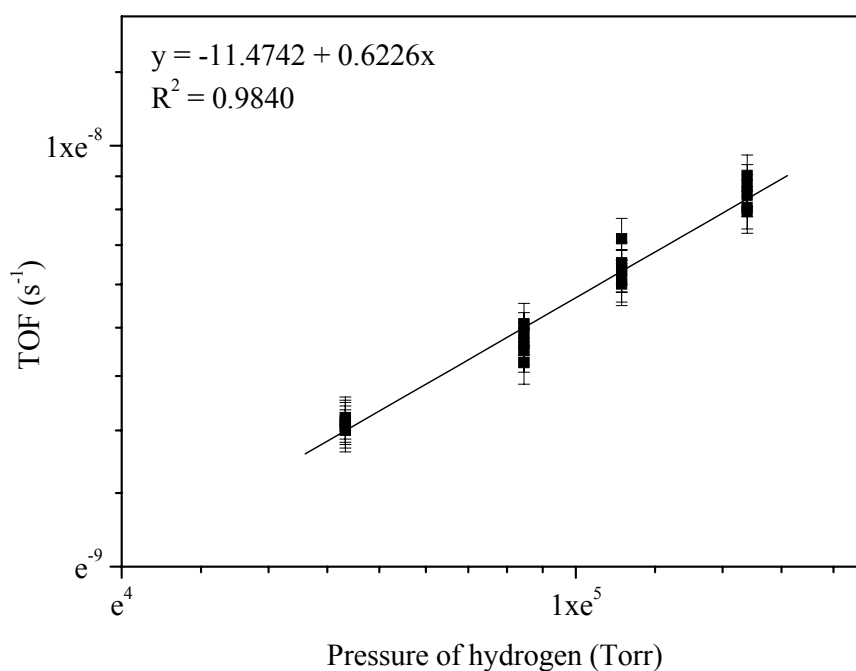


**Figure 3.12** The plot in a natural log scale between TOF and pressure of hydrogen for ethylene hydrogenation catalyzed by PtRu/MgO at  $-75^{\circ}\text{C}$ , 40 Torr ethylene and 80 to 200 Torr hydrogen.

Hydrogen order of PtRu/MgO obtained from slope of linear plot in Figure 3.12 was 0.62. This hydrogen order value was slightly higher than that of 0.04 wt% Pt/Cab-O-Sil which the rate expression for ethylene hydrogenation was found as equation 3.2 (Cortright et al., 1991).

$$\text{rate} = k P_{H_2}^{0.48} P_{C_2H_4}^{-0.17} \quad \dots(3.2)$$

That data for hydrogen order was obtained in a flow reactor at temperature  $-50^{\circ}\text{C}$ ; 25 Torr  $P_{\text{C}_2\text{H}_4}$ ; 50 - 650 Torr  $P_{\text{H}_2}$ . In addition, hydrogen order of PtRu/MgO in this work was higher the value of PtRu/ $\gamma$ - $\text{Al}_2\text{O}_3$  which was 0.46 (see Chapter II).

The effect of ethylene pressure on ethylene hydrogenation activity was investigated at  $-75^{\circ}\text{C}$  at constant hydrogen pressure of 80 Torr and varied pressure of ethylene from 20 to 200 Torr. A plot of TOF as a function of pressure of ethylene was shown in Figure 3.13.

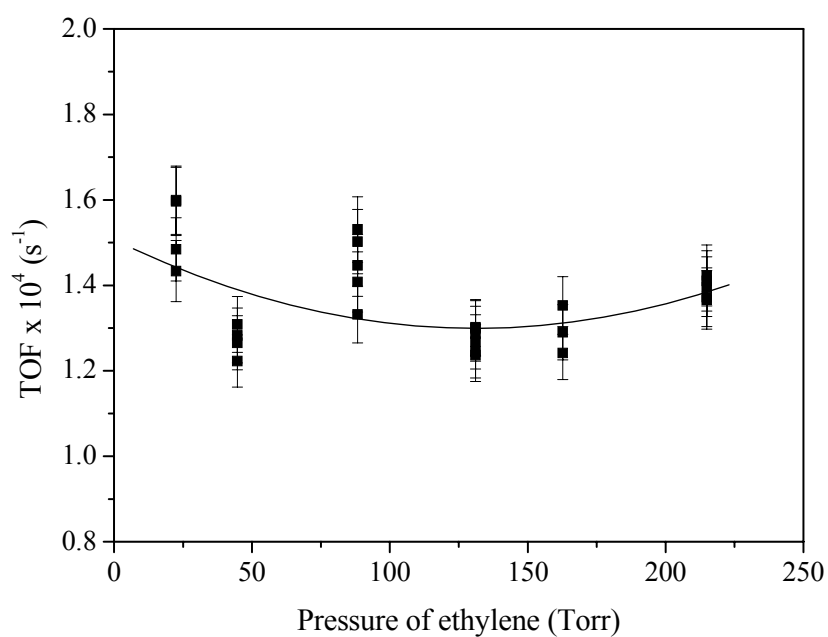


**Figure 3.13** Effect of pressure of ethylene on ethylene hydrogenation catalyzed by PtRu/MgO.

Figure 3.13 indicates that at low pressure ratio hydrogen:ethylene, catalytic activities decrease with ethylene pressure whereas at high ethylene pressure, catalytic activities increase with pressure of ethylene. The order of ethylene could be obtained

with the rate expression (equation 3.1). A plot in a natural log scale of TOF and  $P_{C_2H_4}$  is in Figure 3.14 at hydrogen pressure 80 Torr and low ethylene pressure range 20-40 Torr and high ethylene pressure 120-200 Torr.

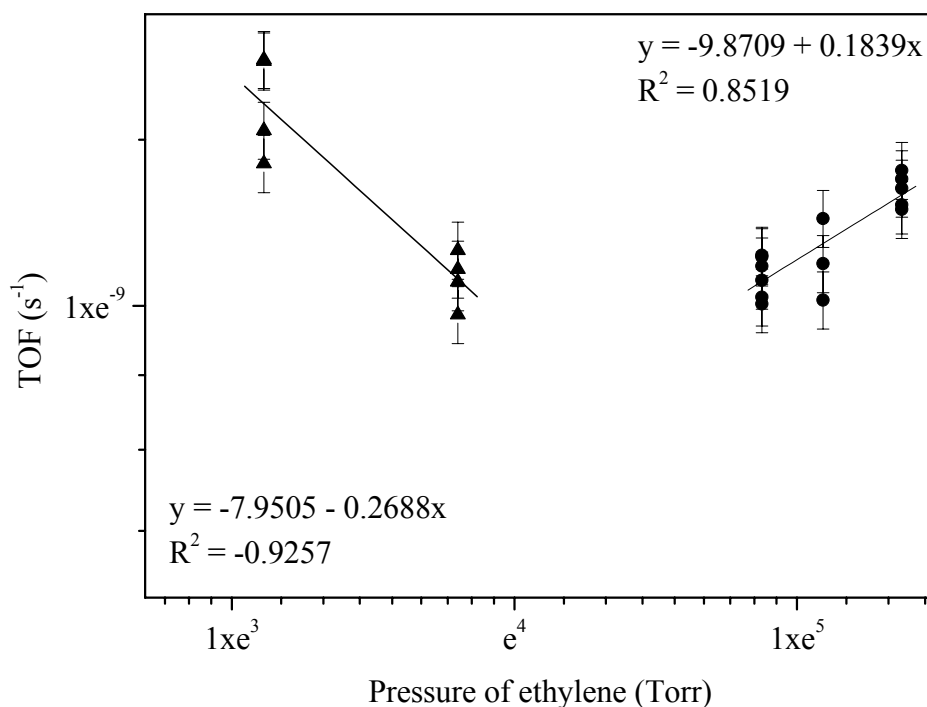


**Figure 3.14** The plot in a natural log scale between TOF and pressure of ethylene for ethylene hydrogenation catalyzed by PtRu/MgO at  $-75^{\circ}\text{C}$ , 80 Torr hydrogen and (▲) 20 to 40 Torr ethylene; and (●) 120 to 200 Torr ethylene.

It was found that ethylene order was negative values at low hydrogen:ethylene ratio, and was positive at hydrogen:ethylene  $> 1:1$ . At low pressure of ethylene, ethylene order obtained from slope of a left graph in Figure 3.14 was  $-0.27$  whereas the order was  $0.18$  at high ethylene pressure, 120 to 200 Torr. The negative ethylene order in this work was slightly lower than that reported by Cortright et al. (1991). The

positive ethylene value was lower than that obtained from PtRu/ $\gamma$ -Al<sub>2</sub>O<sub>3</sub> in Chapter II which was 0.35 during 80-200 Torr ethylene at -75°C and hydrogen pressure at 80 Torr. Therefore, rate expression for ethylene hydrogenation catalyzed by PtRu/MgO at -75°C and hydrogen:ethylene ratio < 1:1 could be written as in equation 3.3.

$$\text{rate} = k P_{\text{H}_2}^{0.52} P_{\text{C}_2\text{H}_4}^{-0.27} \quad \dots(3.3)$$

The rate expression for ethylene hydrogenation catalyzed by PtRu/MgO at -75°C while hydrogen:ethylene ratio > 1:1 could be written as in equation 3.4.

$$\text{rate} = k P_{\text{H}_2}^{0.52} P_{\text{C}_2\text{H}_4}^{-0.18} \quad \dots(3.4)$$

Ethylene could adsorb on surface of metal by three different modes as described in Chapter II;  $\pi$ -bonded ethylene, di- $\sigma$ -bonded ethylene and ethylidyne. The  $\pi$ -bonded ethylene is weakly bound and occurred at high pressure of hydrogen and ethylene in reaction. Hwang and co-workers (2003) reported that most of ethane products of ethylene hydrogenation on Pt(111) were from  $\pi$ -bonded ethylene. This study also concluded that ethylene order at high pressure of ethylene was due to  $\pi$ -bonded ethylene hydrogenation the same as suggested in Chapter II for PtRu/ $\gamma$ -Al<sub>2</sub>O<sub>3</sub>.

#### **3.3.6.4 Change of IR spectrum during ethylene hydrogenation catalyzed by PtRu/MgO**

The adsorption of ethylene on PtRu/MgO was studied by IR spectroscopy during flowing of a mixture of ethylene and He at various pressure of ethylene at room temperature. Details of sample preparation were described in Chapter II. Briefly, self-supporting wafer of treated sample placed in special design IR cell was purged with He, and then mixture of ethylene and He was flowed into the

cell. The IR signal was scanned with scan rate 128 scan/min every 120 s. The difference IR spectra of adsorbed ethylene displayed in Figure 3.15 were obtained by subtraction the spectra from that of gas phase ethylene during flowing ethylene.

Figure 3.15A and 3.15B represented IR spectra in  $\nu_{C-H}$  stretching and angle-deformation during 2700-3300  $\text{cm}^{-1}$  and 1000-2200  $\text{cm}^{-1}$ . The adsorbed ethylene species show IR band at 2964, 2987, 3008, 3076 and 3122  $\text{cm}^{-1}$ . The IR intensity of these bands increased with ethylene pressure. At low pressure of ethylene, around 20 Torr, only IR bands at 2964 and 2987  $\text{cm}^{-1}$  were observed. It was previously reported elsewhere that three adsorbed ethylene species on Pt/SiO<sub>2</sub> catalysts at room temperature: (i) ethylidyne show strong IR bands in bond-stretching and angle-deformation regions at 2885 and 1340  $\text{cm}^{-1}$ ; (ii) di  $\sigma$ -adsorbed species give medium absorptions at 2920 and 1420  $\text{cm}^{-1}$ ; and (iii)  $\pi$ -bonded species show weak absorptions at around 3105 and 1500  $\text{cm}^{-1}$  (Shahid and Sheppard, 1990). Thus, the IR bands at 2964 and 2987  $\text{cm}^{-1}$  in this work could be assigned to ethylidyne species.

The other IR bands at 3008, 3076 and 3122  $\text{cm}^{-1}$  were clearly observed when ethylene pressure was 40 Torr, and their intensity increased quickly with ethylene pressure. These IR bands at 3076 and 3122  $\text{cm}^{-1}$  were assigned to  $\pi$ -bonded ethylene, while IR band at 3008  $\text{cm}^{-1}$  represented di- $\sigma$ -bonded ethylene adsorbed species.

Furthermore, IR spectra during ethylene hydrogenation were collected as in Figure 3.16 in which IR spectra were not subtracted with gas phase ethane due to high conversion of ethylene at room temperature. The IR band represented ethane at 2954  $\text{cm}^{-1}$  occurred immediately after reactant gas flowed to catalyst wafer.

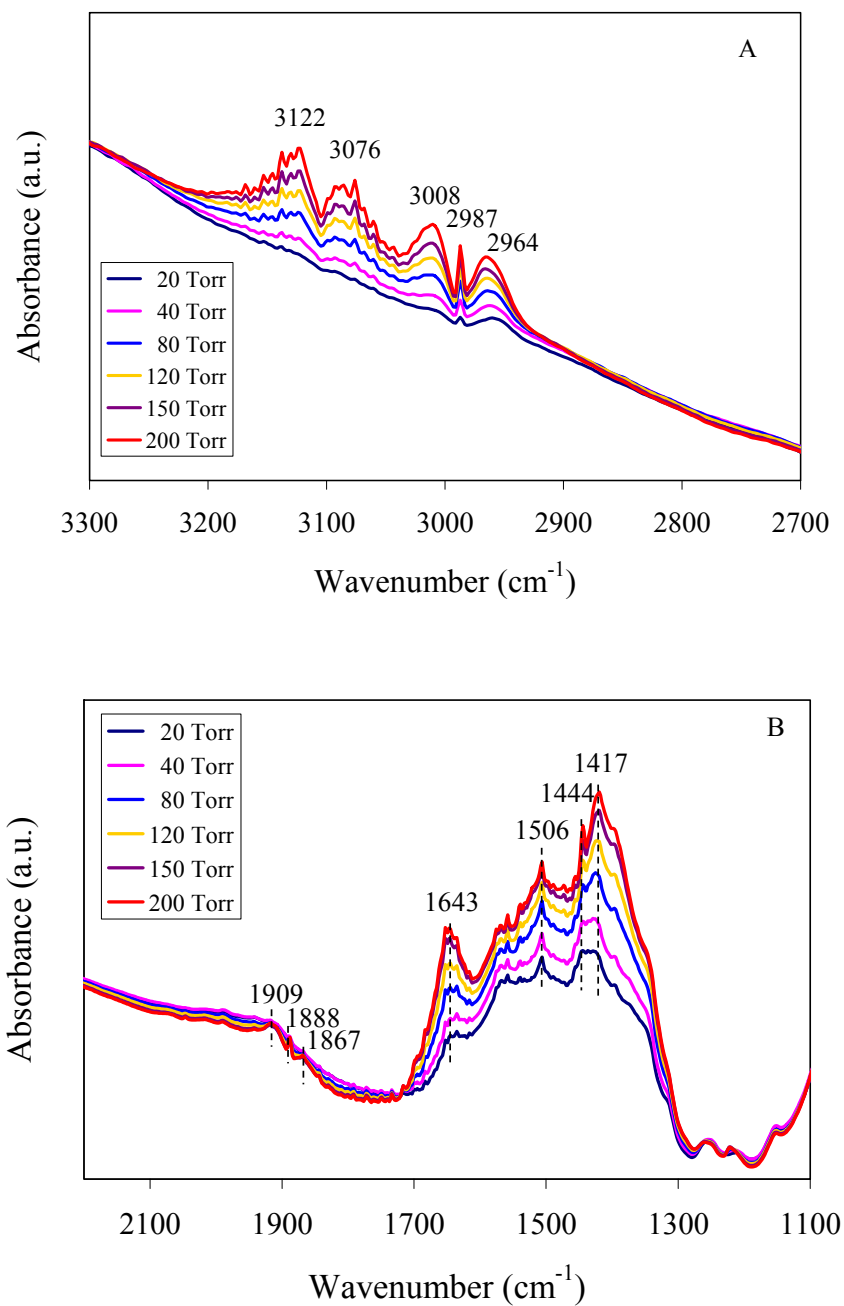


**Figure 3.15** The difference IR spectra during ethylene flow over PtRu/MgO at 30°C in the IR ranges of (A) 2700-3300 cm<sup>-1</sup>; and (B) 2200-1000 cm<sup>-1</sup> at ethylene pressure (1) 20 Torr; (2) 40 Torr; (3) 80 Torr; (4) 120 Torr; 150 Torr; and 200 Torr.

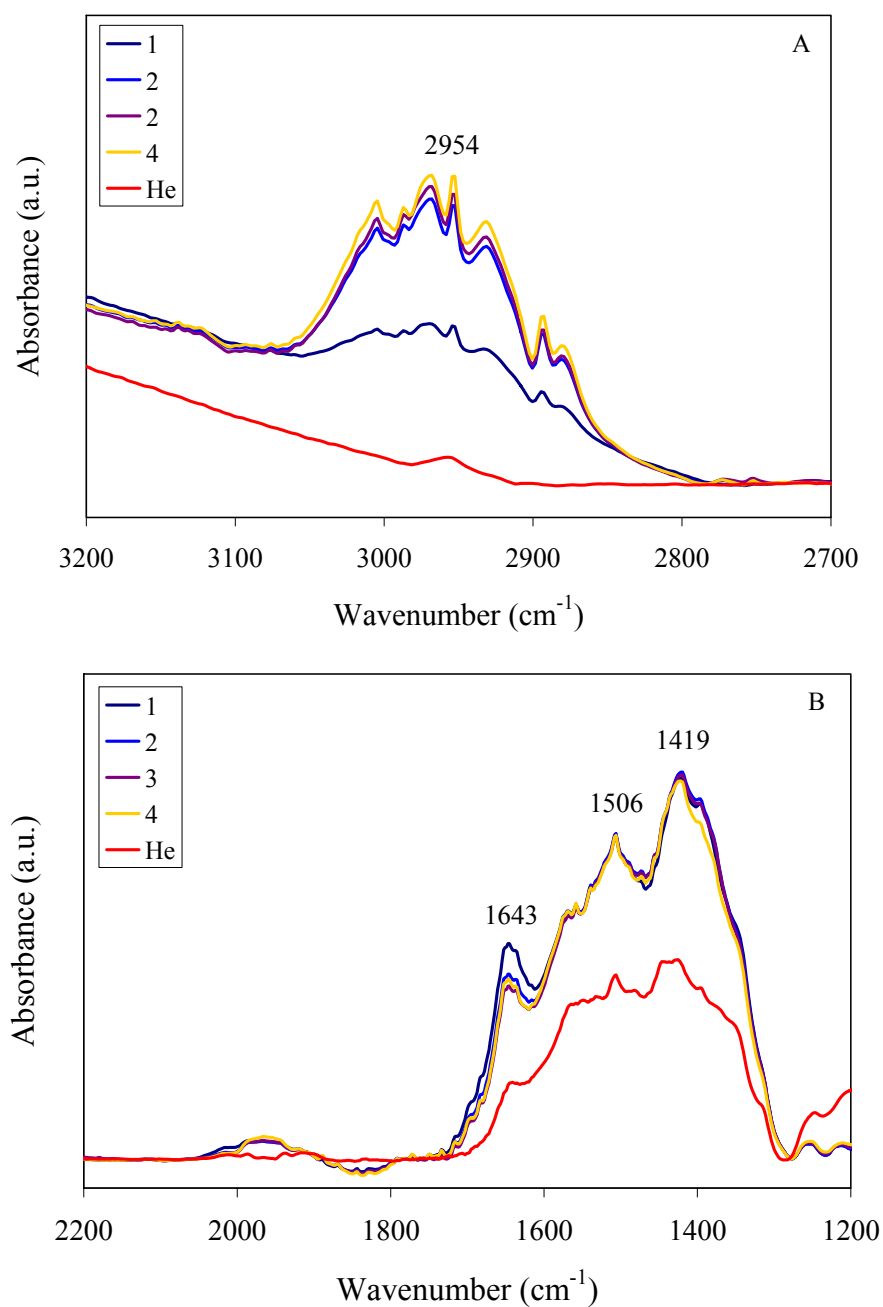


**Figure 3.16** IR spectra during catalysis of ethylene hydrogenation in a flow reactor at 30°C catalyzed by PtRu/MgO in IR ranges of (A) 2700-3200 cm<sup>-1</sup> and (B) 1200-2200 cm<sup>-1</sup> at conditions (1) He, 40 Torr C<sub>2</sub>H<sub>4</sub> and 80 Torr H<sub>2</sub>; (2) at 240 s after flowing reactant gas; (3) at 480 s after flowing reactant gas; (4) at 38 min after flowing reactant gas.

### 3.3.7 Effect of Pt-Ru interactions on *n*-butane hydrogenolysis catalyzed by PtRu/MgO

#### 3.3.7.1 Catalytic activity and TOS

Catalytic activities of *n*-butane hydrogenolysis catalyzed by PtRu/MgO prepared from adsorption of  $\text{Pt}_3\text{Ru}_6(\text{CO})_{21}(\mu_3\text{-H})(\mu\text{-H})_3$  was also investigated.

A blank test for *n*-butane hydrogenolysis was performed in quartz-tubed reactor with inert  $\alpha\text{-Al}_2\text{O}_3$  at  $P_{\text{H}_2} = 540$  Torr,  $P_{n\text{-C}_4\text{H}_{10}} = 60$  Torr with 100 ml (NTP)/min flow rate, and temperature 220°C. Conversion of *n*-butane was plotted as a function of inverse weight hourly space velocity (inv. WHSV, g cat/mol/h) at steady-state operation with conversion < 5% in Figure 3.17.

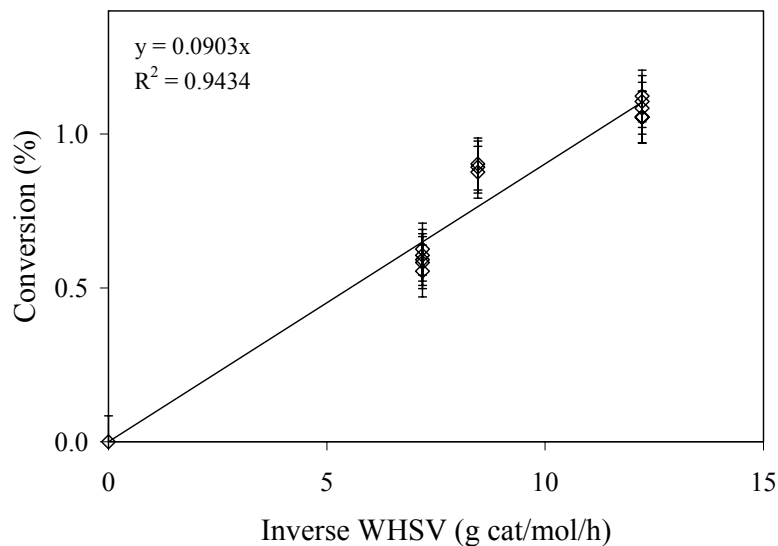


**Figure 3.17** Demonstration of differential reactor operation at 220°C,  $P_{\text{H}_2} = 540$  Torr,  $P_{n\text{-C}_4\text{H}_{10}} = 60$  Torr with 100 ml (NTP)/min flow rate catalyzed by PtRu/MgO.

The plot between activities and inv. WHSV within the ranges of 0-12.2 g cat/mol/h in Figure 3.17 represents linear graph through the origin imply that quartz-tubed flow reactor for *n*-butane hydrogenolysis was a differential reactor at this reaction condition. A plot of selectivity varied with inv. WHSV is in Figure 3.18.

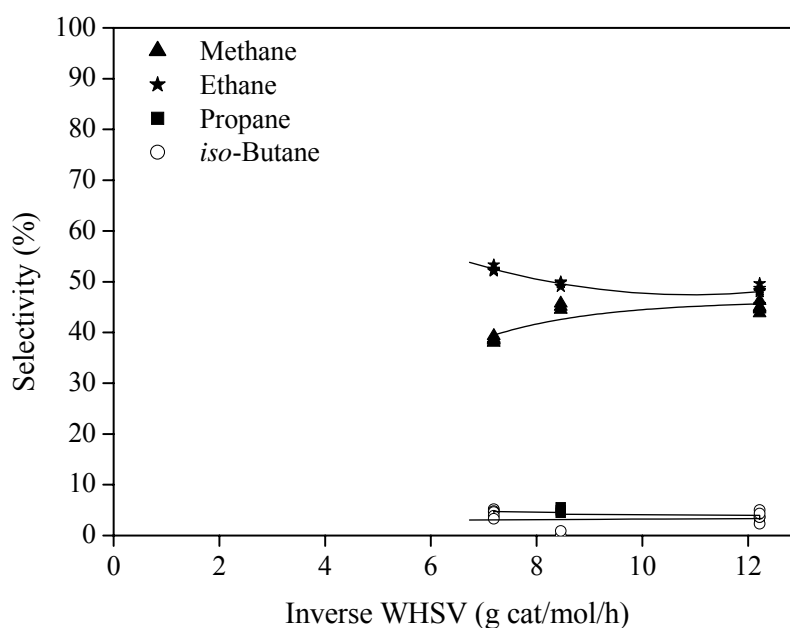


**Figure 3.18** Selectivity varied with inv. WHSV at 220°C,  $P_{H_2} = 540$  Torr,  $P_{n-C_4H_{10}} = 60$  Torr with 100 ml (NTP)/min flow rate catalyzed by PtRu/MgO.

Initial selectivities obtained from extrapolation curves to zero conversion (Figure 3.18) were around 0, 91, 6, and 3% for methane, ethane, propane and *iso*-butane, respectively. These values indicated *n*-butane hydrogenolysis catalyzed by PtRu/MgO gave ethane as primary product.

*n*-Butane hydrogenolysis catalyzed by supported PtRu/MgO was carried out at various reaction temperatures. Catalytic activities at temperature varied from

200-260°C were plotted with TOS in Figure 3.18. Firstly, the reaction was tested at 200°C with  $P_{\text{H}_2} = 540$  Torr,  $P_{n\text{-C}_4\text{H}_{10}} = 60$  Torr with 100 ml (NTP)/min flow rate. As shown in Figure 3.19, the catalytic activities slightly decreased with TOS and then reached steady-state within 30 min. According to endothermic reaction, *n*-butane hydrogenolysis activities increased with temperature when the reaction temperature was varied from 200 to 260°C. There was no sign of deactivation during 150 min TOS.

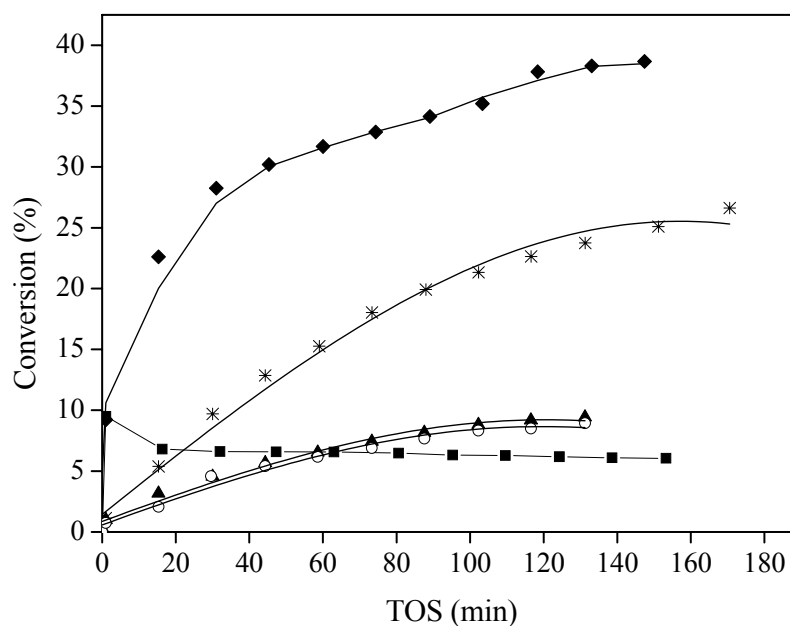


**Figure 3.19** Activity varied with time on stream (TOS) for *n*-butane hydrogenolysis catalyzed by PtRu/MgO (■) 200°C; (○) 210°C; (▲) 220°C; (\*) 240°C; and (◆) 260°C.

In addition, the catalytic activities in terms of TOF at 220°C of PtRu/MgO catalyst was  $(11.7 \pm 0.7) \times 10^{-4} \text{ (s}^{-1}\text{)}$ . This value was higher than that of PtRu/ $\gamma$ -Al<sub>2</sub>O<sub>3</sub> at 220°C which was  $(5.2 \pm 0.2) \times 10^{-4} \text{ (s}^{-1}\text{)}$  implying that PtRu/MgO was more active

in *n*-butane hydrogenolysis than PtRu/ $\gamma$ -Al<sub>2</sub>O<sub>3</sub>. Furthermore, percent product distribution (selectivity) at this reaction condition of PtRu/MgO included 43% methane, 52% ethane, 3% propane and 2% *iso*-butane. A plot of selectivity of *n*-butane hydrogenolysis catalyzed by PtRu/MgO as a function of temperature during 200-260°C is shown in Figure 3.20.

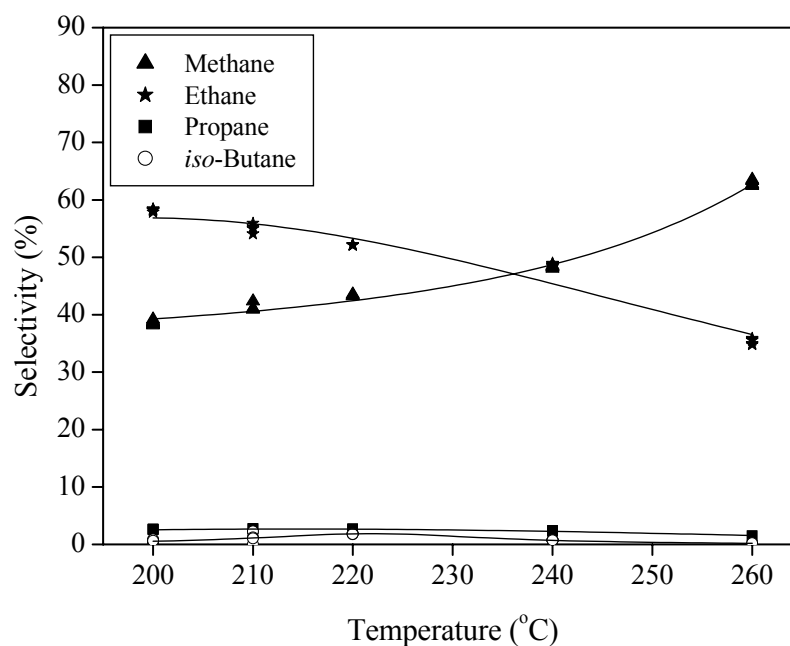


**Figure 3.20** Selectivity varied with reaction temperature of *n*-butane hydrogenolysis catalyzed by PtRu/MgO.

It was shown that selectivities of ethane, propane and *iso*-butane slightly decreased when reaction temperature increased whereas that of methane increased indicating a tendency of multiple hydrogenolysis at high temperature. At reaction temperature 260°C, selectivities of methane were much higher than that of ethane.

From selectivity, it was suggested that *n*-butane molecule mainly adsorbed on MgO through both 2, 3- and 1, 2-adsorbed type as shown in Figure 1.4 (Chapter I).

Compare with *n*-butane hydrogenolysis catalyzed by PtRu/ $\gamma$ -Al<sub>2</sub>O<sub>3</sub>, the selectivity for methane of PtRu/MgO was 43%, higher than that of PtRu/ $\gamma$ -Al<sub>2</sub>O<sub>3</sub> which was 33%, where as selectivity for ethane was 52%, lower than that of PtRu/ $\gamma$ -Al<sub>2</sub>O<sub>3</sub> which was 63%. It was found that *iso*-butane produced on PtRu/MgO was more than that on PtRu/ $\gamma$ -Al<sub>2</sub>O<sub>3</sub> which was 0.3%. Thus, *n*-butane hydrogenolysis catalyzed by PtRu/MgO showed greater tendency for isomerization reaction than that by PtRu/ $\gamma$ -Al<sub>2</sub>O<sub>3</sub>.

For reaction catalyzed by Pt-Ru/ $\gamma$ -Al<sub>2</sub>O<sub>3</sub>, isomerization reaction might be suppressed when Pt atoms incorporated with Ru particles. Ru might have effect to Pt atom, i.e. changes in electronic and chemisorptive properties and lead to greater tendency for isomerization reaction catalyzed by PtRu/MgO catalysts.

### **3.3.7.2 Apparent activation energy of *n*-butane hydrogenolysis catalyzed by PtRu/MgO**

Kinetic data of *n*-butane hydrogenolysis catalyzed by PtRu/MgO catalyst was collected during 200-260°C,  $P_{\text{H}_2} = 540$  Torr,  $P_{n\text{-C}_4\text{H}_{10}} = 60$  Torr with 100 ml (NTP)/min flow rate. A plot of TOF as a natural log with a function of 1/T is in Figure 3.21.

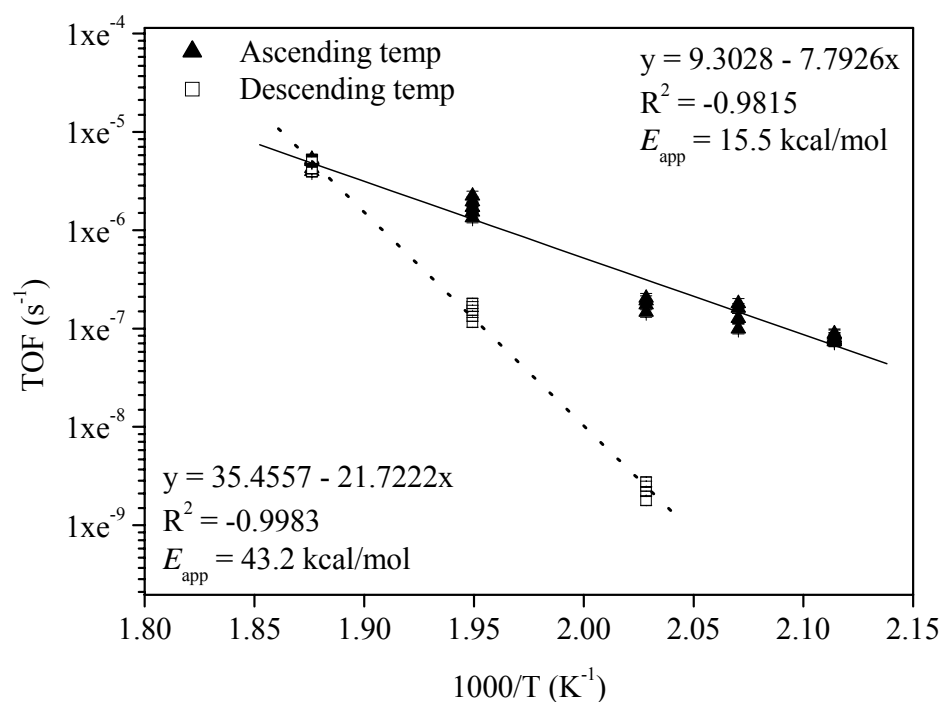


**Figure 3.21** Arrhenius plot of *n*-butane hydrogenolysis catalyzed by PtRu/MgO.

The apparent activation energy obtained from a slope of ascending temperature line from 200 to 260°C was  $15.5 \pm 0.1$  kcal/mol. The apparent activation energy in this work was less than that of reaction catalyzed by Pt on alumina at various reaction conditions (Bond and Cunningham, 1996; Leclercq et al., 1976; Passos et al., 1996). For example, the apparent activation energy over Pt/Al<sub>2</sub>O<sub>3</sub> was 30 kcal/mol obtained at  $P_{n-C_4H_{10}} = 75$  Torr,  $P_{H_2} = 675$  Torr, temperature ranges 266 to 379°C (Leclercq et al.). Moreover, the apparent activation energy of *n*-butane hydrogenolysis catalyzed by PtRu/MgO was also lower than that over supported bimetallic PtRe/Al<sub>2</sub>O<sub>3</sub> which was 34.2 kcal/mol at temperature ranges 244-321°C, with hydrogen:ethylene ratio = 10:1 (Bond and Conningham).

In addition, the apparent activation energy of *n*-butane hydrogenolysis over PtRu/MgO in this work was approximately half the value of that catalyzed by PtRu/ $\gamma$ -Al<sub>2</sub>O<sub>3</sub> which was  $30.9 \pm 0.1$  kcal/mol.

### 3.3.7.3 Evidence of catalyst deactivation at high reaction temperature

Figure 3.18 shows that catalytic activity increased with TOS and there was no sign of deactivation during the test period 150 min at each temperature. However, the Arrhenius plot in Figure 3.21 for descending temperature gave higher the apparent activation energy which was 43.2 kcal/mol. This value was twice larger than the value of that from ascending temperature. Therefore, deactivation occurred after testing reaction at higher temperature.

The catalytic data demonstrated that strong metal-support and Pt-Ru interactions on support might affect ethylene hydrogenation and *n*-butane hydrogenolysis reactions. The Pt-Ru interactions may lead to change electronic and chemisorptive properties of Pt, and then its catalytic properties as suggested for MgO-supported Pt-W catalyst prepared from bimetallic precursor for toluene hydrogenation (Alexeev, Shelef et al., 1996).

## 3.4 Conclusions

PtRu/MgO catalyst with Pt-Ru bonds was successfully prepared by adsorption of Pt<sub>3</sub>Ru<sub>6</sub>(CO)<sub>21</sub>( $\mu_3$ -H)( $\mu$ -H)<sub>3</sub> on MgO. Characterization by IR and EXAFS spectroscopy indicated that the precursor did not adsorb intact on MgO but still in the form of bimetallic carbonyl species. The decreasing in intensity of IR band in  $\nu_{OH}$

region implies that OH groups on support were involved in cluster-support interaction. The cluster precursor adsorbed through oxygen of CO ligands with surface of support such as hydroxyl groups and  $O^{2-}$  sites forming carbonates, carboxylates adsorbed species and hydrogen bonding. In addition, metals could interact with surface oxygen forming  $M-O_{\text{support}}$  bondings as observed by EXAFS spectroscopy indicating structural distortion of cluster core. The strong  $M-O_{\text{support}}$  interactions lead to partial cleavage of Pt-Ru contributions on MgO during adsorption. High dispersion of bimetallic PtRu on MgO was observed by EXAFS spectroscopy after ligand removal. All CO ligands were removed lead to changes in cluster core on support with tendency of Pt and Ru particles to segregate from each other. The average coordination numbers of Pt-Ru and Ru-Pt contributions were  $0.9 \pm 0.1$  and  $1.1 \pm 0.1$ , and coordination numbers of Pt-Pt and Ru-Ru contributions were found to be  $1.3 \pm 0.2$  and  $2.6 \pm 0.1$ , respectively. PtRu/MgO catalyst was active for both ethylene hydrogenation and *n*-butane hydrogenolysis with apparent activation energy  $7.6 \pm 0.1$  and  $15.5 \pm 0.1$  kcal/mol, respectively. Catalytic activity (TOF) of ethylene hydrogenation catalyzed by PtRu/MgO at temperature  $-75^{\circ}\text{C}$  was  $(33.6 \pm 2.5) \times 10^{-5} \text{ (s}^{-1}\text{)}$  while that of *n*-butane hydrogenolysis at temperature  $220^{\circ}\text{C}$  was  $(11.7 \pm 0.7) \times 10^{-4} \text{ (s}^{-1}\text{)}$  with selectivity 43% methane, 52% ethane, 3% propane and 2% *iso*-butane.

**CHAPTER IV**

**CHARACTERIZATION AND CATALYTIC ACTIVITY**

**OF Pt-Ru/TiO<sub>2</sub> CATALYST PREPARED FROM**

**Pt<sub>3</sub>Ru<sub>6</sub>(CO)<sub>21</sub>(μ<sub>3</sub>-H)(μ-H)<sub>3</sub>**

#### **4.1 Introduction**

In the surface science, titanium oxide or titania (TiO<sub>2</sub>) is the most investigated single-crystalline system of metal oxides and also has been used as support in heterogeneous catalysis even its specific surface area is lower than silica and alumina (Diebold, 2003; Serp et al., 2002). TiO<sub>2</sub> surface consists of Brønsted acid and base sites. However, it is much more acidic character than alumina but largely less basic than magnesia. It has been known that the most common commercial TiO<sub>2</sub> support contains two allotropic forms of 70-90% anatase and 10-30% rutile with specific area of 50 m<sup>2</sup>/g.

##### **4.1.1 Supported Pt catalysts incorporating second metal on TiO<sub>2</sub>**

Although platinum is one of the most studied metal overlayers on TiO<sub>2</sub> for photocatalysis, not many of bimetallic Pt incorporating noble metal on TiO<sub>2</sub> has been studied. There were some examples of an incorporation of other metals which were not noble. For example, supported Pt-Fe/TiO<sub>2</sub> and Pt-Sn/TiO<sub>2</sub> were prepared by impregnation of mixed-metal salts and tested for hydrogenation of cinnamaldehyde

(da Silva, Jordão, Mendes, and Fouilloux, 1997). It was suggested that electron donor effects of Fe and electron transfer from titanium species to Pt affected the catalytic activity. Another example of supported bimetallic on  $\text{TiO}_2$  was PtAu/ $\text{TiO}_2$  containing Pt-Au contributions which was prepared by deposition-precipitation of  $\text{HAuCl}_4 \cdot 4\text{H}_2\text{O}$  and  $\text{Pt}(\text{acac})_2$  on  $\text{TiO}_2$  under irradiation with mercury lamp and  $\text{N}_2$  flow (Tada et al., 2002).

#### 4.1.2 Research goals

The goal of this work was to prepare highly dispersed PtRu/ $\text{TiO}_2$  catalyst by adsorption of  $\text{Pt}_3\text{Ru}_6(\text{CO})_{21}(\mu_3\text{-H})(\mu\text{-H})_3$  from  $\text{CH}_2\text{Cl}_2$  onto  $\text{TiO}_2$ . The supported PtRu samples were characterized by IR and EXAFS spectroscopy to study the interactions between the cluster and surface of support before and after ligand removal. The nature of adsorbed species and structural changes of cluster precursor were also investigated. Catalytic activities of PtRu/ $\text{TiO}_2$  catalyst were tested for ethylene hydrogenation and *n*-butane hydrogenolysis reactions. Results were compared with those of PtRu/ $\gamma\text{-Al}_2\text{O}_3$  and PtRu/MgO catalysts prepared from adsorption of  $\text{Pt}_3\text{Ru}_6(\text{CO})_{21}(\mu_3\text{-H})(\mu\text{-H})_3$  and bimetallic catalysts prepared conventionally.

## 4.2 Experimental

### 4.2.1 Chemicals and materials

Organometallic syntheses, solvent purification, supported catalyst preparations and samples handling were performed with the same method as in section 2.2.1 of Chapter II (page 18).

TiO<sub>2</sub> powder (Degussa, P-25, approximately 70% anatase and 30% rutile) was mixed with deionized water to form a paste before drying overnight at 120°C. Prior to use, it was calcined or partially dehydroxylated in O<sub>2</sub> flow at 400°C for 2 h followed by evacuation (pressure  $\approx 10^{-3}$  Torr) at this temperature for an additional 14 h.

#### 4.2.2 Synthesis of organometallic precursor

Pt<sub>3</sub>Ru<sub>6</sub>(CO)<sub>21</sub>( $\mu_3$ -H)( $\mu$ -H)<sub>3</sub> was synthesized by a procedure described by Adams and his group (1994) and details of synthesis method and characterization of cluster precursor are described in section 2.2.2 of Chapter II (page 19). Briefly, Pt<sub>3</sub>Ru<sub>6</sub>(CO)<sub>21</sub>( $\mu_3$ -H)( $\mu$ -H)<sub>3</sub> was synthesized from the reaction between Pt<sub>2</sub>Ru<sub>4</sub>(CO)<sub>18</sub> and H<sub>2</sub> and purified by washing with cold *n*-pentane several times before characterized by IR, <sup>1</sup>H and <sup>13</sup>C NMR spectroscopy.

#### 4.2.3 Preparation of supported catalyst

Supported Pt-Ru catalysts on TiO<sub>2</sub> was prepared by slurring TiO<sub>2</sub> with a solution of Pt<sub>3</sub>Ru<sub>6</sub>(CO)<sub>21</sub>( $\mu_3$ -H)( $\mu$ -H)<sub>3</sub> in CH<sub>2</sub>Cl<sub>2</sub> for 1 day followed by evacuation ( $\approx 10^{-3}$  bar) for an additional 1 day to ensure complete uptake of the precursor by the support. The amount of chosen precursor gave sample containing 1.0 wt% Pt and 1.0 wt% Ru after ligand removal from precursor.

#### 4.2.4 Extraction of adsorbed species on TiO<sub>2</sub>

After removal of solvent by evacuation from the dry supported sample prepared from adsorption of Pt<sub>3</sub>Ru<sub>6</sub>(CO)<sub>21</sub>( $\mu_3$ -H)( $\mu$ -H)<sub>3</sub> onto TiO<sub>2</sub>, the adsorbed species were recovered by extraction with CH<sub>2</sub>Cl<sub>2</sub> for approximately 30 min with

stirring. The extract solution and extracted dry sample were characterized by IR spectroscopy.

#### **4.2.5 PtRu catalyst activation**

Fresh supported sample contained adsorbed species was heated in He flow at 300°C for 2 h to remove ligands from adsorbed precursor.

#### **4.2.6 Characterization techniques**

##### **4.2.6.1 IR spectroscopy**

IR spectra of the dry supported samples supported with  $\text{Pt}_3\text{Ru}_6(\text{CO})_{21}(\mu_3\text{-H})(\mu\text{-H})_3$  were recorded before and after ligand removal with a Bruker IFS-66v spectrometer with a resolution of  $4\text{ cm}^{-1}$ . Each sample was scanned 64 times and the signal averaged. Details for sample preparation and measurement are in section 2.2.6.1 of Chapter II (page 22).

##### **4.2.6.2 EXAFS spectroscopy**

EXAFS experiments were performed at the X-ray beamline X18B at the National Synchrotron Light Source (NSLS), Brookhaven National Laboratory (BNL), Upton, New York, USA. EXAFS instrument, sample preparation and measurement were described in section 2.2.6.3 of Chapter II (page 23).

#### **4.2.7 EXAFS data analysis**

Details of EXAFS data analysis were described in section 2.2.7 of Chapter II (page 23). Briefly, EXAFS data were collected at individual Pt  $L_{\text{III}}$  (11564

eV) and Ru K (22117 eV) absorption edge and analyzed with theoretical reference files. The EXAFS data processing was carried out with ATHENA software (Raval, 2003). Phase shift and backscattering amplitudes of metal-metal and metal-surface oxygen interactions were calculated by FEFF7.0 software (Rehr et al., 1991). EXAFSPAK software (George et al., 2000) was used to fit the EXAFS data with single and multiple scattering paths calculated by FEFF7.0 and the EXAFS parameters were extracted from the raw data with the EXAFSPAK software. The fittings were done both in  $r$  space ( $r$  is interatomic distance from the absorber atom) and  $k$  space ( $k$  is the wave vector) with application of  $k^0$ ,  $k^1$ , and  $k^3$  weightings.

Raw EXAFS data of the dry supported sample on TiO<sub>2</sub> obtained at the Pt L<sub>III</sub> edge were Fourier transformed over the ranges  $3.50 < k < 11.55$  with  $k^3$  weighting without phase correction and  $0.0 < r < 5.0$  Å.

The EXAFS data of this sample scanned at the Ru K edge were Fourier transformed over the ranges  $4.10 < k < 12.00$  and  $0.0 < r < 4.0$  Å. Statistically justified numbers of free parameters estimated from Nyquist theorem (Stern, 1993),  $n = (2\Delta k\Delta r/\pi) + 1$ , for the Pt L<sub>III</sub> and the Ru K edge of sample before ligand removal were about 27 and 34, respectively.

The EXAFS data characterizing Pt-Ru/TiO<sub>2</sub> after treatment in He and scanned at the Pt L<sub>III</sub> edge were Fourier transformed over the ranges  $4.00 < k < 14.31$  and  $0.0 < r < 5.0$  Å. The EXAFS data characterizing this sample scanned at the Ru K edge were Fourier transformed over the ranges  $4.00 < k < 14.20$  and  $0.0 < r < 4.2$  Å. Statistically justified number of free parameters estimated from Nyquist theorem for the Pt L<sub>III</sub> and the Ru K edge of sample after treatment in He were about 21 and 29, respectively.

#### 4.2.8 Catalytic activity of PtRu/TiO<sub>2</sub> for ethylene hydrogenation

Ethylene hydrogenation was carried out in a stainless steel U-tube flow reactor at atmospheric pressure with the same procedure and condition described in section 2.2.8 of Chapter II (page 24). Briefly, in an Ar-filled glovebox, 10 to 20 mg of pretreated catalyst (300°C in He flow for 2 h) diluted with 600 mg of inert nonporous  $\alpha$ -Al<sub>2</sub>O<sub>3</sub> was loaded into the reactor. The reactor was cooled to the desired temperature with He flowing through it before a gas mixture of H<sub>2</sub>, C<sub>2</sub>H<sub>4</sub> and the balance He was allowed to flow into it at a rate of 200 ml (NTP)/min. The effluent gas mixture was analyzed with an online gas chromatograph (Hewlett-Packard HP 6890) equipped with an Al<sub>2</sub>O<sub>3</sub> capillary column (50 m x 0.53 mm x 15.0 micron film thickness) and a flame ionization detector. Testing conditions were as followed:  $P_{\text{H}_2} = 80$  Torr,  $P_{\text{C}_2\text{H}_4} = 40$  Torr and temperature varied from -75 to -20°C.

#### 4.2.9 Catalytic activity of PtRu/TiO<sub>2</sub> for *n*-butane hydrogenolysis

*n*-Butane hydrogenolysis was performed in a quartz tube flow reactor at atmospheric pressure with the same procedure and condition as described in section 2.2.9 of Chapter II (page 25). Briefly, around 25-30 mg of pretreated supported sample (at 300°C in He flow for 2 h) was diluted with inert nonporous  $\alpha$ -Al<sub>2</sub>O<sub>3</sub> before loading into the reactor. The reactor was heated to the desired temperature with He flowing through it before reactant gas mixture of H<sub>2</sub>, *n*-C<sub>4</sub>H<sub>10</sub>, and the balance He was allowed to flow into it at a rate of 100 ml (NTP)/min. The effluent gas mixture was analyzed with the online gas chromatograph (Hewlett-Packard HP 6890) equipped with an Al<sub>2</sub>O<sub>3</sub> capillary column (50 m x 0.53 mm x 15.0 micron film thickness) and a

flame ionization detector. Testing conditions were as followed:  $P_{\text{H}_2} = 540$  Torr,  $P_{n\text{-C}_4\text{H}_{10}} = 60$  Torr and temperature varied from 200 to 280°C.

### 4.3 Results and discussion

#### 4.3.1 IR evidence of interaction between adsorbed precursor and TiO<sub>2</sub> surface

The interaction between cluster precursor and TiO<sub>2</sub> powder support was first investigated by IR spectroscopy. TiO<sub>2</sub> powder (Degussa, P-25) was principally anatase. Prior to use, it was added with water to form paste and dried in hot air oven at 120°C before calcination in O<sub>2</sub> flow at 400°C for 2 h and then evacuated at this temperature for 14 h. The IR spectrum of bare TiO<sub>2</sub> was recorded and compared with that of samples (i) after adsorption with Pt<sub>3</sub>Ru<sub>6</sub>(CO)<sub>21</sub>(μ<sub>3</sub>-H)(μ-H)<sub>3</sub> and (ii) after ligand removal in He flow. The IR bands characterizing hydroxyl groups in ν<sub>OH</sub> region of these samples are shown in Figure 4.1.

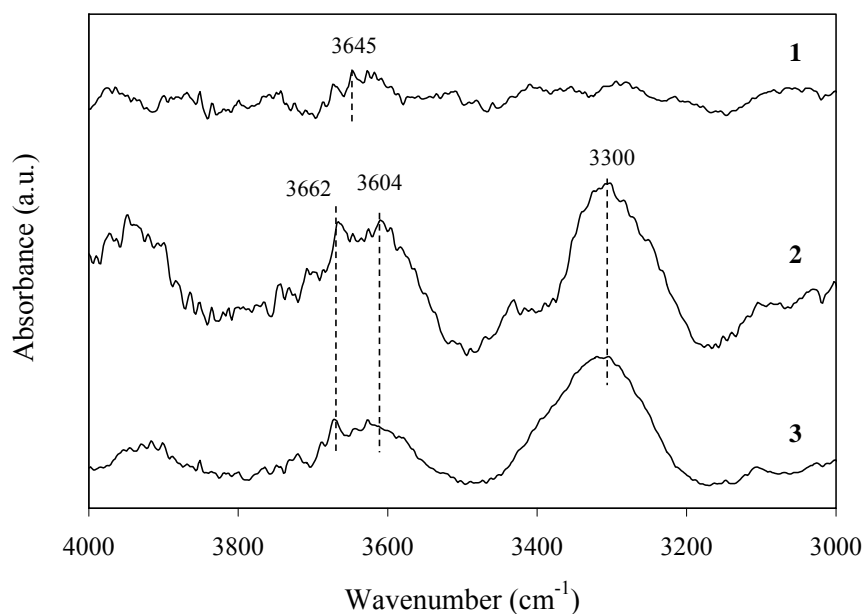


**Figure 4.1** IR spectra in  $\nu_{\text{OH}}$  region of: (1) Dry sample prepared from  $\text{Pt}_3\text{Ru}_6(\text{CO})_{21}(\mu_3\text{-H})(\mu\text{-H})_3$  on  $\text{TiO}_2$ ; (2) sample after ligand removal in He flow at  $300^\circ\text{C}$  for 2 h; (3) calcined  $\text{TiO}_2$ .

The partially dehydroxylated  $\text{TiO}_2$  give two broad IR bands at 3662 (w), 3604 (w) and 3300 (w)  $\text{cm}^{-1}$  as shown in spectrum 3 in Figure 4.1. These peaks were assigned to stretching modes of isolated surface hydroxyl groups on  $\text{TiO}_2$ . More specific assignment of hydroxyl bands were determined, the former two bands were characteristic of anatase and was of terminal OH type, Ti-OH (Hadjivanov, Bushev, Kantcheva, and Klissurski, 1994). On the one hand, the latter band was characteristic of bridging OH groups of rutile (Finklea and Vithanage, 1982).

After  $\text{Pt}_3\text{Ru}_6(\text{CO})_{21}(\mu_3\text{-H})(\mu\text{-H})_3$  in  $\text{CH}_2\text{Cl}_2$  was adsorbed on  $\text{TiO}_2$  and dried by evacuation, the intensity of isolated surface hydroxyl bands at 3662 and 3604  $\text{cm}^{-1}$  decreased and shifted to 3645  $\text{cm}^{-1}$  as in spectrum 1 as shown in Figure 4.1. In addition, the IR band at 3300  $\text{cm}^{-1}$  disappeared after adsorption. The decrease in

intensity and disappearance of IR bands in  $\nu_{\text{OH}}$  region imply that hydroxyl groups involved in the interaction between metal cluster precursor and  $\text{TiO}_2$  support.

It has been known that IR bands of carbonyl ligands of supported metal carbonyl cluster differ from those of the cluster in solid or solution due to cluster-support interaction (Alexeev et al., 2002). In this work, the changes of IR in  $\nu_{\text{CO}}$  region were determined. The IR band in  $\nu_{\text{CO}}$  region of sample after adsorption with  $\text{Pt}_3\text{Ru}_6(\text{CO})_{21}(\mu_3\text{-H})(\mu\text{-H})_3$  is in Figure 4.2 (spectrum 1). These IR peaks were significantly different from those of cluster precursor in  $\text{CH}_2\text{Cl}_2$  [Figure 2.4 in Chapter II: 2081 (w, sh), 2066 (vs), 2052 (m, sh), and 2026 (w)]. Supported  $\text{TiO}_2$  sample gave IR bands in  $\nu_{\text{CO}}$  region at 2131 (w), 2090 (sh), 2042 (vs), 2015 (sh), 1957, 1614 (w) and 1383 (m)  $\text{cm}^{-1}$ .

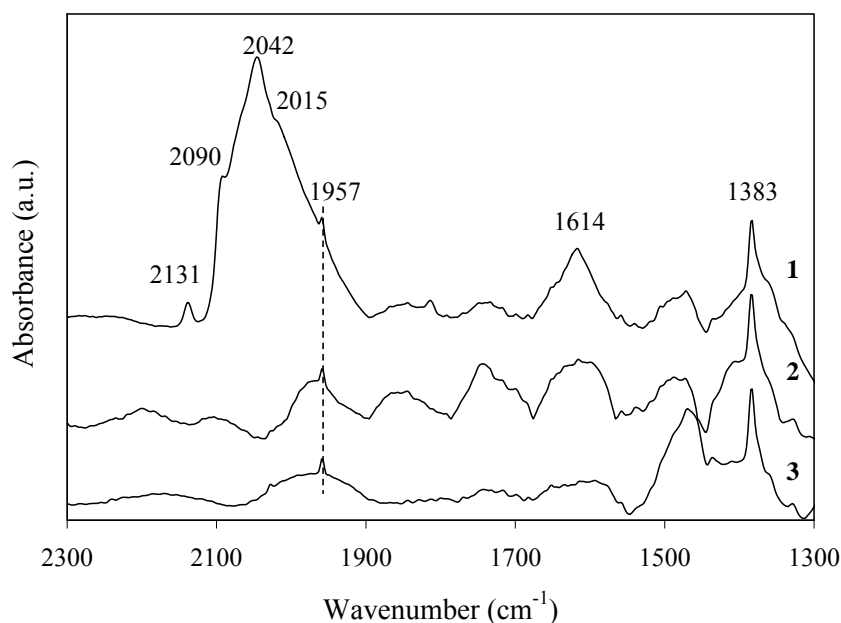


**Figure 4.2** IR spectra in  $\nu_{\text{CO}}$  region of: (1) Dry sample prepared from  $\text{Pt}_3\text{Ru}_6(\text{CO})_{21}(\mu_3\text{-H})(\mu\text{-H})_3$  on  $\text{TiO}_2$ ; (2) sample after ligand removal in He flow at  $300^\circ\text{C}$  for 2 h; (3) calcined  $\text{TiO}_2$ .

Strong IR band at  $2042\text{ cm}^{-1}$  was assigned to be linear M-CO species (M in this work were Pt or Ru). Bridging CO ligand which typically occurred at about  $1850\text{ cm}^{-1}$  for CO adsorbed on metal platinum did not observed in this work (Hadjiivanov, 1998). Small IR band at  $2131\text{ cm}^{-1}$  was similarly found on  $\gamma\text{-Al}_2\text{O}_3$  and MgO impregnated with  $\text{Pt}_3\text{Ru}_6(\text{CO})_{21}(\mu_3\text{-H})(\mu\text{-H})_3$  in Chapter II and III. This band could be from CO ligands of Pt or Ru of supported bimetallic PtRu on  $\text{TiO}_2$  (Hadjiivanov and Vayssilov, 2002). The IR peaks at low frequency,  $1957$  and  $1383\text{ cm}^{-1}$  occurred at the same position as bare  $\text{TiO}_2$ , thus these peaks are characteristic of  $\text{TiO}_2$  support. Moreover, IR band at  $1614\text{ cm}^{-1}$  is near the position of residual carbonates which was found at  $1578\text{ cm}^{-1}$  on  $\text{TiO}_2$  (Hadjiivanov et al., 1994) and also in the same range of asymmetric stretching of adsorbed carboxylates,  $1650\text{-}1560\text{ cm}^{-1}$  (Hadjiivanov and Vayssilov, 2002). Therefore, IR band at  $1614\text{ cm}^{-1}$  was assigned to adsorbed carbonates or carboxylates on  $\text{TiO}_2$  indicating cluster-support interaction.

The changes in intensity of IR bands in  $\nu_{\text{OH}}$  region and shift of IR bands to lower frequency in  $\nu_{\text{CO}}$  region including IR band characterizing carbonates or carboxylates implied that  $\text{Pt}_3\text{Ru}_6(\text{CO})_{21}(\mu_3\text{-H})(\mu\text{-H})_3$  was not adsorbed intact on  $\text{TiO}_2$  but still in the form of metal carbonyl species. Cluster precursor could interact with  $\text{TiO}_2$  through oxygen of CO ligand with hydroxyl group or  $\text{O}^{2-}$  on  $\text{TiO}_2$  forming carbonates or carboxylates.

#### **4.3.2 Strong interaction between cluster precursor and $\text{TiO}_2$**

The strong interaction between cluster precursor and  $\text{TiO}_2$  support was investigated by extraction surface species with  $\text{CH}_2\text{Cl}_2$ . After  $\text{Pt}_3\text{Ru}_6(\text{CO})_{21}(\mu_3\text{-H})(\mu\text{-H})_3$  was brought into contact with  $\text{TiO}_2$  and dried by evacuation, the fresh

supported sample was slurry with  $\text{CH}_2\text{Cl}_2$  around 30 minutes to extract adsorbed species. The extract solution and dry sample after remove extracted solution were characterized by IR spectroscopy. IR in  $\nu_{\text{CO}}$  region at 2079 (sh), 2067 (s), 2046 (w) and 2031 (w)  $\text{cm}^{-1}$  were observed in the extract  $\text{CH}_2\text{Cl}_2$  solution as in Figure 4.3.

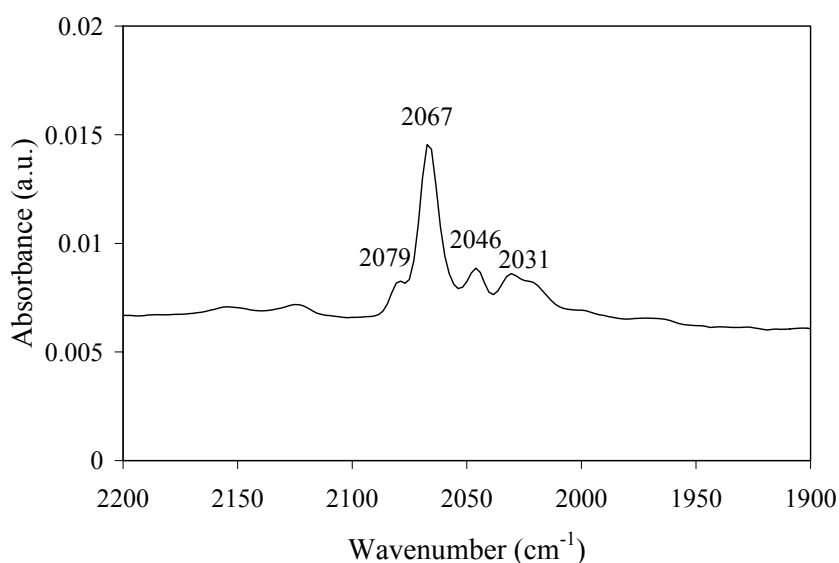


**Figure 4.3** IR spectrum in  $\nu_{\text{CO}}$  region of extract solution after extraction of the supported sample on  $\text{TiO}_2$  with  $\text{CH}_2\text{Cl}_2$ .

The IR spectrum of extracted solution shows strong IR peak at  $2067 \text{ cm}^{-1}$  which could be assigned to terminal CO ligands of metal carbonyl species. This IR spectrum differed from  $\text{Pt}_3\text{Ru}_6(\text{CO})_{21}(\mu_3\text{-H})(\mu\text{-H})_3$  in  $\text{CH}_2\text{Cl}_2$  indicating partial change in structure of extracted metal carbonyl. Structure of adsorbed precursor on  $\text{TiO}_2$  might be changed after adsorption that was discussed later with EXAFS data.

Supported PtRu sample after removal extract solution was dried under vacuum and characterized by IR spectroscopy again. The IR spectrum of dry sample differed from fresh sample after adsorption (Figure 4.4).

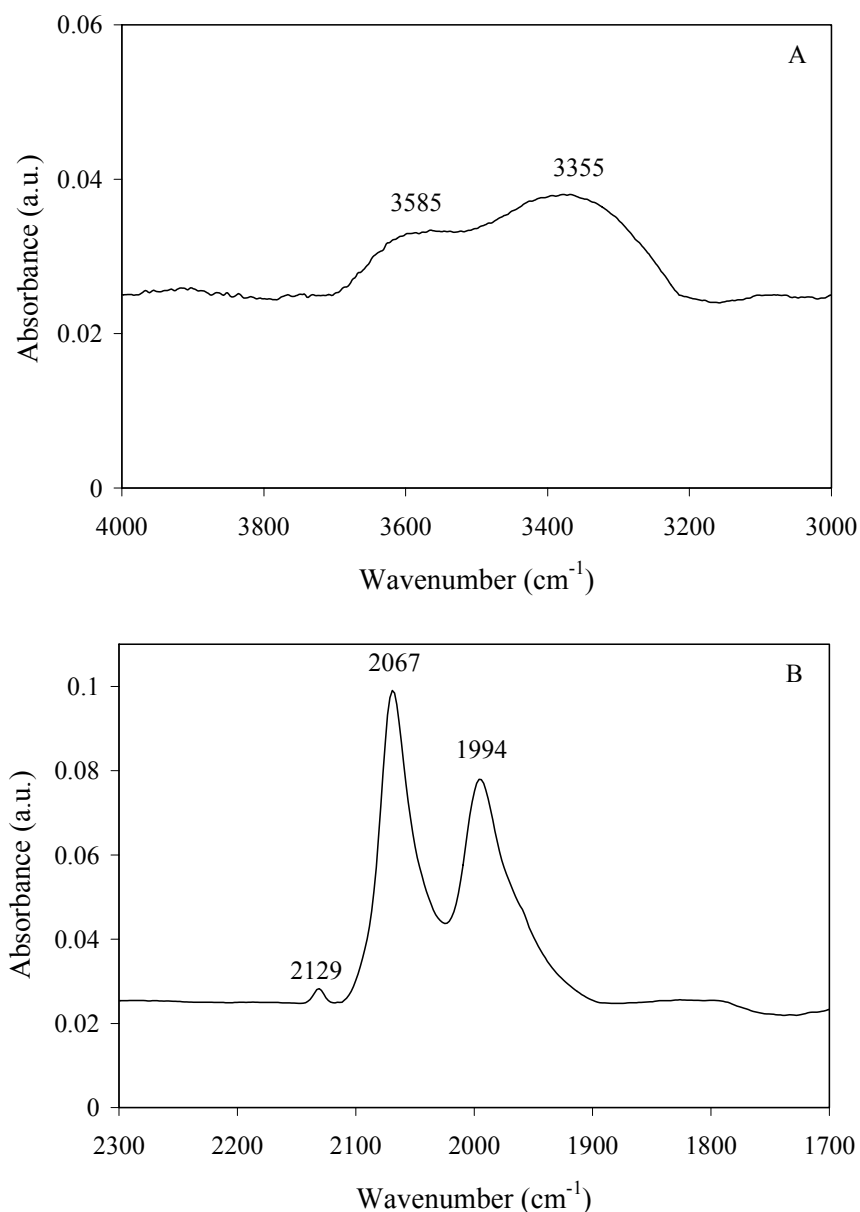


**Figure 4.4** IR spectrum of dry supported sample on  $\text{TiO}_2$  after extraction with  $\text{CH}_2\text{Cl}_2$  in (A)  $\nu_{OH}$ , and (B)  $\nu_{CO}$  region.

IR peaks in  $\nu_{OH}$  region at 3585 and 3355  $\text{cm}^{-1}$  (Figure 4.4A) represented surface hydroxyl groups on supported sample. IR peaks in  $\nu_{CO}$  region were observed at 2129 (w), 2067 (vs) and 1994 (s)  $\text{cm}^{-1}$  indicating changes of adsorbed precursor after extraction with  $\text{CH}_2\text{Cl}_2$ .

Evidence from IR data confirmed that the adsorption of  $\text{Pt}_3\text{Ru}_6(\text{CO})_{21}(\mu_3\text{-H})(\mu\text{-H})_3$  onto  $\text{TiO}_2$  support was not intact and adsorbed precursor could not be completely extracted by  $\text{CH}_2\text{Cl}_2$ . The adsorption on  $\text{TiO}_2$  was through oxygen of CO ligands with  $\text{O}^{2-}$  or OH groups on  $\text{TiO}_2$  resulting in unknown adsorbed metal carbonyl species including carbonates or carboxylates.

### 4.3.3 EXAFS evidence of structural changes of adsorbed precursor on $\text{TiO}_2$

After adsorption of  $\text{Pt}_3\text{Ru}_6(\text{CO})_{21}(\mu_3\text{-H})(\mu\text{-H})_3$  in  $\text{CH}_2\text{Cl}_2$  onto partially dehydroxylated  $\text{TiO}_2$  and dried by evacuation, the sample was characterized by IR and EXAFS spectroscopy to study cluster-support interaction and structure of adsorbed precursor. IR results indicated changes in intensity of IR bands in  $\nu_{\text{OH}}$  region and shift of IR bands to lower frequency in  $\nu_{\text{CO}}$  region including IR band characterizing carbonates or carboxylates. These IR data implied changes in ligands environment and those changes in structure of adsorbed precursor was expected to be seen in EXAFS spectroscopy.

The EXAFS fitting parameters of dried fresh sample after impregnation scanned at the Ru K edge in transmission mode at nearly liquid nitrogen temperature and at the Pt  $L_{\text{III}}$  edge in fluorescence mode at room temperature are summarized in Table 4.1. The EXAFS fitting results in  $k$  and  $r$  space with  $k^0$ ,  $k^1$  and  $k^3$  weighted are in Figures 4.5 and 4.6. The estimated accuracies of coordination number ( $N$ ), distance ( $R$ ), Debye-Waller factor ( $\Delta\sigma^2$ ), and inner potential correction ( $\Delta E_0$ ) are as follows:  $\pm 20\%$ ,  $\pm 1\%$ ,  $\pm 30\%$ , and  $\pm 10\%$ , respectively.

**Table 4.1** Summary of EXAFS data of sample formed by adsorption of  $\text{Pt}_3\text{Ru}_6(\text{CO})_{21}(\mu_3\text{-H})(\mu\text{-H})_3$  on  $\text{TiO}_2$  before ligand removal

Edge	Shell	$N$	$R$ (Å)	$10^3 \times \Delta\sigma^2$ (Å <sup>2</sup> )	$\Delta E_o$ (eV)
Pt L <sub>III</sub>	Pt-Pt	$1.8 \pm 0.1$	$2.72 \pm 0.01$	$2.9 \pm 0.4$	$-4.9 \pm 0.4$
	Pt-Ru	$1.8 \pm 0.1$	$2.71 \pm 0.01$	$2.6 \pm 0.2$	$6.1 \pm 0.2$
	Pt-CO				
	Pt-C	$0.6 \pm 0.1$	$1.89 \pm 0.01$	$-7.1 \pm 0.4$	$10.5 \pm 0.5$
	Pt-O*	$0.6 \pm 0.2$	$2.94 \pm 0.01$	$-4.1 \pm 1.0$	$10.2 \pm 0.5$
	Pt-O <sub>support</sub>				
	Pt-O <sub>s</sub>	$0.5 \pm 0.1$	$2.02 \pm 0.01$	$-6.9 \pm 0.3$	$11.4 \pm 0.3$
	Pt-O <sub>l</sub>	$0.9 \pm 0.1$	$3.48 \pm 0.01$	$-5.6 \pm 0.9$	$-8.2 \pm 0.7$
Ru K	Ru-Ru	$1.7 \pm 0.1$	$2.50 \pm 0.01$	$11.6 \pm 0.6$	$-4.5 \pm 0.4$
	Ru-Pt	$1.3 \pm 0.1$	$2.71 \pm 0.01$	$2.4 \pm 0.2$	$-3.7 \pm 0.3$
	Ru-CO				
	Ru-C	$1.4 \pm 0.1$	$1.86 \pm 0.01$	$2.1 \pm 0.3$	$-12.9 \pm 0.4$
	Ru-O*	$1.4 \pm 0.1$	$3.05 \pm 0.01$	$-2.6 \pm 0.3$	$-0.7 \pm 0.3$
	Ru-O <sub>support</sub>				
	Ru-O <sub>s</sub>	$2.5 \pm 0.1$	$2.09 \pm 0.01$	$4.6 \pm 0.4$	$-7.8 \pm 0.5$
	Ru-O <sub>l</sub>	$1.8 \pm 0.1$	$2.84 \pm 0.01$	$-2.9 \pm 0.3$	$2.1 \pm 0.2$

Notation: subscript s and l refer to short and long distance, respectively

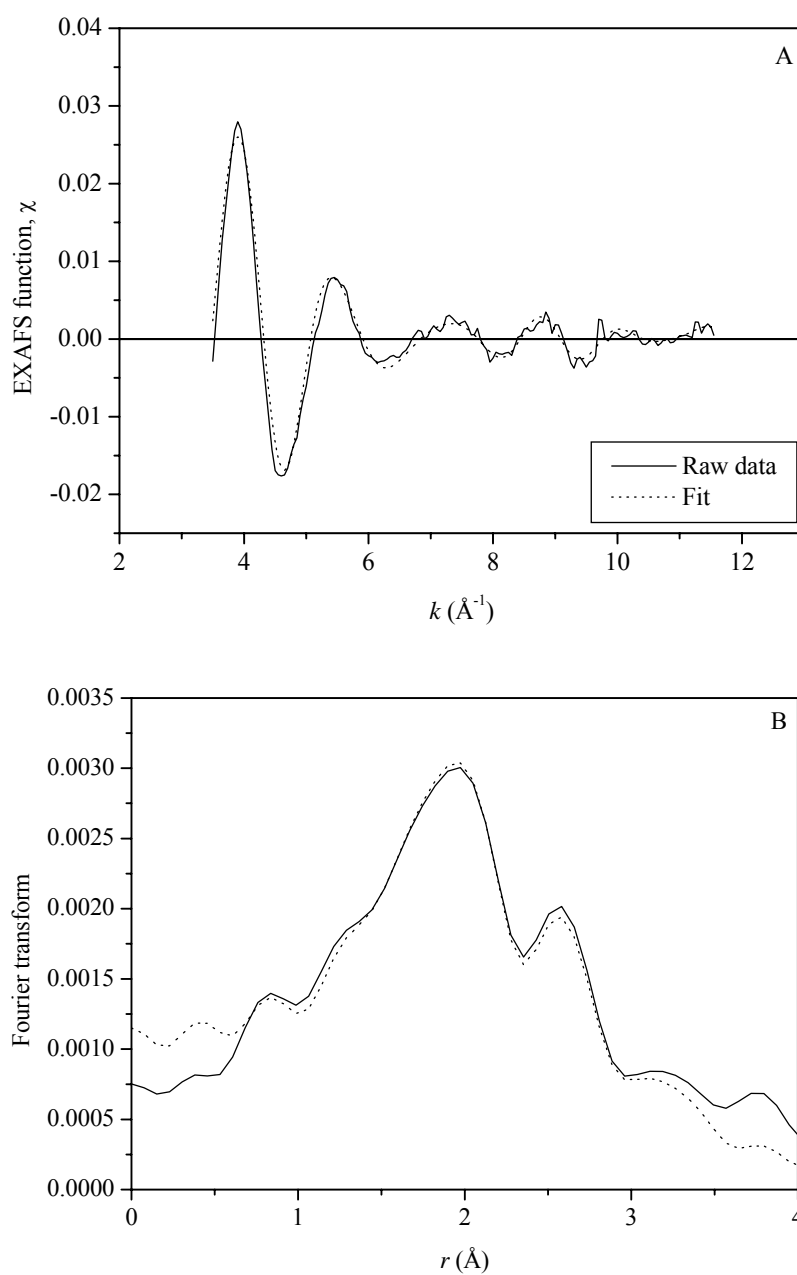


**Figure 4.5** EXAFS results scanned at the Pt L<sub>III</sub> edge characterizing the adsorbed Pt<sub>3</sub>Ru<sub>6</sub>(CO)<sub>21</sub>( $\mu_3$ -H)( $\mu$ -H)<sub>3</sub> on TiO<sub>2</sub>: (A) Experimental EXAFS function (solid line) and sum of the calculated Pt-Pt, Pt-Ru, Pt-C, Pt-O\*, Pt-O<sub>s</sub>, and Pt-O<sub>l</sub> contributions (dotted line). (B) Magnitude of uncorrected Fourier transform ( $k^0$  weighted) of experimental EXAFS function (solid line) and sum of the calculated Pt-Pt, Pt-Ru, Pt-C, Pt-O\*, Pt-O<sub>s</sub>, and Pt-O<sub>l</sub> contributions (dotted line).

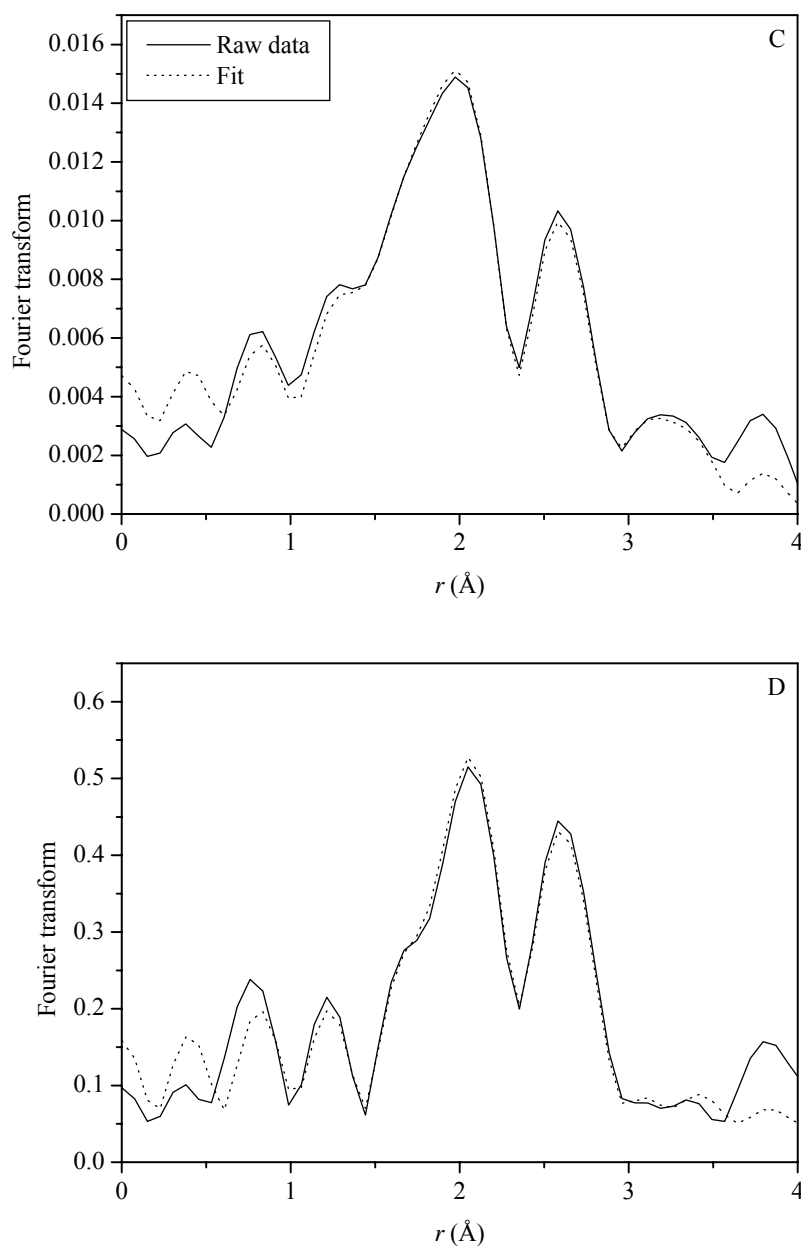


**Figure 4.5** (continued) EXAFS results scanned at the Pt  $L_{III}$  edge characterizing the adsorbed  $\text{Pt}_3\text{Ru}_6(\text{CO})_{21}(\mu_3\text{-H})(\mu\text{-H})_3$  on  $\text{TiO}_2$ : (C) Magnitude of uncorrected Fourier transform ( $k^1$  weighted) of experimental EXAFS function (solid line) and sum of the calculated Pt-Pt, Pt-Ru, Pt-C, Pt-O\*, Pt-O<sub>s</sub>, and Pt-O<sub>l</sub> contributions (dotted line). (D) Magnitude of uncorrected Fourier transform ( $k^3$  weighted) of experimental EXAFS function (solid line) and sum of the calculated Pt-Pt, Pt-Ru, Pt-C, Pt-O\*, Pt-O<sub>s</sub>, and Pt-O<sub>l</sub> contributions (dotted line).

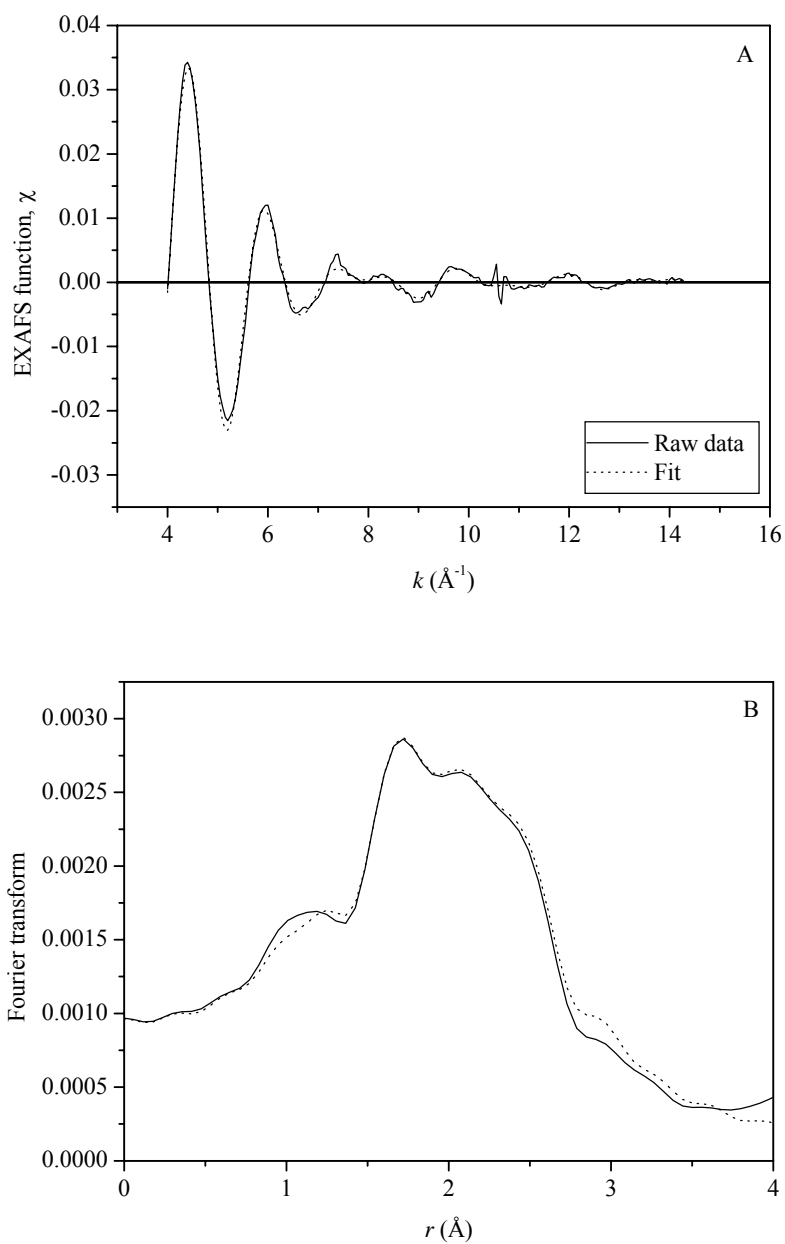


**Figure 4.6** EXAFS results scanned at the Ru K edge characterizing the adsorbed Pt<sub>3</sub>Ru<sub>6</sub>(CO)<sub>21</sub>(μ<sub>3</sub>-H)(μ-H)<sub>3</sub> on TiO<sub>2</sub>: (A) Experimental EXAFS function (solid line) and sum of the calculated Ru-Ru, Ru-Pt, Ru-C, Ru-O\*, Ru-O<sub>s</sub>, and Ru-O<sub>l</sub> contributions (dotted line). (B) Magnitude of uncorrected Fourier transform ( $k^0$  weighted) of experimental EXAFS function (solid line) and sum of the calculated Ru-Ru, Ru-Pt, Ru-C, Ru-O\*, Ru-O<sub>s</sub>, and Ru-O<sub>l</sub> contributions (dotted line).

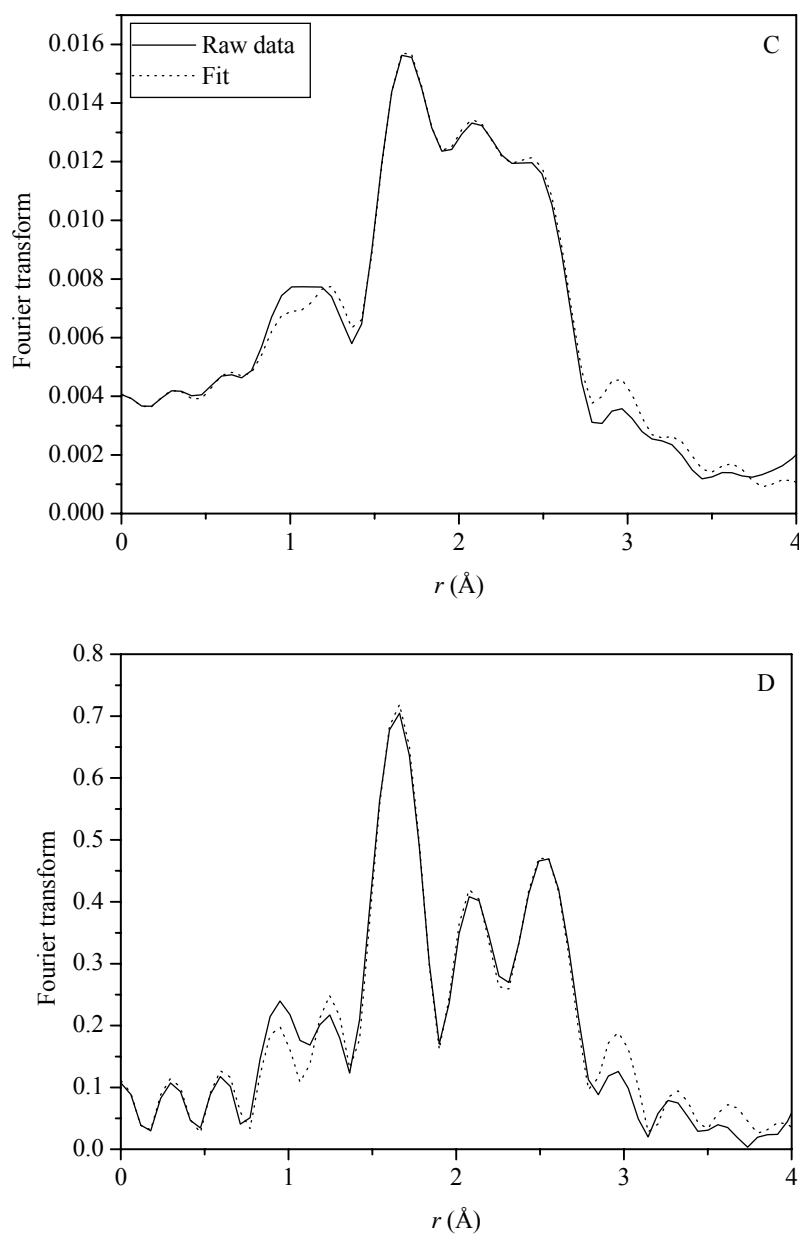


**Figure 4.6** (continued) EXAFS results scanned at the Ru K edge characterizing the adsorbed  $\text{Pt}_3\text{Ru}_6(\text{CO})_{21}(\mu_3\text{-H})(\mu\text{-H})_3$  on  $\text{TiO}_2$ : (C) Magnitude of uncorrected Fourier transform ( $k^1$  weighted) of experimental EXAFS function (solid line) and sum of the calculated Ru-Ru, Ru-Pt, Ru-C, Ru-O\*, Ru-O<sub>s</sub>, and Ru-O<sub>l</sub> contributions (dotted line). (D) Magnitude of uncorrected Fourier transform ( $k^3$  weighted) of experimental EXAFS function (solid line) and sum of the calculated Ru-Ru, Ru-Pt, Ru-C, Ru-O\*, Ru-O<sub>s</sub>, and Ru-O<sub>l</sub> contributions (dotted line).

The reliable and consistence of parameters from EXAFS fitting were determined. The bond distances and Debye-Waller factors must be equivalent for each edge of Pt-Ru contributions, the coordination numbers  $N_{\text{PtRu}}$  related to  $N_{\text{RuPt}}$  by this equation:  $N_{\text{PtRu}}/N_{\text{RuPt}} = n_{\text{Ru}}/n_{\text{Pt}}$ , where  $n_{\text{Ru}}$  and  $n_{\text{Pt}}$  are the total numbers of Ru and Pt atoms in sample.

The EXAFS data in Table 4.1 indicated Pt-O<sub>support</sub> and Ru-O<sub>support</sub> interactions when Pt<sub>3</sub>Ru<sub>6</sub>(CO)<sub>21</sub>(μ<sub>3</sub>-H)(μ-H)<sub>3</sub> adsorbed on TiO<sub>2</sub>. Some changes in CO bonding distances and coordination number were also observed by EXAFS spectroscopy. The EXAFS fitting parameters at the Pt L<sub>III</sub> edge show interaction between Pt and surface oxygen, Pt-O<sub>s</sub> at  $2.02 \pm 0.01$  Å with coordination number  $0.5 \pm 0.1$ . This interatomic distance of Pt-O<sub>s</sub> is slightly shorter than that of common metal-oxygen distances in numerous oxide- and zeolite-supported metal clusters (M: Ru, Rh, Ir, Os, Pt), 2.1-2.2 Å (Koningsberger and Gates, 1992). The short Pt-O<sub>s</sub> distance indicate strong interaction between Pt and surface oxygen and Pt atom might be in cationic form. In addition, few Pt-O<sub>1</sub> contributions were also observed at  $3.48 \pm 0.01$  Å with coordination number  $0.9 \pm 0.1$ .

The interactions between cluster and support through oxygen of CO ligands of precursor lead to change in C-O including Pt-C and Pt-O\* distances. Changes in Pt-CO distances and coordination numbers of sample after adsorption with Pt<sub>3</sub>Ru<sub>6</sub>(CO)<sub>21</sub>(μ<sub>3</sub>-H)(μ-H)<sub>3</sub> analyzed with EXAFS spectroscopy were compared with XRD data of precursor in crystalline form as in Table 4.2. The Pt-C interatomic distances of fresh supported sample were detected at  $1.89 \pm 0.01$  Å

**Table 4.2** Comparison XRD data of crystalline  $\text{Pt}_3\text{Ru}_6(\text{CO})_{21}(\mu_3\text{-H})(\mu\text{-H})_3$  (Adams et al., 1994) and EXAFS of supported species formed from this cluster on  $\text{TiO}_2$

Shell	XRD data of		EXAFS data of adsorbed	
	$\text{Pt}_3\text{Ru}_6(\text{CO})_{21}(\mu_3\text{-H})(\mu\text{-H})_3$		$\text{Pt}_3\text{Ru}_6(\text{CO})_{21}(\mu_3\text{-H})(\mu\text{-H})_3$ on $\text{TiO}_2$	
	<i>N</i>	<i>R</i> (Å)	<i>N</i>	<i>R</i> (Å)
Pt-Pt	2.0	2.64	$1.8 \pm 0.1$	$2.72 \pm 0.01$
Pt-Ru	4.0	2.80	$1.8 \pm 0.1$	$2.71 \pm 0.01$
Pt-CO				
Pt-C	1.0	1.85	$0.6 \pm 0.1$	$1.89 \pm 0.01$
Pt-O*	1.0	2.99	$0.6 \pm 0.2$	$2.94 \pm 0.01$
Ru-Ru	2.0	3.04	$1.7 \pm 0.1$	$2.50 \pm 0.01$
Ru-Pt	2.0	2.80	$1.3 \pm 0.1$	$2.71 \pm 0.01$
Ru-CO				
Ru-C	3.0	1.89	$1.4 \pm 0.1$	$1.86 \pm 0.01$
Ru-O*	3.0	3.03	$1.4 \pm 0.1$	$3.05 \pm 0.01$

The EXAFS data in Table 4.1 showed that Pt-C interatomic distances did not significantly changed, from 1.85 to  $1.89 \pm 0.01$  Å with coordination number  $0.6 \pm 0.1$  indicating that partial decarbonylation did not take place on Pt atom. The Pt-O\* interatomic distances did not significantly changed, from 2.99 to  $2.94 \pm 0.01$  Å with coordination number  $0.6 \pm 0.1$ .

More interaction between cluster cores and surface oxygen were observed at  $\text{Ru-O}_{\text{support}}$  contributions by EXAFS spectroscopy at the Ru K edge in Table 4.1. The EXAFS data showed coordination number of  $\text{Ru-O}_s$  contribution of  $2.5 \pm 0.1$  at distances  $2.09 \pm 0.01$  Å. The high coordination numbers of  $\text{Ru-O}_s$  contributions were agree well with EXAFS data of Ru-C and Ru-O\* contributions. It was found that

coordination numbers of Ru-C significantly decreased from 3.0 to  $1.4 \pm 0.1$  at bond distances  $1.86 \pm 0.01 \text{ \AA}$  implying that partially decarbonylation occurred. The coordination numbers of Ru-O\* were also found to be  $1.4 \pm 0.1$  at bond distances  $3.05 \pm 0.01 \text{ \AA}$ . The EXAFS data indicated that interactions between cluster core and TiO<sub>2</sub> surface in adsorption step occurred more at Ru atoms than at Pt atoms and partially decarbonylation was observed at Ru atoms.

Furthermore, some changes in metal-metal cores of fresh supported sample also presented. It was found that Pt-Pt interactions increased from 2.64 to  $2.72 \pm 0.01 \text{ \AA}$  while its coordination number  $1.8 \pm 0.1$  did not change much. The Pt-Ru interatomic distances decreased from 2.80 to  $2.71 \pm 0.01 \text{ \AA}$  whereas coordination number significantly decreased from 4.0 to  $1.8 \pm 0.1$  indicated that some Pt-Ru contributions were broken upon impregnation. The loss of Pt-Ru contribution resulted from strong cluster-support interaction. The EXAFS fitting parameters at the Ru K edge represented that Ru-Pt coordination numbers also decreased from 2.0 to  $1.3 \pm 0.1$  at average bond distance  $2.71 \pm 0.01 \text{ \AA}$ . More changes in cluster cores were observed at Ru-Ru contributions, the average Ru-Ru bond distances were detected at  $2.50 \pm 0.01 \text{ \AA}$  with coordination number  $1.7 \pm 0.1$ . The significantly decreased in average Ru-Ru bond distances resulted from loss of electron rich hydride ligands which bonded to both Ru<sub>3</sub> stacks of cluster core.

Consequently, Pt<sub>3</sub>Ru<sub>6</sub>(CO)<sub>21</sub>(μ<sub>3</sub>-H)(μ-H)<sub>3</sub> did not adsorb intact on TiO<sub>2</sub> but still in the form of bimetallic carbonyl adsorbed species as shown by IR and EXAFS data. It adsorbed strongly on TiO<sub>2</sub> leading to structural changes and partially decarbonylation at Ru atoms.

#### 4.3.4 EXAFS evidence of Pt-Ru contribution after ligand removal

Supported PtRu sample prepared from adsorption of  $\text{Pt}_3\text{Ru}_6(\text{CO})_{21}(\mu_3\text{-H})(\mu\text{-H})_3$  onto  $\text{TiO}_2$  was treated in He flow at  $300^\circ\text{C}$  for 2 h to remove ligands. From IR spectroscopy, it was found that IR bands in  $\nu_{\text{CO}}$  regions disappeared after ligand removal (spectrum 2 in Figure 4.2) indicating that carbonyl ligands were completely removed at this treatment condition. The IR peaks characterizing isolated hydroxyl groups of  $\text{TiO}_2$  clearly observed at 3662 (sh), 3604 (w) and 3300 (w)  $\text{cm}^{-1}$  (spectrum 3 in Figure 4.1), the same as that of bare  $\text{TiO}_2$ .

The resulting PtRu/ $\text{TiO}_2$  was characterized further with EXAFS spectroscopy. The EXAFS fitting parameters of treated PtRu sample in He flow were summarized in Table 4.3. The EXAFS fitting results in  $k$  and  $r$  space with  $k^0$ ,  $k^1$  and  $k^3$  weighted are in Figures 4.7 and 4.8. The estimated accuracies of coordination number ( $N$ ), distance ( $R$ ), Debye-Waller factor ( $\Delta\sigma^2$ ), and inner potential correction ( $\Delta E_0$ ) are as follows:  $\pm 20\%$ ,  $\pm 1\%$ ,  $\pm 30\%$ , and  $\pm 10\%$ , respectively.

**Table 4.3** Summary of EXAFS data of sample prepared by adsorption of  $\text{Pt}_3\text{Ru}_6(\text{CO})_{21}(\mu_3\text{-H})(\mu\text{-H})_3$  on  $\text{TiO}_2$  after ligand removal in He flow at  $300^\circ\text{C}$  for 2 h

Edge	Shell	$N$	$R$ (Å)	$10^3 \times \Delta\sigma^2$ (Å <sup>2</sup> )	$\Delta E_o$ (eV)
Pt L <sub>III</sub>	Pt-Pt	$1.8 \pm 0.1$	$2.65 \pm 0.01$	$0.9 \pm 0.3$	$-6.8 \pm 0.5$
	Pt-Ru	$1.9 \pm 0.1$	$2.69 \pm 0.01$	$2.8 \pm 0.1$	$7.6 \pm 0.1$
	Pt-O <sub>support</sub>				
	Pt-O <sub>s</sub>	$1.8 \pm 0.1$	$1.96 \pm 0.01$	$9.4 \pm 0.3$	$-0.9 \pm 0.7$
	Pt-O <sub>l</sub>	$0.5 \pm 0.1$	$3.09 \pm 0.01$	$-3.6 \pm 1.7$	$8.6 \pm 1.1$
Ru K	Ru-Ru	$2.4 \pm 0.1$	$2.65 \pm 0.01$	$6.7 \pm 0.4$	$-7.7 \pm 0.3$
	Ru-Pt	$0.9 \pm 0.1$	$2.69 \pm 0.01$	$3.0 \pm 0.4$	$-3.4 \pm 0.6$
	Ru-O <sub>support</sub>				
	Ru-O <sub>s</sub>	$2.4 \pm 0.1$	$2.00 \pm 0.01$	$10.4 \pm 0.3$	$-4.4 \pm 0.2$
	Ru-O <sub>l</sub>	$0.3 \pm 0.1$	$2.80 \pm 0.01$	$-5.5 \pm 1.3$	$-1.4 \pm 1.7$

Notation: subscribe s and l refer to short and long distance

The EXAFS fitting parameters in Table 4.3 represented that cluster core remained after treated supported PtRu sample in He flow. The EXAFS data of treated sample were compared to those of impregnated sample. The average Pt-Pt bond distances slightly decreased from  $2.72 \pm 0.01$  to  $2.65 \pm 0.01$  Å with coordination number  $1.8 \pm 0.1$ . The average Pt-Ru bond distances were also slightly decreased from  $2.71 \pm 0.01$  to  $2.69 \pm 0.01$  Å with coordination number  $1.9 \pm 0.1$  imply strong Pt-Ru interaction on  $\text{TiO}_2$ . The interaction between Pt and surface oxygen slightly increased after treatment in He flow as coordination number of Pt-O<sub>s</sub> increased from  $1.3 \pm 0.1$  to  $1.8 \pm 0.1$  at the same average distances,  $1.96 \pm 0.01$  Å. In addition, the Pt-O<sub>l</sub> interactions were also detected at  $3.09 \pm 0.01$  Å with coordination number  $0.5 \pm 0.1$ .

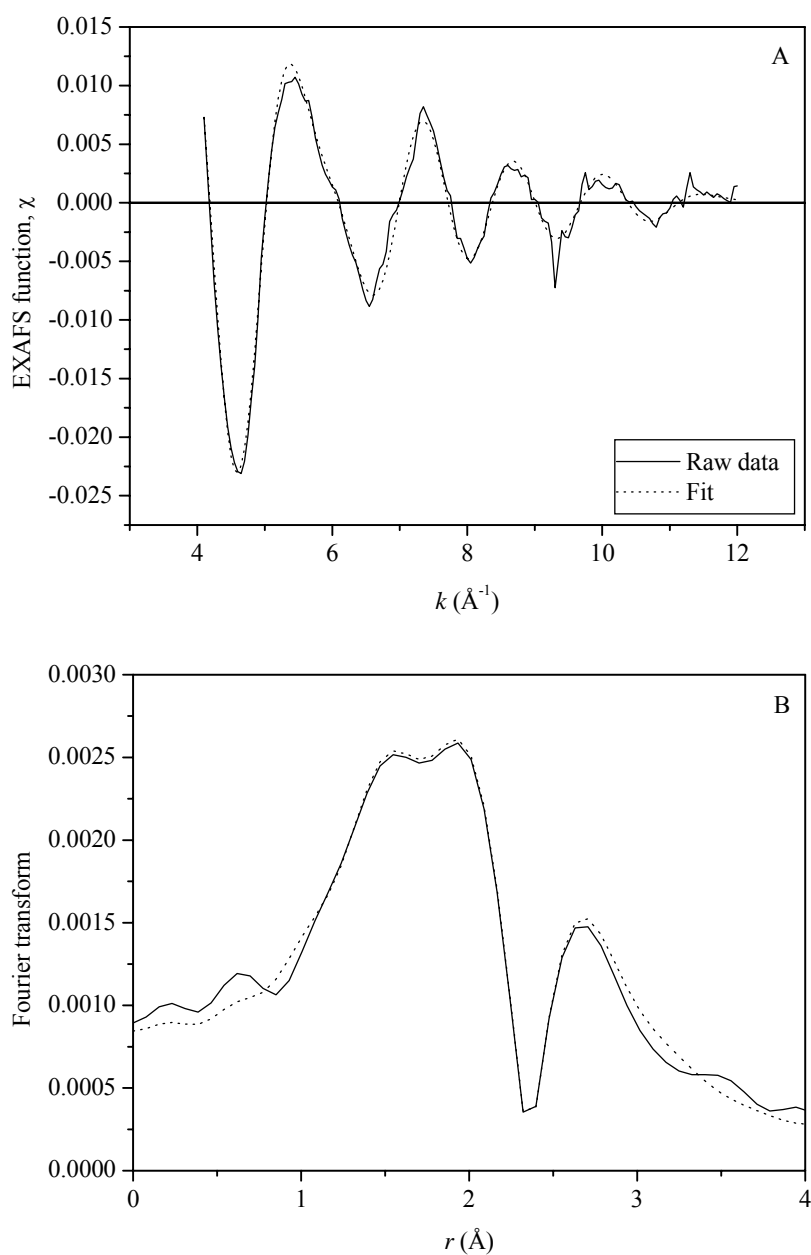


**Figure 4.7** EXAFS results scanned at the Pt  $L_{III}$  edge characterizing the PtRu/TiO<sub>2</sub> sample prepared by adsorption of Pt<sub>3</sub>Ru<sub>6</sub>(CO)<sub>21</sub>( $\mu_3$ -H)( $\mu$ -H)<sub>3</sub> after ligand removal: (A) Experimental EXAFS function (solid line) and sum of the calculated Pt-Pt, Pt-Ru, Pt-C, Pt-O\*, Pt-O<sub>s</sub>, and Pt-O<sub>l</sub> contributions (dotted line). (B) Magnitude of uncorrected Fourier transform ( $k^0$  weighted) of experimental EXAFS function (solid line) and sum of the calculated Pt-Pt, Pt-Ru, Pt-C, Pt-O\*, Pt-O<sub>s</sub>, and Pt-O<sub>l</sub> contributions (dotted line).

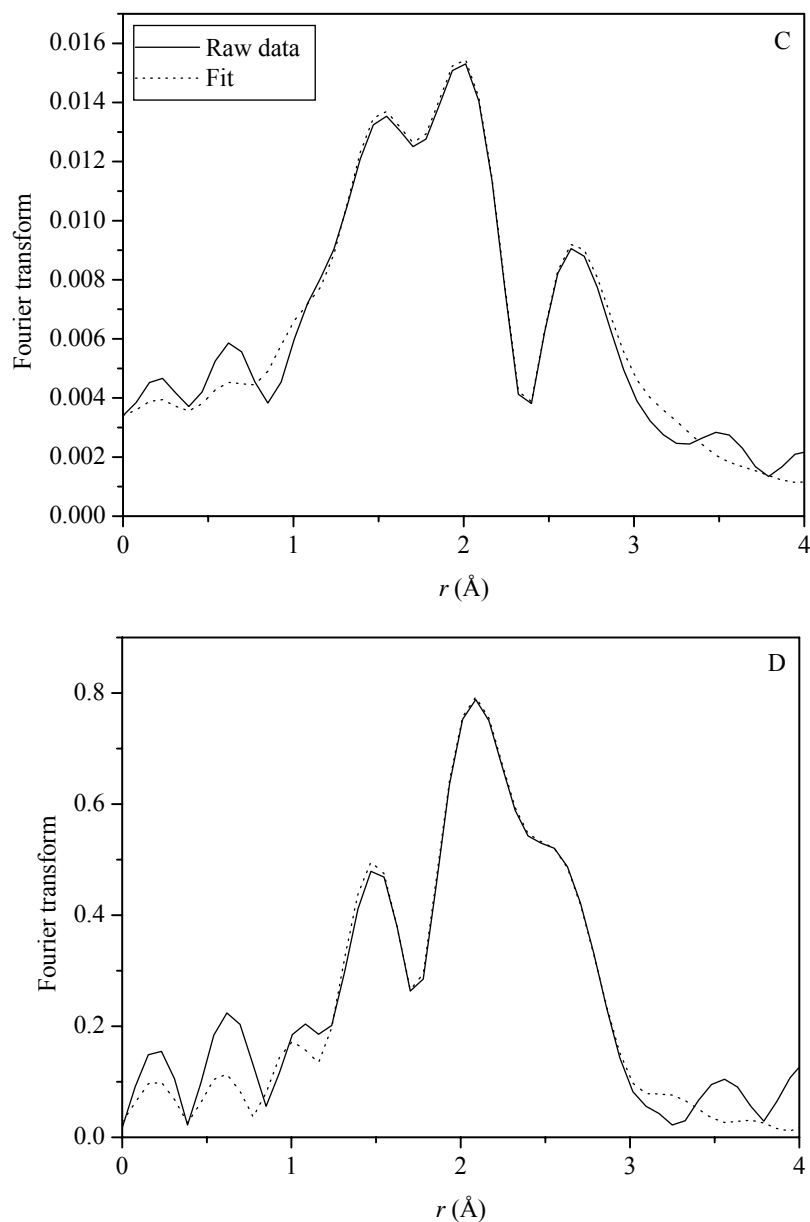


**Figure 4.7** (continued) EXAFS results scanned at the Pt L<sub>III</sub> edge characterizing the PtRu/TiO<sub>2</sub> sample prepared by adsorption of Pt<sub>3</sub>Ru<sub>6</sub>(CO)<sub>21</sub>(μ<sub>3</sub>-H)(μ-H)<sub>3</sub> after ligand removal: (C) Magnitude of uncorrected Fourier transform ( $k^1$  weighted) of experimental EXAFS function (solid line) and sum of the calculated Pt-Pt, Pt-Ru, Pt-C, Pt-O\*, Pt-O<sub>s</sub>, and Pt-O<sub>l</sub> contributions (dotted line). (D) Magnitude of uncorrected Fourier transform ( $k^3$  weighted) of experimental EXAFS function (solid line) and sum of the calculated Pt-Pt, Pt-Ru, Pt-C, Pt-O\*, Pt-O<sub>s</sub>, and Pt-O<sub>l</sub> contributions (dotted line).

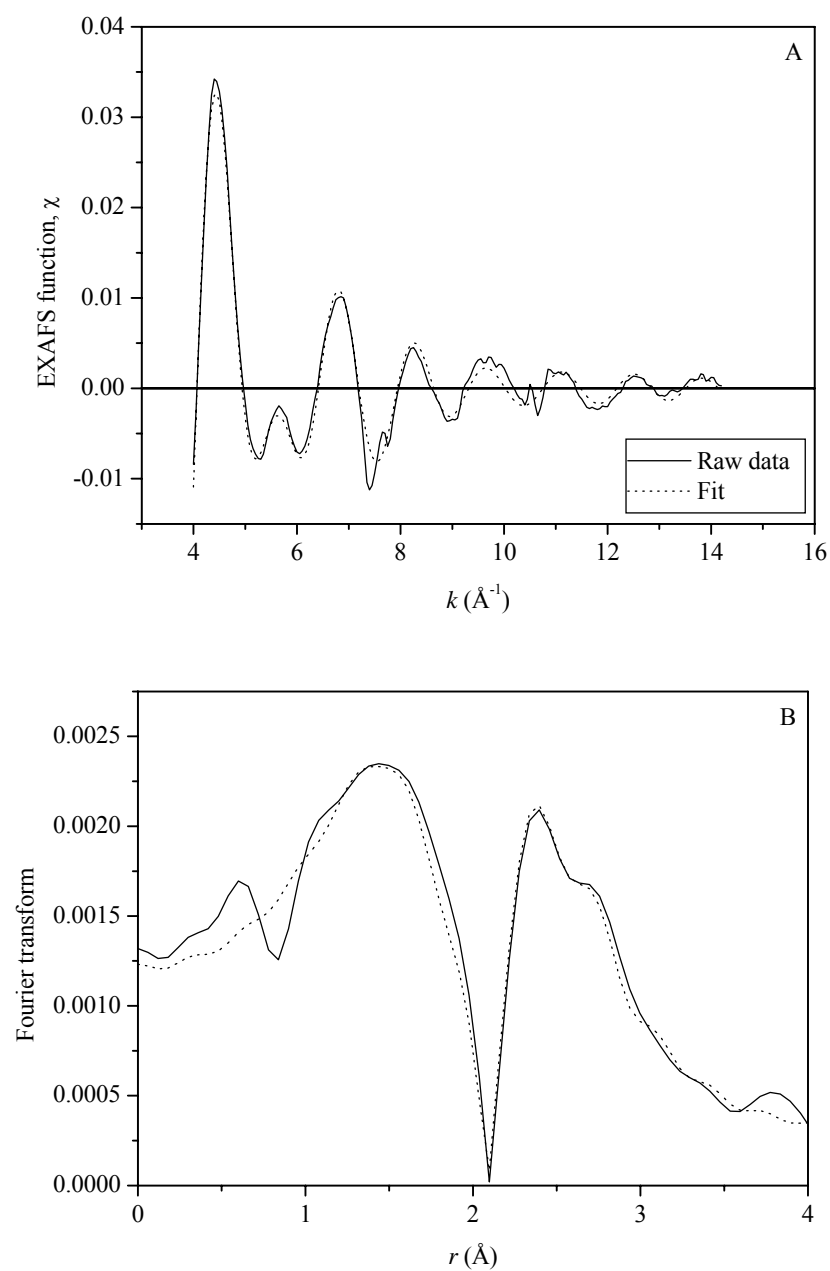


**Figure 4.8** EXAFS results scanned at the Ru K edge characterizing the PtRu/TiO<sub>2</sub> sample prepared by adsorption of Pt<sub>3</sub>Ru<sub>6</sub>(CO)<sub>21</sub>( $\mu_3$ -H)( $\mu$ -H)<sub>3</sub> after ligand removal: (A) Experimental EXAFS function (solid line) and sum of the calculated Ru-Ru, Ru-Pt, Ru-C, Ru-O\*, Ru-O<sub>s</sub>, and Ru-O<sub>l</sub> contributions (dotted line). (B) Magnitude of uncorrected Fourier transform ( $k^0$  weighted) of experimental EXAFS function (solid line) and sum of the calculated Ru-Ru, Ru-Pt, Ru-C, Ru-O\*, Ru-O<sub>s</sub>, and Ru-O<sub>l</sub> contributions (dotted line).

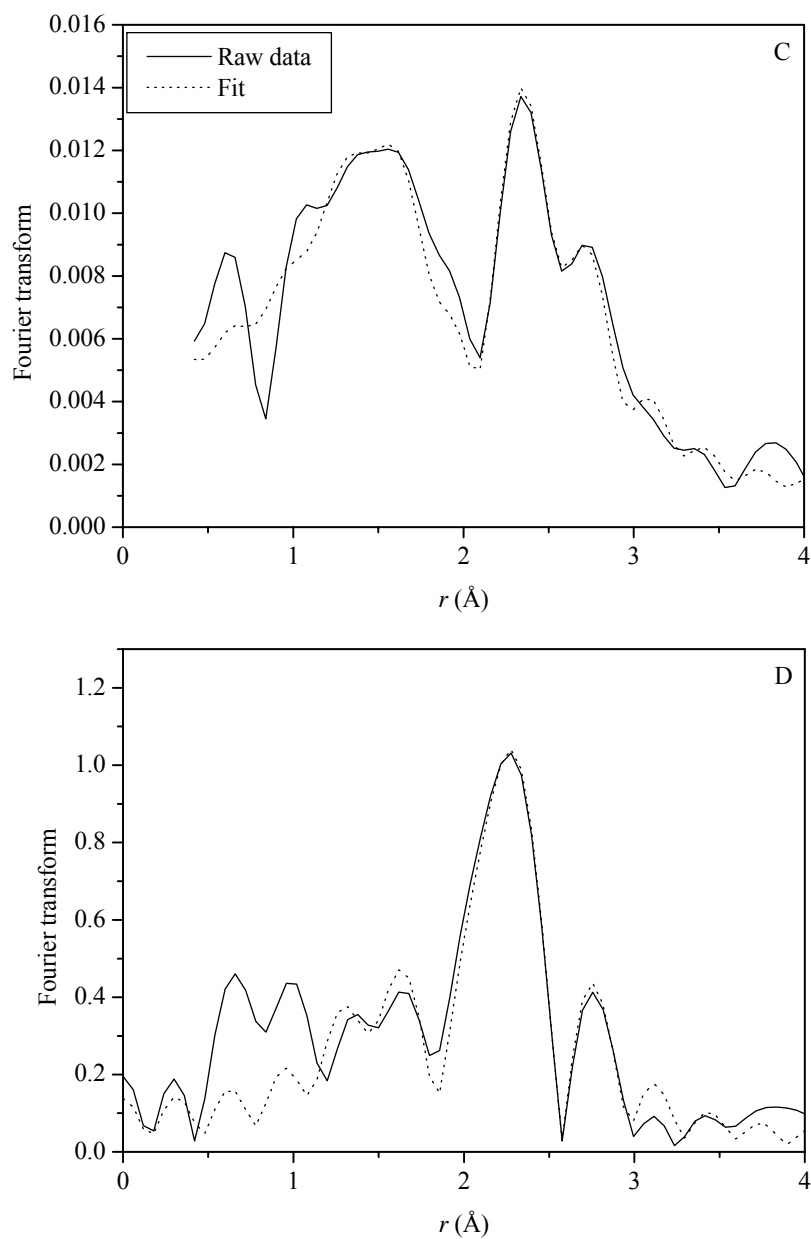


**Figure 4.8** (continued) EXAFS results scanned at the Ru K edge characterizing the PtRu/TiO<sub>2</sub> sample prepared by adsorption of Pt<sub>3</sub>Ru<sub>6</sub>(CO)<sub>21</sub>(μ<sub>3</sub>-H)(μ-H)<sub>3</sub> after ligand removal: (C) Magnitude of uncorrected Fourier transform ( $k^1$  weighted) of experimental EXAFS function (solid line) and sum of the calculated Ru-Ru, Ru-Pt, Ru-C, Ru-O\*, Ru-O<sub>s</sub>, and Ru-O<sub>l</sub> contributions (dotted line). (D) Magnitude of uncorrected Fourier transform ( $k^3$  weighted) of experimental EXAFS function (solid line) and sum of the calculated Ru-Ru, Ru-Pt, Ru-C, Ru-O\*, Ru-O<sub>s</sub>, and Ru-O<sub>l</sub> contributions (dotted line).

The EXAFS fitting parameters at the Ru K edge showed that average Ru-Ru bond distances after treatment in He flow increased from  $2.50 \pm 0.01$  to  $2.65 \pm 0.01$  Å with coordination number  $2.4 \pm 0.1$ , slightly higher than that before ligand removal. It was found that Ru atoms also surrounded by  $0.9 \pm 0.1$  Pt atoms at average bond distances  $2.69 \pm 0.01$  Å. Thus, extremely high dispersion metal and bimetallic particles on TiO<sub>2</sub> could be formed after treatment at this condition.

Moreover, Ru atoms were found to have bonding with  $2.4 \pm 0.1$  surface oxygen atoms at average bond distances  $2.00 \pm 0.01$  Å as similarly to Ru-O<sub>s</sub> interaction of impregnated sample. There was  $0.3 \pm 0.1$  of surface oxygen atom near Ru atom at average distances  $2.80 \pm 0.01$  Å.

Therefore, the EXAFS data indicating that Pt-Ru interactions were stable upon treatment in He flow at 300°C for 2 h and cluster core remained on TiO<sub>2</sub>. The strong interactions of Pt-Ru on support refer to extremely high dispersion of bimetallic that might be effect to catalytic activities over supported PtRu/TiO<sub>2</sub>.

#### **4.3.5 Effect of chemistry of support on cluster-support interaction**

The interactions between cluster and support not only depend on nature of precursor but also the chemistry of support (Alexeev et al., 2002). The difference in surface properties of support such as acidic, neutral or basic support, and degree of hydroxylation are determined. TiO<sub>2</sub>-supported PtRu sample was compared with sample prepared from impregnation of Pt<sub>3</sub>Ru<sub>6</sub>(CO)<sub>21</sub>(μ<sub>3</sub>-H)(μ-H)<sub>3</sub> onto slightly acidic γ-Al<sub>2</sub>O<sub>3</sub> and basic MgO. It was found that cluster-support interactions were difference, especially in the case of sample after treatment in He flow. On basic MgO support, cluster-support interactions were stronger than that on slightly acidic support

such as  $\gamma$ -Al<sub>2</sub>O<sub>3</sub> and TiO<sub>2</sub>. However, partially decarbonylation at Ru atoms before ligand removal only observed at TiO<sub>2</sub>-supported sample. The strong cluster-support interactions lead to partial cleavage of Pt-Ru contributions that were observed by EXAFS data that Pt atom was surrounded by  $0.9 \pm 0.1$  atom of Ru on MgO after treatment in He flow. In contrast, coordination numbers  $2.2 \pm 0.1$  and  $1.9 \pm 0.1$  were found for Pt-Ru contributions of  $\gamma$ -Al<sub>2</sub>O<sub>3</sub>- and TiO<sub>2</sub>-supported PtRu sample after decarbonylation.

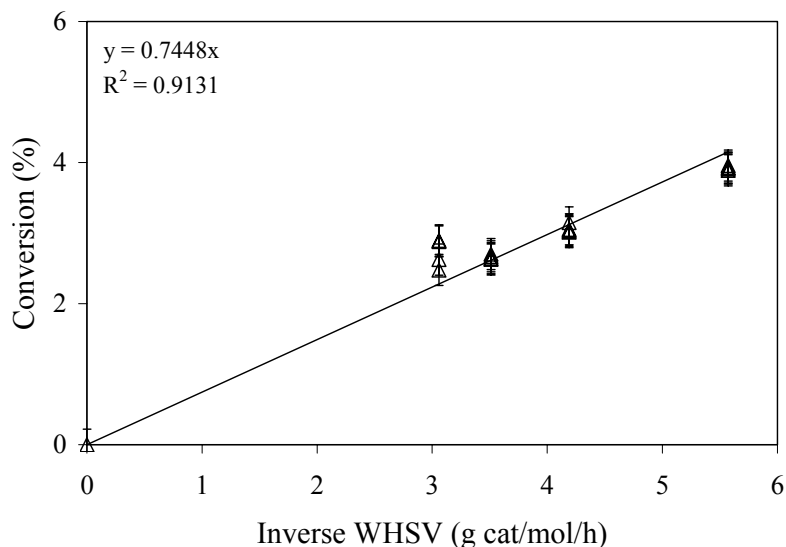
Consequently, surface properties of support also affect to cluster-support interaction.

### **4.3.6 Catalytic activity of ethylene hydrogenation catalyzed by PtRu/TiO<sub>2</sub>**

#### **4.3.6.1 Catalytic activity and time on stream (TOS)**

PtRu/TiO<sub>2</sub> sample prepared from impregnation with Pt<sub>3</sub>Ru<sub>6</sub>(CO)<sub>21</sub>( $\mu_3$ -H)( $\mu$ -H)<sub>3</sub> was used as catalyst in ethylene hydrogenation which is structural-insensitive reaction.

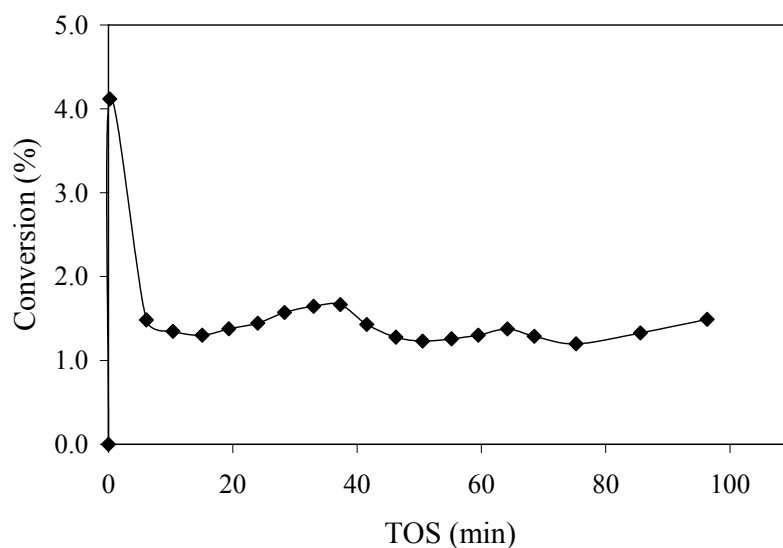
A blank test for ethylene hydrogenation reaction was performed with stainless U-tube reactor containing only inert  $\alpha$ -Al<sub>2</sub>O<sub>3</sub>. The activity and inversed weight hourly space velocity (inv. WHSV, g cat/mol/h) at -75°C was plot as straight line through the origin (Figure 4.9) implying that the reactor testing in inv. WHSV ranges of 0-5.6 g cat/mol/h with conversion < 5% was a differential reactor at this condition.



**Figure 4.9** Demonstration of differential reactor operation at  $-75^{\circ}\text{C}$ ,  $P_{\text{C}_2\text{H}_4} = 40$  Torr,  $P_{\text{H}_2} = 80$  Torr, balanced with He, total feed flow rate = 200 ml (NTP)/min catalyzed by PtRu/TiO<sub>2</sub>.

The catalytic activity of reaction in term of the turnover frequency (TOF) was represented the number of molecules reacting per active sites per second (Fogler, 1999). It was assumed that all metal particles dispersed on TiO<sub>2</sub> were accessible to reactants, so that TOF was defined as the equation 2.3 (Chapter II, page 53).

Catalytic activities of ethylene hydrogenation catalyzed by PtRu/TiO<sub>2</sub> were collected at reaction condition:  $P_{\text{C}_2\text{H}_4} = 40$  Torr,  $P_{\text{H}_2} = 80$  Torr, balanced He with total feed flow rate 200 ml (NTP)/min, catalyst mass 0.012 mg, 1.0 wt% Pt and 1.0 wt% Ru and temperature  $-75^{\circ}\text{C}$ . Ethylene hydrogenation reaction started as soon as reactant gas arrived the catalyst bed. The plot between activity and time on stream (TOS) is shown in Figure 4.10.



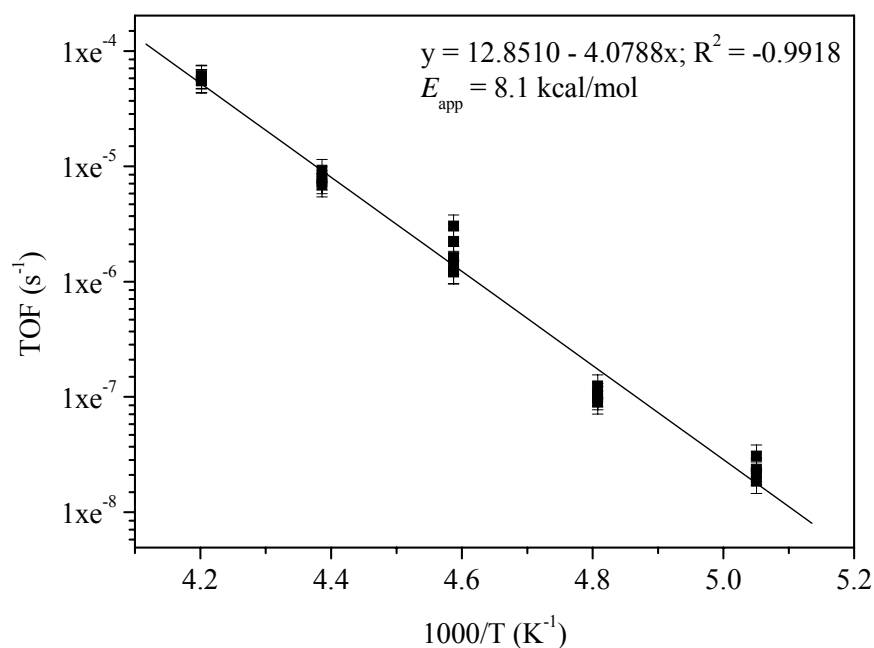
**Figure 4.10** Activity of ethylene hydrogenation with time on stream (TOS) catalyzed by PtRu/TiO<sub>2</sub> at reaction condition:  $P_{\text{C}_2\text{H}_4} = 40$  Torr,  $P_{\text{H}_2} = 80$  Torr, balanced He with total feed flow rate 200 ml (NTP)/min, catalyst mass 0.013 mg, and temperature -75°C.

Figure 4.10 showed that catalytic activity decreased from 4.1 to around 1.5% conversion during 6 minutes and then reached steady-state within 20 minutes with 1.2% conversion.

#### 4.3.6.2 Kinetics of ethylene hydrogenation catalyzed by PtRu/TiO<sub>2</sub>

The kinetic data for ethylene hydrogenation catalyzed by PtRu/TiO<sub>2</sub> catalyst prepared from adsorption of Pt<sub>3</sub>Ru<sub>6</sub>(CO)<sub>21</sub>(μ<sub>3</sub>-H)(μ-H)<sub>3</sub> were investigated. The apparent activation energy of ethylene hydrogenation catalyzed by PtRu/TiO<sub>2</sub> catalyst was collected at around 50 min TOS at reaction condition:  $P_{\text{C}_2\text{H}_4} = 40$  Torr,  $P_{\text{H}_2} = 80$  Torr, balanced He with total feed flow rate 200 ml (NTP)/min, catalyst mass

0.010-0.020 g, 1.0 wt% Pt and 1.0 wt% Ru and temperature range -75 to -35°C. The catalyst was treated in He flow at 300°C for 2 h, diluted with inert  $\alpha$ -Al<sub>2</sub>O<sub>3</sub>, and transferred into stainless steel U-tube reactor in a glovebox. The reactor was isolated from air and moisture and moved to reaction testing. Before flowing reactant gas, the reactor under He flow was cooled down to desired temperature by liquid nitrogen and controlled temperature within  $\pm 1^\circ\text{C}$ . The Arrhenius plot of a natural log scale of TOF as a function of inversed temperature was shown in Figure 4.11.



**Figure 4.11** Arrhenius plot of ethylene hydrogenation catalyzed by PtRu/TiO<sub>2</sub> at reaction condition:  $P_{\text{C}_2\text{H}_4} = 40$  Torr,  $P_{\text{H}_2} = 80$  Torr, balance He with total feed flow rate 200 ml (NTP)/min, catalyst mass 0.013 g.

The apparent activation energy obtained from temperature dependence of rate of ethylene hydrogenation reaction catalyzed by Pt-Ru/TiO<sub>2</sub> was  $8.1 \pm 0.1$  kcal/mol. This apparent activation energy was nearly the same as that of Pt-Ru/ $\gamma$ -Al<sub>2</sub>O<sub>3</sub> which was

$8.4 \pm 0.1$  kcal/mol but slightly higher than that of Pt-Ru/MgO which was  $7.6 \pm 0.1$  kcal/mol. However, the apparent activation energy for ethylene hydrogenation catalyzed by Pt-Ru/TiO<sub>2</sub> was lower than reported on Pt catalysts supported on oxides supports, 8.6-11.7 kcal/mol obtained at various conditions as in Table 2.4 (Chapter II). Moreover, Table 2.4 shows that apparent activation energy obtained from this work is near the valued obtained from polymer-supported Pt-Ru catalysts prepared from bimetallic cluster, [RuPt<sub>2</sub>(CO)<sub>5</sub>(Ph<sub>2</sub>P- $\text{\textcircled{D}}$ )<sub>3</sub>],  $7.8 \pm 1.2$  kcal/mol obtained at  $P_{\text{H}_2} = 555$  Torr and  $P_{\text{C}_2\text{H}_4} = 152$  Torr and temperature range 73 to 98°C (Pierantozzi et al., 1979).

Catalytic activities in term of TOF at -75°C of supported PtRu/TiO<sub>2</sub> was  $(48.6 \pm 4.5) \times 10^{-5}$  (s<sup>-1</sup>), slightly higher than that of PtRu/MgO which was  $(33.6 \pm 2.5) \times 10^{-5}$  (s<sup>-1</sup>) and higher than that of PtRu/ $\gamma$ -Al<sub>2</sub>O<sub>3</sub> which was  $(3.0 \pm 0.1) \times 10^{-5}$  (s<sup>-1</sup>). Thus, order of activity of ethylene hydrogenation was PtRu/TiO<sub>2</sub> > PtRu/MgO > PtRu/ $\gamma$ -Al<sub>2</sub>O<sub>3</sub>.

However, from literature reviews, there was none of catalytic activity of ethylene hydrogenation catalyzed by TiO<sub>2</sub>-supported Pt or Ru catalysts. Therefore, this work could not make a comparison of catalytic activity of ethylene hydrogenation with TiO<sub>2</sub>-supported Pt or Ru or PtRu catalysts.

#### **4.3.6.3 Rate expression for ethylene hydrogenation catalyzed by PtRu/TiO<sub>2</sub>**

The effect of pressure of hydrogen on Pt-Ru/TiO<sub>2</sub> catalyst was investigated at temperature -75°C with conversion < 5% at  $P_{\text{C}_2\text{H}_4} = 40$  Torr,  $P_{\text{H}_2}$

varied from 20 to 200 Torr, balanced He with total feed flow rate 200 ml (NTP)/min, catalyst mass 0.010-0.020 mg, 1.0 wt% Pt and 1.0 wt% Ru. Catalytic activity of ethylene hydrogenation in term of TOF was plotted as a function of hydrogen pressure as in Figure 4.12.

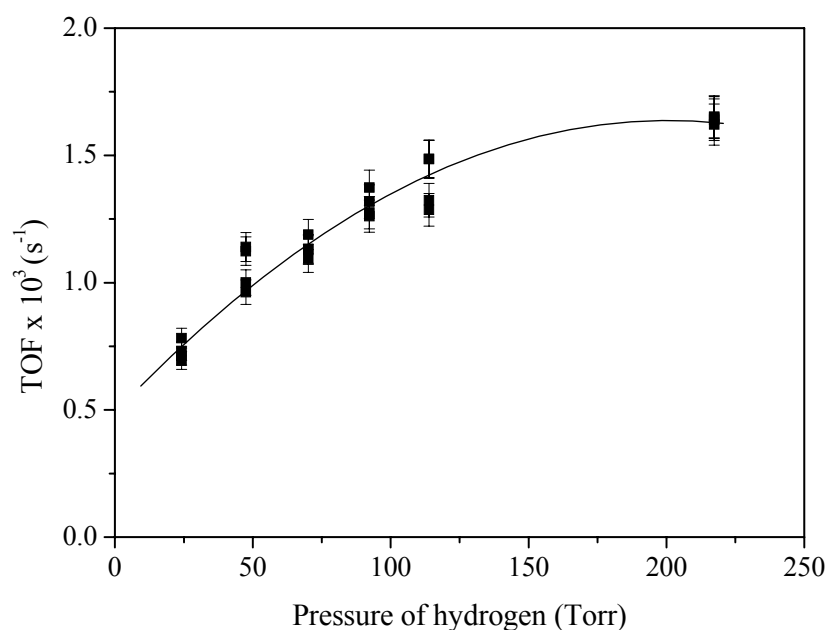


**Figure 4.12** Effect of pressure of hydrogen on ethylene hydrogenation catalyzed by PtRu/TiO<sub>2</sub> at 40 torr ethylene at -75°C.

The catalytic activities of ethylene hydrogenation catalyzed by PtRu/TiO<sub>2</sub> catalyst at 40 Torr ethylene pressure, changed with hydrogen pressure. Orders of hydrogen and ethylene can be determined in the form of rate expression in equation 4.1.

$$\text{rate} = k P_{\text{H}_2}^a P_{\text{C}_2\text{H}_4}^b \quad \dots(4.1)$$

Where  $k$  = reaction rate

$a$  = hydrogen order

$b$  = ethylene order

The slope of a plot of  $\ln(\text{rate})$  as a function of  $\ln P_{\text{H}_2}$  is the hydrogen order. A plot in a natural log scale of TOF and  $P_{\text{H}_2}$  is in Figure 4.13 within the range 80 to 200 Torr hydrogen while ethylene pressure was constant at 40 Torr.

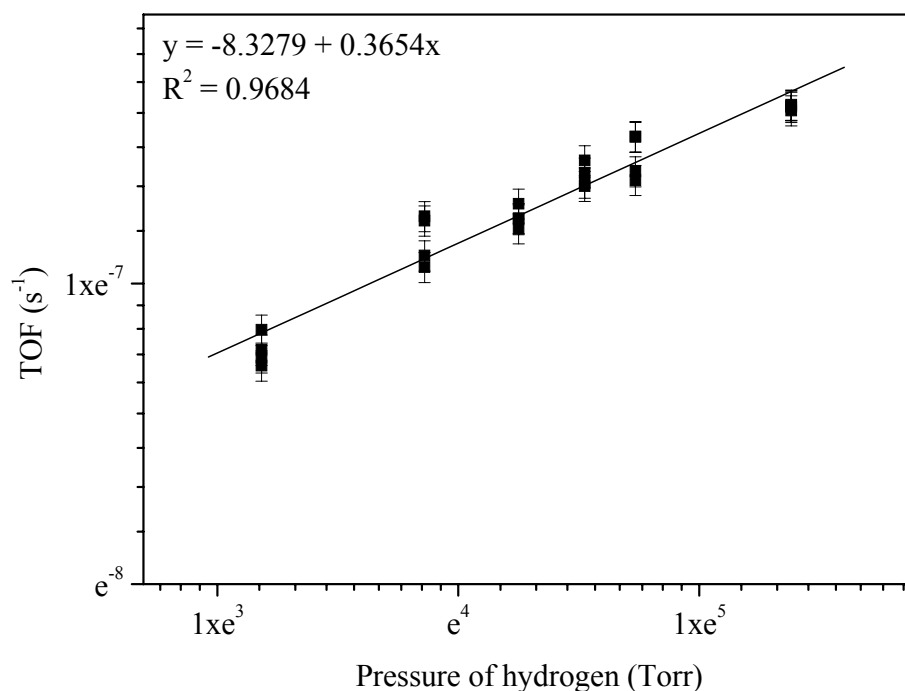


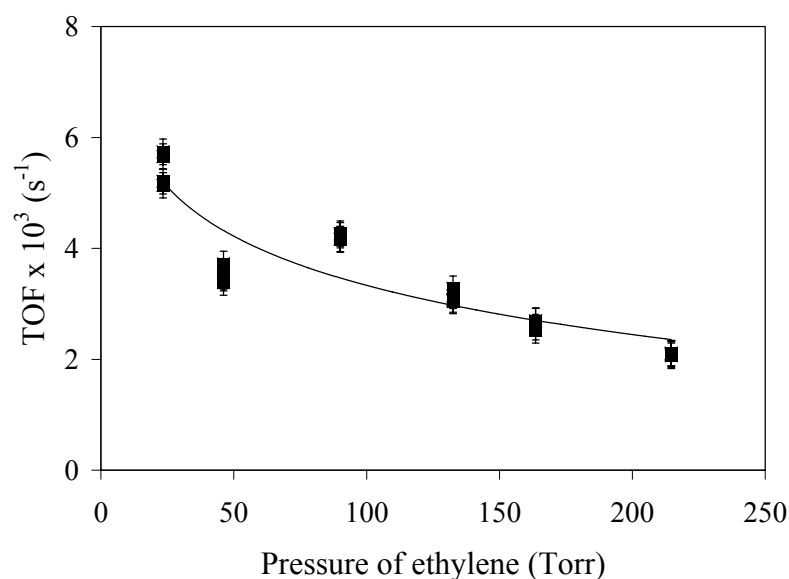
**Figure 4.13** The plot in a natural log scale between TOF and pressure of hydrogen for ethylene hydrogenation catalyzed by PtRu/TiO<sub>2</sub> at -75°C, 40 Torr ethylene and 20 to 200 Torr hydrogen.

A slope of linear plot in Figure 4.13 gave order of hydrogen as 0.36. This hydrogen order value was slightly lower than that of 0.04 wt% Pt/Cab-O-Sil (Cortright et al., 1991). The rate expression for ethylene hydrogenation catalyzed by 0.04 wt% Pt/Cab-O-Sil was reported as in equation 4.2.

$$\text{rate} = k P_{\text{H}_2}^{0.48} P_{\text{C}_2\text{H}_4}^{-0.17} \quad \dots(4.2)$$

When data were obtained for hydrogen order at condition: temperature  $-50^{\circ}\text{C}$ ; 25 Torr  $P_{\text{C}_2\text{H}_4}$ ; 50-650 Torr  $P_{\text{H}_2}$  in flow reactor. In addition, hydrogen order of PtRu/TiO<sub>2</sub> in this work was lower than that of PtRu/ $\gamma$ -Al<sub>2</sub>O<sub>3</sub> which was 0.46 (Chapter II) and that of PtRu/MgO which was 0.62 (Chapter III) at the same reaction condition.

The effect of ethylene pressure on ethylene hydrogenation activity was studied at  $-75^{\circ}\text{C}$  at constant hydrogen pressure at 80 Torr and the ethylene pressure was varied from 20 to 200 Torr. TOF data were plot as a function of ethylene pressure as in Figure 4.14.



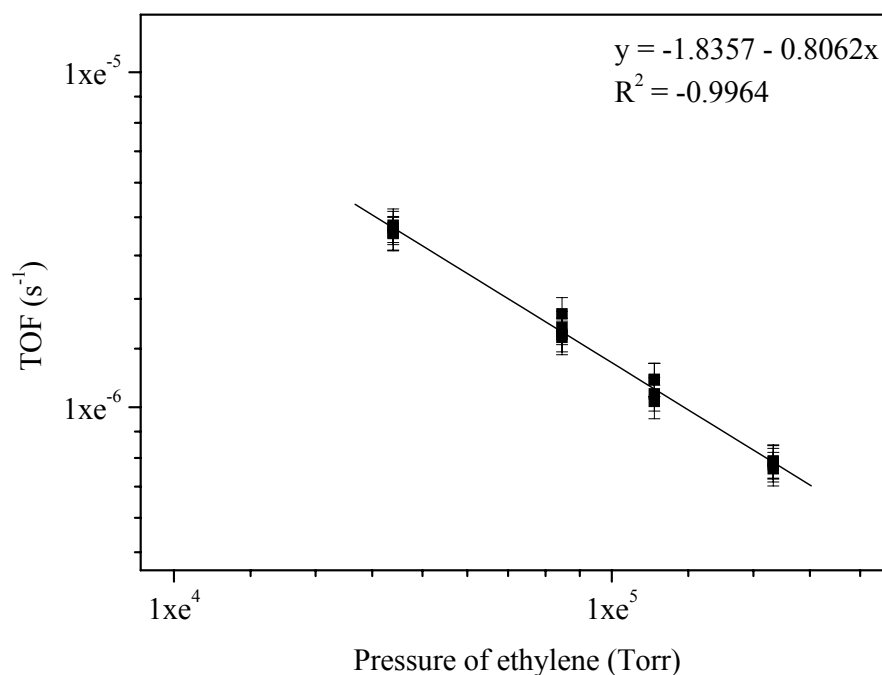
**Figure 4.14** Effect of pressure of ethylene on ethylene hydrogenation catalyzed by PtRu/TiO<sub>2</sub> at 80 Torr hydrogen.

Figure 4.14 shows that catalytic activities decreased with pressure of ethylene. That meant ethylene inhibited the reaction at high pressure of ethylene or at low ratio of hydrogen:ethylene. However, there was a tendency of higher TOF if pressure of ethylene was higher than 250 Torr as shown in Figure 4.14. At high pressure of

ethylene,  $\pi$ -Bonded ethylene which is weakly bound should present on metal surface. Hwang and co-workers (2003) found that most of ethane products from ethylene hydrogenation catalyzed by Pt(111) were from  $\pi$ -bonded ethylene hydrogenation. Thus, it was expected that TOF should increase if pressure of ethylene was higher than 250 Torr for this work.

Compare to catalytic activities over PtRu/MgO, at low ratio hydrogen:ethylene, catalytic activities decreased with pressure of ethylene whereas at high pressure of ethylene, catalytic activities increased with pressure of ethylene as in Figure 3.13 (Chapter III). In addition, catalytic activity of ethylene hydrogenation catalyzed by PtRu/ $\gamma$ -Al<sub>2</sub>O<sub>3</sub> did not change significantly with pressure of ethylene at low pressure of ethylene, < 100 Torr but activities increased with excess of ethylene, pressure of ethylene > 100 Torr as in Figure 2.15 (Chapter II).

Order of ethylene could be obtained with rate expression (4.1). A plot in a natural log scale of TOF and  $P_{C_2H_4}$  is in Figure 4.15 at hydrogen pressure 80 Torr and pressure of ethylene range 80-200 Torr.



**Figure 4.15** The plot in a natural log scale between TOF and pressure of ethylene for ethylene hydrogenation catalyzed by PtRu/TiO<sub>2</sub> at -75°C, 80 Torr hydrogen and 80 to 200 Torr ethylene.

Ethylene order obtained from the slope of linear graph in Figure 4.15 was - 0.80 at ethylene pressure 80 to 200 Torr. The negative ethylene order in this work was lower than that reported by Cortright et al. (1991) which was -0.17 at condition: 5-75 Torr  $P_{C_2H_4}$ ; 150 Torr  $P_{H_2}$  at temperature -50°C. Therefore, rate expression for ethylene hydrogenation catalyzed by PtRu/TiO<sub>2</sub> at temperature -75°C was reported as in equation 4.3.

$$\text{rate} = k P_{H_2}^{0.36} P_{C_2H_4}^{-0.80} \quad \dots(4.3)$$

The comparison was made with rate expression of ethylene hydrogenation catalyzed by PtRu/ $\gamma$ -Al<sub>2</sub>O<sub>3</sub> and PtRu/MgO as shown in Table 4.4.

**Table 4.4** Rate expression of ethylene hydrogenation catalyzed by supported PtRu catalysts prepared from adsorption of  $\text{Pt}_3\text{Ru}_6(\text{CO})_{21}(\mu_3\text{-H})(\mu\text{-H})_3$  on  $\gamma\text{-Al}_2\text{O}_3$ , MgO and  $\text{TiO}_2$

$$\text{rate} = k P_{\text{H}_2}^a P_{\text{C}_2\text{H}_4}^b$$

Catalysts	a	$P_{\text{H}_2}$ (Torr)	$P_{\text{C}_2\text{H}_4}$ (Torr)	b	$P_{\text{H}_2}$ (Torr)	$P_{\text{C}_2\text{H}_4}$ (Torr)
PtRu/ $\gamma\text{-Al}_2\text{O}_3$	0.46	80-200	40	0.35	80	80-200
PtRu/MgO	0.62	80-200	40	-0.27	80	20-40
PtRu/MgO				0.18	80	120-200
PtRu/ $\text{TiO}_2$	0.36	20-200	40	-0.80	80	80-200

Reaction temperature:  $-75^\circ\text{C}$ ; metal loading: 1.0 wt% Pt and 1.0 wt% Ru catalyst

All hydrogen orders in Table 4.4 were positive and varied from 0.36 to 0.62 whereas ethylene orders varied from -0.80 to 0.35. It was suggested that the difference in orders of ethylene might refer to the difference in adsorption process of reaction mechanism.

### 4.3.7 Catalytic activity of *n*-butane hydrogenolysis catalyzed by

#### PtRu/ $\text{TiO}_2$

##### 4.3.7.1 Catalytic activity and TOS

A blank test for *n*-butane hydrogenolysis catalyzed by PtRu/ $\text{TiO}_2$  catalyst prepared from adsorption of  $\text{Pt}_3\text{Ru}_6(\text{CO})_{21}(\mu_3\text{-H})(\mu\text{-H})_3$  was carried out in quartz-tube reactor containing inert  $\alpha\text{-Al}_2\text{O}_3$  at  $P_{\text{H}_2} = 540$  Torr,  $P_{n\text{-C}_4\text{H}_{10}} = 60$  Torr with 100 ml (NTP)/min flow rate and temperature  $220^\circ\text{C}$ . The quartz reactor was tested for differential reactor at this reaction condition. Conversion of *n*-butane was

plotted as a function of inverse weight hourly space velocity (inv. WHSV, g cat/mol/h) at steady-state operation with conversion < 5% in Figure 4.16.

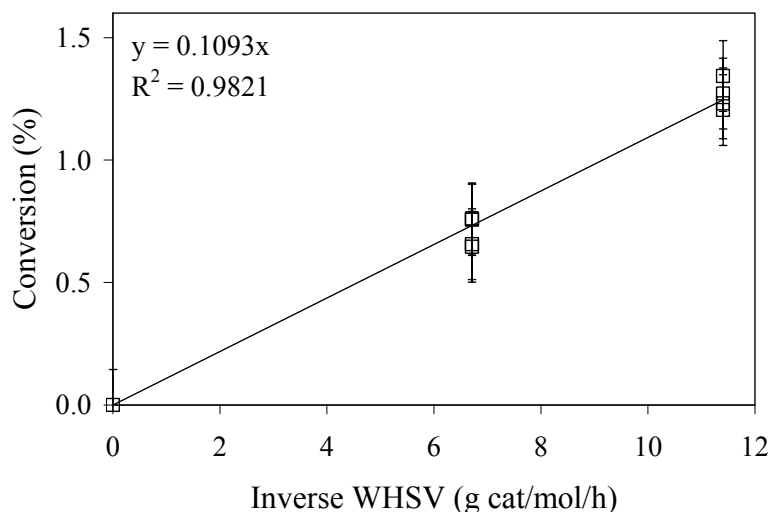


**Figure 4.16** Demonstration of differential reactor operation at 220°C,  $P_{\text{H}_2} = 540$  Torr,  $P_{n\text{-C}_4\text{H}_{10}} = 60$  Torr with 100 ml (NTP)/min flow rate catalyzed by PtRu/TiO<sub>2</sub>.

A linear graph through the origin during inv. WHSV ranges 0-11.4 g cat/mol/h in Figure 4.16 indicates that the quartz reactor containing inert  $\alpha\text{-Al}_2\text{O}_3$  act as differential reactor for *n*-butane hydrogenolysis at this reaction condition. A plot of selectivity varied with inv. WHSV is in Figure 4.17. This figure shows that initial selectivity for methane obtained by extrapolation curve to zero conversion was around 100% indicating the multiple hydrogenolysis.

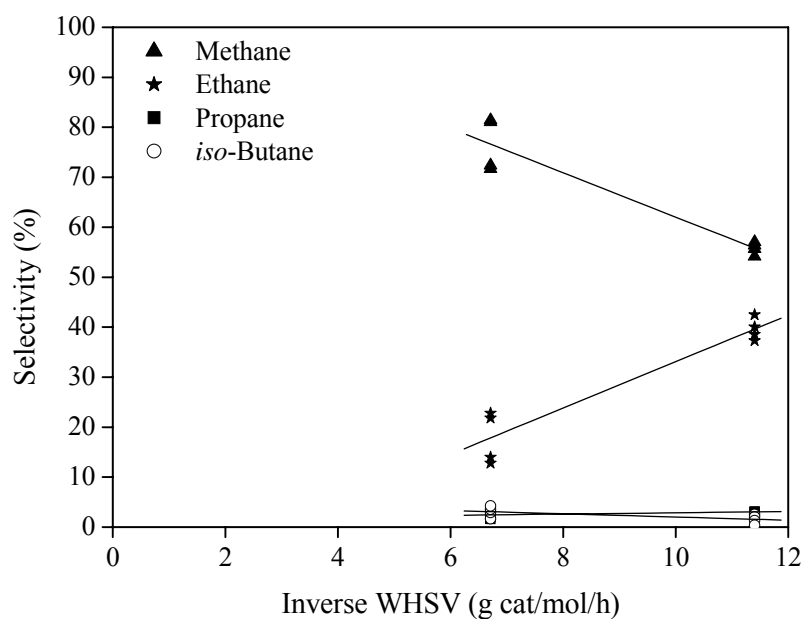


**Figure 4.17** Selectivity varied with inv. WHSV at 220°C,  $P_{\text{H}_2} = 540$  Torr,  $P_{n\text{-C}_4\text{H}_{10}} = 60$  Torr with 100 ml (NTP)/min flow rate catalyzed by PtRu/TiO<sub>2</sub>.

*n*-Butane hydrogenolysis reaction catalyzed by PtRu/TiO<sub>2</sub> catalyst was carried out at various reaction temperatures to study catalytic activities and deactivation. A plot of catalytic activities as a function of time on stream (TOS) at various temperature, 200-280°C is shown in Figure 4.18.

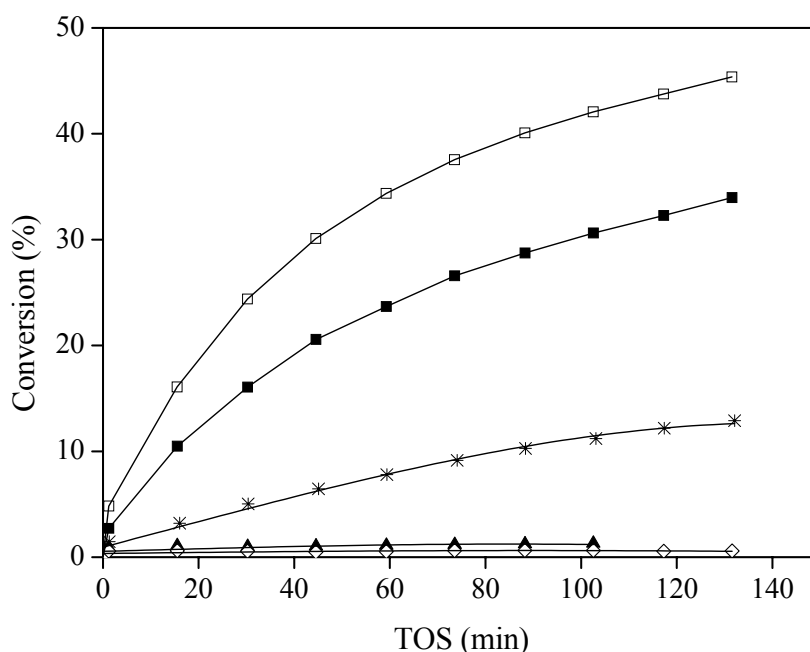


**Figure 4.18** Activity varied with time on stream (TOS) for *n*-butane hydrogenolysis catalyzed by PtRu/TiO<sub>2</sub> (◇) 200°C; (▲) 220°C; (\*) 240°C; (■) 260°C; and (□) 280°C.

For the first test, reaction was carried out at 200°C with  $P_{\text{H}_2} = 540$  Torr,  $P_{n\text{-C}_4\text{H}_{10}} = 60$  Torr with 100 ml (NTP)/min flow rate. It was found that catalytic activity was low and slightly increased with TOS and then reached steady-state. *n*-Butane hydrogenolysis is an endothermic reaction, thus activity increased with temperature as in Figure 4.18 in which reaction temperature was varied from 200 to 280°C. There was no sign of deactivation during 130 min TOS imply that aggregation of metal particles or coking may not occur during catalytic test at each temperature within 130 min.

The catalytic activities in term of TOF at 220°C of PtRu/TiO<sub>2</sub> catalyst was  $(1.3 \pm 0.1) \times 10^{-4}$  (s<sup>-1</sup>). Percent product distribution (selectivity) at this reaction

condition included 48% methane, 32% ethane, 3% propane and 17% *iso*-butane. The plot of selectivity as a function of reaction temperature in the range 200-280°C is shown in Figure 4.19

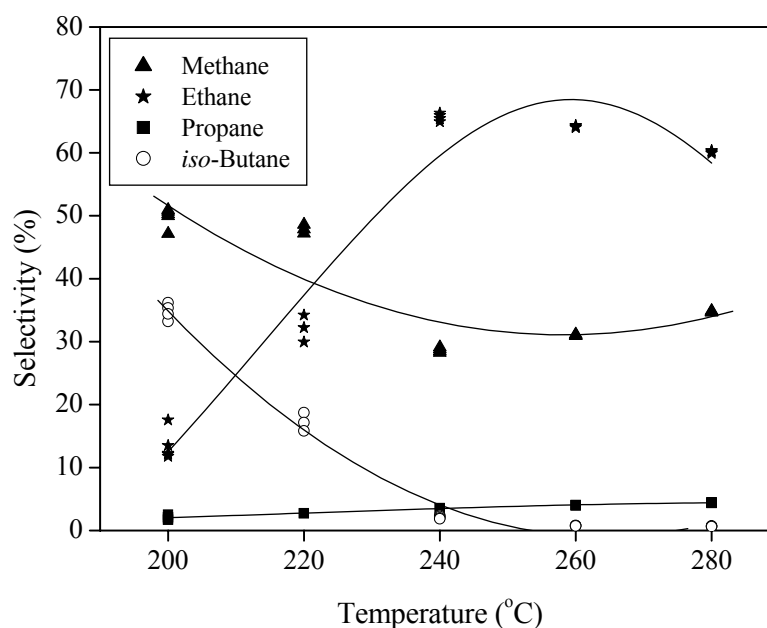


**Figure 4.19** Selectivity varied with various reaction temperature of *n*-butane hydrogenolysis catalyzed by PtRu/TiO<sub>2</sub>.

At reaction temperature range 200-220°C, selectivity of methane was around 50% and slightly decreased while selectivity of ethane increased about twice. In this temperature range, it was found that selectivity of *iso*-butane was about 35% at 200°C but decreased to 18% at 220°C and was less than 2% when reaction was carried out at temperature 240°C. In addition, at 240°C, selectivity of ethane was more than twice higher than that of methane as shown in Figure 4.19. When the reaction temperature was higher than 240°C, the ethane selectivity slightly decreased whereas selectivity of methane increased again but still much lower than that of ethane. Thus, reaction temperature at 240°C is the optimum condition to get highest ethane selectivity in

*n*-butane hydrogenolysis catalyzed by PtRu/TiO<sub>2</sub>. This temperature was higher than the optimum condition for highest ethane selectivity for *n*-butane hydrogenolysis catalyzed by PtRu/MgO and PtRu/γ-Al<sub>2</sub>O<sub>3</sub> were at 200 and 190°C, respectively.

#### 4.3.7.2 Apparent activation energy of *n*-butane hydrogenolysis catalyzed by PtRu/TiO<sub>2</sub>

The catalytic activities of *n*-butane hydrogenolysis catalyzed by PtRu/TiO<sub>2</sub> were collected at steady-state operation during temperature range 200-280°C. Reaction condition was as follow:  $P_{\text{H}_2} = 540$  Torr,  $P_{n\text{-C}_4\text{H}_{10}} = 60$  Torr with 100 ml (NTP)/min flow rate, 1.0 wt Pt and 1.0 wt% Ru metal loading. A plot of TOF in a natural log as a function of 1/T is shown in Figure 4.20.

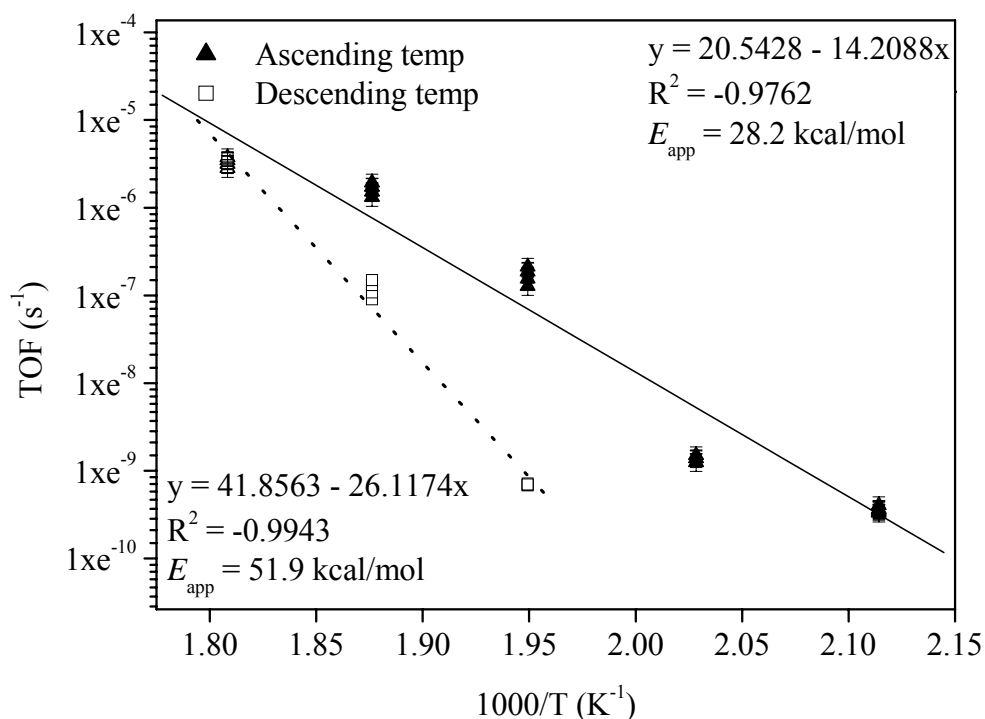


**Figure 4.20** Arrhenius plot of *n*-butane hydrogenolysis catalyzed by PtRu/TiO<sub>2</sub>.

The apparent activation energy obtained from a slope of linear ascending temperature graph from 200 to 280°C was  $28.2 \pm 0.1$  kcal/mol. The apparent activation energy of *n*-butane hydrogenolysis catalyzed by PtRu/TiO<sub>2</sub> was slightly less than that catalyzed by Pt on alumina at various reaction conditions (Bond and Cunningham, 1996; Leclercq et al., 1976; Passos et al., 1996). For example, the apparent activation energy of Pt/Al<sub>2</sub>O<sub>3</sub> was 30 kcal/mol at  $P_{n-C_4H_{10}} = 75$  Torr,  $P_{H_2} = 675$  Torr and temperature range 266 to 379°C (Leclercq et al.). Moreover, the apparent activation energy of *n*-butane hydrogenolysis catalyzed by PtRu/TiO<sub>2</sub> was lower than that of supported bimetallic PtRe/Al<sub>2</sub>O<sub>3</sub> which was 34.2 kcal/mol at temperature range 244-321°C, with hydrogen:ethylene ratio = 10:1 (Bond and Conningham, 1996).

In comparison with other supported PtRu catalysts prepared from adsorption of Pt<sub>3</sub>Ru<sub>6</sub>(CO)<sub>21</sub>(μ<sub>3</sub>-H)(μ-H)<sub>3</sub>, the apparent activation energy of *n*-butane hydrogenolysis over PtRu/TiO<sub>2</sub> was slightly lower than that over PtRu/γ-Al<sub>2</sub>O<sub>3</sub>,  $30.9 \pm 0.1$  kcal/mol but higher than that over PtRu/MgO,  $15.5 \pm 0.1$  kcal/mol.

Therefore, it can be concluded that PtRu/MgO catalyst was the most active catalyst for *n*-butane hydrogenolysis compared to PtRu/γ-Al<sub>2</sub>O<sub>3</sub> and PtRu/TiO<sub>2</sub>.

#### **4.3.7.3 Evidence of catalyst deactivation at high reaction temperature**

There was no sign of deactivation during the test period 130 min at each temperature from 200-280°C as in Figure 4.18. However, the apparent activation energy obtained from the Arrhenius plot in Figure 4.20 for descending temperature was 51.9 kcal/mol. This value was double value of that obtained from ascending

temperature. Therefore, deactivation occurred after performing reaction at higher temperature. Deactivation might be from coking or aggregation of metal particles on support.

#### 4.4 Conclusions

PtRu/TiO<sub>2</sub> catalyst with Pt-Ru bonds could be prepared successfully from adsorption of Pt<sub>3</sub>Ru<sub>6</sub>(CO)<sub>21</sub>(μ<sub>3</sub>-H)(μ-H)<sub>3</sub>. Characterization by IR and EXAFS spectroscopy indicated that Pt<sub>3</sub>Ru<sub>6</sub>(CO)<sub>21</sub>(μ<sub>3</sub>-H)(μ-H)<sub>3</sub> precursor did not adsorb intact on TiO<sub>2</sub> but still in the form of bimetallic carbonyl species and could not be completely extracted by CH<sub>2</sub>Cl<sub>2</sub> solvent. The decreasing in intensity of IR band in ν<sub>OH</sub> region implies that OH groups on support were involved in cluster-support interaction. Cluster precursor interacted with TiO<sub>2</sub> through interaction between oxygen of CO ligands and surface of support forming carbonates, carboxylate species. Moreover, partially decarbonylation was observed at Ru atoms upon adsorption. The EXAFS data representing M-O<sub>support</sub> indicated structural distortion of cluster cores and Pt-Ru contribution were partially broken during adsorption implying strong cluster-support interaction. Carbonyl ligands were completely removed from adsorbed precursor after treatment in He flow at 300°C for 2 h, and cluster cores remain on support. Interactions of Pt-Ru contributions with high dispersion after ligand removal were observed by EXAFS spectroscopy. The average coordination numbers of Pt-Ru and Ru-Pt contributions were 1.9 ± 0.1 and 0.1 ± 0.1, and coordination numbers of Pt-Pt and Ru-Ru contributions were found to be 1.8 ± 0.2 and 2.4 ± 0.1, respectively. The apparent activation energies of ethylene hydrogenation and *n*-butane hydrogenolysis catalyzed by PtRu/TiO<sub>2</sub> catalyst were 8.1 ± 0.1 and 28.2 ± 0.1

kcal/mol, respectively. Catalytic activity (TOF) of ethylene hydrogenation catalyzed by PtRu/TiO<sub>2</sub> at temperature -75°C was  $(48.6 \pm 4.5) \times 10^{-5} \text{ (s}^{-1}\text{)}$ . TOF of *n*-butane hydrogenolysis catalyzed by PtRu/TiO<sub>2</sub> at temperature 220°C was  $(1.4 \pm 0.1) \times 10^{-4} \text{ (s}^{-1}\text{)}$  and selectivity included 48% methane, 32% ethane, 3% propane and 17% *iso*-butane.

# CHAPTER V

## SUPPORTED Pt-Ru CATALYSTS PREPARED FROM A MIXTURE OF PLATINUM AND RUTHENIUM ACETYLACETONATE AND ACTIVITIES FOR ETHYLENE HYDROGENATION

### 5.1 Introduction

Supported bimetallic PtRu catalysts could be prepared from a mixture solution of metal salts by coprecipitation or coimpregnation, sequential impregnation, adsorption and redox surface reaction. Examples of conventional precursors are consisting of (a)  $\text{H}_2\text{PtCl}_6$  and  $\text{RuCl}_3$ , (b)  $\text{Pt}(\text{NH}_3)_4(\text{NO}_3)_2$  and  $\text{Ru}(\text{NH}_3)_6\text{Cl}_3$ , (c)  $\text{Pt}(\text{NO}_2)_2(\text{NH}_3)_2$  and  $\text{Ru}(\text{NO})(\text{NO}_3)_x$ , (d)  $\text{Pt}(\text{NH}_3)_4\text{Cl}_3$  and  $\text{Ru}(\text{NH}_3)_6\text{Cl}_3$ , and (e)  $\text{H}_2\text{PtCl}_6$  and  $\text{Ru}(\text{C}_5\text{H}_5)_2$  (Alerasool and Gonzalez, 1990; Diaz et al., 1995; Martins, Baldanza, and Schmal, 2001; Miura, Taguchi, Sugiyama, Matsuda, and Gonzalez, 1990; Rajesh, Thampi, Bonard, and Viswanathan, 2000; Takasu et al., 2001).

However, the conventional methods using mixture of Pt and Ru compounds especially a mixture chloride salts do not allow an ability to control particle size, structure, composition, and stoichiometry of bimetallic catalysts (Shirai et al., 1999). In addition, a high-temperature reduction causes nonuniform materials with large metal particles and broad particle size distribution.

### 5.1.1 Supported Pt and Ru catalysts prepared from acetylacetonate complexes

To avoid difficulties caused by conventional precursors and compare results with preparation from a molecular precursor in Chapter II-IV. Thus, supported PtRu catalysts were prepared from a mixture of organometallic precursors such as a mixture of  $\text{Pt}(\text{acac})_2$  and  $\text{Ru}(\text{acac})_3$  (acac is acetylacetonate,  $\text{C}_5\text{H}_7\text{O}_2^-$ ). Because acetylacetonato ligands can be completely removed at lower temperature than other ligands in metal salts, many transition metal acetylacetonate compounds has been used as precursors to prepared supported monometallic and bimetallic catalysts. However, there was not much reported on Pt-Ru catalyst (Bernas et al., 2004; Coq et al., 1994; Dossi et al., 2003; Plyuto, Babich, Sharanda, de Wit, and Mol, 1999; Renouprez, Trillat, Moraweck, Massardier, and Bergeret, 1998; Xu, Rheingold, and Gates, 1993; Walter, Coq, Figueras, and Boulet, 1995; Wang, Sigmon, Spivey, and Lamb, 2004).

For instance, bimetallic Pt-Pd/MgO catalyst could be prepared by impregnation of a mixture of  $\text{Pt}(\text{acac})_2$  and  $\text{Pd}(\text{acac})_2$  and the resulting catalyst had a tendency to form bimetallic particles as observed by temperature-programmed reductive decomposition (TPRD) (Dossi et al., 2003). In addition, Pd-Mn contributions on  $\text{SiO}_2$  prepared from impregnation of  $\text{Pd}(\text{acac})_2$  and  $\text{Mn}(\text{acac})_2$  mixture was studied by EXAFS spectroscopy containing 0.2-1.4 Pd-Mn coordination numbers. However, large values of Pd-Pd contributions were found due to high calcination and reduction temperature.

Therefore, it was expected that supported PtRu catalysts prepared from a mixture of  $\text{Pt}(\text{acac})_2$  and  $\text{Ru}(\text{acac})_3$  would give bimetallic particles on support with Pt-Ru connections and possibly high dispersion.

### 5.1.2 Research goals

The goal for this part of thesis was to prepare supported bimetallic PtRu catalysts on  $\gamma\text{-Al}_2\text{O}_3$  and MgO from a mixture solution of  $\text{Pt}(\text{acac})_2$  and  $\text{Ru}(\text{acac})_3$  in which acac ligands could be removed at mild condition, and test catalytic activity with ethylene hydrogenation reaction.

The interaction between precursors and metal oxide supports was characterized by IR spectroscopy. The reductive decomposition temperatures of supported  $\text{Pt}(\text{acac})_2$  and  $\text{Ru}(\text{acac})_3$  were investigated by TPRD technique, and changes in oxidation states during heating in  $\text{H}_2$  flow were observed by XANES spectroscopy. The metal-support interaction after ligand removal was studied as well. The average interatomic distance and coordination number of metals prepared from a mixture solution of  $\text{Pt}(\text{acac})_2$  and  $\text{Ru}(\text{acac})_3$  were studied by EXAFS spectroscopy. The results were used to compare with supported PtRu catalysts prepared from a molecular precursor,  $\text{Pt}_3\text{Ru}_6(\text{CO})_{21}(\mu_3\text{-H})(\mu\text{-H})_3$ .

## 5.2 Experimental

### 5.2.1 Chemicals and materials

The supported PtRu catalyst preparations and samples handling were performed with the same method as described in section 2.2.1 of Chapter II (page 18).

Pt(acac)<sub>2</sub> (Aldrich, 97%) and Ru(acac)<sub>3</sub> (Strem, 99%) were used as received. Prior to use,  $\gamma$ -Al<sub>2</sub>O<sub>3</sub> powder (Degussa, BET surface area 100 m<sup>2</sup>/g), and MgO (EM Science, 97%) were calcined with the procedure as described in Chapter II (page 18) and III (page 77), respectively.

## **5.2.2 Preparation of supported Pt-Ru catalysts from a mixture solution of Pt(acac)<sub>2</sub> and Ru(acac)<sub>3</sub>**

The supported Pt-Ru catalysts containing 1.0 wt% Pt and 1.0 wt% Ru on  $\gamma$ -Al<sub>2</sub>O<sub>3</sub> and MgO were prepared by adsorption of mixture of Pt(acac)<sub>2</sub> and Ru(acac)<sub>3</sub> in toluene over each support, slurring for 1 day, and evacuation for an additional 1 day.

## **5.2.3 PtRu catalyst activation**

Fresh sample after adsorption was heated in H<sub>2</sub> flow at 300°C for 2 h to remove ligands from adsorbed precursor and reduced metal particles.

## **5.2.4 Characterization techniques**

### **5.2.4.1 IR spectroscopy**

IR spectra of solid samples were recorded before and after activation in H<sub>2</sub> flow with a Bruker IFS-66v spectrometer with a resolution of 4 cm<sup>-1</sup>. Each sample was scanned 64 times and the signal were averaged. Details for sample preparation and measurement were mentioned in section 2.2.6.1 in Chapter II (page 22).

#### 5.2.4.2 Temperature-programmed reductive decomposition (TPRD)

Reductive decomposition of Pt and Ru in supported Pt-Ru catalyst prepared from a mixture of Pt(acac)<sub>2</sub> and Ru(acac)<sub>3</sub> in H<sub>2</sub> flow was determined by RXM-100 multifunctional catalyst testing and characterization instrument (Advanced Scientific Designs, Inc. (ASDI) with a vacuum capability of 10<sup>-8</sup> Torr. In a drybox, dry supported sample without treatment (250-300 mg) was loaded into a U-shape quartz tube. It was isolated from air and moisture before transferring to the temperature-programmed apparatus. Reactor was evacuated to around 10<sup>-8</sup> Torr and then Ar was flowed into reactor around 20 min. Gas mixture was then switch to 5 vol% H<sub>2</sub> in Ar and the temperature was ramped to 400°C with a rate of 10°C/min.

#### 5.2.4.3 XANES spectroscopy

XANES experiments were performed at the X-ray beamline X18B at the National Synchrotron Light Source (NSLS), Brookhaven National Laboratory (BNL), Upton, New York, USA. The storage ring energy was 2.5 GeV and the ring current was in the range 110-250 mA. In Ar glovebox at synchrotron, around 0.2 g of sample was loaded in the middle of a flow-through X-ray absorption (XAS) cell (Odzak et al., 2001). Glass wool plugs were used to hold sample in an XAS cell which then was isolated and moved to the beamline without contacting with air or moisture. XANES data of sample in the XAS cell which was approximated as isothermal plug-flow reactor, were collected in transmission mode in the presence of flowing of He or H<sub>2</sub> at individual Pt L<sub>III</sub> edge (11564 eV) and Ru K edge (22117 eV).

#### 5.2.4.4 EXAFS spectroscopy

EXAFS experiments were performed at the X-ray beamline X18B at the National Synchrotron Light Source (NSLS), Brookhaven National Laboratory (BNL), Upton, New York, USA. EXAFS instrument, sample preparation and measurement were described in section 2.2.6.3 of Chapter II (page 23).

#### 5.2.5 EXAFS data analysis

Details of EXAFS data analysis were in section 2.2.7 in Chapter II (page 23). Briefly, EXAFS data were collected at individual Pt L<sub>III</sub> (11564 eV) and Ru K (22117 eV) absorption edge and analyzed with theoretical reference files. The EXAFS data processing was carried out with ATHENA software (Raval, 2003). Phase shift and backscattering amplitudes of metal-metal and metal-surface oxygen interactions were calculated by FEFF7.0 software (Rehr et al., 1991). The EXAFS data fitting done by EXAFSPAK software (George et al., 2000) were accomplished with single and multiple scattering paths calculated by FEFF7.0, and the EXAFS parameters were extracted from the raw data with the EXAFSPAK software. The fitting were done in  $r$  space ( $r$  is interatomic distance from the absorber atom) and  $k$  space ( $k$  is the wave vector) with application of  $k^0$ ,  $k^1$ , and  $k^3$  weightings.

Raw EXAFS data of treated PtRu/ $\gamma$ -Al<sub>2</sub>O<sub>3</sub> in H<sub>2</sub> at 300°C, obtained at the Pt L<sub>III</sub> edge were Fourier transformed over the ranges  $3.60 < k < 14.30$  with  $k^3$  weighting without phase correction and  $0.0 < r < 5.0$  Å. The EXAFS data of treated PtRu/ $\gamma$ -Al<sub>2</sub>O<sub>3</sub> scanned at the Ru K edge were Fourier transformed over the ranges  $3.25 < k < 14.75$  without phase correction and  $0.0 < r < 5.0$  Å.

The EXAFS data of treated PtRu/ $\gamma$ -Al<sub>2</sub>O<sub>3</sub> obtained at the Pt L<sub>III</sub> and the Ru K edge were analyzed with a maximum of 16 free parameters. The statistically justified numbers of free parameters estimated from Nyquist theorem (Stern, 1993),  $n = (2\Delta k\Delta r/\pi) + 1$ , were about 35 and 30, for data obtained at Pt L<sub>III</sub> and the Ru K edge, respectively.

The EXAFS data of treated PtRu/MgO scanned at the Pt L<sub>III</sub> edge were Fourier transformed over the ranges  $3.55 < k < 14.50$  without phase correction and  $0.0 < r < 5.0$  Å. The EXAFS data of treated PtRu/MgO obtained at the Ru K edge were analyzed over the ranges  $3.20 < k < 14.50$  without phase correction and  $0.0 < r < 5.0$  Å.

The raw data of treated PtRu/MgO obtained at the Pt L<sub>III</sub> and the Ru K edge were analyzed with a maximum of 16 free parameters. The statistically justified numbers of free parameters estimated from Nyquist theorem were about 36 and 37, for data obtained at the Pt L<sub>III</sub> and the Ru K edge, respectively.

### **5.2.6 Catalytic activity of ethylene hydrogenation of supported PtRu catalysts prepared from a mixture of Pt(acac)<sub>2</sub> and Ru(acac)<sub>3</sub>**

Ethylene hydrogenation reaction was carried out with the same procedure described in section 2.2.8 of Chapter II (page 24). Briefly, catalyst sample was pretreated in H<sub>2</sub> flow at 300°C for 2 h, diluted with inert  $\alpha$ -Al<sub>2</sub>O<sub>3</sub>, and loaded into the reactor and cooled to desired temperature under He flow before a gas mixture containing H<sub>2</sub>, C<sub>2</sub>H<sub>4</sub> and balance He was flowed into the reactor. The reaction condition was as follow:  $P_{\text{C}_2\text{H}_4} = 40$  Torr,  $P_{\text{H}_2} = 200$  Torr, balanced with He, total feed flow rate = 100 ml (NTP)/min, 1.0 wt% Pt and 1.0 wt% Ru catalyst, and temperature

= -50 to -9°C. The effluent gas mixture was analyzed with an online gas chromatograph (Hewlett-Packard HP 6890) equipped with an Al<sub>2</sub>O<sub>3</sub> capillary column (50 m x 0.53 mm x 15.0 micron film thickness), and a flame ionization detector (FID).

## 5.3 Results and discussion

### 5.3.1 IR evidence of interaction between precursors and support after adsorption

#### 5.3.1.1 PtRu/ $\gamma$ -Al<sub>2</sub>O<sub>3</sub> catalyst prepared from a mixture of Pt(acac)<sub>2</sub> and Ru(acac)<sub>3</sub>

Figure 5.1 shows the IR spectra of sample prepared from deposition of a mixture solution of Pt(acac)<sub>2</sub> and Ru(acac)<sub>3</sub> in toluene onto  $\gamma$ -Al<sub>2</sub>O<sub>3</sub> and dried by evacuation.

Calcined  $\gamma$ -Al<sub>2</sub>O<sub>3</sub> showed IR band in  $\nu_{\text{OH}}$  region at 3786 (w), 3728 (w), 3666 (w) and 3569 (w, sh) cm<sup>-1</sup> (spectrum 1 in Figure 5.1). The first three peaks were assigned to different types of isolated hydroxyl groups (Shelef and Graham, 1994). The broad peak at 3569 cm<sup>-1</sup> represents hydrogen-bonded OH groups.

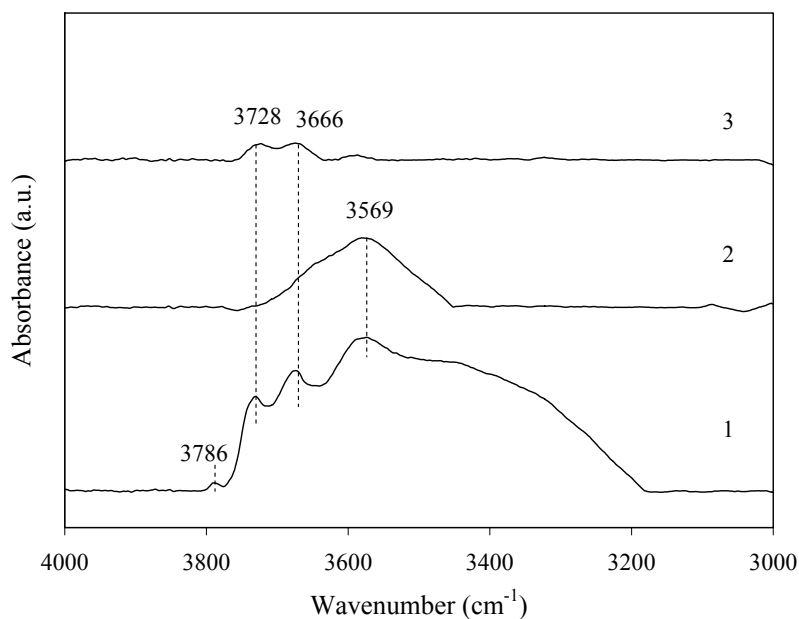


**Figure 5.1** IR spectra in  $\nu_{\text{OH}}$  region of (1) calcined  $\gamma\text{-Al}_2\text{O}_3$ ; (2) dry supported  $\text{Pt}(\text{acac})_2$  and  $\text{Ru}(\text{acac})_3$  on  $\gamma\text{-Al}_2\text{O}_3$ ; (3)  $\text{PtRu}/\gamma\text{-Al}_2\text{O}_3$  after treated in  $\text{H}_2$  flow at  $300^\circ\text{C}$  for 2 h.

After  $\gamma\text{-Al}_2\text{O}_3$  was adsorbed with a mixture of  $\text{Pt}(\text{acac})_2$  and  $\text{Ru}(\text{acac})_3$  in toluene and dried by evacuation, its intensity of isolated hydroxyl groups at  $3728$  and  $3666\text{ cm}^{-1}$  (spectrum 2 in Figure 5.1) significantly decreased indicating that hydroxyl groups involved in precursor-support interaction. In addition, IR band at  $3569\text{ cm}^{-1}$  representing hydrogen bonds was observed clearly after adsorption implies that the interaction between precursor and surface of support was hydrogen bonding.

The dry supported sample shows IR peaks in  $\nu_{\text{C-C}}$  and  $\nu_{\text{C-H}}$  regions at  $1601$  (w),  $1522$  (s),  $1425$  (w),  $1383$  (m) and  $1267$  (sh)  $\text{cm}^{-1}$  (spectrum 3 in Figure 5.2). The peak at  $1383\text{ cm}^{-1}$  overlapped with that of support. These peaks were assigned to acetylacetonate ligands (SADTLER Research Laboratories, 1965; The Coblentz Society, 1970).

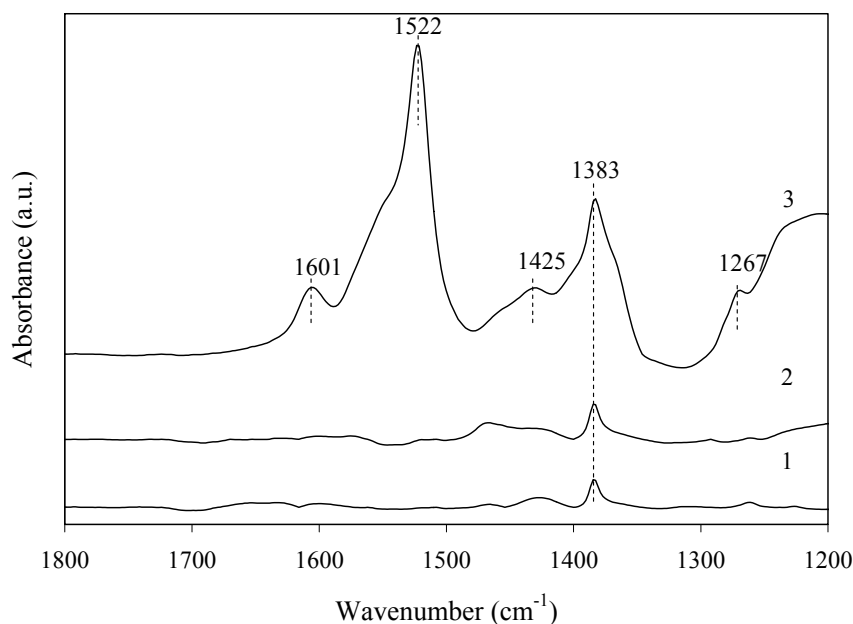


**Figure 5.2** IR spectra in  $\nu_{C-C}$  and  $\nu_{C-H}$  regions of (1) calcined  $\gamma\text{-Al}_2\text{O}_3$ ; (2) PtRu/ $\gamma\text{-Al}_2\text{O}_3$  after treated in  $\text{H}_2$  flow at  $300^\circ\text{C}$  for 2 h; (3) dry supported Pt(acac) $_2$  and Ru(acac) $_3$  on  $\gamma\text{-Al}_2\text{O}_3$ .

Moreover, the adsorption of metal acetylacetonate precursors could also occur through ligand-exchange mechanism forming isolated, covalent bonded species and loss of one or more acetylacetonate ligand (Baltes et al., 1999). However, adsorption interaction could also occur through acetylacetonate ligand and surface of support without loss of any acetylacetonate ligands (Kenvin and White, 1991).

Many researchers used EXAFS to characterized the neighbor atoms of Pt in supported Pt sample prepared from Pt(acac) $_2$  (Fiddy, Newton, and Dent et al., 1999; Fiddy, Newton, and Campbell et al., 1999; Womes et al., 2003). They found coordination number of Pt-O at approximately 4, the same as untreated supported Pt sample implying that Pt(acac) $_2$  adsorbed intact on support.

Moreover, Plyuto et al. (1999) found by thermal study that Ru(acac)<sub>3</sub> adsorbed on Al<sub>2</sub>O<sub>3</sub> without elimination of acetylacetonate ligand.

Consequently, the interaction between metal acetylacetonate precursors and surface of  $\gamma$ -Al<sub>2</sub>O<sub>3</sub> in this work was from hydrogen bonding between acetylacetonate ligands and surface hydroxyl groups on support (OH<sub>(s)</sub>). The adsorption process of M<sup>n+</sup>(acac)<sub>n</sub> on  $\gamma$ -Al<sub>2</sub>O<sub>3</sub> would be explained with the following equation



It was possible that ligand-exchanged mechanism could be confirmed by EXAFS spectroscopy to observed Pt-O coordination number further.

Acetylacetonate ligands were completely removed after treated in H<sub>2</sub> flow at 300°C for 2 h as shown in spectrum 2 (Figures 5.1 and 5.2). The acetylacetonate ligand could be eliminated from adsorbed precursors in the form of acetylacetone, or decomposed into isopropanol and acetone (Kenvin and White, 1991; Dossi et al., 2003).

### **5.3.1.2 PtRu/MgO catalyst prepared from a mixture of Pt(acac)<sub>2</sub> and Ru(acac)<sub>3</sub>**

Partially dehydroxylated MgO obtained from calcination in O<sub>2</sub> flow at 300°C gave characteristic IR peak at 3764 cm<sup>-1</sup> (spectrum 3 in Figure 5.3) indicating isolated hydroxyl groups on MgO (Alexeev, Shelef et al., 1996).

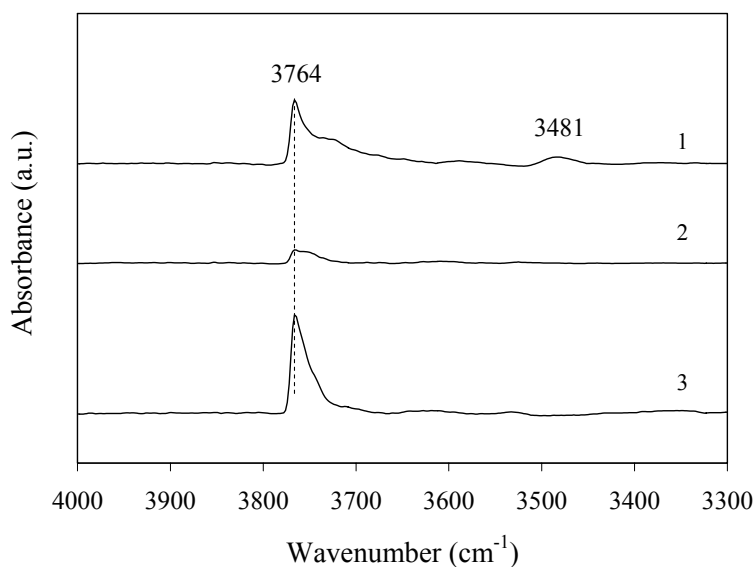


**Figure 5.3** IR spectra in  $\nu_{\text{OH}}$  region of (1) dry supported  $\text{Pt}(\text{acac})_2$  and  $\text{Ru}(\text{acac})_3$  on MgO; (2) PtRu/MgO after ligand removal in  $\text{H}_2$  flow at  $300^\circ\text{C}$  for 2 h; (3) calcined MgO.

After adsorption of a mixture of  $\text{Pt}(\text{acac})_2$  and  $\text{Ru}(\text{acac})_3$  from toluene onto MgO and dry by evacuation, the intensity of isolated hydroxyl groups at  $3764$  ( $\text{vs}$ )  $\text{cm}^{-1}$  decreased indicating that they involved in precursor-support interactions. IR broad band of hydrogen-bonded hydroxyl groups at  $3481$   $\text{cm}^{-1}$  also observed on this sample imply that the interaction between metal acetylacetonate precursors and MgO was hydrogen bonding.

The IR spectrum in  $\nu_{\text{C-C}}$  and  $\nu_{\text{C-H}}$  regions of dry sample after adsorption was shown in spectrum 1 (Figure 5.4).

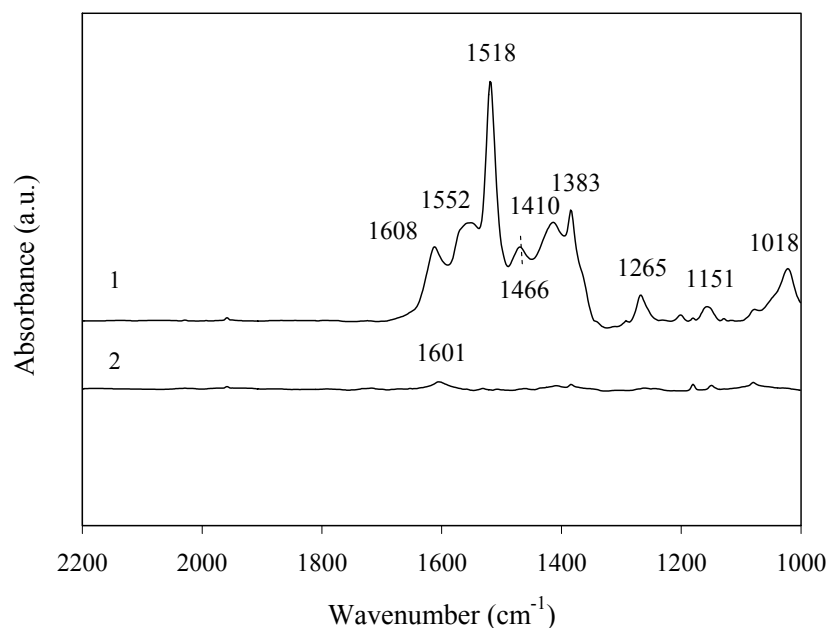


**Figure 5.4** IR spectra  $\nu_{C-C}$  and  $\nu_{C-H}$  regions of (1) dry supported  $Pt(acac)_2$  and  $Ru(acac)_3$  on MgO; (2) PtRu/MgO after ligand removal in  $H_2$  flow at  $300^\circ C$  for 2 h.

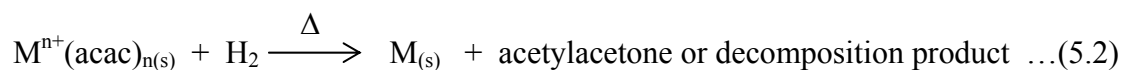
The IR peaks of dry supported sample occurred at 1608 (m), 1552 (sh), 1518 (s), 1466 (sh), 1410 (w), 1383 (m), 1151 (w) and 1018 (m)  $cm^{-1}$  were assigned to acetylacetonate ligands (SADTLER Research Laboratories, 1965; The Coblenz Society, 1970).

Therefore, the interaction between metal acetylacetonate precursors and MgO surface occurred through hydrogen bonding as described by equation 5.1.

Acetylacetonate ligands were completely removed after  $H_2$  flow at  $300^\circ C$  for 2 h as the peaks disappeared in spectrum 2 (Figures 5.3 and 5.4). The acetylacetonate ligand would be eliminated from adsorbed precursors in the form of acetylacetone, or decomposed into isopropanol and acetone (Kenvin and White, 1991; Dossi et al., 2003).

### 5.3.2 TPRD of supported PtRu samples

Temperature-programmed reductive decomposition (TPRD) (Dossi et al., 2003) was used to study reductive decomposition temperature of Pt(acac)<sub>2</sub> and Ru(acac)<sub>3</sub> to form Pt and Ru particles supported on  $\gamma$ -Al<sub>2</sub>O<sub>3</sub> and MgO after deposition of Pt(acac)<sub>2</sub> and/or Ru(acac)<sub>3</sub> as described in equation 5.2 where M was transition metal and decomposition product could be isopropanol and acetone or methane (Dossi et al., 2003).



#### 5.3.2.1 TPRD of Pt(acac)<sub>2</sub> and/or Ru(acac)<sub>3</sub> supported on $\gamma$ -Al<sub>2</sub>O<sub>3</sub>

After  $\gamma$ -Al<sub>2</sub>O<sub>3</sub> was adsorbed with a mixture of Pt(acac)<sub>2</sub> and Ru(acac)<sub>3</sub> in toluene and dried by evacuation, it was studied reduction temperature by TPRD technique. TPRD profiles of sample after adsorption with Pt(acac)<sub>2</sub> and/or Ru(acac)<sub>3</sub> are shown in Figure 5.5.

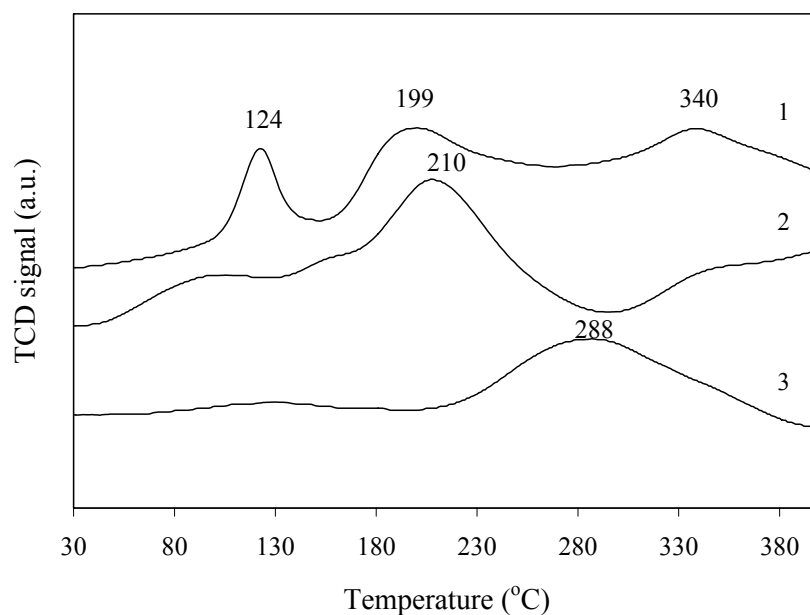


**Figure 5.5** TPRD profiles of (1) Pt(acac)<sub>2</sub> and Ru(acac)<sub>3</sub> adsorbed on  $\gamma$ -Al<sub>2</sub>O<sub>3</sub>; (2) Pt(acac)<sub>2</sub> adsorbed on  $\gamma$ -Al<sub>2</sub>O<sub>3</sub>; (3) Ru(acac)<sub>3</sub> adsorbed on  $\gamma$ -Al<sub>2</sub>O<sub>3</sub>.

TPRD profiles of Pt in Pt(acac)<sub>2</sub> precursor supported on  $\gamma$ -Al<sub>2</sub>O<sub>3</sub> was observed at 210°C whereas that of Pt in mixture precursors supported on  $\gamma$ -Al<sub>2</sub>O<sub>3</sub> decreased to 124 and 199°C indicating that supported Pt(acac)<sub>2</sub> had many decomposition steps on  $\gamma$ -Al<sub>2</sub>O<sub>3</sub>. Reductive decomposition temperature of Ru in mixture of Pt(acac)<sub>2</sub> and Ru(acac)<sub>3</sub> precursors supported on  $\gamma$ -Al<sub>2</sub>O<sub>3</sub> was found at 340°C while that of Ru in Ru(acac)<sub>3</sub> on  $\gamma$ -Al<sub>2</sub>O<sub>3</sub> was observed at 288°C. It was likely that Pt and Ru did not contact with each other due to increasing of reductive decomposition temperature of Ru particles compared to supported Ru(acac)<sub>3</sub>. Because of more hydrogen adsorption on Pt than Ru, hydrogen probably first adsorbed on Pt surface and the reductive decomposition occurred followed by the reductive decomposition of Ru complex.

Dry supported PtRu sample after treated in H<sub>2</sub> flow at 300°C for 2 h was also tested with TPRD apparatus. There was no H<sub>2</sub> consumption in temperature range from

room temperature to 400°C indicating that Pt and Ru particles were completely reduced at 300°C in H<sub>2</sub> flow during 2 h.

### 5.3.2.2 TPRD of Pt(acac)<sub>2</sub> and/or Ru(acac)<sub>3</sub> supported on MgO

Supported PtRu on MgO prepared from a mixture of Pt(acac)<sub>2</sub> and/or Ru(acac)<sub>3</sub> were studied by TPRD technique. Details of sample preparation and apparatus were the same as TPRD study in section 5.3.2.1. The TPRD profiles of bare MgO and dry supported sample prepared from Pt(acac)<sub>2</sub> and/or Ru(acac)<sub>3</sub> are shown in Figure 5.6.

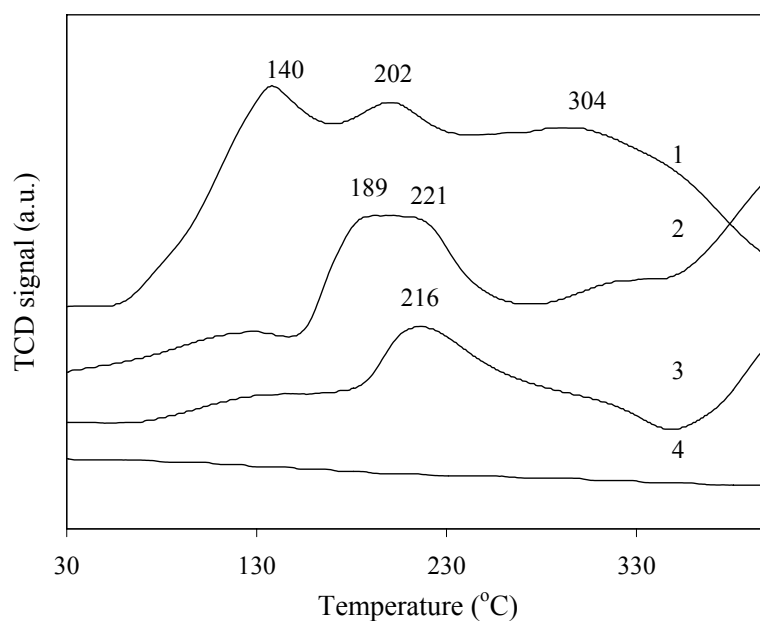


**Figure 5.6** TPRD profiles of (1) Pt(acac)<sub>2</sub> adsorbed on MgO; (2) Pt(acac)<sub>2</sub> and Ru(acac)<sub>3</sub> adsorbed on MgO; (3) Ru(acac)<sub>3</sub> adsorbed on MgO; (4) calcined MgO.

Calcined MgO was tested by TPRD technique as shown in profile 4 (Figure 5.6). As expected, the reduction of MgO support did not occur during TPRD test from

room temperature to 400°C. It was found that reductive decomposition temperatures of Pt(acac)<sub>2</sub> on MgO were observed at 140, 202 and broad TPRD profile at 304°C indicating that supported Pt(acac)<sub>2</sub> had many decomposition steps on MgO. On the other hand, Ru(acac)<sub>3</sub> supported on MgO showed reductive decomposition temperature at 216°C indicating that one step decomposition of supported Ru(acac)<sub>3</sub> on MgO. For supported PtRu sample, reductive decomposition temperatures of Pt and Ru particles were shown in TPRD profile 2 (Figure 5.6). Broad H<sub>2</sub> consumption was observed at 189-221°C indicating that Pt and Ru might contact to each other on MgO or change in oxidation states.

TPRD products probably consisted of acetone and methane as reported by Dossi et al. (2003) on a different system. They prepared supported PtPd/MgO from Pt(acac)<sub>2</sub> and Pd(acac)<sub>2</sub> mixture by chemical vapor deposition and found that acetone fragments were observed by TPRD during TPRD test at 100-300°C, and methane was a main product at above 300°C. The mechanism of reductive decomposition was expected to be complicate and was not investigated further because it was outside the scope of this thesis.

### **5.3.3 XANES spectra of dry supported Pt(acac)<sub>2</sub> and Ru(acac)<sub>3</sub> on $\gamma$ -Al<sub>2</sub>O<sub>3</sub>**

X-ray absorption technique such as X-ray absorption near edge structure (XANES) spectroscopy was used to study changes of oxidation state of Pt and Ru during treatment in H<sub>2</sub> flow. After dry supported sample was loaded in to XAS cell, the XANES spectra were collected at each Pt L<sub>III</sub> (11564 eV) and Ru K (22117 eV)

edge during heating from room temperature to 100°C under H<sub>2</sub> flow. XANES spectra were shown in Figure 5.7.

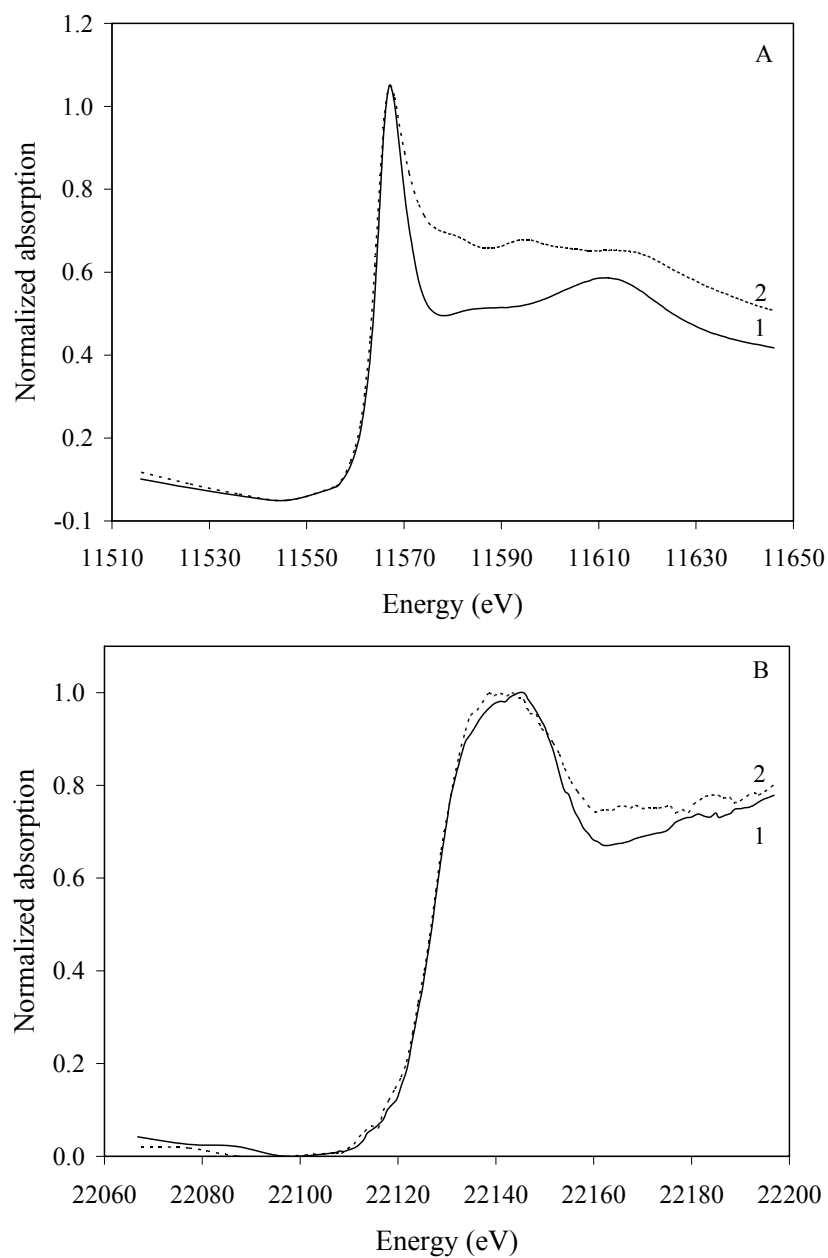


**Figure 5.7** XANES spectra of Pt(acac)<sub>2</sub> and Ru(acac)<sub>3</sub> supported on  $\gamma$ -Al<sub>2</sub>O<sub>3</sub> during H<sub>2</sub> flow from room temperature to 100°C. (A) Scanned at the Pt L<sub>III</sub> edge; (B) the Ru K edge at temperature (1) 25°C and (2) 100°C.

During a treatment in H<sub>2</sub> flow from room temperature to 100°C, XANES data showed that Pt and Ru particles were reduced due to decreasing in white line area while the absorption edge did not change significantly (Figures 5.7A and 5.7B). For XANES at the Pt L<sub>III</sub> edge, Pt atoms showed more decrease of white line area than that of Ru atom in Figure 5.17B. It was suggested that Pt atom was reduced at lower temperature than Ru atoms.

The XANES data agreed with TPRD results that Pt particle was reduced at lower temperature than Ru particle.

In contrast, Wang et al. (2004) found by XANES spectra of supported Pt/MgO prepared from Pt(acac)<sub>2</sub> after reduction by H<sub>2</sub> at 300°C that the Pt L<sub>III</sub> white line area was larger than that of Pt foil indicating that Pt was not completely reduced.

### 5.3.4 EXAFS spectroscopy results

#### 5.3.4.1 EXAFS evidence for PtRu/ $\gamma$ -Al<sub>2</sub>O<sub>3</sub> catalyst prepared from a mixture of Pt(acac)<sub>2</sub> and Ru(acac)<sub>3</sub>

Supported PtRu sample prepared from adsorption of a mixture of Pt(acac)<sub>2</sub> and Ru(acac)<sub>3</sub> from toluene onto  $\gamma$ -Al<sub>2</sub>O<sub>3</sub>, was treated in H<sub>2</sub> flow at 300°C for 2 h to remove acetylacetonato ligands and reduce metals. The interactions of metal-metal and metal-surface oxygen of treated PtRu sample were investigated by EXAFS spectroscopy. The EXAFS fitting parameters of treated PtRu/ $\gamma$ -Al<sub>2</sub>O<sub>3</sub> sample were summarized in Table 5.2. The EXAFS fitting results in The EXAFS fitting results in  $k$  and  $r$  space with  $k^0$ ,  $k^1$  and  $k^3$  weighted are shown in Figures 5.8 and 5.9.

**Table 5.1** Summary of EXAFS data of PtRu/ $\gamma$ -Al<sub>2</sub>O<sub>3</sub> prepared from a mixture of Pt(acac)<sub>2</sub> and Ru(acac)<sub>3</sub> after ligand removal in H<sub>2</sub> flow at 300°C for 2 h

Edge	Shell	$N$	$R$ (Å)	$10^3 \times \Delta\sigma^2$ (Å <sup>2</sup> )	$\Delta E_0$ (eV)
Pt L <sub>III</sub>	Pt-Pt	$2.8 \pm 0.1$	$2.77 \pm 0.01$	$1.1 \pm 0.3$	$7.7 \pm 0.4$
	Pt-Ru	-	-	-	-
	Pt-O <sub>support</sub>				
	Pt-O <sub>s</sub>	$3.4 \pm 0.1$	$2.50 \pm 0.01$	$0.8 \pm 0.5$	$-5.8 \pm 0.3$
	Pt-O <sub>l</sub>	$1.3 \pm 0.1$	$2.95 \pm 0.01$	$-4.5 \pm 1.0$	$8.7 \pm 0.6$
Ru K	Ru-Ru	$3.3 \pm 0.1$	$2.65 \pm 0.01$	$3.9 \pm 0.3$	$-7.3 \pm 0.2$
	Ru-Pt	-	-	-	-
	Ru-O <sub>support</sub>				
	Ru-O <sub>s</sub>	$1.7 \pm 0.1$	$1.98 \pm 0.01$	$14.0 \pm 1.1$	$-3.7 \pm 0.5$
	Ru-O <sub>l</sub>	$0.7 \pm 0.1$	$2.20 \pm 0.01$	$6.5 \pm 2.6$	$-0.8 \pm 0.8$

Notation: subscript s and l refer to short and long, respectively.

The estimated accuracies of coordination number ( $N$ ), distance ( $R$ ), Debye-Waller factor ( $\Delta\sigma^2$ ), and inner potential correction ( $\Delta E_0$ ) are as follows:  $\pm 20\%$ ,  $\pm 1\%$ ,  $\pm 30\%$ , and  $\pm 10\%$ , respectively. Here Pt has higher Pt-O<sub>s</sub> coordination number than that prepared from Pt<sub>3</sub>Ru<sub>6</sub>(CO)<sub>21</sub>( $\mu_3$ -H)( $\mu$ -H)<sub>3</sub>. In contrast, Ru has lower Ru-O<sub>s</sub> coordination number compare to that prepared from Pt<sub>3</sub>Ru<sub>6</sub>(CO)<sub>21</sub>( $\mu_3$ -H)( $\mu$ -H)<sub>3</sub>. In addition, coordination number of Pt-O<sub>s</sub> was higher than that of Ru-O<sub>s</sub>. This trend was opposite to the PtRu/ $\gamma$ -Al<sub>2</sub>O<sub>3</sub> prepared from Pt<sub>3</sub>Ru<sub>6</sub>(CO)<sub>21</sub>( $\mu_3$ -H)( $\mu$ -H)<sub>3</sub>.

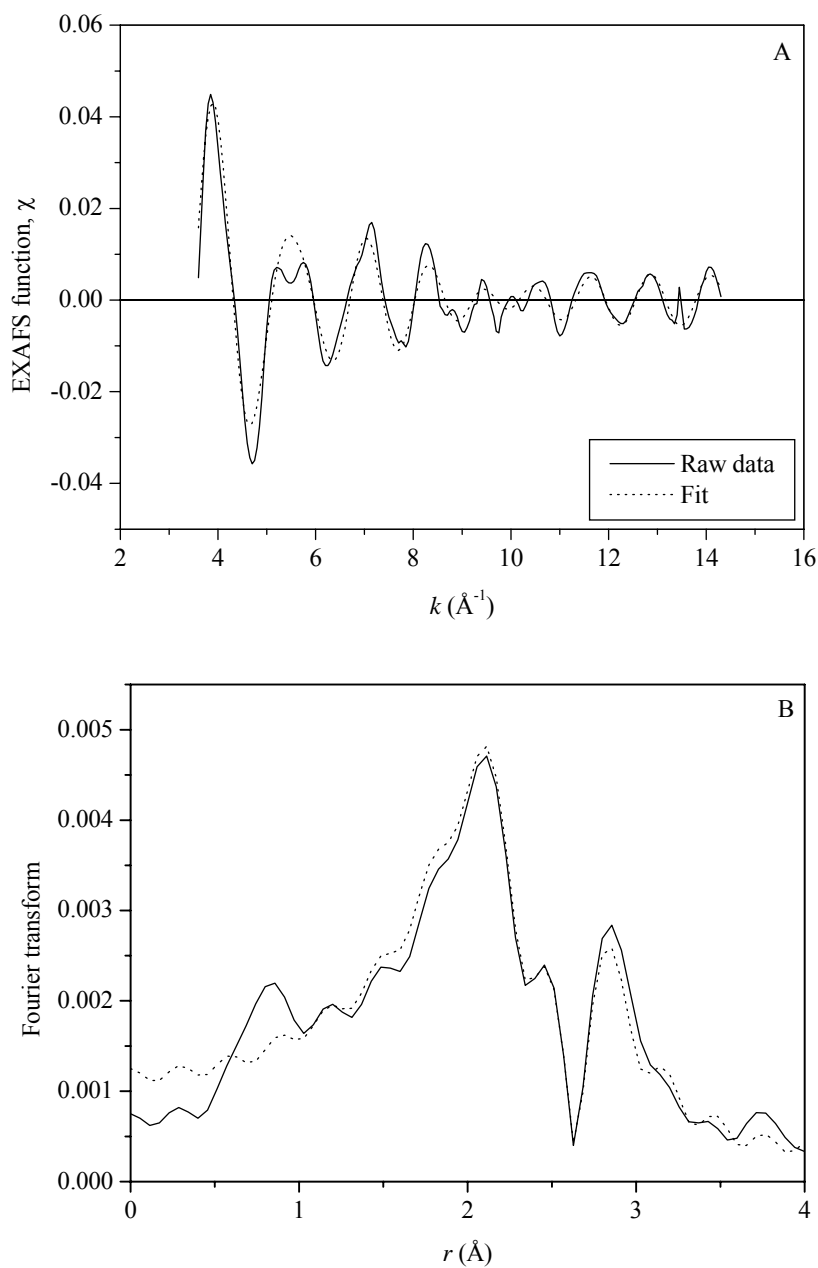


**Figure 5.8** EXAFS results scanned at the Pt  $L_{III}$  edge characterizing the PtRu/ $\gamma$ - $\text{Al}_2\text{O}_3$  sample prepared by adsorption of a mixture of  $\text{Pt}(\text{acac})_2$  and  $\text{Ru}(\text{acac})_3$  after ligand removal in  $\text{H}_2$  flow at  $300^\circ\text{C}$ : (A) Experimental EXAFS function (solid line) and sum of the calculated Pt-Pt, Pt- $\text{O}_s$ , and Pt- $\text{O}_l$  contributions (dotted line). (B) Magnitude of uncorrected Fourier transform ( $k^0$  weighted) of experimental EXAFS function (solid line) and sum of the calculated Pt-Pt, Pt- $\text{O}_s$ , and Pt- $\text{O}_l$  contributions (dotted line).

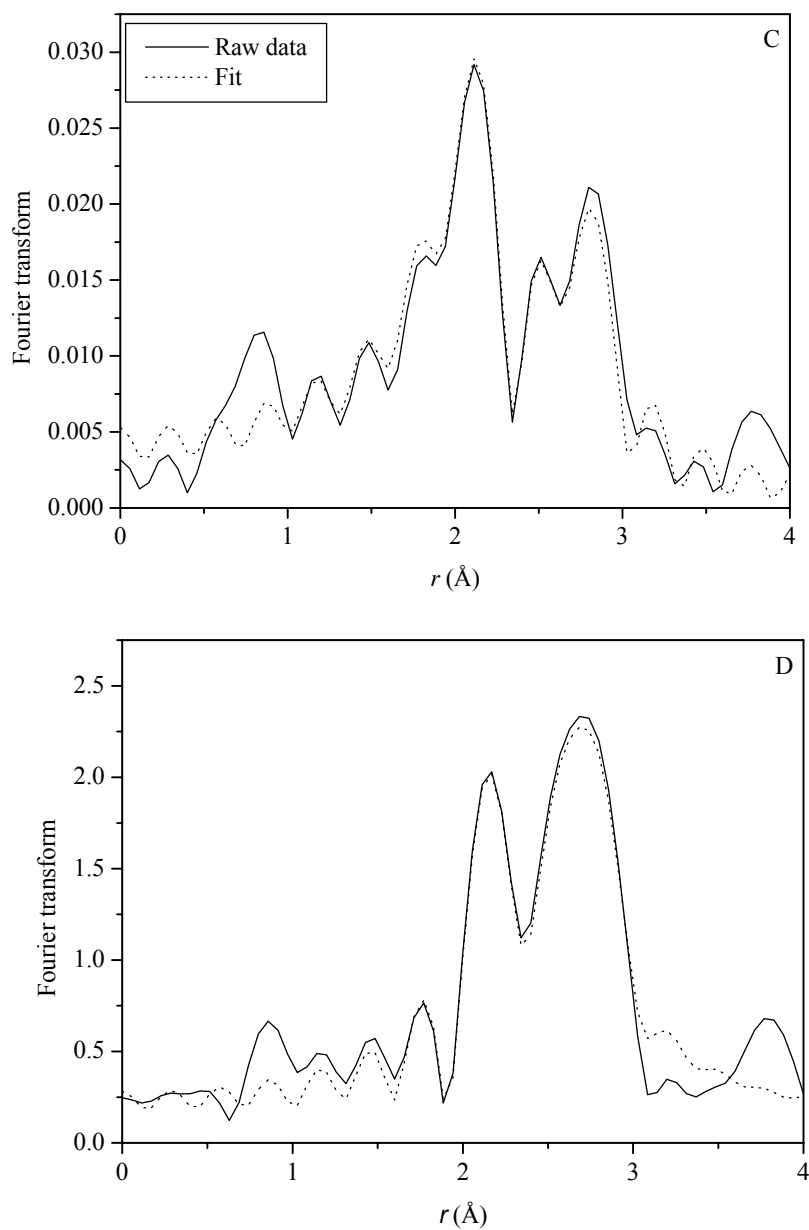


**Figure 5.8** (continued) EXAFS results scanned at the Pt L<sub>III</sub> edge characterizing the PtRu/ $\gamma$ -Al<sub>2</sub>O<sub>3</sub> sample prepared by adsorption of a mixture of Pt(acac)<sub>2</sub> and Ru(acac)<sub>3</sub> after ligand removal in H<sub>2</sub> flow at 300°C: (C) Magnitude of uncorrected Fourier transform ( $k^1$  weighted) of experimental EXAFS function (solid line) and sum of the calculated Pt-Pt, Pt-O<sub>s</sub>, and Pt-O<sub>l</sub> contributions (dotted line). (D) Magnitude of uncorrected Fourier transform ( $k^3$  weighted) of experimental EXAFS function (solid line) and sum of the calculated Pt-Pt, Pt-O<sub>s</sub>, and Pt-O<sub>l</sub> contributions (dotted line).

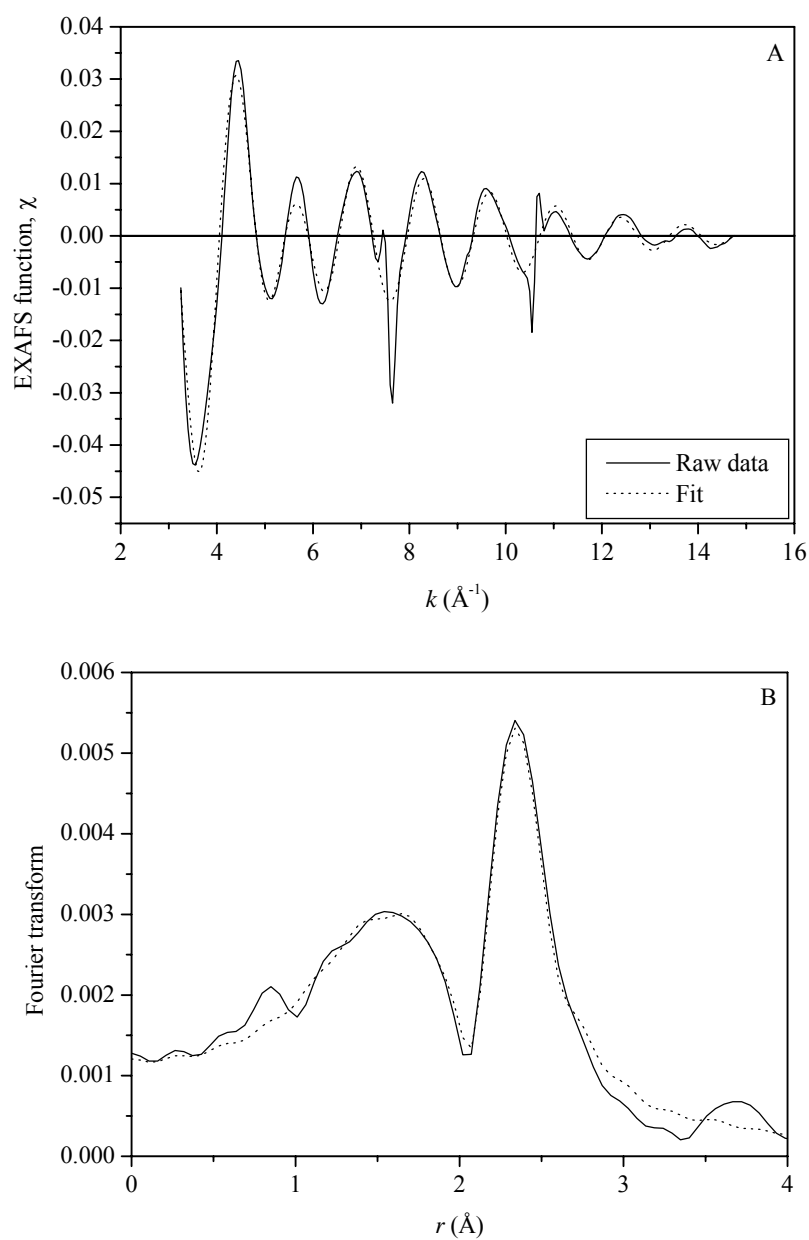


**Figure 5.9** EXAFS results scanned at the Ru K edge characterizing the PtRu/ $\gamma$ -Al<sub>2</sub>O<sub>3</sub> sample prepared by adsorption of a mixture of Pt(acac)<sub>2</sub> and Ru(acac)<sub>3</sub> after ligand removal in H<sub>2</sub> flow at 300°C: (A) Experimental EXAFS function (solid line) and sum of the calculated Pt-Pt, Pt-O<sub>s</sub>, and Pt-O<sub>l</sub> contributions (dotted line). (B) Magnitude of uncorrected Fourier transform ( $k^0$  weighted) of experimental EXAFS function (solid line) and sum of the calculated Pt-Pt, Pt-O<sub>s</sub>, and Pt-O<sub>l</sub> contributions (dotted line).

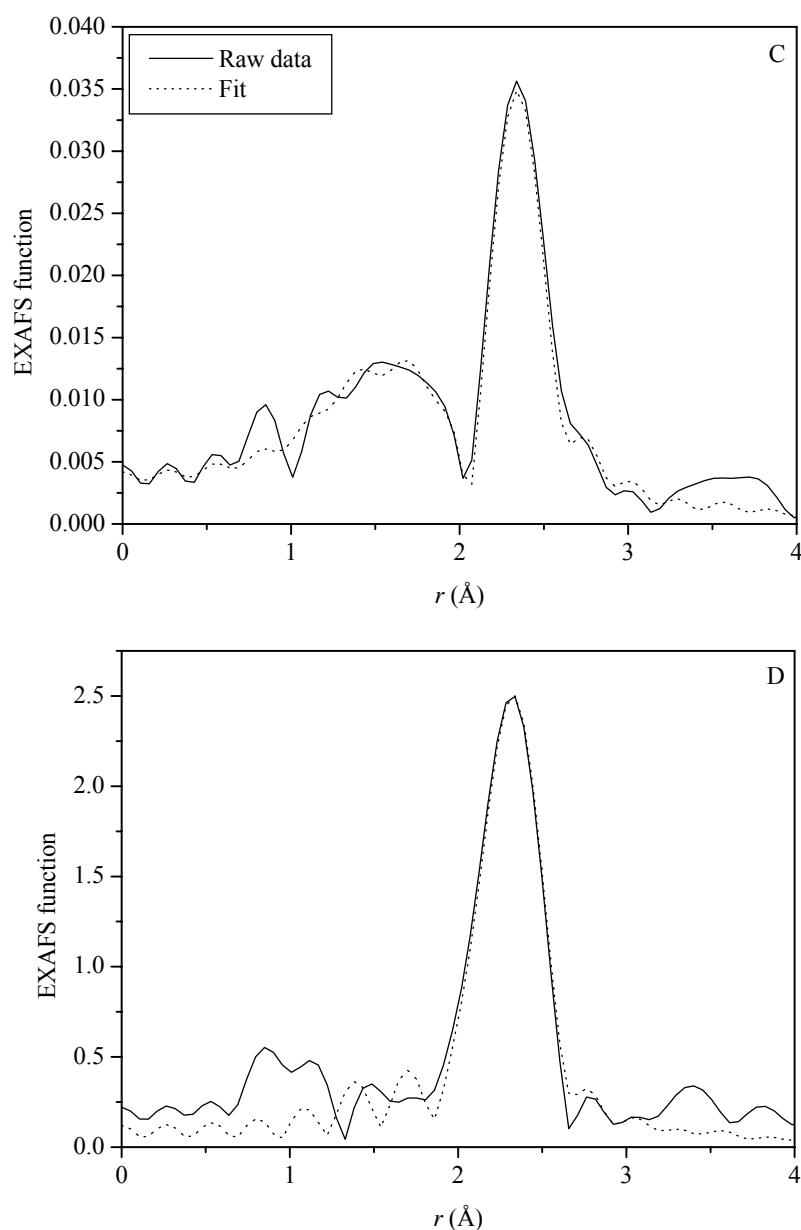


**Figure 5.9** (continued) EXAFS results scanned at the Ru K edge characterizing the PtRu/ $\gamma$ -Al<sub>2</sub>O<sub>3</sub> sample prepared by adsorption of a mixture of Pt(acac)<sub>2</sub> and Ru(acac)<sub>3</sub> after ligand removal in H<sub>2</sub> flow at 300°C: (C) Magnitude of uncorrected Fourier transform ( $k^1$  weighted) of experimental EXAFS function (solid line) and sum of the calculated Pt-Pt, Pt-O<sub>s</sub>, and Pt-O<sub>l</sub> contributions (dotted line). (D) Magnitude of uncorrected Fourier transform ( $k^3$  weighted) of experimental EXAFS function (solid line) and sum of the calculated Pt-Pt, Pt-O<sub>s</sub>, and Pt-O<sub>l</sub> contributions (dotted line).

After treatment in H<sub>2</sub> at 300°C for 2 h, the EXAFS data in Table 5.1 show that the average Pt-Pt coordination number was  $2.8 \pm 0.1$  and that of Ru-Ru was  $3.3 \pm 0.1$ . Pt-Ru and Ru-Pt contributions did not observed on  $\gamma$ -Al<sub>2</sub>O<sub>3</sub> support indicating that Pt and Ru did not contact each other upon treatment in H<sub>2</sub> at 300°C for 2 h. Interaction of Pt-Pt was observed at average bond distance  $2.77 \pm 0.01$  Å with coordination number  $2.8 \pm 0.1$  as shown in Table 5.1.

However, larger coordination numbers of Pt in of Pt/H<sub>1</sub> SiO<sub>2</sub> prepared from Pt(acac)<sub>2</sub> during reduction in H<sub>2</sub> (around 300°C) were observed by *in situ* energy dispersive EXAFS (EDE) (Fiddy, Newton, Dent et al., 1999; Fiddy, Newton, Campbell et al., 1999). The coordination number of Pt-Pt contribution increased to approximately 6 at 300°C. Thus, metal-support interaction on  $\gamma$ -Al<sub>2</sub>O<sub>3</sub> was higher than that on SiO<sub>2</sub> and less aggregation tendency was expected for both Pt and Ru.

The Ru-Ru contribution was also detected at average distance  $2.65 \pm 0.01$  Å with coordination number  $3.3 \pm 0.1$ . The interactions between metal and surface oxygen were found for both Pt and Ru particles.

Thus,  $\gamma$ -Al<sub>2</sub>O<sub>3</sub>-supported PtRu sample prepared from adsorption of a mixture of Pt(acac)<sub>2</sub> and Ru(acac)<sub>3</sub> did not form bimetallic Pt-Ru particles on the support and each metal had high dispersion.

#### **5.3.4.2 EXAFS evidence for PtRu/MgO catalyst prepared from a mixture of Pt(acac)<sub>2</sub> and Ru(acac)<sub>3</sub>**

Supported PtRu sample prepared from adsorption of a mixture of Pt(acac)<sub>2</sub> and Ru(acac)<sub>3</sub> in toluene onto MgO, was treated in H<sub>2</sub> flow at 300°C for 2 h to remove acetylacetonate ligands and reduce metals. The interactions of metal-metal

and metal-surface oxygen of treated PtRu sample were investigated by EXAFS spectroscopy. The EXAFS fitting parameters of treated PtRu/MgO sample were summarized in Table 5.3. The EXAFS fitting results in  $k$  and  $r$  space with  $k^0$ ,  $k^1$  and  $k^3$  weighted are in Figures 5.10 and 5.11. The estimated accuracies of coordination number ( $N$ ), distance ( $R$ ), Debye-Waller factor ( $\Delta\sigma^2$ ), and inner potential correction ( $\Delta E_0$ ) are as follows:  $\pm 20\%$ ,  $\pm 1\%$ ,  $\pm 30\%$ , and  $\pm 10\%$ , respectively.

**Table 5.2** Summary of EXAFS data of PtRu/MgO prepared from a mixture of Pt(acac)<sub>2</sub> and Ru(acac)<sub>3</sub> after ligand removal in H<sub>2</sub> flow at 300°C for 2 h

Edge	Shell	$N$	$R$ (Å)	$10^3 \times \Delta\sigma^2$ (Å <sup>2</sup> )	$\Delta E_0$ (eV)
Pt L <sub>III</sub>	Pt-Pt	$1.0 \pm 0.1$	$3.07 \pm 0.01$	$3.3 \pm 0.5$	$-5.8 \pm 0.6$
	Pt-Ru	-	-	-	-
	Pt-O <sub>support</sub>				
	Pt-O <sub>s</sub>	$0.4 \pm 0.1$	$1.98 \pm 0.01$	$4.9 \pm 1.4$	$7.0 \pm 0.6$
	Pt-O <sub>l</sub>	$2.6 \pm 0.1$	$2.51 \pm 0.01$	$0.5 \pm 0.2$	$2.1 \pm 0.1$
	Pt-O <sub>l2</sub>	$4.3 \pm 0.1$	$3.17 \pm 0.01$	$-0.3 \pm 0.3$	$-11.9 \pm 0.1$
Ru K	Ru-Ru	$3.5 \pm 0.1$	$2.69 \pm 0.01$	$4.4 \pm 0.3$	$-2.8 \pm 0.2$
	Ru-Pt	-	-	-	-
	Ru-O <sub>support</sub>				
	Ru-O <sub>s</sub>	$2.5 \pm 0.1$	$2.01 \pm 0.01$	$8.6 \pm 0.5$	$-2.8 \pm 0.2$
	Ru-O <sub>l</sub>	$0.9 \pm 0.1$	$2.53 \pm 0.01$	$-3.5 \pm 1.0$	$15.0 \pm 0.4$
	Ru-O <sub>l2</sub>	$1.1 \pm 0.1$	$2.96 \pm 0.01$	$1.6 \pm 1.8$	$-3.5 \pm 0.6$

Notation: subscript s and l refer to short and long, respectively.

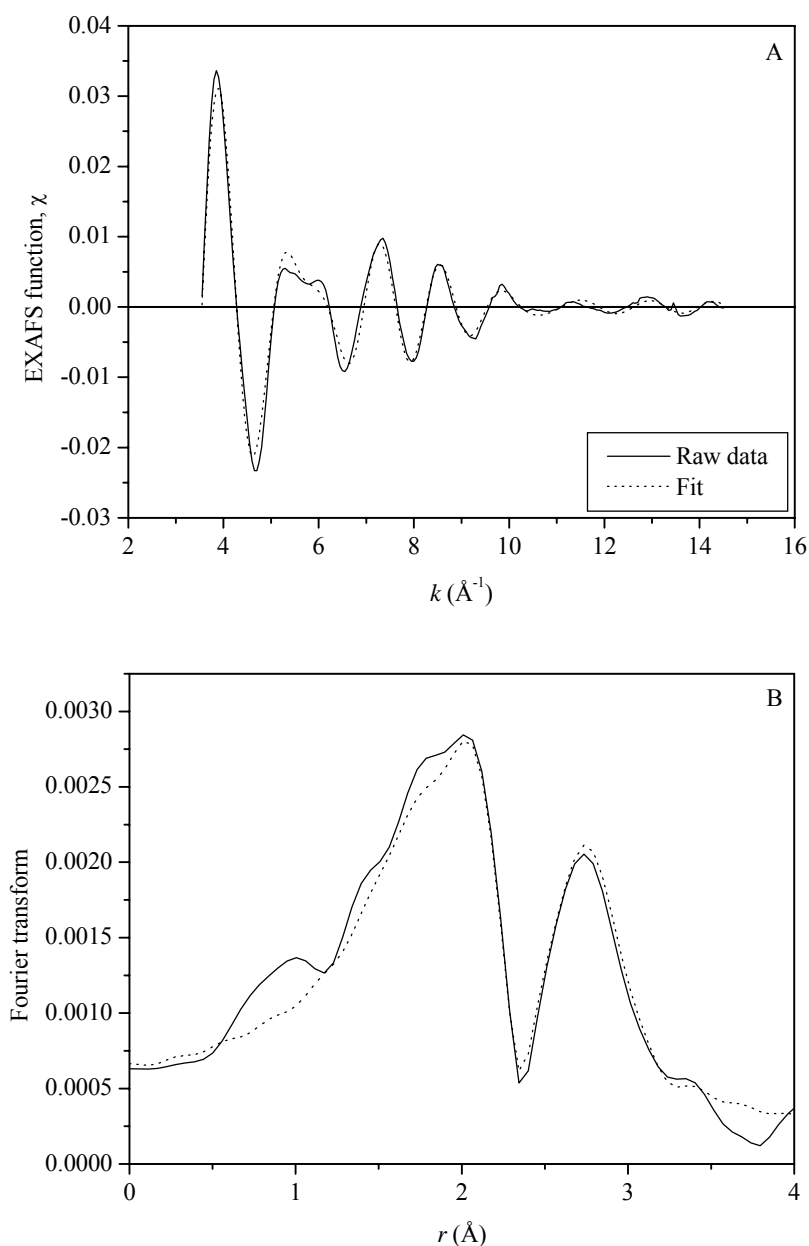


**Figure 5.10** EXAFS results scanned at the Pt  $L_{III}$  edge characterizing the PtRu/MgO sample prepared by adsorption of a mixture of  $\text{Pt}(\text{acac})_2$  and  $\text{Ru}(\text{acac})_3$  after ligand removal in  $\text{H}_2$  flow at  $300^\circ\text{C}$ : (A) Experimental EXAFS function (solid line) and sum of the calculated Pt-Pt, Pt-O<sub>s</sub>, and Pt-O<sub>l</sub> contributions (dotted line). (B) Magnitude of uncorrected Fourier transform ( $k^0$  weighted) of experimental EXAFS function (solid line) and sum of the calculated Pt-Pt, Pt-O<sub>s</sub>, and Pt-O<sub>l</sub> contributions (dotted line).

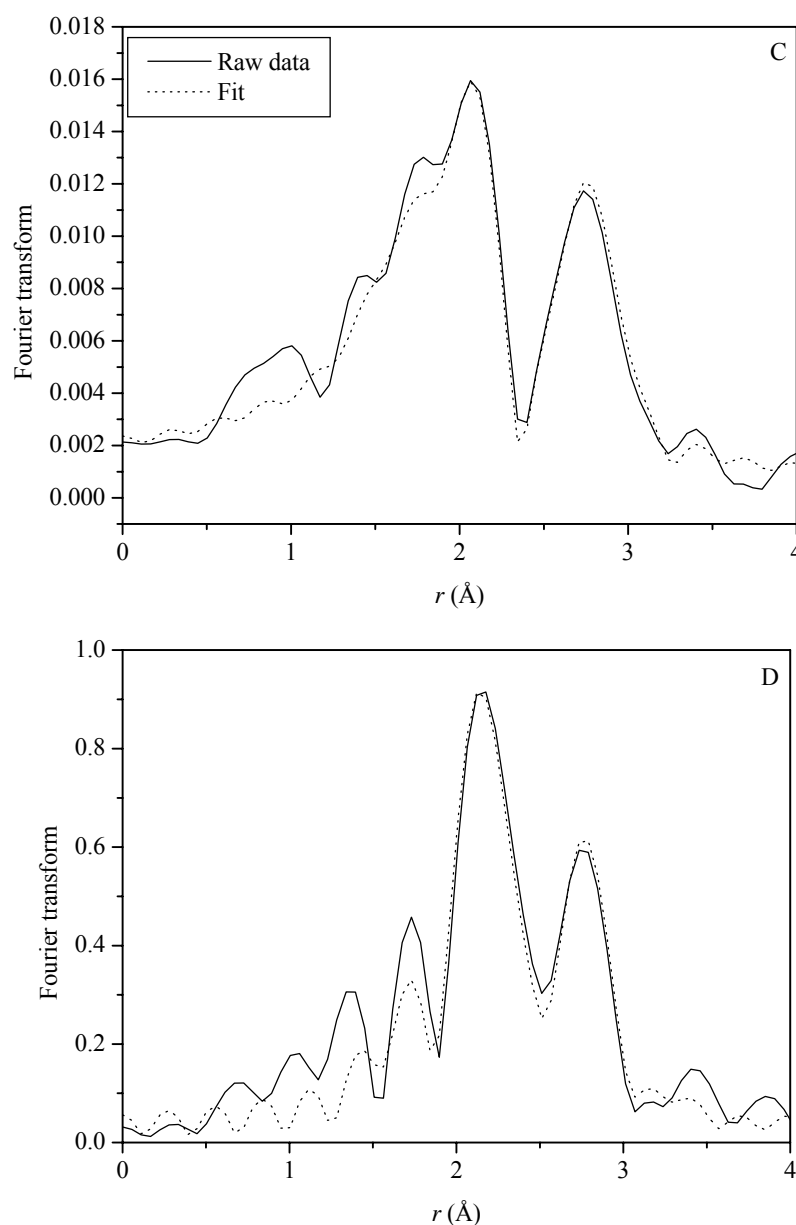


**Figure 5.10** (continued) EXAFS results scanned at the Pt L<sub>III</sub> edge characterizing the PtRu/MgO sample prepared by adsorption of a mixture of Pt(acac)<sub>2</sub> and Ru(acac)<sub>3</sub> after ligand removal in H<sub>2</sub> flow at 300°C: (C) Magnitude of uncorrected Fourier transform ( $k^1$  weighted) of experimental EXAFS function (solid line) and sum of the calculated Pt-Pt, Pt-O<sub>s</sub>, and Pt-O<sub>l</sub> contributions (dotted line). (D) Magnitude of uncorrected Fourier transform ( $k^3$  weighted) of experimental EXAFS function (solid line) and sum of the calculated Pt-Pt, Pt-O<sub>s</sub>, and Pt-O<sub>l</sub> contributions (dotted line).

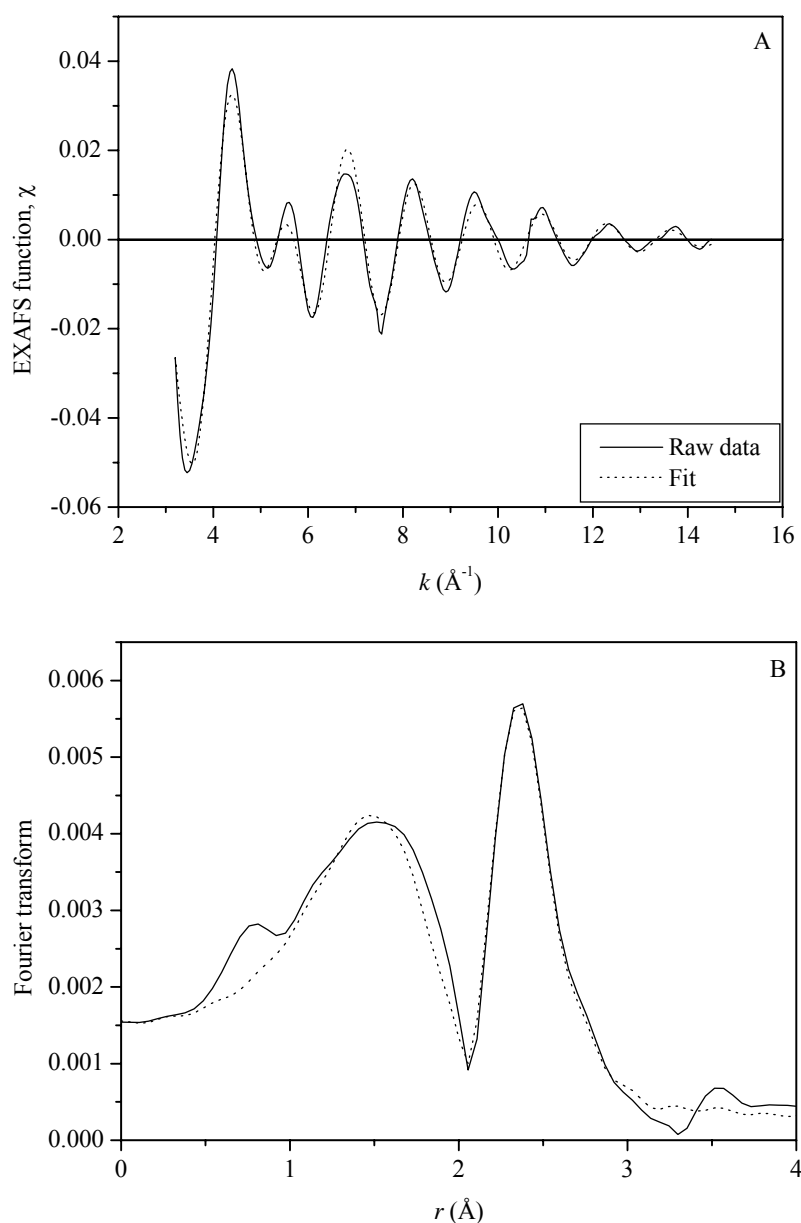


**Figure 5.11** EXAFS results scanned at the Ru K edge characterizing the PtRu/MgO sample prepared by adsorption of a mixture of  $\text{Pt}(\text{acac})_2$  and  $\text{Ru}(\text{acac})_3$  after ligand removal in  $\text{H}_2$  flow at  $300^\circ\text{C}$ : (A) Experimental EXAFS function (solid line) and sum of the calculated Pt-Pt, Pt-O<sub>s</sub>, and Pt-O<sub>l</sub> contributions (dotted line). (B) Magnitude of uncorrected Fourier transform ( $k^0$  weighted) of experimental EXAFS function (solid line) and sum of the calculated Pt-Pt, Pt-O<sub>s</sub>, and Pt-O<sub>l</sub> contributions (dotted line).

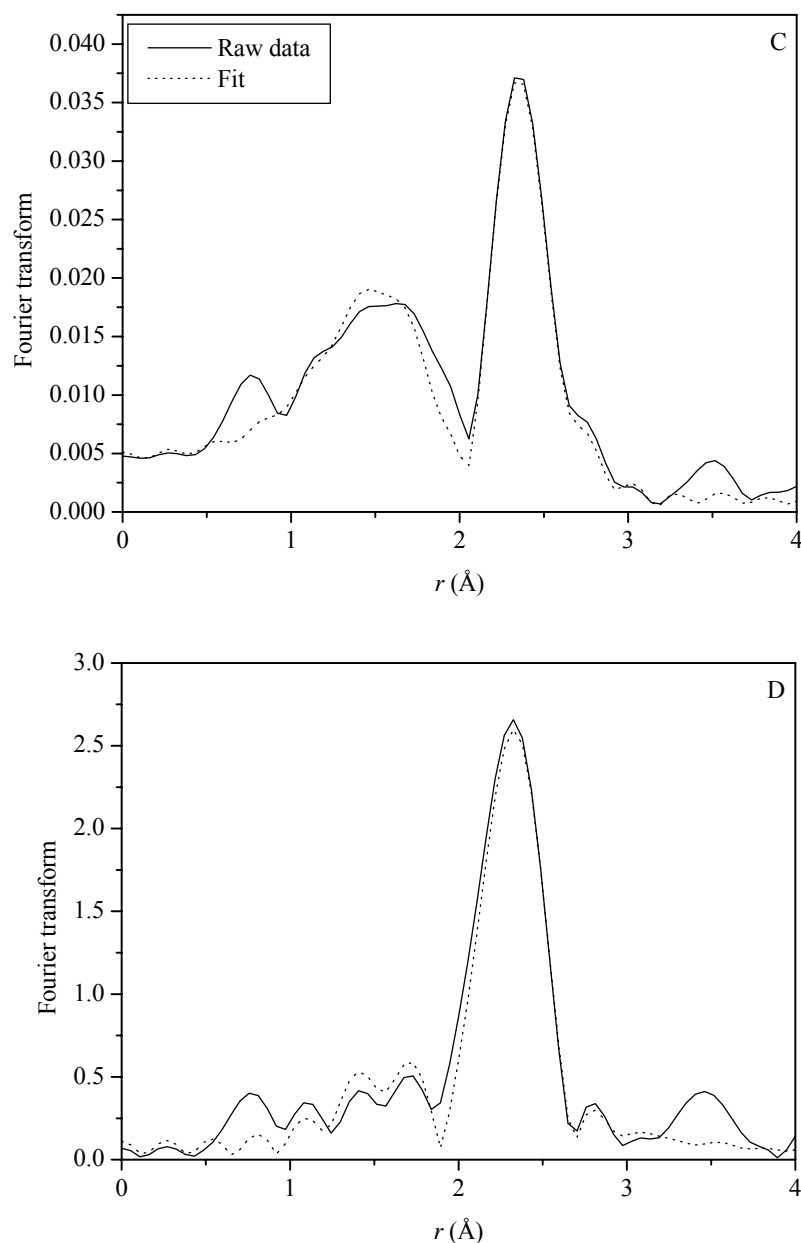


**Figure 5.11** (continued) EXAFS results scanned at the Ru K edge characterizing the PtRu/MgO sample prepared by adsorption of a mixture of  $\text{Pt}(\text{acac})_2$  and  $\text{Ru}(\text{acac})_3$  after ligand removal in  $\text{H}_2$  flow at  $300^\circ\text{C}$ : (C) Magnitude of uncorrected Fourier transform ( $k^1$  weighted) of experimental EXAFS function (solid line) and sum of the calculated Pt-Pt, Pt-O<sub>s</sub>, and Pt-O<sub>l</sub> contributions (dotted line). (D) Magnitude of uncorrected Fourier transform ( $k^3$  weighted) of experimental EXAFS function (solid line) and sum of the calculated Pt-Pt, Pt-O<sub>s</sub>, and Pt-O<sub>l</sub> contributions (dotted line).

After treatment in H<sub>2</sub> flow at 300°C for 2 h, the EXAFS data in Table 5.2 show that the average Pt-Pt coordination number was  $1.0 \pm 0.1$  and that of Ru-Ru was  $3.5 \pm 0.1$ . However, Pt-Ru and Ru-Pt contributions did not observed on MgO support indicating that Pt and Ru did not contact each other upon treatment in H<sub>2</sub> at 300°C for 2 h. Interaction of Pt-Pt was observed at average bond distance  $3.07 \pm 0.01$  Å with coordination number  $1.0 \pm 0.1$  as shown in Table 5.2.

The average coordination of Pt-Pt contribution found in this work was significantly lower than that of Pt/MgO prepared from Pt(acac)<sub>2</sub> and reduced at 300°C, 7.0 at average distance 2.76 Å (Wang et al., 2004).

The Ru-Ru contribution was also detected at average distance  $2.69 \pm 0.01$  Å with coordination number  $3.5 \pm 0.1$ . It was estimated that Ru show greater tendency for aggregation than Pt on MgO upon treatment. The interactions between metal and surface oxygen were found for both Pt and Ru particles.

Thus, PtRu/MgO and PtRu/ $\gamma$ -Al<sub>2</sub>O<sub>3</sub> sample prepared from adsorption of a mixture of Pt(acac)<sub>2</sub> and Ru(acac)<sub>3</sub> did not form bimetallic Pt-Ru particles on each support but contained highly dispersed Pt and Ru particles separately. Because none of Pt-Ru interactions were observed on both Al<sub>2</sub>O<sub>3</sub> and MgO support when using metal acac precursors, it was expected that similar behavior would be observed on TiO<sub>2</sub> support. Thus, further investigation on PtRu/TiO<sub>2</sub> from acetylacetonate salts was not conducted in this thesis.

### 5.3.5 Catalytic activity of ethylene hydrogenation catalyzed by

#### **PtRu/ $\gamma$ -Al<sub>2</sub>O<sub>3</sub> and PtRu/MgO prepared from a mixture of Pt(acac)<sub>2</sub> and Ru(acac)<sub>3</sub>**

Ethylene hydrogenation which is structural-insensitive reaction was used to test catalytic activity over support PtRu catalysts prepared from a mixture of Pt(acac)<sub>2</sub> and Ru(acac)<sub>3</sub>.

#### **5.3.5.1 Time on stream (TOS) for ethylene hydrogenation catalyzed by PtRu/ $\gamma$ -Al<sub>2</sub>O<sub>3</sub> and PtRu/MgO prepared from a mixture of Pt(acac)<sub>2</sub> and Ru(acac)<sub>3</sub>**

Catalytic activity of ethylene hydrogenation catalyzed by supported PtRu/ $\gamma$ -Al<sub>2</sub>O<sub>3</sub> and PtRu/MgO prepared from mixed Pt and Ru compounds were carried out in stainless U-tube reactor at atmospheric pressure. The reaction was tested under condition:  $P_{\text{C}_2\text{H}_4} = 40$  Torr,  $P_{\text{H}_2} = 200$  Torr, balanced with He, total feed flow rate = 100 ml (NTP)/min, 1.0 wt% Pt and 1.0 wt% Ru catalyst and temperature range -50 to -40°C. The reaction temperature was kept at desired temperature with  $\pm 1^\circ\text{C}$  fluctuation. Catalytic activities of ethylene hydrogenation catalyzed by PtRu/ $\gamma$ -Al<sub>2</sub>O<sub>3</sub> and PtRu/MgO prepared from mixed organometallic compounds were plotted as a function of TOS as in Figure 5.12.

Figure 5.12 shows that catalytic activity of ethylene hydrogenation catalyzed by PtRu/MgO prepared from a mixture of Pt(acac)<sub>2</sub> and Ru(acac)<sub>3</sub> in toluene was much higher than that catalyzed by PtRu/ $\gamma$ -Al<sub>2</sub>O<sub>3</sub> catalysts at temperature -50°C. The reaction reached steady-state within 20 minutes for all catalysts and deactivation was not observed during the 100 minute testing period.

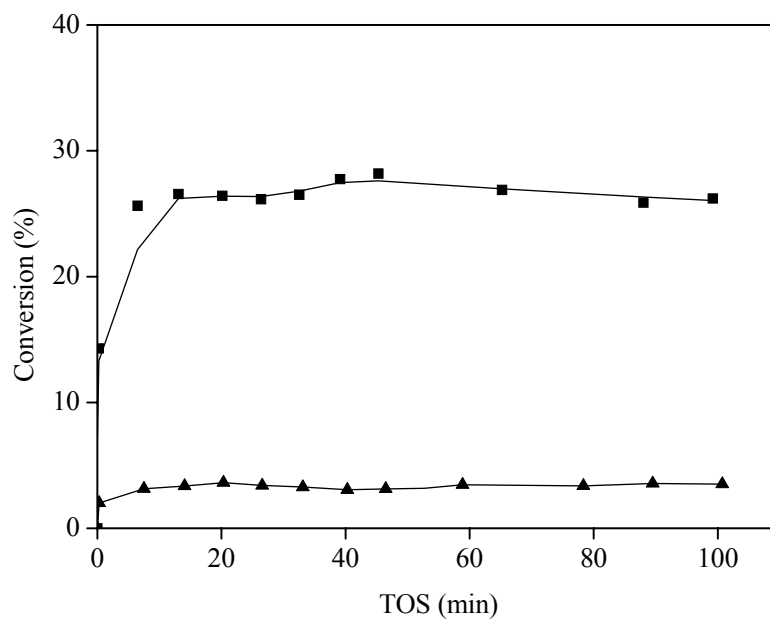


**Figure 5.12** Activity for ethylene hydrogenation catalyzed by (■) PtRu/MgO; (▲) PtRu/ $\gamma$ -Al<sub>2</sub>O<sub>3</sub>, prepared from a mixture solution of Pt(acac)<sub>2</sub> and Ru(acac)<sub>3</sub> at temperature -50°C.

### 5.3.5.2 Apparent activation energy of ethylene hydrogenation catalyzed by PtRu/ $\gamma$ -Al<sub>2</sub>O<sub>3</sub> and PtRu/MgO prepared from a mixture solution of Pt(acac)<sub>2</sub> and Ru(acac)<sub>3</sub>

The apparent activation energy of ethylene hydrogenation catalyzed by supported PtRu catalyst was collected at around 25 min TOS at reaction condition:  $P_{\text{C}_2\text{H}_4} = 40$  Torr,  $P_{\text{H}_2} = 200$  Torr, balanced He with total feed flow rate 100 ml (NTP)/min, catalyst mass 10-20 mg, 1.0 wt% Pt and 1.0 wt% Ru, and temperature ranges -50 to -9°C. Reaction temperature was kept at desired temperature with  $\pm 1^\circ\text{C}$  fluctuation.

The catalytic activity of reaction in terms of the turnover frequency (TOF) was represented the number of molecules reacting per active sites per second (Fogler,

1999). It was assumed that all metal particles dispersed on support were accessible to reactants, so that TOF was defined as the equation 2.3 (Chapter II, page 53). Arrhenius plot of TOF in a natural log scale as a function of inversed temperature was in Figure 5.13.

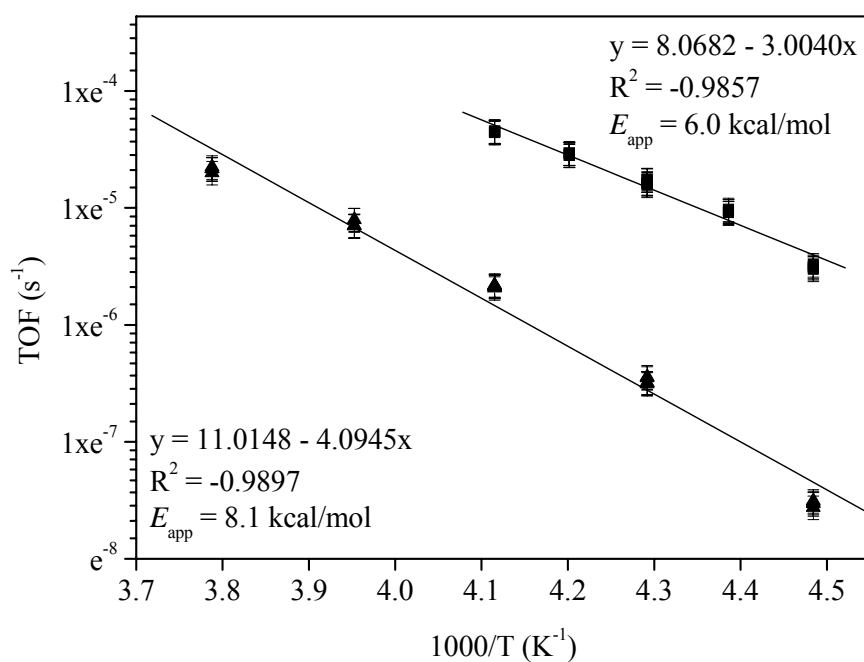


**Figure 5.13** Arrhenius plot for ethylene hydrogenation catalyzed by (■) PtRu/MgO; (▲) PtRu/γ-Al<sub>2</sub>O<sub>3</sub>, prepared from a mixture solution of Pt(acac)<sub>2</sub> and Ru(acac)<sub>3</sub>.

Due to very high activity of ethylene hydrogenation catalyzed by PtRu/MgO prepared from a mixture solution of Pt(acac)<sub>2</sub> and Ru(acac)<sub>3</sub>, complete conversion were obtained at temperature higher than -30°C, thus data was collected in temperature ranges -50 to -30°C. The lower Pt-Ru contributions on MgO than that on γ-Al<sub>2</sub>O<sub>3</sub> probably affect the catalytic activity. The apparent activation energy of

ethylene hydrogenation catalyzed by supported PtRu catalysts could be obtained from slope of linear graph in Figure 5.13 and values are shown in Table 5.3.

**Table 5.3** Apparent activation energy for ethylene hydrogenation catalyzed by PtRu catalysts prepared from mixture solution of Pt and Ru compounds and ligand removal in H<sub>2</sub> flow at 300°C for 2 h

Precursors	Supports	Activity TOF x 10 <sup>4</sup> (s <sup>-1</sup> ) <sup>a</sup>	Apparent activation energy (kcal/mol)	Temperature (°C)
Pt(acac) <sub>2</sub> + Ru(acac) <sub>3</sub>	γ-Al <sub>2</sub> O <sub>3</sub>	1.5 ± 0.1	8.1 ± 0.1	-50 to -9
Pt(acac) <sub>2</sub> + Ru(acac) <sub>3</sub>	MgO	83.9 ± 1.7	6.0 ± 0.1	-50 to -30
Pt(cod)Cl <sub>2</sub> + Ru(cod)Cl <sub>2</sub>	γ-Al <sub>2</sub> O <sub>3</sub>	6.8 ± 0.2	6.7 ± 0.1	-51 to -10 <sup>b</sup>
Pt(cod)Cl <sub>2</sub> + Ru(cod)Cl <sub>2</sub>	MgO	6.9 ± 0.3	6.7 ± 0.1	-50 to -10 <sup>b</sup>

<sup>a</sup>Reaction at -40°C,  $P_{\text{C}_2\text{H}_4} = 40$  Torr and  $P_{\text{H}_2} = 200$  Torr

<sup>b</sup>Chotisuwan, Wittayakun, and Gates, 2004

Table 5.3 shows order of apparent activation energy over PtRu/MgO prepared from Pt(acac)<sub>2</sub> and Ru(acac)<sub>3</sub> > PtRu/MgO ≈ PtRu/γ-Al<sub>2</sub>O<sub>3</sub> prepared from Pt(cod)Cl<sub>2</sub> and Ru(cod)Cl<sub>2</sub> > PtRu/γ-Al<sub>2</sub>O<sub>3</sub> prepared from Pt(acac)<sub>2</sub> and Ru(acac)<sub>3</sub>. The turn over frequency (TOF) at temperature -40°C of PtRu/MgO prepared from Pt(acac)<sub>2</sub> and Ru(acac)<sub>3</sub> was pretty much higher than that of other catalysts.

However, the apparent activation energy of PtRu/γ-Al<sub>2</sub>O<sub>3</sub> catalyst prepared from Pt(acac)<sub>2</sub> and Ru(acac)<sub>3</sub> was slightly lower than that of PtRu/γ-Al<sub>2</sub>O<sub>3</sub> catalyst

prepared from a molecular precursor in Chapter II which was  $8.4 \pm 0.1$  kcal/mol at condition:  $P_{\text{H}_2} = 80$  Torr,  $P_{\text{C}_2\text{H}_4} = 40$  Torr, balance He with 200 ml (NTP)/min flow rate and temperature varied from -75 to -20°C. In addition, the apparent activation energy of PtRu/MgO catalyst prepared from Pt(acac)<sub>2</sub> and Ru(acac)<sub>3</sub> was lower than that of PtRu/MgO catalyst prepared from a molecular precursor in Chapter III which was  $7.6 \pm 0.1$  kcal/mol at condition:  $P_{\text{H}_2} = 80$  Torr,  $P_{\text{C}_2\text{H}_4} = 40$  Torr, balance He with 200 ml (NTP)/min flow rate and temperature varied from -75 to -30°C.

## 5.4 Conclusions

Supported (Pt+Ru) catalysts were prepared by adsorption with the mixture of Pt(acac)<sub>2</sub> and Ru(acac)<sub>3</sub> in toluene. Precursors adsorbed on support by hydrogen bonding. Acetylacetonato ligands of adsorbed precursors could be completely removed by treatment in H<sub>2</sub> flow at 300°C for 2 h. However, metal particles could be reduced at this condition after observed by TPRD technique. The EXAFS results indicated that Pt-Ru or Ru-Pt connection did not form after treatment in H<sub>2</sub> flow at 300°C but contained highly dispersed Pt and Ru particles. The average Pt-Pt and Ru-Ru coordination numbers of PtRu/γ-Al<sub>2</sub>O<sub>3</sub> were  $2.8 \pm 0.1$  and  $3.3 \pm 0.1$  whereas that of PtRu/MgO were  $1.0 \pm 0.1$  and  $3.5 \pm 0.1$ , respectively. Supported PtRu catalysts on both supports were active for ethylene hydrogenation. The apparent activation energies of PtRu/MgO and PtRu/γ-Al<sub>2</sub>O<sub>3</sub> prepared from the mixture of Pt(acac)<sub>2</sub> and Ru(acac)<sub>3</sub> were  $6.0 \pm 0.1$  and  $8.1 \pm 0.1$  kcal/mol, slightly lower than that of PtRu/MgO and PtRu/γ-Al<sub>2</sub>O<sub>3</sub> catalysts prepared from Pt<sub>3</sub>Ru<sub>6</sub>(CO)<sub>21</sub>(μ<sub>3</sub>-H)(μ-H)<sub>3</sub> in Chapter II and III which were  $7.6 \pm 0.1$  and  $8.4 \pm 0.1$  kcal/mol, respectively. Catalytic activities

(TOF) of ethylene hydrogenation catalyzed by PtRu/ $\gamma$ -Al<sub>2</sub>O<sub>3</sub> and PtRu/MgO prepared from the mixture of Pt(acac)<sub>2</sub> and Ru(acac)<sub>3</sub> at temperature -40°C were  $(1.5 \pm 0.1) \times 10^{-4}$  and  $(83.9 \pm 1.7) \times 10^{-4}$  (s<sup>-1</sup>).

## CHAPTER VI

### CONCLUSIONS

Highly dispersed PtRu catalysts on  $\gamma$ -Al<sub>2</sub>O<sub>3</sub>, MgO and TiO<sub>2</sub> were prepared successfully by adsorption with a CH<sub>2</sub>Cl<sub>2</sub> solution of Pt-Ru carbonyl hydride cluster, Pt<sub>3</sub>Ru<sub>6</sub>(CO)<sub>21</sub>( $\mu$ <sub>3</sub>-H)( $\mu$ -H)<sub>3</sub> which is coordinatively saturated and has Pt-Ru bonds. Characterization by IR and EXAFS spectroscopy indicated that the precursor did not adsorb intact on each support except on  $\gamma$ -Al<sub>2</sub>O<sub>3</sub> which cluster core was intact. The adsorbed precursor was still in the form of bimetallic carbonyl species and the structure was slightly changed possibly due to loss of hydrides during impregnation and interaction with the support. This adsorbed precursor on each support could not be recovered completely by CH<sub>2</sub>Cl<sub>2</sub> solvent also due to the strong interaction with support.

The difference in chemistry of supports lead to differences in chemistry of precursor-support interactions. The cluster precursor could bind to  $\gamma$ -Al<sub>2</sub>O<sub>3</sub> support by the interactions between metal and surface oxygen, oxygen of CO ligands and between surface hydroxyl groups and Al<sup>3+</sup> acid sites. For adsorption on MgO, oxygen of CO ligands of the precursor interacted with surface hydroxyl groups and formed carbonates, carboxylates adsorbed species and hydrogen bonding whereas IR results indicated that oxygen of CO ligands of precursor adsorbed on TiO<sub>2</sub> interacted with surface hydroxyl groups forming carbonates, carboxylates adsorbed species. Partial

decarbonylation was observed only at Ru atoms of adsorbed precursor on TiO<sub>2</sub> by EXAFS spectroscopy.

Carbonyl ligands of adsorbed precursor could be completely removed in He flow at 300°C for 2 h resulting in supported bimetallic Pt-Ru particles with high dispersion. The average bond distances for Pt-Ru catalysts supported on  $\gamma$ -Al<sub>2</sub>O<sub>3</sub>, MgO and TiO<sub>2</sub> were  $2.64 \pm 0.01$ ,  $2.69 \pm 0.01$  and  $2.65 \pm 0.01$  Å for Pt-Pt,  $2.68 \pm 0.01$ ,  $2.69 \pm 0.01$  and  $2.69 \pm 0.01$  Å for Pt-Ru,  $2.62 \pm 0.01$ ,  $2.63 \pm 0.01$  and  $2.65 \pm 0.01$  Å for Ru-Ru, respectively. The average coordination numbers for Pt-Ru catalysts supported on  $\gamma$ -Al<sub>2</sub>O<sub>3</sub>, MgO and TiO<sub>2</sub> were  $1.7 \pm 0.2$ ,  $1.3 \pm 0.2$  and  $1.8 \pm 0.1$  for Pt-Pt,  $2.2 \pm 0.1$ ,  $0.9 \pm 0.1$  and  $1.9 \pm 0.1$  for Pt-Ru,  $2.1 \pm 0.1$ ,  $2.6 \pm 0.1$  and  $2.4 \pm 0.1$  for Ru-Ru,  $1.0 \pm 0.1$ ,  $1.1 \pm 0.1$  and  $0.9 \pm 0.1$  for Ru-Pt contribution, respectively.

EXAFS data showed structural changes in bond distances and coordination numbers of Pt-Ru contribution due to partial segregation but the bimetallic frame remained on support. There was greater tendency to segregate on MgO than other supports. However, Pt-Pt and Ru-Ru contributions were stable upon ligand removal. Strong Pt-Ru and cluster-support interactions might lead to high dispersion bimetallic species on  $\gamma$ -Al<sub>2</sub>O<sub>3</sub>.

Supported PtRu catalysts prepared from Pt<sub>3</sub>Ru<sub>6</sub>(CO)<sub>21</sub>( $\mu_3$ -H)( $\mu$ -H)<sub>3</sub> were active for both ethylene hydrogenation and *n*-butane hydrogenolysis. The apparent activation energies for ethylene hydrogenation were  $8.4 \pm 0.1$ ,  $7.6 \pm 0.1$  and  $8.1 \pm 0.1$  kcal/mol for catalysts on  $\gamma$ -Al<sub>2</sub>O<sub>3</sub>, MgO and TiO<sub>2</sub>, respectively. The catalytic activity for ethylene hydrogenation of supported PtRu/TiO<sub>2</sub> catalyst prepared from Pt<sub>3</sub>Ru<sub>6</sub>(CO)<sub>21</sub>( $\mu_3$ -H)( $\mu$ -H)<sub>3</sub> was highest among tested catalysts. The apparent

activation energies for *n*-butane hydrogenolysis were  $30.9 \pm 0.1$ ,  $15.5 \pm 0.1$  and  $28.2 \pm 0.1$  kcal/mol for catalysts on  $\gamma$ -Al<sub>2</sub>O<sub>3</sub>, MgO and TiO<sub>2</sub>, respectively.

Supported PtRu catalysts on  $\gamma$ -Al<sub>2</sub>O<sub>3</sub> and MgO were also prepared successful by adsorption with a mixture of Pt(acac)<sub>2</sub> and Ru(acac)<sub>3</sub> compounds. IR results indicated that interaction of precursors and support could occur through acetylacetonate ligands with surface of support forming hydrogen bond. Acetylacetonate ligands could be removed completely after treatment in H<sub>2</sub> flow at 300°C for 2 h. TPRD and EXAFS data indicated that there were no Pt-Ru connections in treated PtRu samples prepared from the mixture of Pt(acac)<sub>2</sub> and Ru(acac)<sub>3</sub> on both supports, only Pt-Pt and Ru-Ru contributions were observed. However, PtRu/MgO and PtRu/ $\gamma$ -Al<sub>2</sub>O<sub>3</sub> catalysts prepared from the mixture of Pt(acac)<sub>2</sub> and Ru(acac)<sub>3</sub> were active in ethylene hydrogenation and apparent activation energies were  $6.0 \pm 0.1$  and  $8.1 \pm 0.1$  kcal/mol, slightly lower than that of PtRu/MgO and PtRu/ $\gamma$ -Al<sub>2</sub>O<sub>3</sub> catalysts prepared from Pt<sub>3</sub>Ru<sub>6</sub>(CO)<sub>21</sub>( $\mu$ <sub>3</sub>-H)( $\mu$ -H)<sub>3</sub>.

## **REFERENCES**

## REFERENCES

- Adams, R. D., Alexander, M. S., Arafa, I., and Wu, W. (1991). Cluster Synthesis. 36. New platinum-ruthenium and platinum-osmium carbonyl cluster complexes from the reaction of the complexes  $\text{Pt}_2\text{M}_4(\text{CO})_{18}$  ( $\text{M} = \text{Ru}, \text{Os}$ ) with cycloocta-1, 5-diene in the presence of UV irradiation. **Inorganic Chemistry** 30 (25): 4717-4723.
- Adams, R. D., Barnard, T. S., Li, Z., Wu, W., and Yamamoto, J. (1994). Cluster synthesis. 43. New layer-segregated platinum-ruthenium cluster complexes and their reactions with diphenylacetylene. **Organometallics** 13: 2357-2364.
- Adams, R. D., Chen, W., and Wu, W. (1993). The synthesis and structural analysis of  $\text{Pt}_2\text{Ru}_4(\text{CO})_{18}$  and the products obtained from its reactions with 1, 2-bis(diphenylphosphino)ethane. **Journal of Cluster Science** 4 (2): 119-132.
- Alerasool, S., Boecker, D., Rejai, B., Gonzalez, R. D., del Angel, G., Azomosa, M., and Gomes, R. (1988). The role of preparative variables on the surface composition of supported platinum-ruthenium bimetallic clusters. **Langmuir** 4 (5): 1083-1090.
- Alerasool, S., and Gonzalez, R. D. (1990). Preparation and characterization of supported Pt-Ru bimetallic clusters: strong precursor-support interaction. **Journal of Catalysis** 124: 204-216.

Alexeev, O. S., and Gates, B. C. (2003). Supported bimetallic cluster catalysts.

**Industrial & Engineering Chemistry Research** 42 (8): 1571-1587.

Alexeev, O. S., Graham, G. W., Kim, D-W., Shelef, M., and Gates, B. C. (1999).

$\gamma$ -Al<sub>2</sub>O<sub>3</sub>-supported Pt-W catalysts prepared from molecular organometallic precursors: characterization by infrared spectroscopy. **Physical Chemistry Chemical Physics** 1: 5725-5733.

Alexeev, O. S., Graham, G. W., Shelef, M., Adams, R. D., and Gates, B. C. (2002).

$\gamma$ -Al<sub>2</sub>O<sub>3</sub>-supported PtRu clusters prepared from [Pt<sub>2</sub>Ru<sub>4</sub>(CO)<sub>18</sub>]: characterization by infrared and extended x-ray absorption fine structure spectroscopy. **Journal of Physical Chemistry B** 106 (18): 4697-4704.

Alexeev, O. S., Graham, G. W., Shelef, M., and Gates, B. C. (2000).  $\gamma$ -Al<sub>2</sub>O<sub>3</sub>-

supported Pt catalysts with extremely high dispersions resulting from Pt-W interactions. **Journal of Catalysis** 190: 157-172.

Alexeev, O., Kawi, S., Shelef, M., and Gates, B. C. (1996). Synthesis and

characterization of model MgO-supported catalysts with Pt-Mo interactions. **Journal of Physical Chemistry** 100 (1): 253-264.

Alexeev, O., Shelef, M., and Gates, B. C. (1996). MgO-supported platinum–tungsten

catalysts prepared from organometallic precursors: platinum clusters isolated on dispersed tungsten. **Journal of Catalysis** 164: 1-15.

Antos, G. A., Aitani, A. M., and Parera, J. M., (eds.). (1995). **Catalytic Naphtha**

**Reforming**. New York: Marcel Dekker.

Asakura, K., Bando, K. -K., and Iwasawa, Y. (1990). Structure and behaviour of

Ru<sub>3</sub>(CO)<sub>12</sub> supported on inorganic oxide surfaces, studied by EXAFS, infrared

- spectroscopy and temperature-programmed decomposition. **Journal of the Chemical Society-Faraday Transaction** 86 (14): 2645-2655.
- Baltes, M., Collart, O., Van Der Voort, P., and Vansant, E. F. (1999). Synthesis of supported transition metal oxide catalysts by the designed deposition of acetylacetonate complexes. **Langmuir** 15 (18): 5841-5845.
- Bergmeister, J. J., and Hanson, B. E. (1989). Adsorption of ruthenium-cobalt bimetallic clusters on hydroxylated alumina. **Organometallics** 8 (2): 283-286.
- Bernas, A., Kumar, N., Laukkanen, P., Väyrynen, J., Salmi, T., and Murzin, D. Y. (2004). Influence of ruthenium precursor on catalytic activity of Ru/Al<sub>2</sub>O<sub>3</sub> catalyst in selective isomerization of linoleic acid to *cis*-9,*trans*-11- and *trans*-10,*cis*-12-conjugated linoleic acid. **Applied Catalysis A: General** 267: 121-133.
- Bond, G. C., and Cunningham, R. H. (1996). Alkane transformations on supported platinum catalysts Part 3: The stability of Pt/Al<sub>2</sub>O<sub>3</sub> (EUROPT-3) and of PtRe/Al<sub>2</sub>O<sub>3</sub> (EUROPT-4) during the hydrogenolysis of alkanes. **Journal of Catalysis** 163: 328-337.
- Bond, G. C., and Lin, X. (1997). Alkane transformations on supported platinum catalysts 5. Effects of formation and removal of carbon deposits on alkane hydrogenolysis using EUROPT-1 (6.3% platinum/silica). **Journal of Catalysis** 168: 207-216.
- Bond, G. C., and Slaa, J. C. (1995). Catalytic and structural properties of ruthenium bimetallic catalysts: effects of pretreatment on the behaviour of various Ru/Al<sub>2</sub>O<sub>3</sub> catalysts in alkane hydrogenolysis. **Journal of Molecular Catalysis A: Chemical** 96: 163-173.

- Boxall, D. L., Deluga, G. A., Kenik, E. A., King, W. D., and Lukehart, C. M. (2001). Rapid synthesis of a Pt<sub>1</sub>Ru<sub>1</sub>/carbon nanocomposited using microwave irradiation: a DMFC anode catalyst of high relative performance. **Chemistry of Materials** 13 (3): 891-900.
- Braccini, C., Indovina, V., De Rossi, S., and Giorgi, L. (2000). Anodic catalysts for polymer electrolyte fuel cells : the catalytic activity of Pt/C, Ru/C and Pt-Ru/C in oxidation of CO by O<sub>2</sub>. **Catalysis Today** 55: 45-49.
- Braunstein, P., and Rose, J. (1998). Heterometallic Clusters for Heterogeneous Catalysis. In Adams, R., and Cotton, F. A. (eds.). **Catalysis by Di- and Polynuclear Metal Cluster Complexes** (pp. 448). New York: Wiley-VCH.
- Braunstein, P., and Rose, J. (1999). Heterometallic in Catalysis. In : **Metal Clusters in Chemistry**, Vol. 2: Catalysis and dynamics and physical properties. Braunstein, P., Oro, L. A. and Raithby, P. R. (eds). Germany: WILEY-VCH.
- Busca, G., and Lorenzelli, V. (1982). Infrared spectroscopic identification of species arising from reactive adsorption of carbon oxides on metal oxide surfaces. **Materials Chemistry** 7 (1): 89-126.
- Chrzanowski, W., and Wieckowski, A. (1998). Surface structure effects in Platinum/Ruthenium methanol oxidation electrocatalysis. **Langmuir** 14 (8): 1967-1970.
- Chotisuwan, S., Wittayakun, J., and Gates, B. C. (2004). Activities of supported Platinum-Ruthenium catalysts for ethylene hydrogenation. In **Proceeding of the 30<sup>th</sup> Congress on Science and Technology of Thailand** (pp 86). Bangkok, Thailand: The Science Society of Thailand.

- Clark, H. C., and Manzer, L. E. (1973). ( $\pi$ -1,5-Cyclooctadiene)organoplatinum(II) compounds. **Journal of Organometallic Chemistry** 59: 411.
- Coq, B., Kumbhar, P. S., Moreau, C., Moreau, P., and Figueras, F. (1994). Zirconia-supported monometallic Ru and bimetallic Ru-Sn, Ru-Fe catalysts: role of metal support interaction in the hydrogenation of cinnamaldehyde. **Journal of Physical Chemistry** 98 (40): 10180-10188.
- Cortright, R. D., Goddard, S. A., Rekoske, J. E., and Dumesic, J. A. (1991). Kinetic study of ethylene hydrogenation. **Journal of Catalysis** 127: 342-353.
- Cotton, F. A., Wilkinson, G., Murillo, C. A., and Bochmann, M. (1999). **Advanced Inorganic Chemistry** (6<sup>th</sup> ed). New York: John Wiley & Sons. pp 652.
- da Silva, A. B., Jordão, E., Mendes M. J., and Fouilloux, P. (1997). Effect of metal-support interaction during selective hydrogenation of cinnamaldehyde to cinnamyl alcohol on platinum based bimetallic catalysts. **Applied Catalysis A: General** 148: 253-264.
- Dhepe, P. L., Fukuoka, A., and Ichikawa, M. (2003). Novel fabrication and catalysis of nano-structured Rh and RhPt alloy particles occluded in ordered mesoporous silica templates using supercritical carbon dioxide. **Physical Chemistry Chemical Physics** 5: 5565-5573.
- Diaz, G., Garin, F., and Maire, G. (1983). Isomerization and hydrogenolysis of hexanes on an alumina-supported Pt-Ru catalyst. **Journal of Catalysis** 82: 13-25.
- Diaz, G., Garin, F., Maire, G., Alerasool, S., and Gonzalez, R. D. (1995). Hydrogenolysis of methylcyclopentane and isomerization of 2-methylpentane

- over well characterized silica-supported platinum-ruthenium catalysts. **Applied Catalysis A** 124: 33-46.
- Diebold, U. (2003). The surface science of titanium dioxide. **Surface Science Reports** 48: 53-229.
- Dorling, T. A., Eastlake, M. J., and Moss, R. L. (1969). The structure and activity of supported metal catalysts IV. Ethylene hydrogenation on platinum/silica catalysts. **Journal of Catalysis** 14: 23-33.
- Dossi, C., Pozzi, A., Reccia, S., Fusi, A., Psaro, R., and Dal Santo, V. (2003). An organometallic route to mono and bimetallic Pt and Pt-Pd catalysts supported on magnesium oxide: thermoanalytical investigation and catalytic behavior in MCP conversion. **Journal of Molecular Catalysis A: Chemical** 204-205: 465-472.
- Dossi, C., Psaro, R., Fusi, A., Reccia, S., Dal Santo, V., and Sordelli, L. (1998). Thermochemical mass-spectrometric investigation under reducing conditions of [Pd(acac)<sub>2</sub>] adsorbed on magnesium oxide. **Thermochimica Acta** 317: 157-164.
- Drew, D., and Doyle, J. R. (1972). Organometallic compounds 11. Cyclic-diolefin complexes of platinum and palladium. **Inorganic Syntheses** 13: 47-49.
- Farrautao, R. J., and Bartholomew, C. H. (1997). **Industrial Catalytic Processes**. London: Blachie Academic & Professional. pp 88, 145-147.
- Fiddy, S. G., Newton, M. A., Campbell, T., Dent, A. J., Harvey, I., Salvini, G., Turin, S., and Evans, J. (1999). Particle development and characterization in Pt(acac)<sub>2</sub> and Pt(acac)<sub>2</sub>/GeBu<sub>4</sub> derived catalysts supported upon porous and

mesoporous SiO<sub>2</sub>: effect of reductive environment, and support structure.

**Physical Chemistry Chemical Physics** 4: 827-834.

Fiddy, S. G., Newton, M. A., Dent, A. J., Salvini, G., Corker, J. M., Turin, S., Campbell, T., and Evans, J. (1999). In situ energy dispersive EXAFS (EDE) of low loaded Pt(acac)<sub>2</sub>/ H<sub>1</sub> SiO<sub>2</sub> catalyst precursors on a timescale of seconds and below. **Chemical Communications** (9): 851-852.

Finklea, H., and Vithanage, R. (1982). Infrared absorption spectroscopy of chemically modified titanium dioxide. **Journal of Physical Chemistry** 89 (18): 3631-3626.

Fogler, H. S. (1999). **Elements of Chemical Reaction Engineering**. (3<sup>rd</sup> ed.). New Jersey: Prentice-Hall. pp. 587.

Fung, A. S., Kelley, M. J., Koningsberger, D. C., and Gates, B. C. (1997).  $\gamma$ -Al<sub>2</sub>O<sub>3</sub>-supported Re-Pt cluster catalyst prepared from [Re<sub>2</sub>Pt(CO)<sub>12</sub>]: characterization by Extended X-ray absorption fine structure spectroscopy and catalysis of methylcyclohexane dehydrogenation. **Journal of the American Chemical Society** 119 (25): 5877-5887.

George, G. N., George, J. S., and Pickering, I. J. (2000). EXAFSPAK: A Suite of Computer Programs for Analysis of X-ray Absorption Spectra. Stanford Synchrotron Radiation Laboratory, Stanford Linear Accelerator Center. Available: <http://www-ssrl.slac.stanford.edu/exafspak.html> (downloaded 2004).

Granger, P., Lecomte, J. J., Dathy, C., Leclercq, L., and Leclercq, G. (1998). Kinetics of the CO + NO reaction over rhodium and platinum-rhodium on alumina. **Journal of Catalysis** 175: 194-203.

- Grunes, J., Zhu, J., Yang, M., and Somorjai, G. A. (2003). CO poisoning of ethylene hydrogenation over Pt catalysts: a comparison of Pt(111) single crystal and Pt nanoparticle activities. **Catalysis Letters** 86 (4): 157-161.
- Guczi, L., and Beck, A. (1988). Elementary steps in the formation of bimetallic catalysts derived from carbonyl clusters. **Polyhedron** 7 (22): 2387-2392.
- Guzman, J., and Gates, B. C. (2003). Supported molecular catalysis: metal complexes and cluster on oxides and zeolites. **Journal of the Chemical Society-Dalton Transactions** 17: 3303-3318.
- Hadjiivanov, K. I. (1998). IR study of CO and H<sub>2</sub>O coadsorption on Pt<sup>n+</sup>/TiO<sub>2</sub> and Pt/TiO<sub>2</sub> samples. **Journal of the Chemical Society-Faraday Transaction** 94 (13): 1901-1904.
- Hadjiivanov, K. I., Bushev, V., Kantcheva, M., and Klissurski, D. (1994). Infrared spectroscopy study of the series arising during NO<sub>2</sub> adsorption on TiO<sub>2</sub> (anatase). **Langmuir** 10 (2): 464-471.
- Hadjiivanov, K. I., Vayssilov, G. N. (2002). Characterization of oxide surfaces and zeolites by carbon monoxide as an IR probe molecule. In Gates, B. C., and Knözinger, H. (eds.). **Advances in Catalysis** (Vol. 47, pp. 451). Amsterdam: Academic Press.
- Hamnett, A., Kennedy, B. J., and Wagner, F. E. (1990). Pt-Ru anodes for methanol electrooxidation: a ruthenium-99 Mossbauer study. **Journal of Catalysis** 124: 30-40.
- Herrman, W. A., and Salzer, A. (1996). **Synthetic methods of organometallic and inorganic chemistry: Literature, laboratory techniques, and common**

- starting materials.** Vol. I. New York: Georg Thime Verlag Stuttgart. pp. 166-168.
- Hills, C. H., Nasher, M. S., Frenkel, A. I., Shapley, J. R., and Nuzzo, R. G. (1999). Carbon support effects on bimetallic Pt-Ru nanoparticles formed from molecular precursors. **Langmuir** 15 (3): 690-700.
- Hwang, K. S., Yang, M., Zhu, J., Grunes, J., and Somorjai, G. A. (2003). The molecular mechanism of the poisoning of platinum and rhodium catalyzed ethylene hydrogenation by carbon monoxide. **Journal of Molecular Catalysis A: Chemical** 204-205: 499-507.
- Ichikawa, M. (2000). "Ship-in-Bottle" catalyst technology. **Platinum Metals Reviews** 44 (1): 3-14.
- Jackson, S. D., Kelly, G. J., and Webb, G. (1998). Supported metal catalysts; preparation, characterization, and function Part VI. Hydrogenolysis of ethane, propane, n-butane and iso-butane over supported platinum catalysts. **Journal of Catalysis** 176: 225-234.
- Jentoft, R. E., Deutsch, S. E., and Gates, B. C. (1996). Low-cost, heated, and/or cooled flow-through cell for transmission x-ray absorption spectroscopy. **Review of Scientific Instruments** 67 (6): 2111-2112.
- Jongpatiwut, S., Li, Z., Resasco, D. E., Alvarez, W. E., Sughrue, Ed L., and Dodwell, G. W. (2004). Competitive hydrogenation of poly-aromatic hydrocarbons on sulfur-resistant bimetallic Pt-Pd catalysts. **Applied Catalysis A: General** 262: 241-253.
- Kenvin J. C., and White, M. G. (1991). Preparation and characterization of supported mononuclear metal complexes as model catalysts. **Langmuir** 7 (6): 1198-1205.

- Kondarides, D. I., Tomishige, K., Nagasawa, Y., Lee U., and Iwasawa, Y. (1996). Characterization and performance of a [PtMo<sub>6</sub>]/MgO catalyst to alkane-to-alkene conversion. **Journal of Molecular Catalysis A: Chemical** 111: 145-165.
- Koningsberger, D.C., and Gates, B.C. (1992). Nature of the metal-support and metal-promoter interface: Implications of x-ray absorption spectroscopy for catalysis. **Catalysis Letters** 14: 271-277.
- Koningsberger, D. C., Mojet, B. L., van Dorssen, G. E., and Ramaker, D. E. (2000). XAFS spectroscopy; fundamental principles and data analysis. **Topics in Catalysis** 10: 143-155.
- Knözinger, H., and Ratnasamy, P. (1978). Catalytic aluminas: Surface models and characterization of surface sites\*. **Catalysis Reviews: Science and Engineering** 17 (1): 31-70.
- Lai, F., Kim, D-W., Alexeev, O. S., Graham, G. W., Shelef, M., and Gates, B. C. (2000). Temperature-programmed desorption of hydrogen from  $\gamma$ -Al<sub>2</sub>O<sub>3</sub>-supported platinum catalysts with and without tungsten. **Physical Chemistry Chemical Physics** 2: 1997-2003.
- Leclercq, G., Leclercq, L., and Maurel, R. (1976). Hydrogenolysis of saturated hydrocarbons II. Comparative hydrogenolysis of some aliphatic light hydrocarbons on platinum-alumina. **Journal of Catalysis** 44: 68-75.
- Lide, D. R. (ed.). (1993-1994). **CRC Handbook of chemistry and physics** (74<sup>th</sup> ed.). Boca Raton, FL: CRC Press. pp. 9-124-9-126.

- Martins, R. L., Baldanza, M. A. S., and Schmal, M. (2001). An infrared study of NO and CO adsorption on zeolite-supported Ru and Ru-Pt catalysts. **Journal of Physical Chemistry B** 105 (42): 10303-10307.
- Mestl, G. and Knözinger, H. (1997) Vibrational Spectroscopies. In Ertl, G., Knözinger, H., and Weitkamp, J. (eds.). **Handbook of Heterogeneous Catalysis** (Vol. 2: Characterization of solid catalysts, pp. 563). Germany: VCH Verlagsgesellschaft mbH.
- Miura, H., Osawa, M., Suzuki, T., Sugiyama, K., and Matsuda, T. (1982). Synergistic effect in alumina supported Pt-Ru bimetallic cluster catalysis used for dehydrogenation of cyclohexane. **Chemistry Letters** 1803-1804.
- Miura, H., Taguchi, H., Sugiyama, K., Matsuda, T., and Gonzalez, R. D. (1990). The control of metal precursor mobilities as a variable in the preparation of supported Pt-Ru bimetallic clusters: The use of ruthenocene. **Journal of Catalysis** 124: 194-203.
- Nashner, M. S., Frenkel, A. I., Adler, D. L., Shapley, J. R. and Nuzzo, R. G. (1997). Structure characterization of carbon-supported platinum-ruthenium nanoparticles from molecular cluster precursor  $\text{PtRu}_5\text{C}(\text{CO})_{16}$ . **Journal of the American Chemical Society** 119 (33): 7760-7771.
- Nashner, M. S., Frenkel, A. I., Somerville, D., Hills, C. W., Shapley, J. R. and Nuzzo, R. G. (1998). Core shell inversion during nucleation and growth of bimetallic Pt/Ru nanoparticles. **Journal of the American Chemical Society** 120 (32): 8093-8101.

- Neurock, M., and van Santen, R. A. (2000). A first principles analysis of C-H bond formation in ethylene hydrogenation. **Journal of Physical Chemistry B** 104 (47): 11127-11145.
- Niemantsverdriet, J. W. (2000). **Spectroscopy in Catalysis** (2<sup>nd</sup> ed.). Germany: Wiley-VCH.
- O'Grady, W. E., Hagans, P. L., Pandya, K. I., and Maricle, D. L. (2001). Structure of Pt/Ru catalysts using x-ray absorption near edge structure Studies. **Langmuir** 17 (10): 3047-3050.
- Odzak, J. F., Argo, A. M., Lai, F. S., Gates, B. C., Pandya, K., and Feraria, L. (2001). A flow-through x-ray absorption spectroscopy cell for characterization of powder catalysts in the working state. **Review of Scientific Instruments** 72 (10): 3943-3945.
- Passos, F. B., Schmal, M., and Vannice, M. A. (1996). Effect of In and Sn on the adsorption behavior and hydrogenolysis activity of Pt/Al<sub>2</sub>O<sub>3</sub> catalysts. **Journal of Catalysis** 160: 106-117.
- Pierantozzi, R., McQuade, K. J., Gates, B. C., Wolf, M., Knözinger, H., and Ruhmann, W. (1979). Preparation and catalytic properties of polymer- and silica-supported bimetallic clusters. **Journal of the American Chemical Society** 101 (18): 5436-5438.
- Plyuto, Y. V., Babich, I. V., Sharanda, L. F., de Wit, A. M., and Mol, J. C. (1999). Thermolysis of Ru(acac)<sub>3</sub> supported on silica and alumina. **Thermochimica Acta** 335: 87-91.
- Purnell, S. K., Sanchez, K. M., Patrini, R., Chang J. -R., and Gates, B. C. (1994). Genesis and growth of Pt particles on MgO: characterization by x-ray

- absorption spectroscopy and infrared spectroscopy. **Journal of Physical Chemistry** 98 (4): 1205-1212.
- Rajesh, B., Thampi, K. R., Bonard, J. -M., and Viswanathan, B. (2000). Preparation of a Pt-Ru bimetallic system supported on carbon nanotubes. **Journal of Materials Chemistry** 10: 1757-1759.
- Raval, B., (downloaded 2003). Available: <http://feff.phys.washington.edu/~ravel/software/exafs/aboutathena.html>.
- Rehr, J. J., and Albers, R. C. (2000). Theoretical approaches to x-ray absorption fine structure. **Reviews of Modern Physics** 72 (3): 621-654.
- Rehr, J. J., Mustre de leon, J., Zabinsky, S. I., and Albers, R. C. (1991). Theoretical X-ray absorption fine structure standards. **Journal of the American Chemical Society** 113 (14): 5135.
- Renouprez, A. J., Trillat, J. F., Moraweck, B., Massardier, J., and Bergeret, G. (1998). Pd-Mn silica supported catalysts: 1. Formation of the bimetallic particles. **Journal of Catalysis** 179: 390-399.
- Rethwisch, D. G., and Dumesic, J. A. (1986). Effect of metal-oxygen bond strength on properties of oxides. 1. Infrared spectroscopy of adsorbed CO and CO<sub>2</sub>. **Langmuir** 2 (1): 73-79.
- SADTLER Research Laboratories. (1965). **The SADTLER Standard Spectra: High Resolution Spectra of Inorganic and Related Compounds**. Philadelphia: SADTLER Research Laboratories.
- Schlatter, J. C., and Boudart, M. (1972). Hydrogenation of ethylene on supported platinum. **Journal of Catalysis** 24: 482-492.

- Serp, P., Kalck, P., and Feurer, R. (2002). Chemical vapor deposition methods for the controlled preparation of supported catalytic materials. **Chemical Reviews** 102 (9): 3085-3128.
- Shahid, G., and Sheppard, N. (1990). Infrared spectra and the structures of the chemisorbed species resulting from the adsorption of propene and propane on a Pt/SiO<sub>2</sub> catalyst. **Spectrochimica Acta** 46A (6): 999-1010.
- Shelef, M., and Graham, G. W. (1994). Why rhodium in automotive three-way catalysts? **Catalysis Reviews: Science and Engineering** 36 (3): 433-457.
- Shirai, M., Yang, O. -B., Weber, W. A., and Gates, B. C. (1999). Rh-Pt clusters and aggregates on MgO: catalysts for toluene hydrogenation. **Journal of Catalysis** 182 (1): 274-277.
- Sinfelt, J. H. (1983). **Bimetallic Catalysts: Discoveries, Concepts, and Applications**. New York: Wiley.
- Spencer, J. L. (1979). 49. Olefin complexes of platinum. **Inorganic Syntheses** 19: 213-215.
- Stern, E. A. (1993). Number of relevant independent points in x-ray-absorption fine-structure spectra. **Physical Review B** 48 (13): 9825-9827.
- Stievano, L., Wagner, F. E., Calogera, S., Recchia, S., Dossi, C., and Psaro, R. (2000). <sup>119</sup>Sn Mössbauer study and catalytic properties of magnesia-supported platinum-tin catalysts prepared by surface organometallic chemistry. **Studies in Surface Science and Catalysis** 130: 3903-3908.
- Tada, H., Suzuki, F., Ito, S., Akita, T., Tanaka, K., Kawahara, T., and Kobayashi, H. (2002). Au-core/Pt-shell bimetallic cluster-loaded TiO<sub>2</sub> 1. Adsorption of

organosulfur compound. **Journal of Physical Chemistry B** 106 (34): 8714-8720.

Takasu, Y., Itaya, H., Iwazaki, T., Miyoshi, R., Ohnuma, T., Sugimoto, W., and Murakami, Y. (2001). Size effects of ultrafine Pt-Ru particles on the electrocatalytic oxidation of methanol. **Chemical Communications** (4): 341-342.

The Coblenz Society. (1970). **Joint Committee on Atomic and Molecular Physical Data Evaluated Infrared Reference Spectrum**. Norwalk.

Vaarkamp, M., and Koningsberger, D. C. (1997). X-ray absorption spectroscopy (XANES, EXAFS) in catalysis: Experimental methods and data analysis. In Ertl, G., Knozinger, H.G., and Weitkamp, J. (eds.). **Handbook of Heterogeneous Catalysis** (Vol. 2: Characterization of solid catalysts. pp 475-493). Germany: Wiley-VCH.

Walter, C. G., Coq, B., Figueras, F., and Boulet, M. (1995). Competitive reaction of methylcyclohexane and n-hexane over alumina-supported platinum, iridium and ruthenium catalysts. **Applied Catalysis A: General** 133: 95-102.

Wang, X., Sigmon, S. M., Spivey, J. J., and Lamb, H. H. (2004). Supported and particle size effects on direct NO decomposition over platinum. **Catalysis Today** 96: 11-20.

Weber, W. A., Yang, O. -B., Shirai, M., and Gates, B. C. (1999). Corrosive chemisorption of  $[\text{PtRh}_5(\text{CO})_{15}]^-$  on MgO. **Langmuir** 15 (6): 2234-2236.

White, L. (2000). Bimetallic Pt/Ru complexes as catalysts for the electrooxidation of methanol. **Inorganic Chemistry** 39 (17): 3942-3944.

- Womes, M., Lynch, J., Bazin, D., Le Peltier, F., Mosin, S., and Didillon, B. (2003). Interaction between Pt(acac)<sub>2</sub> and alumina surfaces studied by XAS. **Catalysis Letters** 85 (1-2): 25-31.
- Wong, T. C., Chang, L. C., Haller, G. L., Oliver, J. A., Scaife, N. R., and Kemball, C. (1984). Reactions of *n*-butane and 2, 2-dimethylpropane on silica-supported Rh-Pt bimetallic catalysts. **Journal of Catalysis** 87: 389-397.
- Xu, Z., Kawi, S., Rheingold, A. L., and Gates, B. C. (1994). Surface synthesis of [PtRh<sub>5</sub>(CO)<sub>15</sub>]<sup>-</sup> on MgO. **Inorganic Chemistry** 33 (19): 4415-4417.
- Xu, Z., Rheingold, A. L., and Gates, B. C. (1993). [Pt<sub>6</sub>(CO)<sub>12</sub>]<sup>2-</sup> and [Pt<sub>9</sub>(CO)<sub>18</sub>]<sup>2-</sup> supported on magnesia: synthesis and spectroscopic characterization. **Journal of Physical Chemistry** 97 (37): 9465-9469.
- Yang, O. -B., Shirai, M., Weber, W. A., and Gates, B. C. (1998). Decarbonylation of MgO-supported PtRh<sub>5</sub> clusters characterized by infrared and extended x-ray absorption fine structure spectroscopies. **Journal of Physical Chemistry B** 102(44): 8771-8781.

## **APPENDICES**

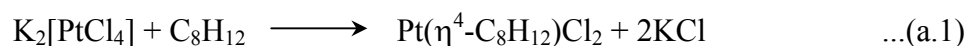
## APPENDIX A

### SYNTHESIS AND CHARACTERIZATION OF

### Bis[1,2,5,6- $\eta$ -(1,5-CYCLOOCTADIENE)]PLATINUM

#### A.1 Synthesis of dichloro[1,2:5,6- $\eta$ -(1,5-cyclooctadiene)]platinum

Pt( $\eta^4$ -C<sub>8</sub>H<sub>12</sub>)Cl<sub>2</sub> or Pt(cod)Cl<sub>2</sub> was prepared by methods modified from three different literatures (Drew and Doyle, 1972; Clark and Manzer, 1973; Herrman and Salzer, 1996) from a reaction between K<sub>2</sub>[PtCl<sub>4</sub>] and C<sub>8</sub>H<sub>12</sub> in acidic conditions as equation a.1, and H<sub>2</sub>PtCl<sub>6</sub>.xH<sub>2</sub>O and C<sub>8</sub>H<sub>12</sub>.



##### A.1.1 Method I

K<sub>2</sub>[PtCl<sub>4</sub>] (2.5 g, Alfa, 46.60% Pt; and Strem, 46.84% Pt) was dissolved in 40 mL of distilled water and filtered to remove undissolved portions. CH<sub>3</sub>COOH (60 mL, Fisher, GR ACS) and C<sub>8</sub>H<sub>12</sub> (2.5 mL, Alfa, 99% purity, density 0.8803 g/mL) were added into the solution of K<sub>2</sub>[PtCl<sub>4</sub>]. The solution was vigorously stirred and heated to 90°C until the fine light yellow crystalline needles were slowly formed. The crystalline needles were filtered on a glass filter plate and washed with 20 mL portions of distilled water and CH<sub>3</sub>CH(OH)CH<sub>3</sub> (EM, 99.5% purity, GR ACS). The product was dried in a hot air oven at 120°C for 1 hour and characterized by IR spectroscopy.

### A.1.2 Method II

$\text{H}_2\text{PtCl}_6 \cdot x\text{H}_2\text{O}$  (5.0 g, Matthey Bishop) was dissolved in 15 mL of  $\text{CH}_3\text{COOH}$  and heated to  $75^\circ\text{C}$ .  $\text{C}_8\text{H}_{12}$  was added to the hot solution and reaction flask was swirled gently. After reaction was cooled to room temperature, it was diluted with 50 mL of water and left to stand at room temperature for 1 hour. The crude product was filtered and washed with 50 mL of water, and then 100 mL of petroleum ether. The crude product was dissolved in 200 mL of  $\text{CH}_2\text{Cl}_2$  and heated until it boiled for 5 min. The solution was cooled to room temperature, and 5.0 g of chromatographic-grade silica gel was added to the solution. The mixture was swirled, and allowed silica gel to settle. Additional silica gel 1 g portions were added to the supernatant liquid until it was colorless. The supernatant liquid was filtered and the residue was washed with two 50 mL portions of  $\text{CH}_2\text{Cl}_2$ . The filtrate was evaporated until the product was crystallized. The solution was heated again and poured into 200 mL of petroleum ether. The white precipitate was filtered and washed with 50 mL of petroleum ether and dried. The product could be recrystallized by dissolving in 150 mL boiling  $\text{CH}_2\text{Cl}_2$  and evaporated until the product crystallized to white macroscopic crystals.

The percentage yields of  $\text{Pt}(\text{cod})\text{Cl}_2$  in this work were 63-85%.  $\text{Pt}(\text{cod})\text{Cl}_2$  was light yellow, needle-like, air-stable solid and gave IR spectrum at 1381 (w), 1207 (sh), 1178 (sh) and 1078 (vs)  $\text{cm}^{-1}$ .

## A.2 Synthesis of dilithiated cyclooctatetraene

$\text{Li}_2\text{C}_8\text{H}_8$  was prepared by the methods described by Spencer (1979) from a direct reaction between Li and  $\text{C}_8\text{H}_8$  in  $(\text{C}_2\text{H}_5)_2\text{O}$  as equation a.2.



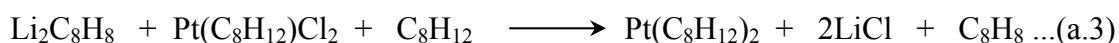
Prior to use,  $(\text{C}_2\text{H}_5)_2\text{O}$  (Acros) was dried over molecular sieve 4A and purged with  $\text{N}_2$  (99.99%) to remove  $\text{O}_2$ . In Ar glovebox, Li wire (0.7 g, Aldrich) was cut into small pieces and suspended in oxygen-free  $(\text{C}_2\text{H}_5)_2\text{O}$  (150 mL) at  $0^\circ\text{C}$ .  $\text{C}_8\text{H}_8$  (2.80 mL, Aldrich, 97%) was added into the mixture and left stirred for 16 hours. After the precipitates were settle, the aliquot of orange solution was checked for molarity of  $\text{Li}_2\text{C}_8\text{H}_8$  solution by hydrolysis (see section A.2.1).

### A.2.1 Molarity check (Total alkali)

A secondary standard solution of 0.1 M HCl was prepared and titrated with diluted NaOH solution which was standardized with tartaric acid. The hydrolysis of  $\text{Li}_2\text{C}_8\text{H}_8$  solution was carried out by transferred 3.00 mL of  $\text{Li}_2\text{C}_8\text{H}_8$  solution into 10.00 mL of  $(\text{C}_2\text{H}_5)_2\text{O}$ , follow by adding 10.00 mL of distilled  $\text{H}_2\text{O}$ . The hydrolyzed solution was titrated with 0.1 M HCl solution with bromothymol blue indicator.

## A.3 Synthesis of bis[1,2,5,6- $\eta$ -(1,5-cyclooctadiene)]platinum

$\text{Pt}(\text{cod})_2$  was synthesized under inert atmosphere by the method described by Spencer (1979) from a reaction between  $\text{Li}_2\text{C}_8\text{H}_8$ ,  $\text{Pt}(\text{C}_8\text{H}_{12})\text{Cl}_2$ , and  $\text{C}_8\text{H}_{12}$  as equation a.3



$\text{Pt}(\text{cod})\text{Cl}_2$  (3.7 g) was slurry with 15 mL of  $\text{C}_8\text{H}_{12}$  at  $-40^\circ\text{C}$ . The freshly prepared solution of  $\text{Li}_2\text{C}_8\text{H}_8$  (about 42 mL) was added dropwise to the vigorously stirred slurry over a period of 45 minutes and the temperature was kept between  $-50$

and  $-30^{\circ}\text{C}$ . The cream-colored mixture was warmed up to  $0^{\circ}\text{C}$  within 30 minutes after complete addition.  $(\text{C}_2\text{H}_5)_2\text{O}$ , excess  $\text{C}_8\text{H}_{12}$  and  $\text{C}_8\text{H}_8$  were removed by evacuation ( $\approx 10^{-3}$  Torr) and the pale-tan solid product was extracted with five 50 mL portions of toluene at  $20^{\circ}\text{C}$  under inert atmosphere. The extract solution was filtered through a column containing activated alumina (EM, activity grade II-III) under inert atmosphere. The alumina column was washed with 50 mL of toluene. The filtrate and washing solution were combined and evacuated at  $20^{\circ}\text{C}$  to a volume of 15 mL. The mother liquor was removed from the off-white precipitates product and washed with four 5 mL portions of petroleum ether.  $\text{Pt}(\text{cod})_2$  product was dried under vacuum and characterized by IR spectroscopy.

The percentage yields of  $\text{Pt}(\text{cod})_2$  in this work were 7-44 %.  $\text{Pt}(\text{cod})_2$  gave IR spectrum at 3010 (s), 2925 (s), 2864 (s), 2816 (s), 1464 (s), 1460 (s), 1429 (s) and 1323 (s)  $\text{cm}^{-1}$ .

**APPENDIX B**

**ARTICLE IN PROCEEDING OF THE 10<sup>TH</sup> ASIAN PACIFIC  
CONFEDERATION OF CHEMICAL ENGINEERING (APCChE)  
CONGRESS 2004 (ORAL PRESENTATION)**

## Characterization of Alumina-Supported Pt-Ru Catalyst and Its Activities for Ethylene Hydrogenation and *n*-Butane Hydrogenolysis

On-line Number 1078

Saowapa Chotisuwan<sup>1</sup>, Jatuporn Wittayakun<sup>1</sup>, and Bruce C. Gates<sup>2</sup>

<sup>1</sup>School of Chemistry, Suranaree University of Technology, Nakhon Ratchasima, Thailand

<sup>2</sup>Department of Chemical Engineering and Materials Science, University of California, Davis, CA, USA

### ABSTRACT

Gamma-alumina supported bimetallic Pt-Ru catalyst (Pt-Ru/ $\gamma$ -Al<sub>2</sub>O<sub>3</sub>) was prepared by impregnation of Pt<sub>3</sub>Ru<sub>6</sub>(CO)<sub>21</sub>( $\mu_3$ -H)( $\mu$ -H)<sub>3</sub> cluster in CH<sub>2</sub>Cl<sub>2</sub> solution on  $\gamma$ -Al<sub>2</sub>O<sub>3</sub> and decarbonylated in helium at 300°C. Changes of the cluster before and after decarbonylation, monitored by infrared (IR) spectroscopy indicated that Pt<sub>3</sub>Ru<sub>6</sub>(CO)<sub>21</sub>( $\mu_3$ -H)( $\mu$ -H)<sub>3</sub> adsorbed strongly to surface of  $\gamma$ -Al<sub>2</sub>O<sub>3</sub> and could not be extracted from support by CH<sub>2</sub>Cl<sub>2</sub> solvent. In addition, Pt-Ru/ $\gamma$ -Al<sub>2</sub>O<sub>3</sub> was characterized by extended X-ray absorption fine structure (EXAFS) spectroscopy which confirmed that Pt and Ru were still intact after decarbonylation. Some changes in the cluster bonding were likely caused by cluster-support interaction. The catalyst was active for ethylene hydrogenation and *n*-butane hydrogenolysis. The temperature dependence of both reactions gave apparent activation energy of 8.4 ± 0.1 and 30.9 ± 0.1 kcal/mol, respectively.

### KEYWORDS

Bimetallic catalyst, Pt-Ru, alumina, ethylene hydrogenation, *n*-butane hydrogenolysis

### INTRODUCTION

Supported bimetallic catalysts have been reported in many applications, for instance, Pt-Re, Pt-Sn and Pt-Ir for naphtha reforming (Antos, et al., 1995), and Pt-Rh for auto exhaust conversion (Shelef and Graham, 1994). An incorporation of second metal to a supported platinum-group metal improves the catalyst performance and stability. In general, the simplest preparation method for bimetallic catalyst is by coimpregnation followed by high-temperature reduction. However, this conventional method gives nonuniform metal structure and usually with large particles on support. For better control of metal particles, bimetallic metal cluster with metal-metal bonds could be used as catalyst precursors to provide well-defined and/or highly dispersed bimetallic structure on support. In a bimetallic cluster consists of a noble metal and oxophilic metal combination, removal of ligands from adsorbed precursor gives the clusters of noble metals in clusters of oxides of the oxophilic metal which bonds strongly to oxide support and stabilized the dispersion of the metals (Alexeev, et al., 1996 and 2002).

The goal of this work was to prepare and characterize Pt-Ru/ $\gamma$ -Al<sub>2</sub>O<sub>3</sub> catalysts from a bimetallic cluster precursor, Pt<sub>3</sub>Ru<sub>6</sub>(CO)<sub>21</sub>( $\mu_3$ -H)( $\mu$ -H)<sub>3</sub> which contained Pt-Ru bond and its CO ligands could be easily removed by thermal treatment in an inert atmosphere. This precursor is in the same family as Pt<sub>2</sub>Ru<sub>4</sub>(CO)<sub>18</sub> which was successfully used as a catalyst precursor on  $\gamma$ -Al<sub>2</sub>O<sub>3</sub> by Alexeev and coworkers (2002).

The characterization methods for Pt-Ru/ $\gamma$ -Al<sub>2</sub>O<sub>3</sub> included infrared (IR), and extended X-ray absorption fine structure (EXAFS) spectroscopy. The Pt-Ru/ $\gamma$ -Al<sub>2</sub>O<sub>3</sub> was tested for ethylene

hydrogenation and *n*-butane hydrogenolysis. The first reaction is simple and widely used to test catalytic activity, while the latter reaction is sensitive to surface structure and can be used as a probe reaction.

## MATERIALS AND METHODS

The organometallic syntheses and supported catalyst preparations were performed in an argon drybox to prevent contact with moisture and air. The  $\gamma$ -Al<sub>2</sub>O<sub>3</sub> powder (Degussa, BET surface area 100 m<sup>2</sup>/g) was calcined in flowing O<sub>2</sub> at 400°C for 2 h and evacuated (pressure  $\approx 10^{-3}$  Torr) for 14 h before use. Hexane, and pentane (Fisher Scientific) were distilled over Na/benzophenone and purged with N<sub>2</sub> to eliminate oxygen. Gases (He and H<sub>2</sub>) were purified by passage through traps containing reduced Cu/Al<sub>2</sub>O<sub>3</sub> and zeolite particles to remove oxygen and water. Trace of water in dichloromethane was removed by molecular sieve 4Å. The Pt<sub>3</sub>Ru<sub>6</sub>(CO)<sub>21</sub>( $\mu_3$ -H)( $\mu$ -H)<sub>3</sub> was synthesized by a procedure described elsewhere (Adams, et al., 1994), and separated from other products by extraction with cold *n*-pentane. The cluster structure in CH<sub>2</sub>Cl<sub>2</sub> solution was confirmed by IR spectroscopy.

### Preparation of Pt-Ru/ $\gamma$ -Al<sub>2</sub>O<sub>3</sub> catalysts

The Pt-Ru/ $\gamma$ -Al<sub>2</sub>O<sub>3</sub> catalyst containing 1 wt% Pt and 1 wt% Ru was prepared by slurring of Pt<sub>3</sub>Ru<sub>6</sub>(CO)<sub>21</sub>( $\mu_3$ -H)( $\mu$ -H)<sub>3</sub> in CH<sub>2</sub>Cl<sub>2</sub> over  $\gamma$ -Al<sub>2</sub>O<sub>3</sub> powder for 1 day and evacuated for 1 day.

### Catalyst characterization

**Infrared Spectroscopy.** IR spectra of  $\gamma$ -Al<sub>2</sub>O<sub>3</sub> impregnated with Pt<sub>3</sub>Ru<sub>6</sub>(CO)<sub>21</sub>( $\mu_3$ -H)( $\mu$ -H)<sub>3</sub> were recorded before and after drying by a Bruker IFS-66v spectrometer with a resolution of 4 cm<sup>-1</sup>. Each sample was scanned 64 times and the signal averaged. For solid, small amount of powder samples were slightly pressed into semitransparent between KBr pellets placed in a cell in a glovebox.

**EXAFS Spectroscopy.** EXAFS experiments were performed at X-ray beamline X18B at the National Synchrotron Light Source, Brookhaven National Laboratory, New York, USA. The storage ring energy was 2.5 GeV and the ring current was in the range 80-220 mA. Sample wafers for transmission EXAFS spectroscopy in a special designed holder (Jentoft, et al., 1996) were cooled to nearly liquid nitrogen temperature before scanning at Pt L<sub>III</sub> edge (11564 eV) and Ru K edge (22117 eV) in transmission mode and integrating for 1 s at each energy in the range from 200 eV below the absorption edge to 975 eV beyond the edge. A double crystal monochromator Si(111) was used.

**EXAFS Data Analysis.** Because of the difference in energy between Pt L<sub>III</sub> edge (11564 eV) and Ru K edge (22117 eV), EXAFS data were collected at individual Pt L<sub>III</sub> and Ru K absorption edge and analyzed with theoretical reference files. The interaction of Pt-Pt, Pt-Ru, Pt-O<sub>support</sub>, Ru-Ru, Ru-Pt, and Ru-O<sub>support</sub> bond were analyzed with phase shift and backscattering amplitudes calculated by FEFF software (Rehr, et al, 1991). The EXAFS data processing was carried out with Athena software (Raval, 2004). The final normalized EXAFS function from ATHENA software for each edge of each sample was obtained from the average of four scans. The EXAFS parameters were extracted from the raw data with the EXAFSPAK software (George, et al., 2000). The fitting were done in *R* space and *k* space with application of *k*<sup>0</sup>, *k*<sup>1</sup>, and *k*<sup>3</sup> weightings.

Raw EXAFS data obtained at Pt L<sub>III</sub> edge of Pt-Ru/ $\gamma$ -Al<sub>2</sub>O<sub>3</sub> prepared from Pt<sub>3</sub>Ru<sub>6</sub>(CO)<sub>21</sub>( $\mu_3$ -H)( $\mu$ -H)<sub>3</sub> after decarbonylation, were Fourier transformed over the ranges  $3.25 < k < 14.25$  with  $k^3$  weighting and no phase correction ( $k$  = the wave vector). The main contributions were isolated by backward Fourier transformation in the ranges  $0.0 < r < 5.0$  Å ( $r$  = interatomic distance from the absorber atom).

The raw data obtained at Ru K edge of  $\gamma$ -Al<sub>2</sub>O<sub>3</sub>-supported Pt<sub>3</sub>Ru<sub>6</sub>(CO)<sub>21</sub>( $\mu_3$ -H)( $\mu$ -H)<sub>3</sub> after decarbonylation, were analyzed over the ranges  $3.40 < k < 14.45$  and  $0.0 < r < 4.0$  Å.

The statistically justified number of free parameters estimated from Nyquist theorem for data obtained at Pt L<sub>III</sub> and Ru K edge of sample after decarbonylation were about 36 and 29, respectively.

## Catalyst Testing

**Ethylene Hydrogenation Reaction.** This study was carried out in a stainless steel U-tubed flow reactor at atmospheric pressure from -75 to -20°C. The sample was pretreated with He at 300°C for 2h prior to reaction testing. Typically, 10 to 20 mg of catalyst was diluted with 600 mg of inert  $\alpha$ -Al<sub>2</sub>O<sub>3</sub>, loaded into the reactor, and cooled to desired temperature before a gas mixture consisting of H<sub>2</sub>, ethylene, and balance He was flowed into reactor with 200 ml (NTP)/min flow rate. The effluent gas mixture was analyzed with an online gas chromatograph (Hewlett-Packard HP 6890) equipped with an Al<sub>2</sub>O<sub>3</sub> capillary column (50 m x 0.53 mm x 15.0 micron film thickness), and a flame ionization detector. Testing conditions included  $P_{\text{hydrogen}} = 80$  Torr,  $P_{\text{ethylene}} = 40$  Torr, and temperature varied from -75 to -20°C.

***n*-Butane Hydrogenolysis Reaction.** This test was performed in a quartz tube flow reactor at atmospheric pressure from 190 to 260°C. The sample was decarbonylated in the conditions as above. Typically, 25 - 30 mg of decarbonylated sample was diluted with inert  $\alpha$ -Al<sub>2</sub>O<sub>3</sub>, loaded into reactor, and heated to desired temperature before exposed to a flow of a gas mixture consisting of H<sub>2</sub>, *n*-butane, and balance He with 100 ml (NTP)/min flow rate. The effluent gas mixture was analyzed with the same online gas chromatograph. Testing conditions were:  $P_{\text{hydrogen}} = 540$  Torr,  $P_{\text{n-butane}} = 60$  Torr, and temperature varied from 190 to 260°C.

## RESULTS AND DISCUSSION

### Evidence of interaction of precursors with $\gamma$ -Al<sub>2</sub>O<sub>3</sub> from IR Spectroscopy

Figure 1 showed an IR spectrum in  $\nu_{\text{OH}}$  and  $\nu_{\text{CO}}$  regions of  $\gamma$ -Al<sub>2</sub>O<sub>3</sub> before and after interaction with Pt<sub>3</sub>Ru<sub>6</sub>(CO)<sub>21</sub>( $\mu_3$ -H)( $\mu$ -H)<sub>3</sub> cluster compared with that of the cluster dissolved in CH<sub>2</sub>Cl<sub>2</sub>. The bands at 3786, 3728 and 3672 cm<sup>-1</sup> of bared  $\gamma$ -Al<sub>2</sub>O<sub>3</sub> (spectrum 1 in Figure 1A) were assigned to different types of isolated hydroxyl groups (Alexeev, et al., 2002). The peak at 3786 cm<sup>-1</sup> was assigned to type Ib, (Al<sup>3+</sup><sub>oct</sub>)OH while the peak at 3728 cm<sup>-1</sup> was assigned to type IIa, (Al<sup>3+</sup><sub>tet</sub>)(OH) (Al<sup>3+</sup><sub>oct</sub>). (Mestl and Knözinger, 1997). The broad at 3579 cm<sup>-1</sup> represents hydrogen-bonded OH groups (Alexeev, et al., 2002 and references therein). The spectrum of vacuum-dried mixture of Pt<sub>3</sub>Ru<sub>6</sub>(CO)<sub>21</sub>( $\mu_3$ -H)( $\mu$ -H)<sub>3</sub> and  $\gamma$ -Al<sub>2</sub>O<sub>3</sub> at 25°C showed only two broad peaks at 3679 and 3587 cm<sup>-1</sup> in the hydroxyl region ((spectrum 2 in Figure 1A)). The change in hydroxyl peaks indicated that they involved in the interaction with the cluster.

Four peaks in carbonyl range were observed at 2081, 2065, 2048 and 2023 cm<sup>-1</sup> for Pt<sub>3</sub>Ru<sub>6</sub>(CO)<sub>21</sub>( $\mu_3$ -H)( $\mu$ -H)<sub>3</sub> in CH<sub>2</sub>Cl<sub>2</sub> solution (spectrum 2 in Figure 1B). After it was impregnated on

$\gamma$ -Al<sub>2</sub>O<sub>3</sub> and dried in vacuum, carbonyl peaks were still present at 2137, 2073, 2038 and 2011 cm<sup>-1</sup> (spectrum 2 in Figure 1B). The small peak at 2137 cm<sup>-1</sup> was likely due to monometallic complex containing terminal carbonyl from cluster decomposition, such as Pt<sup>m+</sup>-CO and/or Ru-CO adsorbed on  $\gamma$ -Al<sub>2</sub>O<sub>3</sub> (Hadjiivanov and Vayssilov, 2002). Whereas the other three peaks corresponded to carbonyl peaks in the cluster interacting with alumina support. The frequency was shifted to lower value due to weakening of C-O bond after interacting with hydroxyl group of alumina. This interaction was suspected because the change of hydroxyl bands was coincident with the shift of carbonyl bands in the cluster.

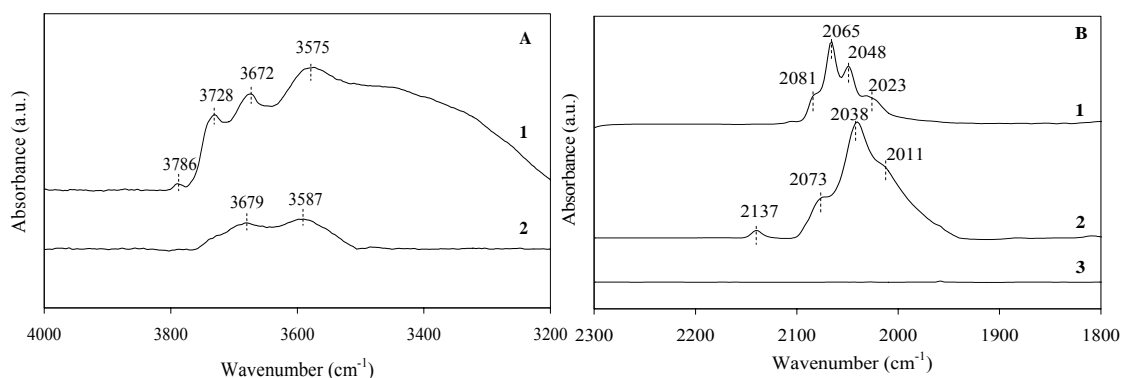


**Figure 1. (A) IR spectrum in  $\nu_{\text{OH}}$  region: (1) Bared  $\gamma$ -Al<sub>2</sub>O<sub>3</sub> calcined at 400°C for 14 h; (2) dried Pt<sub>3</sub>Ru<sub>6</sub>(CO)<sub>21</sub>( $\mu_3$ -H)( $\mu$ -H)<sub>3</sub> on  $\gamma$ -Al<sub>2</sub>O<sub>3</sub>. (B) Infrared in  $\nu_{\text{CO}}$  regions: (1) Pt<sub>3</sub>Ru<sub>6</sub>(CO)<sub>21</sub>( $\mu_3$ -H)( $\mu$ -H)<sub>3</sub> dissolved in dichloromethane; (2) Pt<sub>3</sub>Ru<sub>6</sub>(CO)<sub>21</sub>( $\mu_3$ -H)( $\mu$ -H)<sub>3</sub> adsorbed on  $\gamma$ -Al<sub>2</sub>O<sub>3</sub> after removal of solvent; (3) sample after decarbonylation with He at 300 °C for 2 h.**

An attempt to extract the cluster Pt<sub>3</sub>Ru<sub>6</sub>(CO)<sub>21</sub>( $\mu_3$ -H)( $\mu$ -H)<sub>3</sub> from  $\gamma$ -Al<sub>2</sub>O<sub>3</sub> with CH<sub>2</sub>Cl<sub>2</sub> was not successful because the cluster adsorbed strongly on alumina surface. There were two possible interactions between carbonyl ligands and  $\gamma$ -Al<sub>2</sub>O<sub>3</sub> support: (1) between carbonyl oxygen and surface hydroxyl proton to form hydrogen-bonding; (2) between carbonyl oxygen and Lewis acid sites (Al<sup>3+</sup> ions). After treating the dried mixture with He at 300°C for 2 h, all  $\nu_{\text{CO}}$  bands disappeared, indicating complete decarbonylation. Carbonylation was a conversion of coordinated CO ligands with basic surface sites (O<sup>2-</sup> or OH<sup>-</sup>) to carbon dioxide (Alexeev, et al., 2002).

The interaction between carbonyl ligands and surface hydroxyl groups may be formed by nucleophilic displacement of carbonyl which is energetically favored for  $\gamma$ -Al<sub>2</sub>O<sub>3</sub>-supported metal carbonyls. This decarbonylation was resulted from cleavage of CO ligands of metal carbonyl and formed metal-O<sub>support</sub> bonds (Myllyoja, et al., 1999) and caused a formation of anionic metal carbonyl clusters (Alexeev, et al., 2002). Typically, the formation of anionic metal carbonyl clusters shows the shifting of terminal  $\nu_{\text{CO}}$  bands to lower frequencies (Gates, 1998). However, IR data does not show any anionic species of metal carbonyl cluster on support. However, it was possible that some of surface species after contact  $\gamma$ -Al<sub>2</sub>O<sub>3</sub> with Pt<sub>3</sub>Ru<sub>6</sub>(CO)<sub>21</sub>( $\mu_3$ -H)( $\mu$ -H)<sub>3</sub> were the fragments of Pt<sub>3</sub>Ru<sub>6</sub>(CO)<sub>21</sub>( $\mu_3$ -H)( $\mu$ -H)<sub>3</sub> that had been decarbonylated and coordinated to oxygen atoms on  $\gamma$ -Al<sub>2</sub>O<sub>3</sub> surface.

## Characterization of alumina Pt-Ru catalysts by EXAFS Spectroscopy

EXAFS data of Pt-Ru/ $\gamma$ -Al<sub>2</sub>O<sub>3</sub> give information of local structure such as coordination number of absorbing atom and interatomic distances between absorbing atom and scattering atoms. The EXAFS data analysis of these samples at Pt L<sub>III</sub> edge and Ru K edge were summarized in Table 1. The estimated accuracies of coordination number ( $N$ ), distance ( $R$ ), Debye-Waller factor ( $\Delta\sigma^2$ ), and inner potential ( $\Delta E_0$ ) are as follows:  $\pm 20\%$ ,  $\pm 1\%$ ,  $\pm 30\%$ ,  $\pm 10\%$ , respectively. After decarbonylation in He at 300°C for 2 h, the EXAFS results of Pt-Ru prepared from cluster precursor gave a Pt-Pt interatomic distance of  $2.64 \pm 0.01$  Å which was nearly similar to that of Pt<sub>3</sub>Ru<sub>6</sub>(CO)<sub>21</sub>( $\mu_3$ -H)( $\mu$ -H)<sub>3</sub>, average 2.63 Å. (Adams, et al, 1994). The Pt-Pt had coordination number of  $1.7 \pm 0.2$ , lower than 2.0 in the precursor. The Pt-Ru contribution in Pt-Ru/ $\gamma$ -Al<sub>2</sub>O<sub>3</sub> had interatomic distance of  $2.68 \pm 0.01$  Å, slightly shorter than the average 2.80 Å in the precursor in crystalline form. The coordination number of the first shell of Pt-Ru contribution compared with that of precursor decreased from 4.0 to  $2.2 \pm 0.1$ . The Pt-O<sub>s</sub> contribution was found at  $2.08 \pm 0.01$  Å for interatomic distance and coordination number of  $2.2 \pm 0.1$ .

The EXAFS results at Ru K edge showed Ru-Ru distance of  $2.62 \pm 0.01$  Å, decreased from 3.04 Å of Ru-Ru distance in the precursor. The shorter distance could be resulted from the loss of bridging hydride ligands bonded to Ru<sub>3</sub> faces after decarbonylation. The EXAFS results showed nearly the same of Ru-Ru coordination number for cluster adsorbed on support after decarbonylation and that for precursor in crystalline form, 2.4 and  $2.1 \pm 0.1$ , respectively. The average coordination numbers of Ru-Pt contribution of cluster after decarbonylation decreased from 2.0 to  $1.0 \pm 0.1$ . EXAFS results confirmed metal-metal framework remained intact on alumina support after decarbonylation, the cluster-support interaction was not strong enough to break cluster framework.

**Table 1. Summary of EXAFS data of  $\gamma$ -Al<sub>2</sub>O<sub>3</sub>-supported Pt<sub>3</sub>Ru<sub>6</sub>(CO)<sub>21</sub>( $\mu_3$ -H)( $\mu$ -H)<sub>3</sub> after decarbonylation with He at 300°C for 2 h.**

Edge	Shell	$N$	$R$ (Å)	$10^3 \times \Delta\sigma^2$ (Å <sup>2</sup> )	$\Delta E_0$ (eV)
Pt L <sub>III</sub>	Pt-Pt	$1.7 \pm 0.2$	$2.64 \pm 0.01$	$3.0 \pm 0.7$	$-4.5 \pm 0.8$
	Pt-Ru	$2.2 \pm 0.1$	$2.68 \pm 0.01$	$4.2 \pm 0.5$	$6.0 \pm 0.3$
	Pt-O <sub>support</sub>				
	Pt-O <sub>s</sub>	$2.2 \pm 0.1$	$2.08 \pm 0.01$	$11.3 \pm 1.4$	$8.7 \pm 0.6$
Ru K	Pt-O <sub>l</sub>	$0.8 \pm 0.1$	$2.99 \pm 0.02$	$-2.3 \pm 2.0$	$-7.6 \pm 1.4$
	Ru-Ru	$2.1 \pm 0.1$	$2.62 \pm 0.01$	$4.1 \pm 0.3$	$-13.3 \pm 0.3$
	Ru-Pt	$1.0 \pm 0.1$	$2.68 \pm 0.01$	$4.5 \pm 0.7$	$-11.5 \pm 1.0$
	Ru-O <sub>support</sub>				
	Ru-O <sub>s</sub>	$1.2 \pm 0.1$	$2.06 \pm 0.01$	$10.9 \pm 1.7$	$4.1 \pm 0.7$
	Ru-O <sub>l</sub>	$2.1 \pm 0.1$	$2.89 \pm 0.01$	$0.1 \pm 0.7$	$11.8 \pm 0.2$
	Ru-O <sub>l2</sub>	$1.4 \pm 0.2$	$3.32 \pm 0.02$	$5.2 \pm 2.8$	$6.2 \pm 0.6$

Notation: the subscript s and l refer to short and long, respectively

## Catalyst Testing for Ethylene Hydrogenation and *n*-Butane Hydrogenolysis

The Pt-Ru/ $\gamma$ -Al<sub>2</sub>O<sub>3</sub> prepared from the cluster precursor was treated by decarbonylation in He at 300°C for 2h prior to test catalytic reactions. The raw data were collected at steady-state operation and represented in units of mol of ethylene converted (g catalyst·s)<sup>-1</sup> (Figure 2A and 2B). Figure 2A shows Arrhenius plot of ethylene hydrogenation over  $\gamma$ -Al<sub>2</sub>O<sub>3</sub>-supported Pt<sub>3</sub>Ru<sub>6</sub>(CO)<sub>21</sub>( $\mu_3$ -H)( $\mu$ -H)<sub>3</sub> under catalysis condition of  $P_{\text{ethylene}} = 40$  Torr,  $P_{\text{hydrogen}} = 80$  Torr; total feed flow rate: 200 ml (NTP)/min; catalyst mass: 10 mg, 1 wt% Pt and 1 wt% Ru, and temperature = -75 to -20°C.

The result for these reactions was summarized in Table 2. The catalytic activity of ethylene hydrogenation in terms of turn over frequency (TOF) at  $-40^{\circ}\text{C}$  of Pt-Ru/ $\gamma\text{-Al}_2\text{O}_3$  catalysts prepared from  $\text{Pt}_3\text{Ru}_6(\text{CO})_{21}(\mu_3\text{-H})(\mu\text{-H})_3$  was  $6.5 \times 10^{-4} \pm 0.1$ . The apparent activation energy obtained from temperature dependence of ethylene hydrogenation reaction for this catalyst was  $8.4 \pm 0.1$  kcal/mol. This value is comparable to that reported for ethylene hydrogenation catalyzed by Pt catalysts, and Ru catalysts consisting of metallic particles on metal oxide supports (Dorling, et al., 1969; Hwang, et al., 2003).

From this catalytic data, it can be concluded that this catalyst prepared from the molecular precursor is very active for ethylene hydrogenation, which is structural insensitive. In addition, there was no sign of catalyst deactivation during the test period.

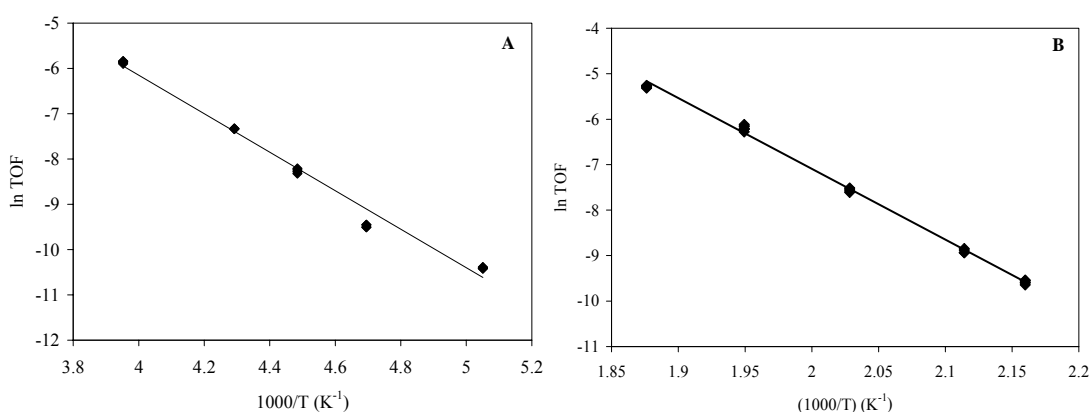


**Figure 2.** Arrhenius plot for (A) ethylene hydrogenation catalyzed by PtRu/ $\gamma\text{-Al}_2\text{O}_3$  prepared from  $\text{Pt}_3\text{Ru}_6(\text{CO})_{21}(\mu_3\text{-H})(\mu\text{-H})_3$ ; reaction condition:  $P_{\text{ethylene}} = 40$  Torr,  $P_{\text{hydrogen}} = 80$  Torr; total feed flow rate: 200 ml (NTP)/min; catalyst mass: 10 mg, 1 wt% Pt and 1 wt% Ru. (B) *n*-Butane hydrogenolysis; reaction condition:  $P_{n\text{-butane}} = 60$  Torr,  $P_{\text{hydrogen}} = 540$  Torr; total feed flow rate: 100 ml (NTP)/min; catalyst mass: 26 mg, 1 wt% Pt and 1 wt% Ru.

**Table 2.** Ethylene hydrogenation and *n*-butane hydrogenolysis catalyzed by  $\gamma\text{-Al}_2\text{O}_3$ -supported PtRu catalysts treated in He at  $300^{\circ}\text{C}$  for 2 h

Ethylene hydrogenation		<i>n</i> -Butane hydrogenolysis				
Activity	Apparent activation	Activity	Apparent activation	Product distribution (%) <sup>d</sup>		
TOF $\times 10^4$ (s <sup>-1</sup> ) <sup>c</sup>	Energy (kcal/mol)	TOF $\times 10^4$ (s <sup>-1</sup> ) <sup>d</sup>	Energy (kcal/mol)	CH <sub>4</sub>	C <sub>2</sub> H <sub>6</sub>	C <sub>3</sub> H <sub>6</sub>
$6.5 \pm 0.1$	$8.4 \pm 0.1$	$5.2 \pm 0.2$	$30.9 \pm 0.1$	33	63	4

<sup>c</sup> Reaction at  $-40^{\circ}\text{C}$ ,  $P_{\text{ethylene}} = 40$  Torr and  $P_{\text{hydrogen}} = 200$  Torr.

<sup>d</sup> Reaction at  $220^{\circ}\text{C}$ ,  $P_{n\text{-butane}} = 60$  Torr and  $P_{\text{hydrogen}} = 540$  Torr

For *n*-butane hydrogenolysis reaction, the catalytic activity in terms of turn over frequency (TOF) at  $220^{\circ}\text{C}$  of this Pt-Ru/ $\gamma\text{-Al}_2\text{O}_3$  catalyst was found to be  $5.2 \times 10^{-4} \pm 0.2$ . The apparent activation energy obtained from temperature dependence was  $30.9 \pm 0.1$  kcal/mol. This value is approximately the same as the value reported for *n*-butane hydrogenolysis catalyzed by Pt and Ru catalysts consisting of metallic particles on metal oxide supports (Bond and Slaa, 1995; Bond and Cunningham 1996). Product distribution percentages or selectivity in table 2 at  $220^{\circ}\text{C}$ , indicate high selectivity for ethane.

However, selectivity for CH<sub>4</sub> is much higher than that for C<sub>3</sub>H<sub>8</sub>, this can be suggested that multiple hydrogenolysis occurred over this bimetallic catalyst in *n*-butane hydrogenolysis.

From catalytic testing of Pt-Ru/ $\gamma$ -Al<sub>2</sub>O<sub>3</sub>, the catalyst which was prepared from the molecular precursor was active for *n*-butane hydrogenolysis, which is structural sensitive. Again, there was no sign of catalyst deactivation during the test period.

## CONCLUSIONS

The characterization of  $\gamma$ -Al<sub>2</sub>O<sub>3</sub>-supported Pt<sub>3</sub>Ru<sub>6</sub>(CO)<sub>21</sub>( $\mu_3$ -H)( $\mu$ -H)<sub>3</sub> were carried out by IR and EXAFS spectroscopy. The data suggested that Pt<sub>3</sub>Ru<sub>6</sub>(CO)<sub>21</sub>( $\mu_3$ -H)( $\mu$ -H)<sub>3</sub> adsorbed strongly on surface of  $\gamma$ -Al<sub>2</sub>O<sub>3</sub> by nucleophilic displacement between coordinated CO ligands of precursor and surface hydroxyl group on support. Decarbonylation occurred by the cleavage of CO ligands of metal carbonyl upon heating and resulted metal-O<sub>support</sub> bonds forming partially decarbonylated surface species on  $\gamma$ -Al<sub>2</sub>O<sub>3</sub> surface. The carbonyl ligands can be removed completely in flowing He at 300°C for 2h to give bimetallic Pt-Ru/ $\gamma$ -Al<sub>2</sub>O<sub>3</sub>. Results from EXAFS spectroscopy confirmed that Pt and Ru were still intact after decarbonylation.

Pt-Ru/ $\gamma$ -Al<sub>2</sub>O<sub>3</sub> from a molecular precursor was active for both ethylene hydrogenation and *n*-butane hydrogenolysis.

## ACKNOWLEDGMENTS

We thank Prof. Neil E. Schore at Department of Chemistry, University of California, Davis, CA, USA, for UV lamp used to synthesize the molecular precursor. The EXAFS experiments were performed at the National Synchrotron Light Source at Brookhaven National Laboratory, Upton, New York. The EXAFS data were processed with ATHENA software developed by Bruce Ravel, and analyzed with EXAFSPAK software developed by George, G. N., et al.

## REFERENCES

- Adams, R. D., Barnard, T. S., Li, Z., Wu, W., Yamamoto, J.; "Cluster Synthesis. 43. New Layer-Segregated Platinum-Ruthenium Cluster Complexes and Their Reactions with Diphenylacetylene," *Organometallics*, 13, 2357-2364 (1994)
- Alexeev, O., Graham, G. W., Shelef, M., Adams, R. D., Gates, B. C.; " $\gamma$ -Al<sub>2</sub>O<sub>3</sub>-Supported PtRu Clusters Prepared from [Pt<sub>2</sub>Ru<sub>4</sub>(CO)<sub>18</sub>]: Characterization by Infrared and Extended X-ray Absorption Fine Structure Spectroscopies," *J. Phys. Chem. B*, 106, 4697-4704 (2002)
- Alexeev, O., Shelef, M., Gates, B. C.; "MgO-Supported Platinum-Tungsten Catalysts Prepared from Organometallic Precursors: Platinum Clusters Isolated on Dispersed Tungsten," *J. Catal.*, 164, 1-15 (1996)
- Antos, G. A., Aitani, A. M., Parera, J. M., Eds, "Catalytic naphtha Reforming," Marcel Dekker, New York (1995)
- Bond, G. B., Cunningham, R. H., "Alkane Transformations on Supported Platinum Catalysts, Part 3: the Stability of Pt/Al<sub>2</sub>O<sub>3</sub> (EUROPT-3) and of Pt/Al<sub>2</sub>O<sub>3</sub> (EUROPT-3) during the hydrogenolysis of Alkanes," *J. Catal.* 163, 328-337 (1996)

- Bond, G. B., Slaa, J. C.; "Catalytic and structural properties of ruthenium bimetallic catalysts: effects of pretreatment on the behaviour of various Ru/Al<sub>2</sub>O<sub>3</sub> catalysts in alkane hydrogenolysis," *J. Mol. Catal.* 96, 163-173 (1995)
- Dorling, T. A., Eastlake, M. J., Moss, R. L.; "The Structure and Activity of Supported Metal Catalysts IV. Ethylene Hydrogenation on Platinum/Silica Catalysts," *J. Catal.*, 14, 23-33 (1969)
- Gates, B. C. in *Catalysis by Di- and Polynuclear Metal Cluster Complexes*, Adams, R. D., Cotton, F. A. Eds.; "Metal Cluster Catalysts Dispersed on Solid Supports," Wiley-VCH, Weinheim, pp. 509 (1998)
- George, G. N., George, J. S., Pickering, I. J.; "EXAFSPAK: A Suite of Computer Programs for Analysis of X-ray Absorption Spectra," Stanford Synchrotron Radiation Laboratory, Stanford Linear Accelerator Center, (2000); Home page, <http://www-ssrl.slac.stanford.edu/exafspak.html> (downloaded 2004)
- Hadjiivanov, K. I., Vayssilov, G. N. in *Advances in Catalysis Volume 47*, Gates, B. C., Knözinger, H. Eds.; "Characterization of Oxide Surfaces and Zeolites by Carbon Monoxide as an IR Probe Molecule" Academic Press, Amsterdam, pp. 451-480 (2002)
- Hwang, K. S., Yang, M., Xhu, J., Grunes, J., Somorjai, G. A.; "The Molecular Mechanism of the poisoning of platinum and rhodium catalyzed ethylene hydrogenation by carbon monoxide," *J. Mol. Catal.*, 204-205, 499-507 (2003)
- Jentoft, R. E., Deutsch, S. E., Gates, B. C.; "Low-cost, heated, and/or cooled flow-through cell for transmission x-ray absorption spectroscopy," *Rev. Sci. Instrum.*, 67, 2111-2112 (1996)
- Mestl, G. and Knözinger, H., in *Handbook of Heterogeneous Catalysis*, Ertl, G., Knözinger, H., and Weitkamp, J., Eds; "Vibrational Spectroscopies," VCH Verlagsgesellschaft mbH, Weinheim, Germany, pp.563-568 (1997)
- Myllyoaha, S., Suvanto, M., Kurhinen, M., Hirva, P., Pakkanen, T. A., "Interactions of M(CO)<sub>6</sub> (M=Cr, Mo, W) with surface sites of Al<sub>2</sub>O<sub>3</sub>: a theoretical study," *Surf. Sci.*, 441, 454-460 (1999)
- Raval, B., Home page, <http://feff.phys.washington.edu/~raval/software/exafs/aboutathena.html> (downloaded 2003)
- Rehr, J. J., Mustre de leon, J., Zabinsky, S. I., Albers, R. C.; "Theoretical x-ray absorption fine structure standards," *J. Am. Chem. Soc.* 113, 5135 (1991)
- Shelef, M., Graham, G. W.; "Why rhodium in automotive three-way catalysts?," *Catal. Rev-Sci. Eng.*, 36, 433-457 (1994)
- Vaarkamp, M., Linders, J. C., Koningsberger, D. C.; "A new method for parameterization of phase shift and backscattering amplitude," *Physica B*, 208-209 159-160, (1995)

**APPENDIX C**

**ARTICLE IN PROCEEDING OF THE 14<sup>TH</sup> REGIONAL  
SYMPOSIUM ON CHEMICAL ENGINEERING (RSCE) 2004  
(ORAL PRESENTATION)**

## CHARACTERIZATION OF SUPPORTED PtRu CATALYSTS AND ACTIVITIES FOR ETHYLENE HYDROGENATION

Chotisuwana, Saowapa<sup>1\*</sup>, Wittayakun, Jatuporn<sup>1</sup>, and Gates, Bruce. C.<sup>2</sup>

<sup>1</sup>School of Chemistry, Suranaree University of Technology, Nakhon Ratchasima, Thailand

<sup>2</sup>Department of Chemical Engineering and Materials Science, University of California, Davis, CA, USA

E-mail address: csaowapa@yahoo.com, jatuporn@ccs.sut.ac.th

**ABSTRACT** Supported bimetallic PtRu catalysts were prepared by deposition a mixture solution of Pt(acac)<sub>2</sub> and Ru(acac)<sub>3</sub> (acac = acetylacetonate anion) in toluene on  $\gamma$ -Al<sub>2</sub>O<sub>3</sub> and MgO. The organic ligand of precursors could be removed completely after heated in H<sub>2</sub> flow at 300°C for 2 h. The nature of metal and interaction with support was studied by temperature-programmed reductive decomposition (TPRD), infrared (IR) and extended X-ray absorption fine structure (EXAFS) spectroscopy. The EXAFS data indicated high dispersion of Pt and Ru particles but none of Pt-Ru connections in both treated samples. Ethylene hydrogenation reaction over Pt-Ru/ $\gamma$ -Al<sub>2</sub>O<sub>3</sub> and Pt-Ru/MgO catalysts were carried out at -40°C and 1 atm. The temperature dependence of ethylene hydrogenation of both catalysts gave apparent activation energy of 8.1 ± 0.1 and 6.0 ± 0.1 kcal/mol, respectively.

**KEYWORDS:** Pt-Ru, acetylacetonate, alumina, magnesium oxide, EXAFS, ethylene hydrogenation

### 1. INTRODUCTION

Supported bimetallic catalysts, for instance, Pt-Re, Pt-Sn and Pt-Ir have been reported in many applications, e.g. for naphtha reforming [1], and Pt-Rh for auto exhaust conversion [2]. Supported platinum incorporating with second metal could improve the catalyst performances and stability of catalysts. In general, the simplest preparation method for bimetallic catalyst is by coimpregnation followed by high-temperature reduction. However, high temperature treatment could lead to large metal particles on support or aggregation of metal particles. In this work, a mixture of platinum and ruthenium acetylacetonate (acac) complex was employed as catalyst precursor. The acac ligands could be removed from adsorbed precursor by heat at lower temperature than chloride ligand.

The goal of this work was to prepare and characterize PtRu/ $\gamma$ -Al<sub>2</sub>O<sub>3</sub> and PtRu/MgO catalysts from a mixture of Pt(acac)<sub>2</sub> and Ru(acac)<sub>3</sub> in toluene. The acac ligands would be removed by thermal treatment in hydrogen atmosphere.

The catalyst characterization methods included temperature-programmed reductive decomposition (TPRD) technique [3], infrared (IR) and extended X-ray absorption fine structure (EXAFS) spectroscopy. The catalysts were tested for ethylene hydrogenation which is simple, structural-insensitive and widely used to test catalytic activity.

### 2. METHODOLOGY

#### 2.1 Chemicals and materials

The supported PtRu catalyst preparations and samples handling were performed under dry N<sub>2</sub> or Ar and kept in an Ar drybox to prevent contact with moisture and air. Trace of O<sub>2</sub> and moisture in gases [He, N<sub>2</sub> (Airgas, 99.99%), H<sub>2</sub> from H<sub>2</sub> generator (99.99%), and C<sub>2</sub>H<sub>4</sub> (Matheson, 99.5%)] were removed by passing each gas through traps containing reduced Cu/Al<sub>2</sub>O<sub>3</sub> and molecular sieve particles. Pt(acac)<sub>2</sub> (Aldrich, 97%) and Ru(acac)<sub>3</sub> (Strem, 99%) were used as received.

Prior to use as support, each of  $\gamma$ -Al<sub>2</sub>O<sub>3</sub> (Degussa, BET surface area 100 m<sup>2</sup>/g) and MgO powder (EM Science, 97%) was added with deionized water to form paste before drying overnight at 120°C and then calcined in flowing O<sub>2</sub> at 400°C for 2 h and evacuated for an additional 14 h.

#### 2.2 Preparation of supported samples

The PtRu catalysts containing approximately 1.0 wt % Pt and 1.0 wt % Ru were prepared by impregnation of a mixture solution of Pt(acac)<sub>2</sub> and Ru(acac)<sub>3</sub> in dry toluene onto  $\gamma$ -Al<sub>2</sub>O<sub>3</sub> and MgO followed by solvent evacuation and treatment in H<sub>2</sub> at 300°C for 2 h.

#### 2.3 Characterization

IR spectra of dry impregnated samples were recorded with a Bruker IFS-66v spectrometer with a resolution of 4 cm<sup>-1</sup>. Each sample was scanned 64 times and the signal averaged. Reductive decomposition temperatures of Pt(acac)<sub>2</sub> and Ru(acac)<sub>3</sub> to form supported PtRu catalysts were determined with RXM-100 multifunctional catalyst testing and characterization instrument (Advanced Scientific Designs, Inc. (ASDI). Dry

impregnated sample was treated in flowing H<sub>2</sub> at 300°C for 2 h to remove acac ligands and then characterized by EXAFS spectroscopy at beamline X18B of the National Synchrotron Light Source (NSLS) at Brookhaven national Laboratory (BNL), New York, USA. The storage ring energy was 2.5 GeV and the ring current was in the range 110-250 mA. Self-supporting wafer was pressed from 0.3 g of sample in the Ar glovebox at the synchrotron laboratory, and placed in a special designed XAS holder [4]. After the XAS cell was evacuated, it was installed at the beamline and cooled to nearly liquid nitrogen temperature before scanning at Pt L<sub>III</sub> edge (11564 eV) and Ru K edge (22117 eV) in transmission mode and integration for 1 s at each energy in the range from 200 eV below the absorption edge to 975 eV beyond the edge. A double crystal monochromator Si(111) was used.

#### 2.4 EXAFS data analysis

The EXAFS data were collected in transmission mode at individual Pt L<sub>III</sub> (11564 eV) and Ru K (22117 eV) absorption edge and analyzed with theoretical reference files. The EXAFS data processing was carried out with ATHENA software [5]. The final normalized EXAFS function from ATHENA software for each edge of each sample was obtained from the average of four scans. Phase shift and backscattering amplitudes of Pt-Pt, Pt-Ru, Pt-O<sub>support</sub>, Ru-Ru, Ru-Pt, and Ru-O<sub>support</sub> interactions were calculated by FEFF7.0 software [6]. The EXAFS data fittings by EXAFSPAK software [7] were accomplished with single and multiple scattering paths calculated by FEFF7.0, and the EXAFS parameters were extracted from the raw data with the EXAFSPAK software. The fitting were done in *r* space (*r* is interatomic distance from the absorber atom) and *k* space (*k* is the wave vector) with application of *k*<sup>0</sup>, *k*<sup>1</sup>, and *k*<sup>3</sup> weightings.

Raw EXAFS data obtained at Pt L<sub>III</sub> edge of ligand-free PtRu/γ-Al<sub>2</sub>O<sub>3</sub> and PtRu/MgO were Fourier transformed over the ranges 3.60 < *k* < 14.30, and 3.55 < *k* < 14.50 with *k*<sup>3</sup> weighting without phase correction, respectively. The main contributions were isolated by backward Fourier transformation in the ranges 0.0 < *r* < 5.0 Å for both samples after treatment in H<sub>2</sub>.

The raw data obtained at Ru K edge of ligand-free PtRu/γ-Al<sub>2</sub>O<sub>3</sub> were analyzed over the ranges 3.25 < *k* < 14.75 and 0.0 < *r* < 4.0 Å whereas that of ligand-free PtRu/MgO were analyzed over the ranges 3.20 < *k* < 14.50 and 0.0 < *r* < 5.0 Å.

The raw data of PtRu/γ-Al<sub>2</sub>O<sub>3</sub> obtained at Pt L<sub>III</sub> and Ru K edge were analyzed with a maximum of 16 free parameters. The statistically justified numbers of free parameters estimated from Nyquist theorem [8],  $n = (2\Delta k\Delta R/\pi) + 1$ , were about 35 and 30, for data obtained at Pt L<sub>III</sub> and Ru K edge, respectively. The raw data of treated PtRu/MgO obtained at Pt L<sub>III</sub> and Ru K edge were analyzed with a maximum of 20 free parameters. The statistically justified numbers of free parameters estimated from Nyquist theorem were about 36 and 37, for data obtained at Pt L<sub>III</sub> and Ru K edge, respectively.

#### 2.5 Catalytic test for ethylene hydrogenation

The catalytic test for ethylene hydrogenation was carried out in a stainless steel U-tubed flow reactor at atmospheric pressure. Prior to reaction testing, catalyst sample was pretreated with H<sub>2</sub> at 300°C for 2 h. Typically, 10 to 20 mg of 1.0 wt% Pt and 1.0 wt% Ru catalyst was diluted with 600 mg of inert α-Al<sub>2</sub>O<sub>3</sub>, loaded into the reactor, and cooled to desired temperature under He flow before a gas mixture of H<sub>2</sub>, ethylene, and balance He was flowed into reactor. The reaction condition was as follow: *P*<sub>ethene</sub> = 40 Torr, *P*<sub>hydrogen</sub> = 200 Torr, balanced with He, total feed flow rate = 100 ml (NTP)/min, and temperature = -50 to -9°C. The effluent gas mixture was analyzed with an on-line gas chromatograph (Hewlett-Packard HP 6890) equipped with an Al<sub>2</sub>O<sub>3</sub> capillary column (50 m x 0.53 nm x 15.0 micron film thickness), and a flame ionization detector.

### 3. RESULTS AND DISCUSSION

#### 3.1 Evidence of adsorbed precursor on supports from IR

The decreasing in intensity of IR peaks of isolated hydroxyl groups of γ-Al<sub>2</sub>O<sub>3</sub> at 3786(w), 3728(m), and 3366(m) cm<sup>-1</sup> of dry impregnated Pt(acac)<sub>2</sub> and Ru(acac)<sub>3</sub> on γ-Al<sub>2</sub>O<sub>3</sub> indicated that the hydroxyl groups on γ-Al<sub>2</sub>O<sub>3</sub> involved in the interaction with the mixture of Pt(acac)<sub>2</sub> and Ru(acac)<sub>3</sub>. IR broad band at 3569(m) indicates hydrogen-bonded on support [9].

After impregnation of a mixture of Pt(acac)<sub>2</sub> and Ru(acac)<sub>3</sub> in toluene onto MgO and evacuation to remove solvent, the intensity of isolated hydroxyl groups at 3764(s) cm<sup>-1</sup> decreased indicating that they were involved in precursor-support interactions.

A small IR band at 1601 cm<sup>-1</sup> of dry impregnated Pt(acac)<sub>2</sub> and Ru(acac)<sub>3</sub> on γ-Al<sub>2</sub>O<sub>3</sub> and at 1608 cm<sup>-1</sup> of that on MgO were observed, each peak was assigned to the formation of Al-acac and Mg-acac species which was reported at 1590 cm<sup>-1</sup> for Al-acac imply ligand-exchange mechanism [9]. The acac ligands showed IR peaks in region of 1610-1100 cm<sup>-1</sup> [10, 11]. These ligands were removed completely after treatment in H<sub>2</sub> at 300°C.

#### 3.2 Reductive decomposition temperature of supported samples by TPRD

The reductive decomposition temperature based on hydrogen consumption of dry impregnated Pt(acac)<sub>2</sub>, Ru(acac)<sub>3</sub>, and Pt(acac)<sub>2</sub> + Ru(acac)<sub>3</sub> on  $\gamma$ -Al<sub>2</sub>O<sub>3</sub> and MgO are presented in Table 1. All observed peaks were broad indicating that the decomposition was a slow process. Alumina supported Pt(acac)<sub>2</sub> had a peak at 210°C while that of Ru(acac)<sub>3</sub> had a peak at 288 °C. The supported mixture of Pt(acac)<sub>2</sub> + Ru(acac)<sub>3</sub> on  $\gamma$ -Al<sub>2</sub>O<sub>3</sub> had 3 peaks: at 124 and 199°C indicated at least two types of supported Pt on support, and at 340°C indicated reduction temperature of supported Ru. TPRD profile indicated that Pt and Ru particles were isolated from one another on  $\gamma$ -Al<sub>2</sub>O<sub>3</sub> after treatment.

Broad H<sub>2</sub> consumption temperatures during reductive decomposition of Pt(acac)<sub>2</sub> on MgO had 3 peaks at 140, 202, and 340°C indicating that Pt had various oxidation states or various adsorption modes on MgO. On the other hand, Ru in Ru(acac)<sub>3</sub> supported on MgO showed decomposition temperature at 216°C indicating that only one oxidation state or one adsorption mode of Ru(acac)<sub>3</sub> supported on MgO. For supported PtRu sample on MgO, broad H<sub>2</sub> consumption was observed at 189-221°C indicating that Pt and Ru might contact to each other on MgO or change in oxidation states. The Pt-Ru connectivity could be characterized by EXAFS spectroscopy.

**Table 1** Reduction temperatures of Pt(acac)<sub>2</sub> and Ru(acac)<sub>3</sub> supported on  $\gamma$ -Al<sub>2</sub>O<sub>3</sub> and MgO

Samples	Reduction temperature (°C)
Pt(acac) <sub>2</sub> / $\gamma$ -Al <sub>2</sub> O <sub>3</sub>	210 (b)
Ru(acac) <sub>3</sub> / $\gamma$ -Al <sub>2</sub> O <sub>3</sub>	288 (b)
[Pt(acac) <sub>2</sub> + Ru(acac) <sub>3</sub> ]/ $\gamma$ -Al <sub>2</sub> O <sub>3</sub>	124 (sh), 199 (b), 340 (b)
Pt(acac) <sub>2</sub> /MgO	140 (b), 202 (b), 340 (b)
Ru(acac) <sub>3</sub> /MgO	216 (b)
[Pt(acac) <sub>2</sub> + Ru(acac) <sub>3</sub> ]/MgO	189 - 221 (b)

Notation: b = broad, sh = shoulder

### 3.3 Metal-metal contributions in treated samples by EXAFS

The EXAFS data of decarbonylated sample scanned at Pt L<sub>III</sub> and Ru K edges at nearly liquid nitrogen temperature were processed by ATHENA software and fitted with EXAFSPAK software. The EXAFS fitting parameters of supported PtRu/ $\gamma$ -Al<sub>2</sub>O<sub>3</sub> and PtRu/MgO were summarized in Table 2. The estimated accuracies of coordination number (*N*), distance (*R*), Debye-Waller factor ( $\Delta\sigma^2$ ), and inner potential correction ( $\Delta E_0$ ) are as follows:  $\pm 20\%$ ,  $\pm 1\%$ ,  $\pm 30\%$ ,  $\pm 10\%$ , respectively.

**Table 2** Summary of EXAFS fitting parameters of supported Pt-Ru/ $\gamma$ -Al<sub>2</sub>O<sub>3</sub> and Pt-Ru/MgO

Samples	Edge	Shell	<i>N</i>	<i>R</i> (Å)	10 <sup>3</sup> x $\Delta\sigma^2$ (Å <sup>2</sup> )	$\Delta E_0$ (eV)
PtRu/ $\gamma$ -Al <sub>2</sub> O <sub>3</sub>	Pt L <sub>III</sub>	Pt-Pt	2.8 $\pm$ 0.1	2.77 $\pm$ 0.01	1.1 $\pm$ 0.3	7.7 $\pm$ 0.4
		Pt-Ru	-	-	-	-
		Pt-O <sub>support</sub>				
	Ru K	Pt-O <sub>s</sub>	3.4 $\pm$ 0.1	2.50 $\pm$ 0.01	0.8 $\pm$ 0.5	-5.8 $\pm$ 0.3
		Pt-O <sub>l</sub>	1.3 $\pm$ 0.1	2.95 $\pm$ 0.01	-4.5 $\pm$ 1.0	8.7 $\pm$ 0.6
		Ru-Ru	3.3 $\pm$ 0.1	2.65 $\pm$ 0.01	3.9 $\pm$ 0.3	-7.3 $\pm$ 0.2
		Ru-Pt	-	-	-	-
		Ru-O <sub>support</sub>				
		Ru-O <sub>l</sub>	1.7 $\pm$ 0.1	1.98 $\pm$ 0.01	14.0 $\pm$ 1.1	-3.7 $\pm$ 0.5
PtRu/MgO	Pt L <sub>III</sub>	Ru-O <sub>l</sub>	0.7 $\pm$ 0.1	2.20 $\pm$ 0.01	6.5 $\pm$ 2.6	-0.8 $\pm$ 0.8
		Pt-Pt	1.0 $\pm$ 0.1	3.07 $\pm$ 0.01	3.3 $\pm$ 0.5	-5.8 $\pm$ 0.6
		Pt-Ru	-	-	-	-
	Ru K	Pt-O <sub>support</sub>				
		Pt-O <sub>s</sub>	0.4 $\pm$ 0.1	1.98 $\pm$ 0.01	4.9 $\pm$ 1.4	7.0 $\pm$ 0.6
		Pt-O <sub>l</sub>	2.6 $\pm$ 0.1	2.51 $\pm$ 0.01	0.5 $\pm$ 0.2	2.1 $\pm$ 0.1
		Pt-O <sub>l2</sub>	4.3 $\pm$ 0.1	3.17 $\pm$ 0.01	-0.3 $\pm$ 0.3	-11.9 $\pm$ 0.1
		Ru-Ru	3.5 $\pm$ 0.1	2.69 $\pm$ 0.01	4.4 $\pm$ 0.3	-2.8 $\pm$ 0.2
		Ru-Pt	-	-	-	-
		Ru-O <sub>support</sub>				
Ru-O <sub>s</sub>	2.5 $\pm$ 0.1	2.01 $\pm$ 0.01	8.6 $\pm$ 0.5	-2.8 $\pm$ 0.2		
Ru-O <sub>l</sub>	0.9 $\pm$ 0.1	2.53 $\pm$ 0.01	-3.5 $\pm$ 1.0	15.0 $\pm$ 0.4		
Ru-O <sub>l2</sub>	1.1 $\pm$ 0.1	2.96 $\pm$ 0.01	1.6 $\pm$ 1.8	-3.5 $\pm$ 0.6		

Notation: the subscript s, l and l2 refer to short and long distance, respectively

The EXAFS fitting data in Table 2 included metal-metal (Pt-Pt and Ru-Ru) and metal-support (M-O<sub>support</sub>: M-O<sub>s</sub>, and M-O<sub>i</sub>) contributions of supported PtRu samples on  $\gamma$ -Al<sub>2</sub>O<sub>3</sub> and MgO. The EXAFS data showed that there were no Pt-Ru or Ru-Pt contributions on both  $\gamma$ -Al<sub>2</sub>O<sub>3</sub> and MgO after treatment in H<sub>2</sub> flow at 300°C. High dispersion of Pt and Ru particles was observed by EXAFS spectroscopy. The coordination numbers of Pt-Pt on  $\gamma$ -Al<sub>2</sub>O<sub>3</sub> was 2.8 at average distance  $2.77 \pm 0.01$  Å, shorter than that on MgO,  $3.07 \pm 0.01$  Å with coordination number 1.0 indicating that Pt-Pt interaction on  $\gamma$ -Al<sub>2</sub>O<sub>3</sub> was stronger than that on MgO. Interactions of Ru-Ru contributions on both  $\gamma$ -Al<sub>2</sub>O<sub>3</sub> and MgO were not significantly different in terms of both average distance and coordination number. After treatment in H<sub>2</sub> flow at 300°C to remove acac ligands, the average Pt-O<sub>s</sub> and Ru-O<sub>s</sub> bond distances were found at  $2.50 \pm 0.01$  and  $1.98 \pm 0.01$  Å with coordination numbers  $3.4 \pm 0.1$  and  $1.7 \pm 0.1$ , respectively for PtRu/ $\gamma$ -Al<sub>2</sub>O<sub>3</sub>. The average Pt-O<sub>s</sub> and Ru-O<sub>s</sub> bond distances of PtRu/MgO were found at  $1.98 \pm 0.01$  and  $2.01 \pm 0.01$  Å with coordination numbers  $0.4 \pm 0.1$  and  $2.5 \pm 0.1$ , respectively indicating strong interaction of metal-support interactions. Normally the average M-O bond distances were observed at 2.1 - 2.2 Å for supported metal on oxide support [12].

### 3.4 Ethylene Hydrogenation reaction catalyzed by supported PtRu catalysts

Catalytic activity of ethylene hydrogenation catalyzed by supported PtRu/ $\gamma$ -Al<sub>2</sub>O<sub>3</sub> and PtRu/MgO prepared from mixed Pt and Ru compounds were carried out in stainless U-tubed reactor at atmospheric pressure under condition:  $P_{\text{ethene}} = 40$  Torr,  $P_{\text{hydrogen}} = 200$  Torr, balanced with He, total feed flow rate = 100 ml (NTP)/min, 10 to 20 mg of 1.0 wt% Pt and 1.0 wt% Ru catalyst, temperature ranges -50 to -9°C. Reaction temperature was kept at desired temperature with  $\pm 1$ °C. Catalytic activities of ethylene hydrogenation catalyzed by PtRu/ $\gamma$ -Al<sub>2</sub>O<sub>3</sub> and PtRu/MgO prepared from the mixture solution of Pt(acac)<sub>2</sub> and Ru(acac)<sub>3</sub> were plotted as a function of time on stream (TOS) as shown in Figure 1. The activities over PtRu/MgO were much higher than that over PtRu/ $\gamma$ -Al<sub>2</sub>O<sub>3</sub> at temperature -50°C. The reaction reached steady-state within 20 minutes for both catalysts and deactivations was not observed during 100 minutes of the test.

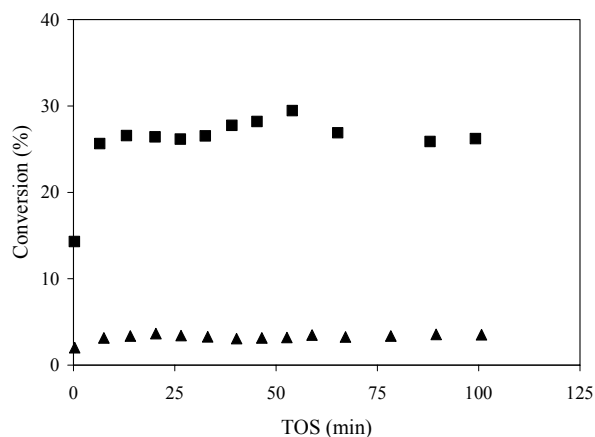


**Figure 1** Activity for ethylene hydrogenation over (■) PtRu/MgO; (▲) PtRu/ $\gamma$ -Al<sub>2</sub>O<sub>3</sub>, prepared from the mixture solution of Pt(acac)<sub>2</sub> and Ru(acac)<sub>3</sub> at temperature -50°C.

The apparent activation energy of ethylene hydrogenation over supported PtRu catalysts was collected at around 25 min TOS at this condition at temperature ranges -50 to -9°C. The catalytic activity of reaction in terms of the turnover frequency (TOF) was represented the number of molecules reacting per active sites per second [13]. It was assumed that metal particles dispersed on support accessible to reactants, so that TOF was defined as units of mole of ethylene converted to ethane per gram catalyst per second. Arrhenius plot of natural logarithm of TOF as a function of inversed temperature was in Figure 2. Due to very high activity of ethylene hydrogenation over PtRu/MgO prepared from a mixture solution of Pt(acac)<sub>2</sub> and Ru(acac)<sub>3</sub>, conversion at higher temperature than -30°C was too high, thus data was collected in temperature ranges -50 to -30°C.

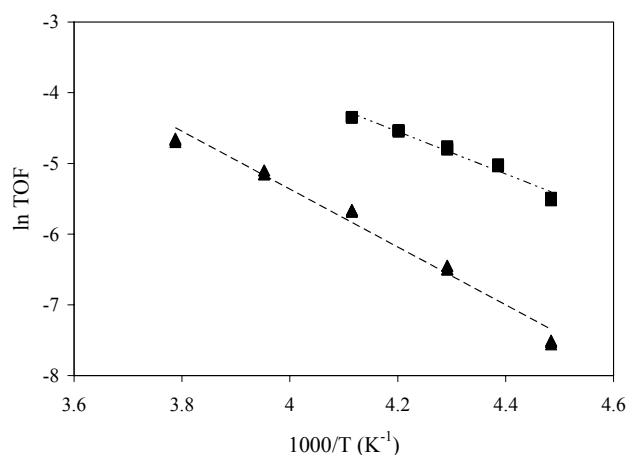


**Figure 2** Arrhenius plot for ethylene hydrogenation over (■) PtRu/MgO; (▲) PtRu/ $\gamma$ -Al<sub>2</sub>O<sub>3</sub>, prepared from the mixture solution of Pt(acac)<sub>2</sub> and Ru(acac)<sub>3</sub>.

The apparent activation energy of ethylene hydrogenation catalyzed by supported PtRu catalysts could be obtained from slope of linear graph in Figure 2 and values are shown in Table 3. The apparent activation energy of supported PtRu/MgO was lower than that of PtRu/ $\gamma$ -Al<sub>2</sub>O<sub>3</sub> and activity (TOF) at temperature -40°C of PtRu/MgO was pretty much higher than that of PtRu/ $\gamma$ -Al<sub>2</sub>O<sub>3</sub> indicating that PtRu/MgO catalyst was more active than PtRu/ $\gamma$ -Al<sub>2</sub>O<sub>3</sub>.

**Table 3** Apparent activation energy for ethylene hydrogenation over PtRu catalysts prepared from mixture solution of Pt(acac)<sub>2</sub> and Ru(acac)<sub>3</sub> and treated in H<sub>2</sub> at 300°C for 2 h

Precursors	Supports	Activity TOF x 10 <sup>4</sup> (s <sup>-1</sup> ) <sup>a</sup>	Apparent activation energy (kcal/mol)	Temperature (°C)
Pt(acac) <sub>2</sub> + Ru(acac) <sub>3</sub>	$\gamma$ -Al <sub>2</sub> O <sub>3</sub>	1.5 ± 0.1	8.1 ± 0.1	-50 to -9
Pt(acac) <sub>2</sub> + Ru(acac) <sub>3</sub>	MgO	83.9 ± 1.7	6.0 ± 0.1	-50 to -30

<sup>a</sup> Reaction at -40°C,  $P_{\text{ethene}} = 40$  Torr and  $P_{\text{hydrogen}} = 200$  Torr.

#### 4. CONCLUSIONS

TPRD, IR and EXAFS spectroscopy were used to characterize supported PtRu catalysts prepared by impregnation of the mixture of Pt(acac)<sub>2</sub> and Ru(acac)<sub>3</sub> in toluene onto  $\gamma$ -Al<sub>2</sub>O<sub>3</sub> and MgO. The data suggested that precursors adsorbed on surface of  $\gamma$ -Al<sub>2</sub>O<sub>3</sub> and MgO through interaction between acac ligands of precursor and surface hydroxyl group on support. The acac ligands could be removed completely in flowing H<sub>2</sub> at 300°C for 2 h to give PtRu/ $\gamma$ -Al<sub>2</sub>O<sub>3</sub> and PtRu/MgO. TPRD data showed that Pt(acac)<sub>2</sub> decomposed at lower temperature than Ru(acac)<sub>3</sub>. Results from EXAFS spectroscopy indicated that there were no Pt-Ru interactions after ligand removal. Highly dispersed PtRu/ $\gamma$ -Al<sub>2</sub>O<sub>3</sub> and PtRu/MgO catalysts prepared from the mixture of Pt(acac)<sub>2</sub> and Ru(acac)<sub>3</sub> precursor were active for ethylene hydrogenation giving apparent activation energy 8.1 ± 0.1 and 6.0 ± 0.1 kcal/mol, respectively.

#### ACKNOWLEDGEMENT

S. Chotisuwan thanks for financial support from Ministry University Affair and Prince of Songkla University, Pattani campus, Thailand. We acknowledge the National Synchrotron Light Source at Brookhaven National Laboratory, Upton, NY. The EXAFS data were processed by ATHENA software developed by Bruce Ravel, and analyzed with EXAFSPAK software developed by George, G. N., et al.

#### REFERENCES

- [1] Sinfelt, J. H. "Bimetallic Catalysts: Discoveries, Concepts, and Applications," Wiley, New York, (1983).
- [2] Shelef, M., Graham, G. W. *Catal. Rev-Sci. Eng.*, **36**, pp 433-457 (1994).
- [3] Dossi, C., Pozzi, A., Recchia, S., Fusi, A., Psaro, R., Santo, V. D. *J. Mol. Catal. A* **204-205**, pp 465-472 (2003).
- [4] Jentoft, R. E., Deutsch, S. E., Gates, B. C. *Rev. Sci. Instrum.*, **67**, pp 2111-2112 (1996).

- [5] Raval, B., Home page, <http://feff.phys.washington.edu/~ravel/software/exafs/aboutathena.html> (downloaded 2003).
- [6] Rehr, J. J., Mustre de leon, J., Zabinsky, S. I., Albers, R. C. *J. Am. Chem. Soc.*, **113**, pp 5135-5140 (1991).
- [7] George, G. N., George, J. S., Pickering, I. J.; "EXAFSPAK: A Suite of Computer Programs for Analysis of X-ray Absorption Spectra," Stanford Synchrotron Radiation Laboratory, Stanford Linear Accelerator Center, (2000); Home page, <http://www-ssrl.slac.stanford.edu/exafspak.html> (downloaded 2004).
- [8] Stern, E. A. *Phys. Rev. B*, **48**, pp 9825-9827 (1993).
- [9] Baltes, M., Collart, O., Van Der Voort, P., Vansant, E. F., *Langmuir*, **15(18)**, pp 5841-5845 (1999).
- [10] Nakamoto, K., "The SADTLER Standard Spectra: High Resolution Spectra of Inorganic and Related Compounds". SADTLER Research Laboratory, Inc., Philadelphia, (1965).
- [11] Southern Research Institute. "Joint Committee on Atomic and Molecular Physical Data Evaluated Infrared Reference Spectrum". The Coblenz Society, Inc, (1970).
- [12] Guzman, J., Gates, B. C., *Dalton Trans.*, **17**, pp 3303-3318 (2003).
- [13] Fogler, H. S., "Elements of Chemical Reaction Engineering". 3<sup>rd</sup> ed., Prentice-Hall, Inc., New Jersey, p. 587 (1999).

# CURRICULUM VITAE

## SAOWAPA CHOTISUWAN

**E-mail:** csaowapa@yahoo.com

**Birth Date and Place:** 12 February, 1972 in Phang-nga, Thailand

**Citizenship:** Thailand

### **Education:**

1989-1993 B.Sc. Industrial Chemistry, Chiang Mai University, Chiang Mai, Thailand

1993-1996 M.Sc. (Chemistry), Chiang Mai University, Chiang Mai, Thailand

2001-2005 Ph. D. (Chemistry) Suranaree University of Technology, Thailand

### **Experience:**

1996-present Lecturer, Prince of Songkla University, Pattani campus, Pattani, Thailand

November-December 1998 Training visit in industrial chemistry at Institut Universitaire de Technologie du Mans, Le Mans, France

April-May 2000 Training visit in chemistry at University of Wollongong and University of Technology, Sydney, Australia

August 2002 Ph.D. research at Tokyo Institute of Technology, Tokyo, Japan

2002-2003 Ph.D. research at University of California, Davis, USA

**Scholarship:** Commission on Higher Education, Ministry of Education, Thai Government, Thailand